

**Preventing Loss of Aircraft Control**  
**Aiding pilots in manual recovery from roll-limited situations**

Koolstra, Herman

**DOI**

[10.4233/uuid:96053b94-0f1a-45cd-9e45-1f39e78c55de](https://doi.org/10.4233/uuid:96053b94-0f1a-45cd-9e45-1f39e78c55de)

**Publication date**

2017

**Document Version**

Final published version

**Citation (APA)**

Koolstra, H. (2017). *Preventing Loss of Aircraft Control: Aiding pilots in manual recovery from roll-limited situations*. [Dissertation (TU Delft), Delft University of Technology]. <https://doi.org/10.4233/uuid:96053b94-0f1a-45cd-9e45-1f39e78c55de>

**Important note**

To cite this publication, please use the final published version (if applicable).  
Please check the document version above.

**Copyright**

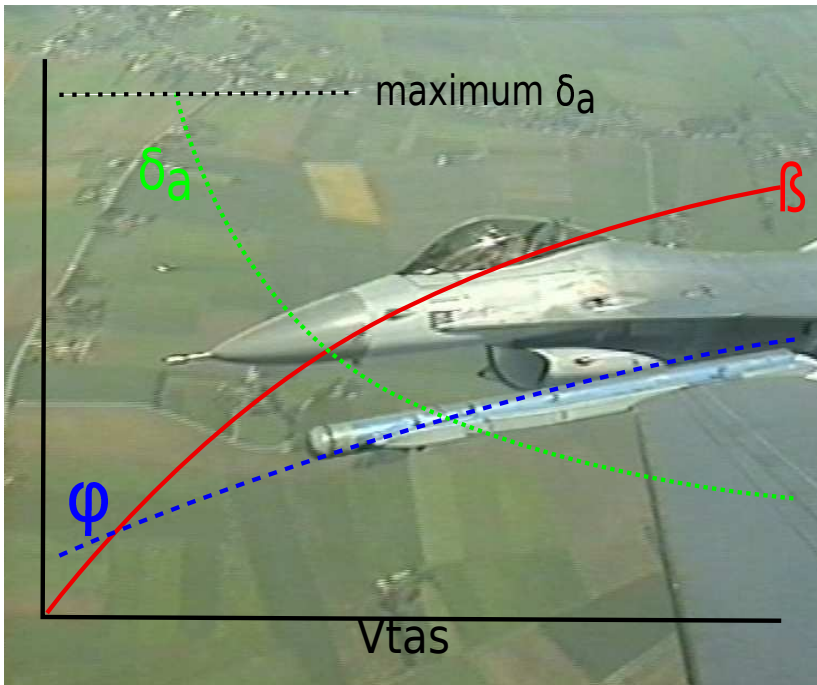
Other than for strictly personal use, it is not permitted to download, forward or distribute the text or part of it, without the consent of the author(s) and/or copyright holder(s), unless the work is under an open content license such as Creative Commons.

**Takedown policy**

Please contact us and provide details if you believe this document breaches copyrights.  
We will remove access to the work immediately and investigate your claim.

# PREVENTING AIRCRAFT LOSS OF CONTROL

AIDING PILOTS IN MANUAL RECOVERY FROM ROLL-LIMITED SITUATIONS





# **PREVENTING AIRCRAFT LOSS OF CONTROL**

**AIDING PILOTS IN MANUAL RECOVERY FROM ROLL-LIMITED  
SITUATIONS**

## **Proefschrift**

ter verkrijging van de graad van doctor  
aan de Technische Universiteit Delft,  
op gezag van de Rector Magnificus prof. ir. K. C. A. M. Luyben,  
voorzitter van het College voor Promoties,  
in het openbaar te verdedigen op 6 juli 2017 om 15:00 uur

door

**Herman Johan KOOLSTRA**

Experimenteel Testvlieger  
geboren te Rijk, Nederland

Dit proefschrift is goedgekeurd door de promotor:

Prof. dr. ir. M. Mulder

Copromotor:

Dr. ir. M. M. van Paassen

Samenstelling promotiecommissie:

Rector Magnificus,	voorzitter
Prof. dr.ir. M. Mulder,	Technische Universiteit Delft, promotor
Dr. ir. M.M. van Paassen,	Technische Universiteit Delft, copromotor
Prof. dr. ir. J.A. Mulder,	Technische Universiteit Delft
Onafhankelijke commissieleden:	
Prof. dr. Ing. R. Luckner,	Technische Universität Berlin, Germany
Prof. dr. A.R. Pritchett,	Georgia Institute of Technology, USA
Ir. W. Huson,	Chief test pilot (ret), Fokker Aircraft
Prof. dr. ir. E.C.T. van der Helm,	Technische Universiteit Delft
Prof. dr. D.G. Simons	Technische Universiteit Delft, reservelid



*Keywords:* Aircraft lateral-directional control, minimum control speed, damaged aircraft.

*Printed by:* Gildeprint

*Front & Back:* Front cover: The roll performance with maximum asymmetric power as function of the airspeed; background an F-16 not affected by any asymmetry in a close formation steep turn. Back cover: Stills of a video of the Beachcraft King Air accident on 11 December 2011 in Paranaque, Philippines. The aircraft lost an engine shortly after take off and lost lateral control, causing a fatal crash. Source:<https://www.youtube.com/watch?v=vTQwkKameLg>

Copyright © 2017 by H.J. Koolstra

ISBN 978-94-6186-816-9

An electronic version of this dissertation is available at

<http://repository.tudelft.nl/>.

*Science is a wonderful thing  
if one does not have to earn one's living at it.*

Albert Einstein



# PREFACE

There is a well-known story about a father and son watching take-offs and landings at a military airbase. Impressed by all these fighter aircraft the boy exclaims: 'Father, when I grow up, I want to be a fighter pilot'. To this, his father says: 'Both isn't possible son, you have to make a choice'. Being myself a typical example of somebody that fulfilled all boyhood dreams: a career at sea, in the merchant marine as well as the navy, joining the Air Force and becoming a fighter pilot and an experimental test pilot, you may wonder: Is this work before you the result of finally growing up or just another endeavour that shows I have never grown up. I will leave it to the reader to decide.

Writing a thesis was actually not the original plan. When I retired from the Air Force, I wanted to improve my theoretical knowledge and try to combine my practical experience with a better understanding of the underlying theory, so I could do some useful research for the flying community. Thanks to Lt. Gen. (ret) B.A.C. Droste, at that moment the dean of the faculty, I was introduced to professor Bob Mulder. It was Bob's idea that my efforts should result in a thesis. Bob is an inspiring personality, so I embarked on the journey. However, Bob's initial expectations about the time required were slightly optimistic. I found out that age is not an obstacle to learning, but simply requires more time, in the same way that my time required to run half a marathon doesn't come close to the time I could set 30 years ago. So the first years were devoted to pure study and working part-time for the Dutch Military Aviation Authority. Both were challenging and rewarding experiences.

It was after the promotion of Thomas Lombaerts, who designed an adaptive flight control system for damaged aircraft, that I realized what a nice subject this was for an experimental test pilot. However, my aim would not be to design a new controller, but to determine how to aid the pilot in the safe recovery of a damaged aircraft. My initial research used our faculty's well-known Citation Model. Initially, it seemed quite easy to predict manoeuvrability for this model. However, Herman Damveld convinced me that it was a much better idea to work on a twin propeller aircraft. And he was right, most accidents, especially with 'one-engine-inoperative' occur with those aircraft. The downside of this decision was that everything that once seemed easy turned out to be much more difficult. Predictions of the remaining manoeuvrability were way off, error detection did not work and questions arose whether working with a simple linear model was possible at all.

A few years later the model worked and the next phase could start, tests with pilots-in-the-loop. These experiments would never have been possible without the excellent support of Olaf Stroosma. We overcame all Dueca obstacles and had two sets of wonderful experiments in the SIMONA flight simulator. These tests were a rewarding ex-

perience. Pilots remained enthusiastic, even in the most severe and difficult scenarios. Transforming results into a decent thesis was the last challenge. Fortunately, my Co-promoter René van Paassen was instrumental in getting the argumentation straight and I was more than impressed with the talents of my Promoter Max Mulder to formulate things clearly and with his keen eye for details that easily escaped mine. Last but not least, my wife read the very first as well as the last version of this thesis-and also some versions in between- which greatly helped to correct typos as well as the grammatical mistakes that I so easily make.

Finally, I hope that the results of this work will find their way into the flying community and may aid in making flying even safer than it already is. Having had the opportunity to complete this thesis and having received so much support is a reason for thankfulness. Or in the words of my tradition, I feel blessed.

*Herman Johan Koolstra  
Amersfoort, March 2017*

# NOMENCLATURE

## ABBREVIATIONS

AoA	Angle of Attack
AIC	Akaike Information Criterion
AICC	Akaike Information Criterion Corrected
BIC	Bayesian Information Criterion
c.g.	Centre of Gravity
CS	Common (EU) Standards
CUSUM	Cumulative Sum
DD	Direct Division
FA	Forgetting Algorithm
FAD	Forgetting Algorithm with Damping
FAR	Federal Aviation Regulations
IBM	Innovation Based Methods
ICAO	International Civil Aviation Organization
IMC	Instrument Meteorological Conditions
IMU	Inertial Measurement Unit
INU	Inertial Navigation Unit
KF	Kalman Filter
KIAS	Knots Indicated Airspeed
KTAS	Knots True Airspeed
LOC-I	Loss of Control in flight
Mil. Spec.	Military Specifications
MKM	Modified Kalman Method
MV	Multivariate (Type of SPRT)
NTSB	National Transportation Safety Board
OEI	One engine inoperative
OLS	Ordinary Least Squares
PFD	Primary Flight Display
PID	Parameter Identification
RLS	Recursive Least Squares
RNLAF	Royal Netherlands Air Force
SHS	Steady Heading Side slip
SL	Sequential Learning
SPRT	Sequential Probability Ratio Test
SRS	SIMONA Research Simulator
$SS_{reg}$	Regression (or explained) Sum of Squares
$SS_{res}$	Residual Sum of Squares
$SS_{tot}$	Total Sum of Squares

TAS	True Airspeed
TUD	Technical University Delft
USAF	United States Air Force
VIF	Variation Inflation Factor
VPS	$V_c$ Prediction System
SIMONA	Simulation, Motion and Navigation
TPS	Test Pilot School

## GREEK SYMBOLS

$\alpha$	Angle of attack
$\beta$	Angle of side slip, Parameter vector
$\gamma$	Climb angle
$\delta$	Incremental change; Control deflection
$\epsilon$	Error value
$\zeta$	Damping ratio
$\theta$	Angle between body X-axis with horizontal plane
$\lambda$	Forgetting factor
$\rho$	Air density ( $kg/m^3$ )
$\mu$	Mean of Distribution
$\sigma$	Standard deviation
$\phi$	Roll Angle
$\psi$	Heading
$\omega$	Frequency (rad/s)

## LATIN SYMBOLS

$b$	Wingspan; Signal to noise ratio = $\frac{\mu_1 - \mu_0}{\sigma}$
$\bar{c}$	mean aerodynamic chord
$g$	Test Statistic
$k$	Factor used to correct thrust moment for cross flow effect
$k$	Number of model parameters
$m$	mass, meter
$m_{x,y,z}$	Moment around respectively x, y and z axis
$n$	Load factor
$p\theta_0$	Probability distribution before change
$p\theta_1$	Probability distribution after change
$p$	Rotation rate around body x-axis
$q$	Rotation rate around body y-axis
$r$	Rotation rate around body z-axis
$s_i$	Log likelihood ratio from observation $i$
$t_a$	Alarm time
$u$	Velocity component in body x-axis
$v$	Velocity component in body y-axis

$v$	State space noise vector on measurement
$w$	Velocity component in body z-axis
$y_i$	Observation at instant $i$
$A$	State space transition matrix
$B$	State space input gain matrix
$C$	State space sensor dynamics matrix
$C$	Normalize aerodynamic coefficient
$D$	State space direct control input matrix
$H$	Input vector
$I$	Inertia tensor
$K$	Kalman gain
$L$	Moments around body x-axis
$M$	Moments around body y-axis
$M$	Matrix with extended state blocks used by the MKF
$N$	Moments around body z-axis
$P$	Weighting matrix for RLS $P = \Sigma M_i H_i^T$ , Power
$P_k$	Covariance matrix of the Kalman filter
$R$	Kalman filter measurement noise matrix, Multiple Correlation Coefficient
$R^2$	Coefficient of Determination (Squared Multiple Correlation Coefficient)
$S$	Wing Surface Area
$S_i^j$	Cumulative log likelihood ratio from observation $i$ to $j$
$\tilde{S}_i^j$	Weighted log likelihood ratio
$V$	Velocity with respect to air
$V_c$	Minimum velocity for sufficient lateral control
$V_{c1}$	Minimum velocity for sufficient lateral control with aileron only
$V_{c2}$	Minimum velocity for sufficient lateral control with aileron and rudder
$V_{mca}$	Minimum Control Speed Air
$V_{NE}$	Never Exceed Speed
$V_S$	Stall speed
$V_{SR}$	Reference stall speed
$Z$	Measurement vector

## SUBSCRIPTS

$a$	Aileron
$c$	Control
$c1$	Control using aileron
$c2$	Control using aileron and maximum rudder
$cR$	Control to the right
$cL$	Control to the left
$e$	Elevator
$i$	Index number
$r$	Rudder
$tl$	Normalized Torque left engine

$tr$	Normalized Torque right engine
$x$	X-axis
$y$	Y-axis
$z$	Z-axis

# CONTENTS

<b>1</b>	<b>Introduction</b>	<b>1</b>
1.1	Safe Flight	3
1.1.1	Present Research	4
1.1.2	Focus of this Thesis	6
1.2	Research Questions	7
1.3	Approach to Solve the Research Questions	8
1.4	Scope and Assumptions	8
1.5	Structure of Thesis	9
	References	12
<b>2</b>	<b>Discriminating Flight Envelopes</b>	<b>13</b>
2.1	Introduction	15
2.2	Flight envelope division	15
2.3	Performance Envelope	16
2.4	Structural Envelope	17
2.5	Stability and Control envelope	19
2.5.1	Stability	19
2.5.2	Control envelope	22
2.6	Situation Awareness Limits	23
2.7	Discussion	23
2.8	Conclusion	25
	References	26
<b>3</b>	<b>Control Authority</b>	<b>29</b>
3.1	Introduction	31
3.2	Defining control authority	32
3.2.1	General	32
3.2.2	Reference frames and Coordinate systems	33
3.2.3	Longitudinal Control	36
3.3	Lateral and Directional Control	39
3.3.1	Directional control	39
3.3.2	Acceptable directional envelope in case of damage	42
3.3.3	Lateral Control	43
3.4	One Engine Inoperative and $V_{mca}$	48
3.4.1	Forces, Moments and Reference frames	49
3.4.2	Steady Heading Side Slip	51
3.4.3	One Engine Out and $V_{mca}$	56
3.5	Conclusions	61
	References	63

<b>4</b>	<b>Design of the <math>V_c</math>-algorithm</b>	<b>65</b>
4.1	Introduction . . . . .	67
4.2	Derivation of State Space Model around an arbitrary reference point . . . . .	67
4.3	Basic Roll Performance using a Linear Model Approach. . . . .	76
4.3.1	Derivation basic $V_c$ equations . . . . .	78
4.4	Conclusions. . . . .	89
	References . . . . .	90
<b>5</b>	<b>Model selection</b>	<b>91</b>
5.1	Introduction . . . . .	93
5.2	Experiment Set-up . . . . .	94
5.3	Statistical Model Size Selection Methods . . . . .	101
5.4	Results . . . . .	110
5.5	Additional Simulations . . . . .	113
5.6	Investigating possible Causes of Over-fitting . . . . .	117
5.7	Conclusion . . . . .	124
	References . . . . .	127
<b>6</b>	<b>Configuration Choices and Prediction Accuracy</b>	<b>129</b>
6.1	Introduction . . . . .	131
6.2	Configuration Choices for VPS . . . . .	131
6.2.1	VPS Design. . . . .	131
6.2.2	Parameter Identification Options . . . . .	133
6.2.3	Initial model parameter values and normalization . . . . .	138
6.3	Lateral Control Velocity Prediction . . . . .	144
6.3.1	Results $V_c$ calculation . . . . .	150
6.3.2	Engine failures . . . . .	153
6.3.3	Adverse Yaw . . . . .	158
6.3.4	The Final Results . . . . .	161
6.3.5	Conclusion. . . . .	163
	References . . . . .	166
<b>7</b>	<b>Initial Evaluation of Pilot Behaviour in Scenarios with Limited Roll Control</b>	<b>167</b>
7.1	Introduction . . . . .	169
7.2	Objectives. . . . .	169
7.3	Experiments . . . . .	170
7.3.1	Simulator and Models . . . . .	170
7.3.2	Pilot Interface . . . . .	171
7.3.3	Subjects . . . . .	173
7.4	Experiment 1; Traffic Pattern . . . . .	175
7.4.1	Design and Procedures. . . . .	175
7.4.2	Results Experiment 1. . . . .	178
7.5	Experiment 2; Go-around. . . . .	184
7.5.1	Experiment Design and Procedures . . . . .	184
7.5.2	Results Experiment 2, Go-Around . . . . .	185

7.6	Experiment 3; Rudder Hardover. . . . .	191
7.6.1	Experiment Design and Procedure. . . . .	191
7.6.2	Results Rudder Hardover. . . . .	192
7.7	Display Comments and Rudder Control . . . . .	192
7.8	Discussion . . . . .	193
7.9	Recommendations . . . . .	194
	References . . . . .	195
<b>8</b>	<b>Final Tests</b>	<b>197</b>
8.1	Introduction . . . . .	199
8.1.1	Objectives . . . . .	199
8.1.2	Overview. . . . .	199
8.2	Experiments . . . . .	200
8.2.1	Simulator and Models . . . . .	200
8.2.2	Pilot Interface . . . . .	201
8.2.3	Subjects . . . . .	202
8.2.4	Data presentation and analysis . . . . .	203
8.3	Experiment 1; One engine out climb . . . . .	205
8.3.1	Design and Procedures. . . . .	205
8.3.2	Results Experiment 1. . . . .	207
8.4	Experiment 2; Go-around. . . . .	214
8.4.1	Experiment Design and Procedures . . . . .	214
8.4.2	Results Experiment 2, Go-Around . . . . .	215
8.5	Training the go-around . . . . .	220
8.5.1	Experiment Design and Procedures . . . . .	220
8.5.2	Results Experiment 5, Go-Around training. . . . .	221
8.6	Experiment 3; EFATO . . . . .	225
8.6.1	Experiment Design and Procedure. . . . .	225
8.6.2	Results EFATO . . . . .	226
8.7	Experiment 4; Damaged aircraft . . . . .	228
8.7.1	Experiment Design and Procedure. . . . .	228
8.7.2	Results Asymmetry. . . . .	231
8.8	Discussion . . . . .	235
8.9	Conclusions. . . . .	237
8.10	Recommendations . . . . .	238
	References . . . . .	239
<b>9</b>	<b>Discussion, conclusion and recommendations</b>	<b>241</b>
9.1	Discussion . . . . .	243
9.1.1	Introduction . . . . .	243
9.1.2	$V_c$ prediction- theory . . . . .	244
9.1.3	Off-Line Simulations with the PA-34 . . . . .	246
9.1.4	Result Pilot-in-the-Loop Simulations . . . . .	249
9.1.5	Final Tests . . . . .	250
9.2	Conclusions. . . . .	252
9.3	Recommendations . . . . .	253

---

References . . . . .	254
<b>A Propeller-induced flow effects on control</b>	<b>255</b>
References . . . . .	261
<b>B Propeller simulation</b>	<b>263</b>
<b>C Error Detection in Realistic Scenarios with Lateral Control Problems</b>	<b>269</b>
C.1 Problem outline. . . . .	269
C.2 SPRT for error detection. . . . .	270
C.2.1 Theory. . . . .	271
C.2.2 Error Detection in Control and Stability Parameters . . . . .	273
C.2.3 Settings, Improvements and Results . . . . .	275
C.2.4 Results. . . . .	277
C.2.5 Conclusion. . . . .	279
References . . . . .	280
<b>Summary</b>	<b>281</b>
<b>Samenvatting</b>	<b>287</b>
<b>Curriculum Vitæ</b>	<b>293</b>
<b>List of Publications</b>	<b>295</b>

# 1

## INTRODUCTION



### 1.1. SAFE FLIGHT

Commercial aviation is one of the safest means of transport. An indication of the relative safety in relation to other means of transport is given in the overview of the National Transportation Safety Board (NTSB). The NTSB overview [1] over the year 2013 shows that out of the 34,678 transport fatalities in the USA, only 443 were aviation related. And out of these 443 fatalities, the majority (387) was in general aviation. While the accident rate between general and commercial aviation differs, there is also a remarkable similarity. In commercial aviation the Loss of Control in Flight (LOC-I) has been the major cause of fatalities over the last years as can be seen in Fig.1.1, which shows the number of accidents and fatalities from 2004 through 2013. LOC-I accounts for almost 40% of all fatalities. Likewise, the overview of the NTSB over 2010 [1] shows that in general aviation LOC-I causes the highest number of fatalities, 72 out of the total of 191, accounting for 38%.

#### Fatalities by CICTT Aviation Occurrence Categories

Fatal Accidents | Worldwide Commercial Jet Fleet | 2004 through 2013

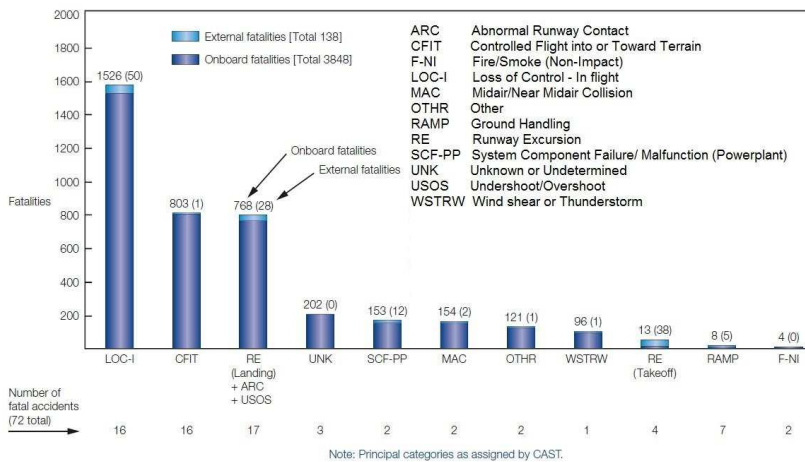


Figure 1.1: Overview Civil Aviation Accidents; Copyright 2013, Boeing; Courtesy of Boeing Corporation

It is therefore not surprising that a large research effort exists<sup>1</sup> to decrease the number of accidents caused by loss of control in-flight. However, most of this research is focused on commercial aviation. This might be caused by the fact that more funding is available for commercial aviation research than for general aviation research, but it would be beneficial if the LOC-I related fatalities could be reduced for airliners as well as for general aviation aircraft. One of the reasons why the LOC-I accident rate in general aviation might be higher is the fact that the controllability of propeller aircraft in case of

<sup>1</sup>Based on www.scopus.com search 2nd June 2015 with key words 'Loss of control' and 'aircraft' : 1023 articles and conference papers were published since 2005 related to loss of control.

an engine failure is much more limited than for turbojet driven aircraft, as will be further discussed in Chapter 3. Other reasons might be that excess power in case of an engine failure is usually less and training and certification requirements are less strict. These are the reasons for focusing on propeller driven general aviation aircraft in this thesis. Because the majority of these aircraft is manually flown, and not by an advanced automatic flight control system, we aim to improve the pilot's situation awareness to prevent loss of control instead of improving or modifying a control system.

### SAFE FLIGHT ENVELOPE

Part of the research to reduce LOC-I focuses on the determination of the safe flight envelope. Knowledge about this safe flight envelope might either be incorporated into a warning system, or be incorporated into the flight control system in which case we call it flight envelope protection. Present airliners have at least a warning system that includes several types of speed warnings, angle of attack (AoA) warnings, warnings at certain bank and pitch angles and warnings against high load factors.

1

#### 1.1.1. PRESENT RESEARCH

In civil aviation, LOC-I is the common term used in accident investigation and in research to improve flight safety. In [2] a description is given of the Quantitative Loss-of-Control Criteria (QLC) that the Boeing Company and the NASA Langley Research Center jointly developed. In this analysis, based on 24 LOC-I events, the authors defined five envelopes (adverse aerodynamic, structural, unusual attitude, dynamic pitch control and dynamic roll control) and found that LOC-I accidents involve the exceedance of three to four of these envelopes. The authors conclude that: *'the excursion of three envelopes is a clear indication of LOC-I; thus the third envelope excursion should be considered the point at which control was lost.'*

This also implies that many types of LOC-I are possible<sup>2</sup>. The drawback of this approach is that the LOC-I accidents mix inadequate pilot assessment and inappropriate control of the aircraft state—which is the prime cause of unusual attitudes and exceeding the dynamic control limits—with the exceedance of technical limitations of the airframe like AoA and structural limits. The first type of limits are very pilot- and situation-dependent. For example, pitch and roll angle limits in airliners are typically set to  $-20^\circ < \theta < 20^\circ$  and  $-45^\circ < \phi < 45^\circ$ , and these limits were used by [2]. But for other operations like ground attack, dog fight, intercepts and aerobatic display a  $120^\circ$  bank and  $30^\circ$  pitch down attitude is not exceptional. On the other hand, even for a fighter pilot  $10^\circ$  nose down and  $30^\circ$  bank will be excessive at night in approach configuration close to the ground. The second type of limits involve AoA limits, side slip limits and structural limits that are pilot- and operation-independent.

Current research [3], [4] and [5] into new safe flight envelopes focuses on two areas: the first area is the development of a new type of safe flight envelope based on safe

<sup>2</sup>Mathematical 30 types of LOC-I; 10 different initial conditions consisting of two envelopes where boundaries are already exceeded combined with the exceedance of three possible other envelopes.

manoeuvrability and the second area is the incorporation of failure states of damaged aircraft into this new envelope. The effect of damage on the safe flight envelope can be determined by either identifying the type of failure and applying the limits corresponding to the specific failure, or by identifying the change in stability and control derivatives.

The safe manoeuvrability envelope as defined by [4] is a subset of the allowable aircraft state space for which an admissible control input exists, that gives a trajectory that remains within the allowable state space for all  $t > 0$ . If we compare this definition with the initial division of [2] we notice an extension: now each allowable aircraft state has to be inside the performance envelope as well because of the requirement that the aircraft remains within the allowable state space for all  $t > 0$ . This is, however, inconsistent with pilot perception of controllability; an example may clarify this. When an aircraft is climbing more steeply than can be sustained with maximum power, it can not stay in this envelope for all  $t > 0$ , however when the pilot can still manoeuvre the aircraft, he will consider the aircraft controllable. A further refinement was made in [5] where the previous envelope was extended with all points that could be reached from the initial state and from which the aircraft could return to the initial state within a certain time period. In [6] the authors used a 5 seconds time limit.

With this last extension the safe flight envelope is extended. However, manoeuvres like a parabolic flight, that are considered manoeuvrable by pilots, will still be outside this extended envelope because it takes more than 5 seconds to return from the apex point, below the 1-g stall speed, to the initial state. One might argue that this is an extreme case and that this safe flight envelope is suitable for most flight conditions, but on the other hand this definition deviates from what pilots would consider manoeuvrable. Two other aspects are noteworthy regarding the way manoeuvrability is used in these studies to define the safe envelope. Firstly, as a sufficient condition for the aircraft state they require that roll rate ( $p$ ) and pitch rate ( $q$ ) can be made zero, and secondly, manoeuvrability is defined as the turn rate ( $\dot{\psi}$ ). But to be manoeuvrable, and to be able to correct any disturbance, the pilot needs at least a minimum roll and pitch rate and not just a capability to change heading. In this respect these new limits seem to be too lenient.

The main achievement of the above-mentioned research is that it maps all achievable aircraft states that can be combined with external limits, such as obstructions and danger areas, to calculate an optimal routing as for example was done in [7]. One disadvantage is that the combination of performance and achievable trim condition gives an envelope that might be overly restrictive in some areas but too permissive in others, and the fundamental question arises whether this manoeuvrability envelope is a good representation of the controllability of an aircraft. The second possible disadvantage is that these envelopes are based on a calculation with optimal inputs, and do not sufficiently consider the pilot's strategy in generating inputs. In actual flight conditions the pilot might use less than the optimal inputs, an example may clarify this.

If an aircraft has a rudder hard-over, lateral-directional control is affected. But by

using differential thrust much of the lateral-directional control can be regained. We can define the safe envelope for this aircraft based on the use of optimum asymmetric thrust, however, if the pilot is not using this strategy the prediction is too optimistic. This leads to a basic question: do we present envelope limits to the pilot based on present control inputs, based on optimal control inputs or both? Present studies did not address (yet) the problem of asymmetric thrust, which is particularly interesting, first because it is a common emergency and second because thrust levels will not only affect the performance but also the lateral-directional flight control.

In all this recent research much effort is devoted to calculating the trimmed states and optimal path, most studies assume that for a damaged aircraft the stability and control parameters, together named model parameters, are known or determined by parameter identification (PID). We know from [8] that in-flight PID is feasible given sufficiently exciting inputs and [9] showed that in-flight PID could be used to make a dynamic inversion controller for a damaged Boeing 747.

In the studies investigated [3], [4], [5], [7] and [6], safe flight envelopes were presented for damaged aircraft, however, the complete process from failure detection to achieving an accurate safe flight envelope, including the required time, required inputs and achieved accuracy were not presented. Furthermore, there are different options for PID and the PID method used should be able to cope with turbulence. All these issues are important for the practical applicability of any safe flight envelope warning system. A particularly important issue is what happens if model parameters become non-linear beyond the present operating range. For example, if the vertical tail is damaged, it must be possible to find the changes in 'weather cock stability' or  $Cn_{\beta}$ , with moderate side slip excursions. But a change in the stall angle of the damaged vertical tail might only be detected by the time the side slip has approached the  $\beta$  stall angle of the vertical tail. This might put a severe limit on the possibility to predict changes of the extremes of the envelope if the parameter identification is based on measurements conducted somewhere else in the flight envelope.

### 1.1.2. FOCUS OF THIS THESIS

This thesis proposes a different approach, based on the aerodynamic control envelope. Based on literature and analysis we will try to define this aerodynamic control envelope. This envelope does not include additional performance limitations or restrictions in attitude. We do not consider those limits unimportant, studies like [10] about US military aviation accidents related to spatial disorientation, which is a prime cause for unusual attitudes, underline its importance. But we learn also from this study that spatial disorientation is very dependent on type of operation, atmospheric condition, time of the day, pilot fatigue and many other factors. Therefore, these limits may be considered a possible –mission dependent– add-on to the basic aerodynamic limits that we aim to develop here. Second, we propose to take into account the actual pilot control inputs and make the aerodynamic control envelope dynamic. Third, we intend to incorporate the effect of aircraft damage into the aerodynamic control envelope using parameter identification and want to establish the effects of pilot inputs, turbulence and different PID methods

on the accuracy and timeliness of the estimated control envelope.

In the further analysis of the aerodynamic control envelope in Chapter 3, it will be shown that a longitudinal control envelope is already feasible. It will also be shown that the lateral aerodynamic control limits are normally reached prior to the directional limits. Therefore, in this thesis we focus on the lateral control envelope.

#### ACCURATE PRESENTATION OF AERODYNAMIC CONTROL LIMITS

The control limits must be presented to the pilot in an easily interpretable way. For longitudinal control these limits can be displayed as a maximum angle of attack (AoA), that still guarantees adequate pitch performance. It is also possible to use aircraft velocity instead of AoA, as long as this velocity is corrected for the current mass and load factor. These types of displays are implemented already in many aircraft. If the allowable AoA is also corrected for damage, as was already shown to be feasible in [11], a new damage-tolerant aerodynamic longitudinal control envelope can be presented to the pilot.

Presently, the only lateral-directional control limit used by pilots is the Minimum Control Speed Air ( $V_{mca}$ ). This speed is defined as the minimum speed where the aircraft can maintain its heading based on the assumptions that the most critical engine has failed, the other engines are set at maximum power or thrust, the rudder is at its maximum deflection (or the pilot is using a defined<sup>3</sup> maximum rudder force) and the bank angle is less than 5°. However, when the pilot is using less than maximum thrust on the operating engines, flight at speeds below  $V_{mca}$  is possible. At present no lateral-directional control indicator exists that incorporates present control inputs and damage. In this thesis we will show that this can be done by presenting the minimum lateral control speed, that we label  $V_c$ , and that takes into account the aircraft state and control inputs. We will also investigate if it is possible to accurately predict the  $V_c$  in case of changed aircraft aerodynamics, mass and mass distribution, due to damage.

## 1.2. RESEARCH QUESTIONS

The basic research questions this thesis will address are:

- Can we determine a dynamic lateral control envelope for damaged and undamaged aircraft? Note that we will use the term ‘dynamic envelope’ for an envelope that takes into account the present aircraft state and control inputs.
- Can we display the lateral control envelope in an easily interpretable way to the pilot?
- Will the Situation Awareness (SA) of pilots be enhanced by presenting a dynamic lateral limit?

A dynamic lateral control envelope can not be determined by a simple instrument

<sup>3</sup>The limit differs for military and civilian aircraft. The military limit is 180 lbs and the civilian limit is 150 lbs.

like the AoA indicator<sup>4</sup> in the longitudinal case. To determine this envelope we have to know the actual aircraft model parameters, for which we need in-flight aircraft parameter identification. Therefore, additional research questions are:

- What is the best model to estimate the lateral aerodynamic control envelope?
- Which PID method yields the best results?
- Are special pilot inputs required to estimate the lateral control envelope more accurately?

### 1.3. APPROACH TO SOLVE THE RESEARCH QUESTIONS

The basic approach to solve the research questions was firstly to find a practical measure for sufficient lateral-directional control, and compare this measure with the  $V_{mca}$  limit that is presently used. Secondly, an algorithm was developed, based on the standard aerodynamic equations, to determine the new  $V_c$  that will adapt to control inputs and changes in the aircraft state. Thirdly, optimum model size, optimum error detection and the accuracy of the estimated lateral control envelope were determined in off-line simulations with a non-linear Piper Seneca (PA-34) model. Finally, the usability of presenting  $V_c$  in the cockpit was evaluated with pilot in the loop experiments, conducted in the SIMONA Research Simulator (SRS) of TU Delft.

A non-linear flight simulation model of PA-34 was modified and implemented to demonstrate lateral-directional flight control problems. With this model, in off-line simulations, the truth data were gathered and the actual lateral flight control was calculated. To determine the flight control envelope, a model was used that was linear in parameters. The model parameters were found using conventional PID methods. The size and structure of this linear model were chosen to minimize the error in the predicted aircraft roll angle at maximum control deflections, and the prediction accuracy of the linear model was found by comparing the predicted roll angle against the measured roll angle of the non-linear model.

To determine whether pilot situation awareness could be enhanced by the information, tests were performed in the SRS of TU Delft. The lateral control information was integrated into the Pilot Flight Display (PFD). The simulator used the same non-linear model as was used for the off-line simulations, while the lateral-directional control envelope was determined with the linear model. Pilots were given scenarios where lateral control was impaired and tests were performed with and without the additional envelope information.

### 1.4. SCOPE AND ASSUMPTIONS

The method developed for determining the lateral-directional control envelope is valid for all fixed wing aircraft. However, lateral control problems are more pronounced in

<sup>4</sup>For a damaged aircraft an AoA indicator is still useful, but the stall angle of attack might have shifted. For the calculation of this shift parameter identification is also required.

propeller aircraft because of the high thrust levels at low airspeed. Furthermore, propeller aircraft have additional lateral effects caused by the propeller slipstream over the wing and around the tail. Therefore, this thesis concentrates on twin propeller aircraft. We assume that the aircraft has a traditional control with a direct mechanical linkage between stick (or yoke) and rudder control inputs and deflections of the aerodynamic control surfaces.

To make parameter estimation possible, we assume that information about AoA ( $\alpha$ ), side slip angle ( $\beta$ ), body accelerations, body rates and the True Airspeed (TAS) is available. Furthermore, we assume that yoke and rudder deflections are known, and to determine engine thrust we use engine torque, Brake Horsepower, or fuel flow. The absolute thrust level is not required, but it must be possible to transform the chosen metric to an input that can be used in the linear-in-parameter model<sup>5</sup>. Although most small twin props are presently not equipped with these instruments, it is technically feasible to equip these aircraft appropriately. We validate our method with a non-linear model in a simulation environment only. Evaluating the method in a real flying environment is an important next step but out of scope for this thesis.

## 1.5. STRUCTURE OF THESIS

The thesis is structured in three parts. The first part zooms in, starting from the general concept of envelope protection on how control authority can be defined and how lateral control relates to the  $V_{mca}$ ; this is the topic of Chapters 2 to 4. The second part is the optimization and evaluation of the  $V_c$  prediction in off-line simulations; this topic is addressed in Chapters 5 and 6. In the third part, Chapters 7 and 8, the results of the pilot-in-the-loop simulations are discussed.

### CHAPTER 2

In this chapter we discuss the concept of safe flight envelope. We partition the flight envelope into sub-envelopes to be able to make a clear distinction between the aerodynamic control envelope, that we want to determine, and other envelopes that are required and used to enable safe flight.

### CHAPTER 3

In Chapter 3 we zoom in on the control envelope, for which many different definitions are used in literature. For example, some definitions will not allow us to define control when the aircraft is flown below the 1-g stall speed or when it can not be trimmed in that state. We therefore propose a new way to define control, that is not related to heading or pitch, but related to  $\alpha$ ,  $\beta$  and roll. Zooming in on the lateral-directional control we will prove that aircraft will reach the roll control limit before the directional control is lost. Because the lateral limit is exceeded before the directional limit we can concentrate on finding the lateral control limit.

---

<sup>5</sup>For example, if BHP is known then  $\frac{BHP}{VTAS}$  gives a reasonable good linear relation with thrust, except at very low airspeed [12].

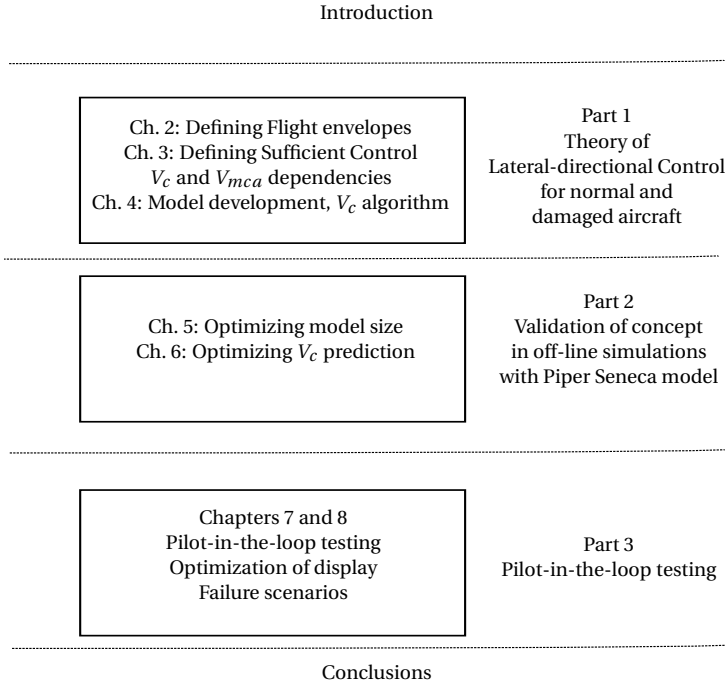


Figure 1.2: The structure of the thesis

A lot of research has been done regarding  $V_{mca}$  and much can be learned about the engine effects that are also applicable for the calculation of the minimum lateral control velocity. Therefore we will discuss  $V_{mca}$  in detail and point out the differences with using a minimum lateral control velocity.

#### CHAPTER 4

To predict the lateral-control envelope, first a suitable model is needed. We start from the assumptions that, for a damaged aircraft, the inertia tensor and mass might be unknown and the aircraft Centre of Gravity (c.g.) may not necessarily be in the plane of symmetry. After having developed this aircraft model, the parameters of this model are used to develop the  $V_c$  algorithm.

#### CHAPTER 5

Because the number of variables in the developed aircraft model is high, we investigate whether the model size can be reduced. We investigate if traditional methods used to determine the optimum size of a model, like Akaike Information Criteria and Bayesian Information Criteria, work for prediction purposes as well. We will show that these traditional methods are not adequate to predict optimum model size, and an alternative method is developed, based on the prediction accuracy, to determine the optimum model.

### CHAPTER 6

In this chapter we combine the results of the two previous chapters and develop the ‘ $V_c$  Prediction System’ or VPS. Besides the choice of model size used, as discussed in Chapter 5, several other configuration choices are possible: initial model parameter values, Parameter Identification (PID) methods used and normalization. The most promising configuration is found by evaluating all VPS options for  $V_c$  prediction accuracy and convergence speed using simulated failure scenarios. The generated failure scenarios, using a non-linear PA-34 model, include runs in smooth atmospheric conditions as well as under conditions with turbulence and include control failures, engine failures, lateral asymmetries and rudder hardovers. Furthermore, the level of additional control inputs is varied over the runs.

### CHAPTER 7

This chapter discusses the results of the first pilot-in-the-loop flight simulator evaluation. It describes the interface, how the  $V_c$  information and side slip are presented on the PFD. Second, it analyses the results of the evaluation in the simulator. Using ten professional pilots, with different backgrounds and experience levels, several scenarios were run in which the lateral control was limited.

### CHAPTER 8

This chapter is devoted to the results of the second series of pilot-in-the-loop tests with an improved display. First the display differences are discussed, followed by the test results. A total of nineteen pilots, with different backgrounds and experience levels, participated.

### CHAPTER 9

In this chapter we draw the final conclusions and make suggestions for further research.

## REFERENCES

- [1] Anon., *Data and Statistics*, Tech. Rep. (NTSB, 2014)  
<http://www.nts.gov/data/index.html>.
- [2] J. E. Wilborn and J. V. Foster, *Defining Commercial Transport Loss-of-Control: A Quantitative Approach*, in *Collection of Technical Papers - AIAA Atmospheric Flight Mechanics Conference, Providence, RI; USA; August 16-19*, Vol. 1 (2004) pp. 205–215.
- [3] L. Tang, M. Roemer, J. Ge, A. Crassidis, J. V. R. Prasad, and C. Belcastro, *Methodologies for Adaptive Flight Envelope Estimation and Protection*, in *Proc. of the AIAA Guidance, Navigation, and Control Conference and Exhibit, Chicago, USA, Aug. 10-13* (2009).
- [4] R. C. Allen and H. G. Kwatny, *Maneuverability and Envelope Protection in the Prevention of Aircraft Loss of Control*, in *ASCC 2011 - 8th Asian Control Conference - Final Program and Proceedings, Kaohsiung; Taiwan; May 15-18* (2011) pp. 381–386.
- [5] T. J. L. Lombaerts, S. Schuet, K. Wheeler, D. Acosta, and J. Kaneshige, *Robust Maneuvering Envelope Estimation Based on Reachability Analysis in an Optimal Control Formulation*, in *Proc. of the Conference on Control and Fault-Tolerant Systems, SysTol. Nice, France, Oct. 9-11* (2013) pp. 318–323.
- [6] T. L. J. Lombaerts, S. Schuet, D. Acosta, J. Kaneshige, K. Shish, and L. Martin, *Piloted Simulator Evaluation of Maneuvering Envelope Information for Flight Crew Awareness*, in *Proc. of the AIAA Guidance, Navigation, and Control Conference 2015, MGNC 2015 - Held at the AIAA SciTech Forum 2015, Kissimmee, USA* (2015).
- [7] D. Asadi, M. Sabzehparvar, E. M. Atkins, and H. A. Talebi, *Damaged Airplane Trajectory Planning Based on Flight Envelope and Motion Primitives*, *Journal of Aircraft* **51**, 1740 (2014).
- [8] M. Laban, *On-line Aircraft Model Identification*, Ph.D. thesis, Technical University Delft (1994).
- [9] T. J. J. Lombaerts, *Fault Tolerant Flight Control*, Ph.D. thesis, Technical University Delft (2010).
- [10] R. J. Poisson and M. E. Miller, *Spatial Disorientation Mishap Trends in the U.S. Air Force 1993 -2013*, *Aviation Space and Environmental Medicine* **85**, 919 (2014).
- [11] K. N. Hossain, V. Sharma, M. B. Bragg, and P. G. Voulgaris, *Envelope Protection and Control Adaptation in Icing Encounters*, in *41st Aerospace Sciences Meeting and Exhibit, Reno, NV; USA; Jan. 6-9* (2003).
- [12] J. A. Mulder, J. C. van der Vaart, and M. Mulder, *Atmospheric Flight Dynamics* (Technical University Delft, Faculty LR, 2007).

# 2

## DISCRIMINATING FLIGHT ENVELOPES



## 2.1. INTRODUCTION

The term flight envelope is used in many aerodynamic text books, but its meaning depends on the subject that is covered. When the topic is performance, the term often refers to the 1-g sustainable flight envelope. If the topic is structures, then the envelope can be described by the maximum positive and negative g-lines, augmented by the maximum speed line and the stall limit. And especially important for our research, the control envelope is also not uniformly defined.

A clear distinction between the different envelopes would be helpful. After discussion of an earlier flight envelope division, we will introduce in this chapter a different flight envelope division, based on a (test)pilot perspective. We will particularly discuss the impact of reaching or exceeding the envelope limits on pilot actions. Other points of interest are whether the envelope is primarily needed for pre-flight planning or, more importantly, for in-flight use and whether new envelope limits are obtainable and useful for the pilot in case the aircraft is damaged. We will first discuss the flight envelope division. Thereafter we will discuss each envelope separately.

## 2.2. FLIGHT ENVELOPE DIVISION

Attempts to classify the different envelopes have been made before; an interesting classification was derived by [1]. Here the authors recognize five different categories, in order to classify Loss of Control In-flight (LoC-I) accidents:

- The adverse aerodynamics envelope,
- The unusual attitude envelope,
- The structural integrity envelope,
- The dynamic pitch control envelope, and
- The dynamic roll control envelope.

However, for reasons explained hereafter, the following division into four envelopes will prove to be more useful:

- Performance envelope,
- Structural envelope,
- Stability and Control envelope, and
- Situation Awareness envelope.

There is much commonality between the division used in this thesis and the one from [1], however, there are also some important differences. The dynamic roll and pitch envelopes can be considered to be a dynamic extension to the unusual attitude envelope, and these three together are then similar to what we will define as the Situation Awareness envelope in this thesis. Common is the Structural envelope, but the adverse

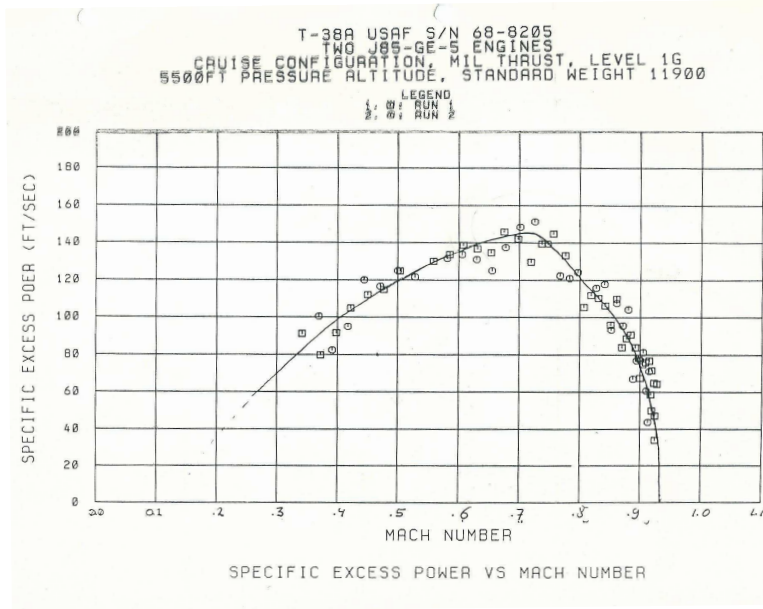


Figure 2.1: Specific Excess Power T-38 at 5000'; Test performed by author at USAF TPS 1984

aerodynamic envelope differs from the control envelope. The authors of [1] restrict the adverse aerodynamics envelope to  $\alpha$  and  $\beta$  limits, and we will also include the roll limit in the Stability and Control envelope. Finally, the authors of [1] do not cover the performance limits, but other authors (e.g., [2], [3]) do include performance limits in the safe flight envelope therefore, we will include them here as well.

### 2.3. PERFORMANCE ENVELOPE

We define the Performance envelope as a set of limits that are derived from the energy control of the aircraft. The most important performance parameters are derived from the Specific Excess Power ( $P_s$ ) charts, which are determined during flight tests [4]. From these charts, the optimum aircraft climb profile, ceiling, maximum speed and best sustained turn performance can be found.

Quite often, the curve for  $P_s = 0$  on the Specific Excess Power charts is considered the (attainable) flight envelope (Fig. 2.1). Performance limits can be exceeded without damaging the aircraft. In case a pilot pulls more g than can be sustained at the present speed, the aircraft will only decelerate. In a similar way the maximum ceiling can be exceeded in, e.g., zoom flights, and the maximum sustainable speed can temporarily be exceeded in a dive. Consequently, these performance limits do not necessarily demand any form of warning or protection.

These are not the only performance limits. Some performance characteristics will

indeed lead to hard limits. Specifically, take off and landing performance will give maximum refusal speeds ( $V_1$ ) and limits on usable runways. A similar situation exists for payload and range envelopes. Normally, all these limits are considered in the pre-flight planning process, but in-flight real-time calculation can also prove to be advantageous. To some extent, this is already being done. For example, the F-16 mission computer will calculate constantly whether the home base can be reached with the present available fuel using optimum climb and descent. This calculation is, however, based on the standard drag for the configuration and not (yet) on the actual drag.

For a damaged aircraft, all these performance limits can change and it may be advantageous to inform the pilot about these changes. The most simple realization is a system that updates the drag coefficients to calculate the new best range speed, optimum cruising altitude and remaining range. In [5] this information was presented for selected emergencies and in relation to ground collision avoidance problems. While this calculation is important, it is less time critical than an exceedance of other limits, such as structural limits.

In conclusion, performance limits can often be exceeded without imminent danger, with the exception of take-off and landing limits. However, in most cases there is ample planning time to re-calculate these limits, and the same holds for range and payload limits. In flight presentation of these limits is not a hard necessity, however, providing some guidance about optimum performance can be useful. Especially when the aircraft is damaged and the drag and lift characteristics have changed, some guidance about changed range, and changed optimum climb speed can be advantageous.

## 2.4. STRUCTURAL ENVELOPE

We define the aircraft Structural envelope as the set of all limits that guarantee the structural integrity of the aircraft. The most important structural limits are g-limits and speed limits. G-limits include positive and negative symmetric and rolling g-limits, while speed limits include gear and flap speed limits and a maximum velocity ('V never exceed' or  $V_{ne}$ ). Quite often, especially for high performance aircraft, the maximum speed is both defined as a maximum KCAS and as a Mach number<sup>1</sup>. Some aircraft have additional limits on roll rates. Furthermore, military aircraft have extra limits for store releases, weapon employment, slung loads and the opening of cargo or para doors.

The number of structural limits for one aircraft type can be impressive; for the F-16 for instance, it is a complete manual [7]. Because these limits are all known, it is relatively easy to implement a warning system to alert the pilot when approaching or even exceeding a limit. If there is any form of an automated flight control system, these limits could be implemented into the flight control system to provide some form of envelope protection. Airbus was the first company to implement this type of protection in passenger aircraft [8], but definitely not the first aircraft builder to implement it. General Dynamics

<sup>1</sup>In a flight test, the structural limit at maximum speed [6] is always tested at the point where the maximum KCAS and maximum Mach number coincide.

had no choice but to implement it in the F-16, because in this unstable aircraft the flight control computer has the ultimate authority and can not control the g-level without setting limits. And even earlier than that are the bob-weight, used in many aircraft, and q-dependent stick forces of the F-4<sup>2</sup> that provided limited protection.

There is a small margin between the Structural envelope presented to the pilot and the point where the aircraft structure will fail, however the pilot's aim is that an exceedance of the structural limit is always prevented. Because structural limits normally change during flight, and the constant monitoring of these limits might be tedious, it is advantageous for the pilot to have an automated warning or protection system that warns or protects against exceeding structural limits.

### FULL STRUCTURAL PROTECTION

It should be noted that the objective of a 'care free aircraft that can never be overstressed', can not always be attained. For example, flying into turbulence with a too high airspeed has been the cause of many accidents. Probably the most well known aircraft structural failure in the Netherlands is the F28 accident at Moerdijk, on 6 October 1981, where the aircraft most likely flew into a tornado, which induced excessive g-loading that caused the right wing to break from the fuselage.[9]. Furthermore, especially in military aircraft there may be multiple limits for the same flight conditions and the designer has to make a choice for which limit he will set the protection or alarm. For example, when the normal g-limit for a configuration is 6-g and the stores jettison limit is 3-g, the manufacturer will always set the warning at 6-g, because stores jettison hardly ever happens and setting the g-limit at the lowest level would reduce the usability of the aircraft significantly. In conclusion, even with structural protection, the protection is never 'full'.

### DAMAGED AIRCRAFT STRUCTURAL LIMITS

While the normal Structural envelope is an important and known envelope that is useful to implement in a warning system or in a protection system, the Structural envelope of a damaged aircraft is very likely to be unknown. Whereas real-time health monitoring, to optimize maintenance, is currently implemented in many aircraft, structural failure detection is still in its infancy [10]. Research [11] showed that some structural limits like wing divergence speed could be calculated when the damaged area was known. But even if the remaining structural strength could be calculated, its operational value might be limited. If a pilot is aware of structural failure, good airmanship dictates to fly carefully, with the load factor as close to one as possible at moderate velocity, even when the calculated envelope would guarantee a large Structural envelope. Information about the aircraft damage is useful to the pilot, especially if guidance could be given about the proper use of systems and controls, like information about allowable flap settings and the use of spoilers etc.

### CONCLUSION

Structural limits can not be exceeded without imminent danger. Therefore, a Structural envelope protection or warning system is important, but does not always guarantee a

<sup>2</sup>The F-4 had a system of bellows around the stick that were connected with the dynamic pressure source.

care-free aircraft, especially because of conflicting limits. An adapted Structural envelope for damaged aircraft is still not yet feasible, but providing pilots with information that the aircraft is damaged could be helpful. However, by simply flying slow and minimizing g-load, pilots have already a practical approach to minimize the load on the aircraft, one that can be used without any knowledge about the remaining aircraft strength.

## 2.5. STABILITY AND CONTROL ENVELOPE

In this thesis we define the Stability envelope as the envelope within which the aircraft's dynamic behaviour, as given by its eigenmodes, is still acceptable for pilot control. In practice, this envelope has lead to specific limits on the eigenmodes, as presented for instance in the MIL. Spec 8785C. An initial definition for the Control envelope is: the envelope in which adequate control of attitude and speed is possible. This automatically leads to the question what adequate control is. In Chapter 3 this subject will be extensively discussed and a new definition will be given. There is a general consensus, however, what the situation 'out of control' is: when the aircraft is stalled, when the aircraft is in a spin or when the aircraft roll or side slip rates can not be stopped. Exceeding the Control envelope is potentially dangerous<sup>3</sup> and over the years many warning systems and control systems have been designed to prevent departure from controlled flight.

The control limits, best known by pilots, are the stall angle of attack, the minimum control airspeed with one engine out  $V_{mca}$  and the aircraft centre of gravity limits for longitudinal stability. These limits are always presented in the aircraft flight manual because the pilot has to prevent the exceedance of these limits<sup>4</sup>. But there are many more stability and control limits presented in the Mil. Specs. [12] and civil aviation publications [13],[14], for example minimum roll performance, damping and frequency requirements for Dutch roll and short period. However, because aircraft are designed to conform to these limits and the pilot can not exceed these limits either, they are under normal conditions not a concern to the pilot, seldom mentioned in aircraft flight manuals, and most likely also seldom known by any pilot.

### 2.5.1. STABILITY

The most complete set of aircraft stability limits is found in the Mil. Specs. [12]. These limits are based on (test)pilot experience and must guarantee acceptable aircraft behaviour for all pilots. Consequently, not all these limits are hard limits in the sense that an exceedance of these limits will automatically cause a departure from controlled flight. However, exceedance of these limits will always increase pilot workload. Because the stability limits of an undamaged aircraft should not be a concern to the pilot, the first

---

<sup>3</sup>Many aircraft have benign stall and spin characteristics and are authorized to perform these manoeuvres. Given enough altitude, these manoeuvres can be executed safely, therefore potentially dangerous is perhaps the more correct term.

<sup>4</sup>This does not mean that the pilot knows every specific limit because a limit like  $V_{mca}$  might be embedded in other limits like  $V_1$  and  $V_2$ .

question to solve is how much loss of stability a pilot can handle in case of damage.

The Mil. Spec. defines limits for different levels, where Level-1 limits are the most stringent requirement and Level 3 and higher are for aircraft with failures. Furthermore, there are different categories for different phases of flight. Because the prime concern for the pilot of a damaged aircraft is to safely land the aircraft, it is appropriate to use the category C, (i.e., the limits for approach and landing), combined with the level for aircraft with failures. The five dynamic modes of an aircraft can be divided into two fast modes (the Dutch roll and the short period), two slow modes (the phugoid and the spiral mode) and a first order roll mode that usually has a small time constant. For the fast modes the Mil. Spec. defines an allowable frequency range and damping ratio, the slow modes are not required to be stable but the minimum time to double amplitude is used as a limit, and for the roll mode a maximum is set for the time constant.

### STABILITY RELATED ACCIDENTS

There are several known accidents where the loss of stability of the aircraft was a factor [9]. In most cases the loss of stability was caused by a (sudden) cargo shift. Tests have shown that a pilot can control a marginally unstable aircraft as long as he is aware of the instability, and the time to double amplitude is not too short.<sup>5</sup> However, to regain control of an aircraft that has suddenly become unstable is close to impossible. If the pilot is aware of the instability, a high-frequency anticipative control could be used to control the aircraft but because of the high-frequency control inputs required, an automatic control system will do much better.

2

### THE B1B ACCIDENT

Yet, even an automatic control system has limitations as to the amount of instability it can handle. A classic example is the B1B accident in 1984 [15]. The aircraft had performed tests with the wings swept aft and was moving the wings forward for a new test point, without having moved the fuel forward first. The resulting instability was not detected by the crew until the aircraft suddenly pitched up. If the aircraft would have been flown manually, the instability might have been detected earlier, but now the flight control system masked the instability until the aircraft ran out of elevator control. This case represents the rather rare occasion in which a warning system that monitors aircraft parameters could have warned the pilot against the impending instability.

### LOSS OF VERTICAL TAIL

An even harder instability to tackle is the loss of the vertical tail. The directional stability must now be regained (if at all possible) by alternate control means like, e.g., differential thrust or the combined use of spoilers and ailerons. Clearly, these types of alternate control strategies are difficult for humans, especially when the engines have a large lag time. Research shows that this type of control can be performed automatically when the flight control systems are optimized to handle this type of instability [16].

<sup>5</sup>In the USAF Test Pilot School syllabus, students were given the opportunity to fly the CALSPAN T-33 with the control laws of the unstable F-16. Most pilots could control this unstable aircraft for a limited period.

### EFFECT OF VELOCITY CHANGE

When the damage to the aircraft causes a more benign change in stability characteristics, the most important issue for the pilot is to know how stability will be affected when he decelerates to approach speed and changes to the approach configuration. The expected effect of a speed change on the dynamic modes are known and if there is no change in the stability derivatives themselves the effect is generally as follows [17]:

- Short period: The damping ratio is independent of velocity, while the frequency changes linear with velocity. Consequently, a speed decrease will lower the short period frequency, making the control easier for the pilot.
- Phugoid: The damping ratio is independent of velocity but the frequency is inversely proportional to velocity. If the phugoid is damped there will be no effect of speed change on the stability of this mode. If the phugoid is unstable the time to double amplitude will decrease making the aircraft more difficult to control.
- Dutch roll: The damping ratio is independent of velocity while the frequency will change linear with velocity. Consequently, a speed decrease will lower the frequency, making the control easier for the pilot.
- Spiral mode: The time constant is inversely proportional to airspeed. If the mode is unstable it will become easier to control the mode at lower velocities because of the increased value of the time constant.
- Roll mode: The roll mode lag time constant is inversely proportional to airspeed, a lower speed will affect the time response but not the stability.

Here, the only mode for which a speed decrease might negatively affect stability is the phugoid when it is unstable. Theoretically [18] the phugoid should always be stable because the damping ratio depends on the  $\frac{C_D}{C_L}$ . However, variation in thrust due to speed and altitude changes can make the phugoid unstable, as is shown in [19]. Fortunately, these altitude and speed deviations decrease with the increase in frequency caused by the lower velocity which in turn decreases the instability. Furthermore, the stability of the phugoid can be increased by increasing  $C_D$ , e.g., lowering the gear. Finally, the phugoid is by far the slowest aircraft eigenmode, even a considerable decrease in time to double amplitude will not make it hard to control.

It is much harder to predict the effect of a configuration change on the aircraft stability, and PID methods only predict the values of the model parameters for the present configuration. It is therefore considered good airmanship to reconfigure a damaged aircraft at altitude where there is ample room to undo the configuration change if the aircraft stability or control deteriorates beyond acceptable levels. This is also in line with, e.g., the US Navy Air Operations Publication (NATOPS)<sup>6</sup> for performing a controllability check.

<sup>6</sup><http://navyflightmanuals.tpub.com/P-1242/P-12420132.htm>.

## CONCLUSION

From this short analysis, the conclusion is that the Stability envelope is essentially a design and test flight issue. A warning system for an impending instability is only useful in the rare situation that the instability is caused by a slowly developing process, where the pilot has ample time to take appropriate action. In case of a sudden cargo shift or loss of vertical tail, the change is very abrupt and a Stability envelope warning system cannot timely warn the pilot, but only confirm the rapid instability. Furthermore, the stability limits are no hard limits, and if a pilot is able to control a damaged aircraft at the velocity where the damage occurred, a subsequent speed decrease to approach speed will normally improve the handling for the pilot.

### 2.5.2. CONTROL ENVELOPE

Considerable differences exist in the provisions taken for the prevention of losing longitudinal control as compared to the provisions taken to prevent lateral-directional loss of control, therefore we will discuss longitudinal and lateral-directional control separately.

#### LONGITUDINAL CONTROL

Maintaining longitudinal control in practice means avoiding that the aircraft stalls; many stall warning and stall prevention systems have indeed been invented. The prevention systems include stick shakers, stick pushers, aural stall warnings and not least angle of attack (AoA) indicators; a selection of those is common in airliners and military aircraft. In General Aviation there have also been several attempts to build 'The Safe Aircraft' [20], which included attempts to make unstallable aircraft. All AoA-based alarms and indicators are dynamic, that is, they adapt to changes in g-level and preferably also to different flap settings. In the case of a damaged aircraft, those angle of attack limits are likely to have changed. Several studies [21] showed the feasibility of systems to identify and quantify the change in angle of attack range. Change in longitudinal control limits can be caused by a damaged elevator, a particularly interesting case is when the elevator position can not be changed at all. Depending on aircraft type, some longitudinal control may then still be possible. This case will be further discussed in Chapter 3.

#### LATERAL-DIRECTIONAL CONTROL

Pilots are less familiar with lateral-directional control limitations because they will not encounter these during normal operation. The most well know case<sup>7</sup> where a pilot might experience limited lateral-directional control is an engine failure. And for this situation they are given the  $V_{mca}$  limit. This  $V_{mca}$  limit is in fact the only limit the pilot has for this case, it is static, based on one power setting and one rudder position. Similar as longitudinal control is related to changing pitch angle, we will relate the lateral-directional envelope with the possibility to change roll and yaw angles, irrespective of stability and performance issues.

For a *damaged* aircraft this situation might change and the minimum speed at which the aircraft could be controlled could in fact become higher than the given  $V_{mca}$ . Presently,

<sup>7</sup>Other possibilities are wake turbulence, fuel asymmetry and roll reversal at high Mach numbers.

pilots are not warned about a change in the minimum velocity for lateral-directional control. Determining this minimum lateral-directional control speed for a damaged aircraft, and presenting it as a dynamic limit to the pilot is the main problem investigated in this thesis.

### CONCLUSION

The longitudinal Control envelope is well known and normally well protected. The lateral-directional Control envelope is presently only defined by the static  $V_{mca}$ . In Chapter 3 we will derive a new lateral-directional control that is also usable for damaged aircraft.

## 2.6. SITUATION AWARENESS LIMITS

Most larger aircraft have limits on roll angles and pitch angles, and because these limits are also presented in aircraft handbooks, they could be interpreted as hard envelope limits. However, aerodynamically, bank angles and pitch angles can be combined with any g-load<sup>8</sup>. Consequently, exceeding a 'situation awareness' limit, such as the maximum bank angle, does not imply an approximation or exceedance of structural or control limits.

The same is true for the aircraft control and stability. When the aircraft velocity, and  $\alpha$  and  $\beta$  are within limits<sup>9</sup>, and the controls are not at their maximum deflection, control is possible, independently of bank and flightpath angle. However, it is clear that there is no need for transport aircraft to perform manoeuvres of this sort. Hence, we propose to qualify them as 'Situation Awareness' limits, to warn the pilot that the aircraft has an unusual attitude.

It is also important to notice that the main issue in the Situational Awareness envelope is the fact that pilots must recognize this situation. The recovery from an unusual attitude requires neither abnormal flight inputs nor extremely difficult pilot performance<sup>10</sup>. Furthermore, these limits are dependent on human factors like pilot training, type of mission, possibilities for spatial disorientation etc., which raises a question whether these limits should be adjustable. We will not pursue this item further in this thesis.

## 2.7. DISCUSSION

### HIERARCHY GENERAL

Based on the above description of the different flight envelopes, we can establish a hierarchy in flight envelopes, based on their importance and urgency for pilot action. We can

<sup>8</sup>As long as the g-load is available and allowed. An example is a wing-over manoeuvre where the 90° roll angle point is combined with a small g-load around 1.

<sup>9</sup> $\beta$  limits are only displayed in special aircraft, but for fighter aircraft it is common to have roll limitations in order not to exceed  $\beta$  limits.

<sup>10</sup>In military flight training, unusual attitude recovery is typically given before even the first solo flight.

use the same hierarchy that is used in flight manuals for different types of failures. ‘Warning’ for situations that require immediate pilot actions and are potentially life threatening, ‘Caution’ for situations that might involve risk and ‘Advisory’ for information that might be useful to the pilot. We will do this separately for a healthy aircraft and an aircraft that is damaged.

### NORMAL HIERARCHY

In normal operation, the Structural and Control envelopes will be the two envelopes at the ‘Warning’ level. Immediate pilot action is required to prevent or recover from a potentially dangerous situation. The Situational Awareness envelope can be set at the ‘Caution’ level. Pilot attention is required, but the aircraft is still functioning normally and there is no direct threat to the integrity of the airframe. The Performance envelope is typically on the ‘Advisory’ level, it is convenient for a pilot to have information about best climb, optimum flight level etc., but it is more of an enhancement. In normal functioning aircraft, stability is guaranteed and the Stability envelope is not really an issue for pilots.

### HIERARCHY FOR DAMAGED AIRCRAFT

In discussing the hierarchy for damaged aircraft we will also discuss whether the envelope is known in the first place, and also whether pilots can still take appropriate actions if the new envelope is not known. We will discuss each envelope separately.

- The Structural envelope remains at the ‘Warning Level’, however the new boundaries might not be known. The pilot can still take appropriate action by always minimizing the loads on the aircraft and reducing speed.
- The Control envelope remains also at the ‘Warning level’, however boundaries are not known. New control boundaries can be estimated by careful manoeuvres or with the help of in-flight parameter identification.
- The Stability envelope moves to the ‘Warning level’, because loss of stability is potentially life-threatening. However, the most frequent occurrence is a sudden shift of the c.g.. It is impossible to warn or protect the pilot from this sudden occurrence and the pilot can either cope with the situation or not. If he is able to deal with the initial change in stability, he can later reduce workload by reducing speed.
- The Performance envelope could move to the cautionary level, especially when different speeds and altitudes are required to be able to reach the nearest suitable airport. However, these data are not available, but could be made available with in-flight aircraft parameter identification.
- The Situational Awareness envelope, being based on aircraft type and normal use is still valid, however, other restrictions from the above-mentioned envelopes might have become much more restrictive than the Situational Awareness envelope.

### MIXING HIERARCHIES

Because of the above developed hierarchy it seems prudent not to mix different hierarchy levels in one protection or warning system. The result of doing so will be that the

system becomes overly protective, limiting the pilot in his available actions. However, this mixing does occur in aircraft design as well as in research on flight envelope protection (e.g., [2], [22], [23]). Using the hierarchy principle might also be useful in the (prolonged) discussion between advocates of warning systems and advocates of envelope protection.

#### PROTECTION OR WARNING

There is no common opinion between operators and aircraft manufacturers as to which is better, envelope protection or warning. Typically, advocates of warning systems will give examples of accidents that could have been prevented by exceeding aircraft limits [24], while advocates of protection argue that those accidents could also have been prevented by other means [8]. Both arguments are true, and are in line with the author's flight experience, when he had to exceed the negative g-limit in an NF-5 to prevent a head-on collision with an F-4 in uncontrolled airspace. Typically, those accidents can better be prevented by a good working Traffic Collision Avoidance System (TCAS) or a good airborne radar. Whatever the choice may be, we believe it is prudent not to combine different hierarchy levels into a single protection or warning system.

## 2.8. CONCLUSION

We have developed a flight envelope classification from a (test)pilot perspective. Our classification leads to a hierarchy of flight envelopes and to the conclusion that a flight envelope warning system or protection system should avoid mixing different categories. In the remainder of this thesis we will focus on developing a lateral-directional envelope warning system, that aims to exclude performance and situational awareness limits.

Investigation into damaged aircraft flight envelopes revealed that structural damage and reduced stability both favour low airspeed. However, the Control envelope might, on the contrary, require an increase in minimum velocities. So, even in the case that the new Structural envelope and Stability envelope are unknown, the Control envelope limit will give a practical limit to be used by pilots when having to cope with a damaged aircraft. This underlines the importance of the determination of the Control envelope for damaged aircraft.

## REFERENCES

- [1] J. E. Wilborn and J. V. Foster, *Defining Commercial Transport Loss-of-Control: A Quantitative Approach*, in *Collection of Technical Papers - AIAA Atmospheric Flight Mechanics Conference, Providence, RI; USA; August 16-19*, Vol. 1 (2004) pp. 205–215.
- [2] T. L. J. Lombaerts, S. Schuet, D. Acosta, J. Kaneshige, K. Shish, and L. Martin, *Piloted Simulator Evaluation of Maneuvering Envelope Information for Flight Crew Awareness*, in *Proc. of the AIAA Guidance, Navigation, and Control Conference 2015, MGNC 2015 - Held at the AIAA SciTech Forum 2015, Kissimmee, USA* (2015).
- [3] L. Tang, M. Roemer, J. Ge, A. Crassidis, J. V. R. Prasad, and C. Belcastro, *Methodologies for Adaptive Flight Envelope Estimation and Protection*, in *Proc. of the AIAA Guidance, Navigation, and Control Conference and Exhibit, Chicago, USA, Aug. 10-13* (2009).
- [4] Anon., *Performance Theory and Flight Test Techniques* (USAF TPS, Edwards AFB, CA, 1979).
- [5] C. Borst, M. Mulder, and M. M. Van Paassen, *Design and Simulator Evaluation of an Ecological Synthetic Vision Display*, *Journal of Guidance, Control, and Dynamics* **33**, 1577 (2010).
- [6] Anon., *System Testing Theory and Flight Test Techniques* (USAF TPS, Edwards AFB, CA, 1984).
- [7] Anon., *T.O.F-16M-4* (LMTAS, 2001).
- [8] D. Briere and P. Traverse, *Airbus A320/A330/340 Electrical Flight Controls a Family of Fault-Tolerant Systems*, in *Digest of Papers - International Symposium on Fault-Tolerant Computing, Toulouse, France; June 22-24* (1993) pp. 616–623.
- [9] Anon., *Aviation-Safety-Database*, Aviation Safety Network website (2014), <http://www.aviation-safety.net/database/dblist.php?Event=WXT>.
- [10] H. Moncayo, M. G. Perhinschi, and J. Davis, *Aircraft Failure Detection and Identification over an Extended Flight Envelope Using an Artificial Immune System*, *Aeronautical Journal* **115**, 43 (2011).
- [11] P. K. Menon, P. Sengupta, S. Vaddi, B. J. Yang, and J. Kwan, *Impaired Aircraft Performance Envelope Estimation*, *Journal of Aircraft* **50**, 410 (2013).
- [12] Anon, *Military Standard, Flying Qualities of Piloted Airplanes; MIL-STD-1797*, Tech. Rep. (DoD, 1987).
- [13] Anon., *Part 23—Airworthiness Standards: Normal, Utility, Acrobatic, and Commuter Category Airplanes*, Tech. Rep. (FAA, 2015).
- [14] Anon., *Part 25—Airworthiness Standards: Transport Category Airplanes*, Tech. Rep. (FAA, 2015).

- [15] Anon., *The Crash of the B-1A*, Check-six website (1984), [http://www.check-six.com/Crash\\_Sites/B-1\\_crash\\_site.htm](http://www.check-six.com/Crash_Sites/B-1_crash_site.htm).
- [16] V. Stepanyan, K. Krishnakumar, and N. Nguyen, *Adaptive Control of a Transport Aircraft Using Differential Thrust*, in *Proc. of the AIAA Guidance, Navigation, and Control Conference and Exhibit, Chigago, USA, Aug. 10-13* (2009).
- [17] Anon., *Volume II, Flying Qualities Phase, Chapter 8, Dynamics* (USAF TPS, Edwards AFB, CA, 1988).
- [18] J. A. Mulder, J. C. van der Vaart, and M. Mulder, *Atmospheric Flight Dynamics* (Technical University Delft, Faculty LR, 2007).
- [19] H. J. Koolstra and M. M. van Paassen, *Investigation in the Boundaries of Thrust Based Longitudinal Control*, TBD (To be published).
- [20] R. Harris, *Editorial, for In Flight USA, Flight USA* (2007).
- [21] J. D. Keller, R. M. McKillip Jr., and S. Kim, *Aircraft Flight Envelope Determination Using Upset Detection and Physical Modeling Methods*, in *Proc. of the AIAA Guidance, Navigation, and Control Conference and Exhibit, Chigago, USA, Aug. 10-13* (2009).
- [22] W. Falkena, Q. P. Borst, C. Chu, and J. A. Mulder, *Investigation of Practical Flight Envelope Protection Systems for Small Aircraft*, *Journal of Guidance, Control, and Dynamics*, Vol. 34, No. 4, 976 (2011).
- [23] J. M. Wilson, M. E. Peters, and G. W. Pettit, *Flight Tests of a General Aviation Envelope Protection and Stability Augmentation System*, *Proceedings AIAA Guidance, Navigation, and Control Conference, National Harbor, MD; USA; (2014)*, 10.2514/6.2014-0602.
- [24] R. Rogers, *Pilot Authority and Aircraft Protection*, Tech. Rep. (Air Line Pilots Association, 1999).



# 3

## CONTROL AUTHORITY



### 3.1. INTRODUCTION

A well-known adage in flight safety is ‘aviate, navigate, communicate’<sup>1</sup> – clearly stating the required pilot priorities to execute a safe flight. That flying comes first is logical, but the prerequisite for flying is that the available aircraft control, or control authority, is sufficient. Normally this will be the case and the pilot can forget this prerequisite, but when for some reason aircraft control is jeopardized, regaining or maintaining sufficient control authority becomes the first priority.

In Chapter 2 it was noted that the control envelope was not well defined, however pilots will be quite aware of what situations are out-of-control, typically the stall and departures in yaw and roll. If we realize that controlling an aircraft is changing its state, it may follow that the change in the states<sup>2</sup> can be used to express control quantitatively. Minimum requirements for aircraft control can be found in publications such as Federal Aviation Regulations (FAR), Common Standards (CS) and Military Specifications (Mil.Specs.), and can be used to define *sufficient* control authority. However, the set of these requirements is not easily interpretable for the pilot; so, typically airspeed limits are used. These speed limits can be dependent on several flight parameters such as load factor, aircraft c.g. and power setting. This means that the control envelope can be considered as the complete set of all aircraft parameters that will guarantee *sufficient* control authority. However, it is our intent to present this envelope to the pilot in the form of a simple speed limit that takes all of these parameters into account. This means that rather than presenting the complete control envelope we will provide the pilot with the limit to which *sufficient* control authority is available. There are flight envelope regions where some aircraft are controllable, but not in the normal (or anticipated) sense. Typical examples are spin and (deep) stall. We have to set limits so these flight regimes are avoided and this is typically what FAR, CS and Mil. Spec. limits do.

So the first task at hand is to define the change in aircraft state in a way that makes it easy to set quantitative limits. Even when the number of state variables is high, as in [1], all aircraft state variables are controlled by only four different types of pilot inputs: two with the stick, one with rudder and one the power levers. As shown below, it is feasible to select a smaller number of state variables that are ‘directly’ (to be discussed below) related to these controls that we can use as measure to quantify *sufficient* control authority. We will also address the differences between manoeuvrability, controllability and agility.

When we have found a suitable measure, we should determine applicable limits for the normal situation, which includes engine failures, as well as for the case where the aircraft is damaged and aerodynamic and mass properties have changed. In the derivation of the lateral and directional control we use the longitudinal limits as guidelines, because good practical limits already exist for longitudinal control, as will be shown below. After having derived and explored the lateral and directional limits, we will show

---

<sup>1</sup>More common in military flying is ‘fly, navigate, talk’.

<sup>2</sup>For example, the NASA paper [1] defines 12 states, three rotations, three velocities and their derivatives.

that lateral control limits are reached before directional control limits. Therefore, we can restrict ourselves to deriving the lateral control limit. Next we explore the options for presenting this to the pilot.

The next step is to compare our derived limits to the present limit that is used for lateral and directional control:  $V_{mca}$ . The limits for  $V_{mca}$  are described in FAR part 25.149. Because these limits refer to a ‘sudden’ loss of power these may be regarded as dynamic requirements. On the other hand, except for one requirement: a heading change of less than 20 degrees, all other requirements can be tested in a static test. This is also the way the author performed  $V_{mca}$  tests in the USAF [13] and this also a test required in civil testing before the dynamic test is performed. The interesting fact about the dynamic test, where a sudden failure is given in a steep climb just above the ‘static’ determined  $V_{mca}$  speed, is that this test primarily verifies the longitudinal manoeuvrability and not in the least part the test pilot’s ability to perform this manoeuvre. Because our focus in this thesis is on the lateral and directional controllability we will focus on the static equilibrium requirements described in FAR and CS.

For a static equilibrium situation, we need the aircraft equations of motion as expressed in many textbooks like [2, p. 134],[3, p.186]. We will review the parts of these equations at the moment they are first needed and point out where we will deviate from the standard approach, which is for example necessary in order to account for an unknown c.g. location. We will also discuss turning with ‘One Engine Inoperative’ (OEI), because turning is an essential manoeuvre when proceeding to land. Furthermore, in the pilot community, the question whether you should not turn ‘into the dead engine’ is still a hotly debated<sup>3</sup> issue see e.g., [4].

Historically, much research has been carried out into the effect of the propeller slipstream on  $V_{mca}$ . We review some of this research and use some of our own simulations in order to get a better understanding of the relationship between airspeed and required control inputs. These relationships are of paramount importance for the prediction of the speed at which lateral-directional control limits are reached.

## 3.2. DEFINING CONTROL AUTHORITY

### 3.2.1. GENERAL

In this chapter we will use the term controllability, however other terms often used are manoeuvrability and agility. Useful definitions to distinguish between the three are given by [5]:

- Manoeuvrability: the ability to change the magnitude and direction of the aircraft velocity vector;
- Controllability: the ability to change the aircraft pointing axis through rotation

<sup>3</sup>The search terms ‘turning into the dead engine’ and ‘aircraft’ gave more than two million hits in Google on September 23, 2016.

about the centre of gravity, independent to the flight path vector<sup>4</sup>; and

- Agility: The combination of the previous two.

These definitions are helpful, but we have to realize that an overlap still exists, because the change of flightpath and attitude are related. However, there is also another distinction: manoeuvrability is mostly used in the context of maximum performance. For example, maximum turn performance is an important aspect of manoeuvrability, while controllability is normally used in situations where the aircraft movements are limited. Therefore the manoeuvrability is a term more applicable to the performance envelope, as discussed in Chapter 2. Furthermore, in this thesis we focus on loss of control and not on loss of manoeuvrability, hence we prefer the term controllability.

A further study into definitions for control and controllability leads to the NASA definition for control [6]:

‘To direct the movements of an aircraft with particular reference to changes in attitude and speed.’

The USAF Test Pilot School definition[7] for controllability is:

‘Controllability is the capability of the aircraft to perform any manoeuvring required in total mission accomplishment at the pilot’s command. The aircraft characteristics should be such that these manoeuvres can be performed precisely and simply with minimum pilot effort’.

The NASA definition is quite in line with [5] and seems a good starting point, that is applicable such as when considering an aircraft that is flying straight and level. The USAF Test Pilot School definition emphasizes the importance of the controllability in relation to the task. In our approach we want to determine the minimum required controllability in normal as well as in abnormal conditions. We will focus on the minimum controllability for the safe recovery of the aircraft in abnormal conditions. However, we realize that there are other tasks, like spinning with a training aircraft, that might need different sets of controllability requirements.

#### THE APPROACH CHOSEN

Using the NASA definition as a starting point, we have a choice of coordinate systems to express attitude change and have to determine the most convenient one. We then have to define the minimum requirements for controllability and finally investigate to what extent these requirements are also usable in case of abnormal flight conditions. We will first choose the coordinate systems and then discuss the controllability measure.

### 3.2.2. REFERENCE FRAMES AND COORDINATE SYSTEMS

There are many aerodynamic textbooks that describe reference frames and coordinate systems. Later in this chapter we will use the book by Zipfel, [3] for the derivation of the

<sup>4</sup>This last addition ‘independent of the flightpath vector’ in [5] is, according to the author, not really necessary.

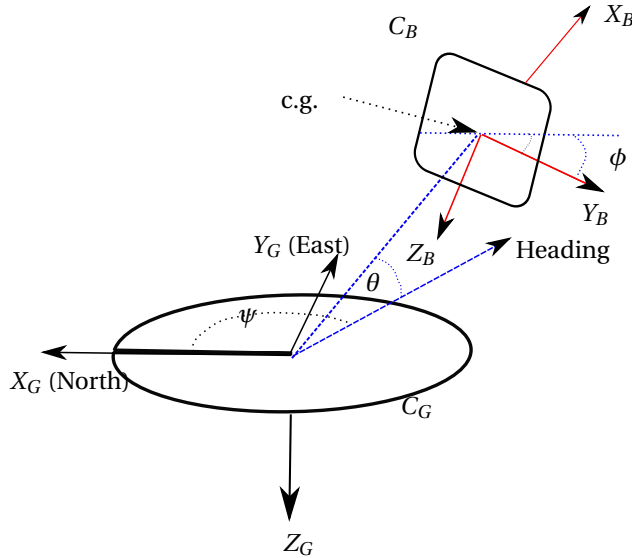


Figure 3.1: Geographic Coordinate system  $C_G$  and Body Coordinate system  $C_B$ . Both coordinate systems are displaced for clarity, which can be done because only the relative orientation is important and not their relative position.

## 3

dynamic equations for asymmetric bodies. In order to be consistent in this thesis, we also use his definitions for reference frames and coordinate systems. This implies the following definitions:

- Reference Frame: a Cartesian triad with location and orientation but without an enumeration;
- Coordinate system: the enumeration of a reference system, chosen to fit the problem and which does not have to emanate from the origin of a reference frame.

For our discussion on controllability we can restrict ourselves to coordinate system, because we are interested in the orientation only and need the enumeration. We limit ourselves to three coordinate systems [3, p. 82]. The first (Fig. 3.1) is the Body-Fixed Coordinate system,  $C_B$ . The  $X_B$  axis is in the plane of symmetry of the aircraft and pointing forward, its exact direction is normally chosen by the aircraft manufacturer. The  $Y_B$  axis is pointing to the right wingtip and is perpendicular to the plane of symmetry. The  $Z_B$  axis is also in the plane of symmetry, perpendicular to the  $X_B$  and  $Y_B$  axes. The aircraft velocity vector in  $C_B$  is:  $[u \ v \ w]^T$  and the rotations around  $[X_B \ Y_B \ Z_B]^T$  are  $[p \ q \ r]^T$ .

The second coordinate system used is the Geographic Coordinate system or  $C_G$ . In this coordinate system the  $Z_G$  axis is aligned with the local gravity vector as seen from the aircraft c.g., the  $X_G$  axis is pointing North and the  $Y_G$  axis is pointing East also as seen from the c.g. Because the orientation is changing with the c.g. position of the aircraft it is

often said that ‘its origin’ moves with it. However, as pointed out by Zipfel [3, p. 73], this is just a coordinate system, a purely mathematical entity that does not need an origin, its orientation only depends on aircraft latitude and longitude and is independent of the aircraft altitude.

The transformation angles between  $C_G$  and  $C_B$  are defined as:  $\psi$ ,  $\theta$  and  $\phi$ , where  $\psi$  is the angle between the projection of  $X_B$  in the horizontal plane and  $X_G$ ,  $\theta$  is the angle between the  $X_B$  and the horizontal plane, and the roll angle  $\phi$  is defined as the angle between the  $Y_B$  axis and the intersection of the local horizontal plane with the plane perpendicular to  $X_B$ .

The third coordinate system we use is the Aerodynamic Reference coordinate system  $C_A$  that resembles  $C_B$ , but now the  $X_a$  axis is aligned with the aircraft velocity vector. This coordinate system is the most convenient for expressing thrust, drag (aligned with  $X_a$ ) and lift (aligned with  $Z_a$ ). The transformation angles between  $C_B$  and  $C_A$  are  $\alpha$  and  $\beta$ . In the no-wind situation, we can use the relation that the airspeed  $V = \sqrt{u^2 + v^2 + w^2}$ , the transformation angles are:  $\alpha = \arctan \frac{w}{u}$  and  $\beta = \arcsin \frac{v}{V}$ .

For our discussion on attitude changes these coordinate systems are sufficient. However, for the discussion of the aircraft dynamics, later this chapter, we need an inertial frame as the laws of motion are expressed in this frame. Because we limit ourselves to aircraft motions of relatively short duration where the effect of earth rotation and curvature can be neglected, the Earth can be presumed to be an inertial reference frame [3, p 81]. This enables us to use the Local Level coordinate system<sup>5</sup>. This coordinate system uses the same orientation as the  $C_G$  coordinate system and its origin can be chosen at any convenient point on the earth surface. In controllability research quite often the starting point of the manoeuvre is used.

#### CHOSEN COORDINATE SYSTEM FOR CONTROLLABILITY

The question at hand is which reference coordinate system we want to use to define controllability. As we have seen in Chapters 1 and 2, some authors use the  $C_G$  coordinate system. They regard controllability as the capability to change climb angle ( $\theta - \alpha$ ) and track. From an airline pilot and an air-traffic controller perspective, this may seem a logical choice. However, an aerobatic pilot or a fighter pilot will most likely express controllability in the Body coordinate system as the capability to pitch, roll and yaw the aircraft. In this thesis we adopt this second approach because it enables us to describe yaw and roll control more directly. In the first approach the no-wind track change follows primarily from a sustained roll angle, but it does not take into account how rapidly this roll angle change was made.

Having made the choice to use the Body coordinate system as the principal reference to express controllability, the logical initial choice is then to use the attainable  $p$ ,  $q$  and  $r$  range, or their integral over time, as measure to express controllability. However, some-

<sup>5</sup>Also referred to as ‘Flat not rotating earth assumption’.

times it is easier to use a different, but related, measure instead. For longitudinal control other measures, like angle of attack or airspeed limits during approach and landing are used to guarantee sufficient controllability. We will discuss longitudinal control first, and after having done so, we will investigate whether changes in the initial chosen measure are required for directional and lateral control.

### 3.2.3. LONGITUDINAL CONTROL

#### CONTROLLABILITY MEASURE: THEORY

If we use  $q$  as measure for longitudinal control, the longitudinal control authority is the  $q$  that can be achieved by the maximum lift coefficient ( $C_{Lmax}$ ). This is indirectly dependent on available elevator input to change the  $\alpha$  to the required value for  $C_{Lmax}$ . An accurate way would be to derive the change in  $q$  from the linearised dynamic equations for symmetric motions as given by [2, p. 476]. Based on the aerodynamic coefficients, this second order differential equation can be solved for  $q$ . However, assuming a manoeuvre with a steady  $q$ <sup>6</sup>,  $q$  will be related to the centripetal acceleration caused by the change in lift due to the change in AoA. This centripetal acceleration is defined by the load factor  $n$  times  $g$  minus the component of the gravitational acceleration parallel to the lift vector. For any, not necessarily level turn,  $q$  follows from:

$$q = \frac{(n - \cos\phi \cos\gamma)g}{V}, \quad (3.1)$$

where the load factor  $n$  is defined as:

$$n = \frac{\frac{1}{2}\rho V^2 SC_L + T \sin\alpha}{mg} \quad (3.2)$$

Here  $T \sin\alpha$  is the contribution of the engines parallel to the lift force. With Eq. 3.1 we have a tool to calculate the minimum aircraft velocity that is needed to achieve a required minimum  $q$ . This  $q$  is the instantaneous  $q$  that depends only on the maximum  $C_L$  value, the flightpath angle and the airspeed.

#### CONTROLLABILITY MEASURE: PRACTICE

In practice an even easier method is used during approaches and landing that can be related to the load factor, namely a minimum speed related to the stall speed. However, the stall speed and stall AoA that are determined in flight test can, dependent on the aircraft type, be based on different features. It can be based on wing drop, buffet level, which typically occurs past maximum  $C_L$ , or on the start of a sink rate in a level deceleration which coincides with the maximum  $C_L$  point, or at a fixed AoA. Traditionally the  $V_s$  mentioned in the flight manuals was often based on the highest possible AoA. The consequence for this stall speed ( $V_s$ ) so derived, is that at this AoA and airspeed, the aircraft can not maintain level flight, and consequently, this stall speed is not an accurate basis for a safety margin. Therefore, FAR25.125 defines the reference stall speed or

<sup>6</sup>The time until the AoA reaches its new final value for the first time is short, hence the name 'short period', which is reason to concentrate on the steady state part.

$V_{SR} = \frac{V_{C_Lmax}}{\sqrt{n_{zw}}}$ , this reference stall speed may never be less than the speed where the maximum  $C_L$  value is reached. Typically the approach speed is  $1.3 V_S$ , but when  $V_{SR}$  is used, the approach speed may be as low as  $1.23 V_{SR}$ . For the remainder of this thesis we will use as stall speed the  $V_{SR}$  speed.

Using Eq. 3.2, and setting  $T = 0$ ,  $V = 1.3 V_{SR}$  gives an attainable load factor of 1.69 that will be even higher if thrust is applied. It can be debated whether a lower value than  $1.3 V_{SR}$ <sup>7</sup> can be used as the minimum speed to maintain longitudinal control, however, the focus here is that starting from a required pitch change over time to express minimum longitudinal control, we arrive at an airspeed in relation to the stall speed, or an AoA limit, which are both easy to interpret by pilots.

Because the aircraft stall speed depends on the aircraft mass, we must be able to update the estimate of the aircraft mass during flight to present the correct  $V_{SR}$  to the pilot. However, the  $1.3 V_{SR}$  value is always at a fixed AoA value, and therefore an AoA limit is even easier to use to guarantee sufficient control authority.

While both the  $\frac{V}{V_{SR}}$  and AoA are usable measures for longitudinal controllability, the consequences for the pilot are different. Using the AoA, the pilot has an indication that is valid under any g-load, but being within the allowable AoA range does not guarantee the ability of 1g level flight. Therefore the pilot has to check the airspeed as well. On the other hand, having an airspeed above  $V_{SR}$  does guarantee the capability of level flight, but does not guarantee that the aircraft will not stall at the present g-level. A reasonable compromise would be that the  $V_s$  presented is the higher of the 1g stall speed and the stall speed at the present load factor<sup>8</sup>. With this last small modification, both the AoA and  $V_{SR}$  indicator have become dynamic indicators that take into account the pilot longitudinal inputs that have generated a certain load factor. A prerequisite is of course that the  $V_{SR}$  is adjusted for the mass and c.g. of the aircraft and both  $V_{SR}$  and AoA are corrected for the available elevator control.

### CHANGES IN LONGITUDINAL CONTROL

Changes in longitudinal control can be caused by a shift in c.g. location, a loss of elevator effectiveness or by control surfaces of damaged aircraft generating additional pitch moments. These situations become serious when the required angle of attack for a safe landing can not be attained<sup>9</sup>. If the damage to the aircraft is such that at least some elevator control is available, the reduced AoA range must be determined. With online parameter identification this is feasible. Studies like [9] and [10] showed for example

<sup>7</sup>It can be argued that a lower number is acceptable. According to [8], US Navy pilots make their approach at  $1.05 V_s$ , which allows for only a maximum of 1.1g pitch authority. This is not quite in accordance with the approach speeds the author used flying US Navy planes at the USAF TPS, however, he only performed simulated carrier landings.

<sup>8</sup>For aircraft that are flying regularly at less than 1g the AoA indication is preferable.

<sup>9</sup>For example because the landing distance required exceeds the available runway length.

that with in-flight parameter identification, the detection of such a reduced range due to icing could be determined. If this reduction in AoA range, and the corresponding revised stall speed, is known, pilots can be provided with the appropriate AoA or speed limits to guarantee sufficient control.

### SPECIAL EMERGENCIES

A more serious situation arises when elevator control is completely lost. For an aircraft without longitudinal stability, this will lead to a departure from controlled flight. Classical longitudinal stable aircraft do in principle have some options for a safe recovery.

The first option to regain control is to use the horizontal stabilizer trim as an alternate source. A second option, available to some aircraft, is to use alternate devices like speed brakes or spoilers to generate a pitching moment. For example, the KC-135[11] can generate a positive and negative change in pitching moment using outboard or inboard spoilers. A third option is to use engine thrust. In the specific case of vertically displaced engines, the thrust difference can be used to generate a pitching moment, which in turn can affect the AoA. Even without vertically displaced engines, it has been shown in the past that engine thrust could be used to control the pitch. Examples are the United Airlines DC-10 accident<sup>10</sup> on 19 July 1989 and the DHL A300 accident on 22nd November 2003 in Baghdad. Both accidents showed the possibility and difficulty of controlling pitch with engine thrust.

3

A classical longitudinally stable aircraft will maintain its AoA, and thrust changes can be used to descend or climb, however, it is also necessary that the phugoid mode is suppressed to prevent airspeed and altitude deviations. An analysis [12] shows that engine thrust can be used to dampen the phugoid, depending on the vertical distance of the engines from the c.g. However, that analysis started from trimmed flight, where elevator change was inhibited. In this situation, thrust is an option for longitudinal control but in order to make a safe landing possible, a reconfiguration and a lower speed are normally required. Depending on the situation and the type of aircraft, the changed configuration may not have an equilibrium at landing speed.

### CONCLUSIONS ON THE LONGITUDINAL CONTROL AUTHORITY

Our choice of measure to express longitudinal control authority is the measure already used in practice: the  $1.3V_{SR}$  and the AoA for this speed. This measure is related to the attainable steady state pitch rate ( $q$ ) as shown in Eq. 3.1. With parameter identification this measure can also be adjusted to show the change in  $V_s$  and attainable AoA range as has been shown for example in [9], [10]. For some special emergencies, especially those where elevator control is lost, the control authority is not clear and might not even be present. In the next section we will investigate if a similar measure can also be applied to lateral and directional control.

<sup>10</sup>The DC-10 has a vertically displaced centre engine, but this engine was inoperative due to the fan disk failure that caused the accident.

### 3.3. LATERAL AND DIRECTIONAL CONTROL

#### INTRODUCTION

Lateral and directional control limitations are less familiar to pilots than longitudinal control limitations. A likely reason is that a normally functioning aircraft will have adequate roll and yaw control from high airspeed until the stall speed. This means that longitudinal control problems will normally manifest themselves before lateral or directional control becomes an issue. The exception is the asymmetric engine thrust after an engine failure, for this situation the  $V_{mca}$  is defined and is often published in the aircraft flight manual. Instead of looking for a single lateral-directional control limit we will discuss directional and lateral control separately.

#### 3.3.1. DIRECTIONAL CONTROL

For expressing directional control in the body axis, the first candidate as measure for control authority is yaw rate ( $r$ ). As with longitudinal control, we could opt for a steady yaw rate or the dynamic yaw response after a step input. Let us first look at the FAR<sup>11</sup> requirements for directional control. The required directional control is defined in FAR par. 25.147 and reads as follows:

- (a) Directional control; general. It must be possible, with the wings level, to yaw into the operative engine and to safely make a reasonably sudden change in heading of up to  $15^\circ$  in the direction of the critical inoperative engine. This must be shown at  $1.3 V_{SR1}$  for heading changes up to  $15^\circ$  (except that the heading change at which the rudder pedal force is 150 pounds need not be exceeded), ...

Here  $V_{SR1}$  stands for reference stall speed in a specific configuration. This rule is followed by many additional requirements.

If we first focus on the initial part of the requirement, where a wings-level yaw is required into the operative engine, we notice that in the FAR a choice is made for a steady yaw rate. Furthermore, a wings-level (continuous) yaw implies also a flightpath curvature that requires a centripetal side force into the direction of the operative engine. This situation is depicted in Fig. 3.2. The side force must be generated by the sum of the side force due to side slip  $\beta$  and by the side force due to rudder deflection. Because the rudder is deflected in the direction of the operating engine, its side force is away from the operative engine and will generate a moment away from the operative engine. Consequently, to enable a turn into the operative engine there must be a (small) side slip angle ( $\beta$ ) from the side of the inoperative engine to generate a side force into the operative engine that exceeds the rudder side force.

Three things are noticeable in the initial part of this requirement: Firstly, the required yaw rate into the operative engine is not defined quantitatively, meaning that

<sup>11</sup>We can use the Common Standards CS of the EU as well. However there is high degree of commonality between the two. Therefore we can restrict ourselves to one of the two.

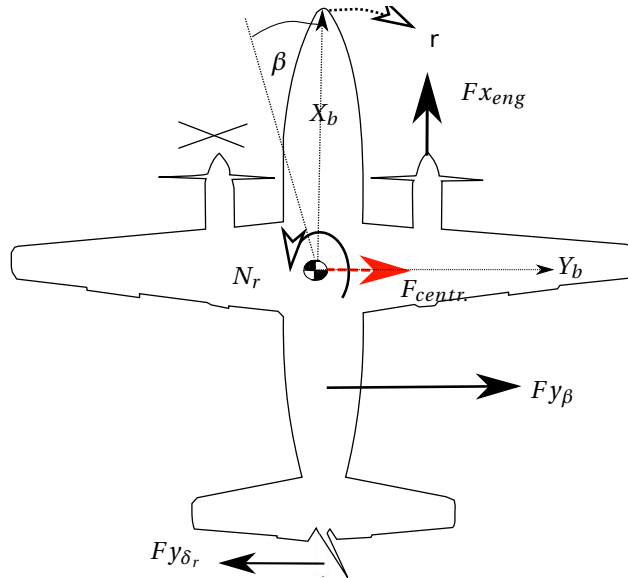


Figure 3.2: Forces in a flat turn into the operative right engine with  $\phi = 0$  and left engine inoperative.

## 3

in the limiting case a side force due to  $\beta$  slightly larger than the rudder side force would be sufficient. The second observation is that for a particular airspeed (in this case  $1.3 V_s$ ) and thrust setting<sup>12</sup>, the asymmetric moment due to inoperative engine is known, the required rudder to counter the asymmetric thrust moment is also known and hence the side force generated by the rudder can also be derived. Next, the side force due to  $\beta$  must be larger in magnitude and opposite in sign, consequently this is also a minimum requirement for  $\beta$ . Thirdly, the rule applies for  $1.3 V_s$  at *maximum gross weight for landing*, and, as will be discussed later in Section 3.4, this is not the condition with the largest engine moment in case of propeller aircraft. The engine moment will increase with decreasing airspeed, hence the maximum moment is reached at the lowest gross weight, with the lowest permitted approach speed combined with maximum power setting. Consequently, the required directional performance is not defined here for the most restrictive case.

The second part of the requirement is slightly confusing. It requires a sudden change into the inoperative engine that can be flown safely. The change into the inoperative engine is of course easy because of the asymmetric power. The fact that a sudden change is required gives the impression that the legislator wants to see a change in heading that affects primarily  $\beta$ , because  $\beta$  is changing more rapidly than flight path. However, based on the author's experience with engine-out tests [13], the requirement to execute a change primarily of  $\beta$  is hard to meet. A rapid rudder deflection induces a quick roll on-

<sup>12</sup>The FAR requires power to maintain level flight in the most heavy landing condition, but not more than maximum continuous power.

set (mainly due to the change in  $\beta$ ) making it hard to remain wings level. Consequently, part of the heading change will be caused by the turn due to roll angle and part by the  $\beta$ . When the rudder deflection is reduced more gently, maintaining wings level is easier, however, the heading change is now partly due to the changed side force that causes the flightpath change and partly due to the change in  $\beta$ .

The conclusion is that the requirement of FAR par. 25.147 is quantitatively not very strong, but is in essence equivalent to requiring a minimum  $\beta$  and not necessarily for the most limiting case. There is, however, one additional requirement: the  $V_{mca}$  limit, that will be discussed in Section 3.4. In that section we will show that the  $V_{mca}$  requirement can also be expressed as a requirement for side slip. We think that making an explicit choice for a  $\beta$  range as measure for directional control authority has several advantages. Listing a few:

1.  $\beta$  can be measured accurately in flight test and makes it a better measure than a heading change that is partly  $\beta$  and partly a lateral flight path change.
2. When using yaw rate as a measure for directional control, all measurements are limited to straight flight. In a turn the roll angle will cause a heading change which transforms to a pitch and yaw rate in the body axis. Consequently, this yaw rate requirement does not easily translate into a requirement that can be used in all flight conditions. However,  $\beta$  is hardly influenced by roll angle as will be proven later in Section 3.4 and can also be used as measure in a turn.
3. A step rudder input will excite a dynamic mode, the Dutch roll, but the final steady state result will be a certain value of  $\beta$ . For a given speed and c.g. there is a direct relation between this value of  $\beta$  and the fixed rudder deflection.
4. Increasing  $\beta$  from zero side slip angle increases the aircraft drag. A zero  $\beta$  under conditions of maximum asymmetric power guarantees that drag due to  $\beta$  can be prevented.

Our conclusion is that directional controllability can be treated similarly to longitudinal controllability. For longitudinal controllability a useful measure is based on AoA, for directional controllability it is based on  $\beta$ . Directional control can then be redefined as: The capability to maintain  $\beta$  in the required operational range and is *not* limited to wings level flight. The determination of the required directional envelope is discussed next.

#### REQUIRED DIRECTIONAL ENVELOPE

The required  $\beta$  value is zero in normal flight conditions, except for crosswind landings where a certain  $\beta$  angle is necessary to align the aircraft with the runway, and a roll angle is used to prevent drifting sideways. But the most important requirement is that zero  $\beta$  can be maintained under adverse conditions, specifically the most common; asymmetric power. FAR par. 25.147 states the requirement to slip into the operative engine, which is an even stricter requirement than zero  $\beta$ . Meeting this last requirement will ensure the availability of some directional control, even during a crosswind take-off with

one engine inoperative. For landings there are fewer problems, because they are normally performed with a low thrust setting, allowing even some control in crosswind<sup>13</sup>. So, if we define the required directional envelope as the envelope where zero  $\beta$  can be maintained with one engine inoperative and the other(s) at maximum take off power, this envelope is limited by a minimum airspeed. The fact that most aircraft don't have a  $\beta$  indicator is not a problem. When the pilot is flying above the speed limit he should simply use as much rudder as is needed to control the aircraft. This speed does not guarantee sufficient roll control, the requirements for roll control will be discussed later.

### 3.3.2. ACCEPTABLE DIRECTIONAL ENVELOPE IN CASE OF DAMAGE

In the case where the side slip angle is not caused by asymmetric power but by damage to the aircraft, rudder and asymmetric power can correct  $\beta$ . A typical problem that illustrates the directional control options in case of damage is the rudder hardover. In this situation, the pilot has the option to use asymmetric thrust to counter the yaw caused by the rudder hardover. Even if the aircraft can not maintain zero  $\beta$ , it may be still possible to safely land. For a damaged aircraft the requirement should just be that it will not depart in yaw, which will only happen if the disturbing yaw moment can not be compensated by the moment due to rudder and  $\beta$ . However, a combination of damage and asymmetric thrust can create a situation where level flight can not be maintained.

#### $\beta$ CANNOT BE KEPT IN THE OPERATIONAL RANGE

If  $\beta$  can not be maintained in the operational envelope, the aircraft will encounter a yaw departure or a spin. Fighter aircraft with stores at high altitude at high angle of attack occasionally experience yaw departures [14]. While these yaw departures are abrupt and may surprise the pilot, and can even involve high lateral g-levels<sup>14</sup>, the aircraft recovers quickly when AoA is reduced<sup>15</sup>. Fortunately these types of departure normally do not happen close to the ground. A more serious case is when the vertical tail area is damaged. Studies like [15] prove that even under these conditions automated differential engine control can be used to stabilize the yaw, however this type of control is hard to maintain by the pilot, especially when engine response time is long when compared to the frequency of the Dutch roll, as was the case in the JAL B747 accident in 1985 [16].

#### CONCLUSION ON DIRECTIONAL CONTROL

For certification purposes, the available directional control must be sufficient to maintain zero  $\beta$  in a situation with maximum asymmetric thrust. A non-zero  $\beta$  due to aircraft damage is only a problem when a fin stall cannot be prevented using maximum rudder and asymmetric thrust. In all simulated emergencies with the PA-34 that we investigated

<sup>13</sup>One can however argue that an aircraft faced with an engine failure can choose a runway with crosswind from the favoured side (The side of the operative engine).

<sup>14</sup>The A-7 yaw departure, which can be invoked by a high AoA turn with the automated Leading Edge Flap disabled, can cause a 3-g lateral acceleration.

<sup>15</sup>Typically, these situations can be a result of reduced  $C_{N\beta}$  due to stores forward of the c.g., a vertical tail which is partly blended combined with a disturbing yaw moment due to roll.

Table 3.1: Class III roll performance. Time to Achieve 30° Bank Angle Change (Seconds)

Level	Speed Range	Category A	Category B	Category C
1	L	1.8	2.3	2.5
	M	1.5	2.0	2.5
	H	2.0	2.3	2.5
2	L	2.4	3.9	4.0
	M	2.0	3.3	4.0
3	H	2.5	3.9	4.0
	All	3.0	5.0	6.0

in this thesis, directional control was never the limiting factor. However, the additional drag caused by the  $\beta$  deteriorates the performance level of the aircraft that is already reduced in case of an engine failure and the uncorrected  $\beta$  will also affect lateral control. This lateral control could become the real limiting factor and will be discussed next.

### 3.3.3. LATERAL CONTROL

The candidate measure for lateral controllability is roll rate ( $p$ ). We can express lateral controllability in different ways, a maximum roll rate, an initial roll rate, or a predefined roll angle change in a specific time. FAR25.147 requires ‘sufficient’ initial roll rate even in adverse control conditions like engine failure and a minimum bank angle of 20° to either side. Mil. Spec. F8785C however, defines the required lateral control in terms of a roll angle change in a specific time. Our choice is to use the latter method. The rationale is that a pilot’s intent is normally not to roll at a certain rate, but to achieve a certain roll angle within a specific time frame. Also, roll angle changes may be quite frequent, e.g., to stay on the localizer, while  $\beta$ , e.g., in a wing low approach, is normally set to a value and maintained. It is therefore more logical to look at the roll angle change in a specific time and not at a final roll rate value, which might not even be reached.

The required lateral control authority will then become a minimum roll angle change in a predetermined time. The lateral envelope is normally neither known nor of concern to the pilot. The only (inaccurate) indication of available lateral control authority is the amount of roll travel available at the yoke or stick. This indication only works with manual control and not when autopilot modes like Control Wheel Steering (CWS) are used. While under normal conditions lateral control is sufficient, in the event of a damaged aircraft or an engine failure, lateral control may be significantly reduced.

#### SUFFICIENT LATERAL CONTROL AUTHORITY

Mil. Spec. F8785C defines minimum roll angle changes for different classes of aircraft and for different flight phases (categories). Also, limits are defined for certain workload levels (1 to 3), with level three giving the highest workload. The absolute minimum roll performance, see Table 3.1, is 6 seconds for a 30° roll angle change. This limit is applicable in Class III aircraft (Large transport) during the landing phase (Cat C) for level 3.

However, for light aircraft (Class I) the maximum time allowed for a 30° roll angle change is only 2.6 seconds (see Table 3.2).

Table 3.2: Excerpt from Mil. Spec. 8785C, TABLE IXa. Roll performance for Class I aircraft.

Level	Category A	Category B	Category C
	60°	60°	30°
1	1.3	1.7	1.3
2	1.7	2.5	1.8
3	2.6	3.4	2.6

Strangely enough, the maximum allowable roll- subsidence time constant (see Table 3.3) for level 3 is the same for all classes, namely 10 seconds. If we combine these minimum requirements ( $\tau = 10$ s and a required roll angle change 30° in 6 s), and assume a first order, single axis response to a maximum step input we need a maximum roll rate of no less than 20°/s which reduces to 12°/s if we use  $\tau = 5$ s.

Table 3.3: Maximum roll subsidence time constant in seconds, according Mil. Spec. 8785C Table VII

Flight Phase Category	Class	Level		
		1	2	3
A	I, IV	1.0	1.4	10
A	II,III	1.4	3.0	10
B	All	1.4	3.0	10
C	I. II-C, IV	1.0	1.4	10
C	II-L, III	1.4	3.0	10

This time constant requirement seems superfluous. If the aircraft roll angle is disturbed, for instance due to a gust, the roll angle deviation should be corrected within a certain time frame, and it is not really important with which combination of maximum roll rate and time constant this change is accomplished. It is also logical to have more stringent limits on light, easily disturbed aircraft, than on the larger transport aircraft. This category-dependent required roll angle change in a fixed amount of time is a good starting point for defining sufficient lateral control authority. Because the roll performance is directly dependent on airspeed, the boundary of the lateral control envelope can be expressed as a minimum allowable airspeed, which we will label  $V_c$ .

### EXCEEDING THE LATERAL ENVELOPE

Loss of lateral control will lead to a roll rate that can not be stopped with aileron and is particularly dangerous close to the ground. One remedy is to increase airspeed. When the roll control is lost, the aircraft will roll towards the ground and this will increase airspeed, however, sufficient altitude should be available to recover from the nose down attitude. Lateral control can also be regained by using asymmetric thrust and rudder.

Close to the ground this may not always prevent a crash but can make the difference between an unsurvivable crash or a possibly survivable crash. A typical example is the Dakota crash in the Waddensee in 1996 [17], where one engine failed and could not be feathered correctly. When lateral control is lost it can be regained by reducing the throttle of the working engine. This will automatically lead to a forced landing or in this particular case to ditching, but the survivability greatly increases when the aircraft ditches or even crashes upright. If we want to prevent pilots from exceeding lateral control limits, we have to make them aware of these limits. However, presently, there does not exist an instrument nor an indication to warn the pilot about these limits. Furthermore, these lateral limits are less straight-forward than AoA limits and different options to define and present them exist. These will be discussed next.

#### AN EXAMPLE; LATERAL CONTROL AUTHORITY OF THE PA-34

The pilot has three ways to influence roll performance: using aileron, rudder and differential thrust. It therefore seems reasonable to express the lateral envelope as a function of these three variables. We will illustrate these relations using the PA-34 model that is used for parameter identification and  $V_c$  calculation, and derived later on in Chapter 6, to show the initial roll rate acceleration as a function of aileron and rudder deflection and asymmetric thrust. The effect of rudder and asymmetric power on roll is primarily caused by the change in  $\beta$ , in the calculation this is addressed in the following way. First the steady state  $\beta$  is derived based on asymmetric thrust and rudder setting. Thereafter, based on this  $\beta$ , the initial roll rate acceleration is calculated as a function of rudder and aileron deflection. This acceleration does not reflect a step input in rudder and aileron, where  $\beta$  builds up, but rather an aileron step input from a situation where  $\beta$  is stabilized and aileron is positioned to counter the roll due to  $\beta$ ,  $\delta_r$  and asymmetric thrust.

In Fig. 3.3 this envelope is presented for the PA-34, in a situation where there is no power difference between the left and right engine and the true airspeed is 85 knots. This figure clearly shows the non-linear behaviour of the aileron<sup>16</sup> and the symmetrical roll performance to the right and to the left.

In Figs. 3.4a and 3.4b the envelopes are presented for the situation where the left engine performs at maximum power and the right engine is off and feathered. The difference in roll performance to the left is clearly visible. While engine power is constant over the speed range, engine thrust and moments are not. If the velocity is only reduced to 80 KTAS, the usable lateral envelope for a left turn becomes significantly smaller, as shown in Fig. 3.4b.

While these graphs are useful, they don't present the actual flight conditions. In actual flight, power will be set to maintain steady flight conditions and optimum pilot control requires that  $\beta = 0^\circ$  is maintained. In Fig. 3.5a these trim conditions are calculated using the non-linear trim model for the PA-34. In this trim model,  $\beta$  is maintained at

<sup>16</sup>The non-linear behaviour of the aileron is accounted for by first transforming the actual aileron deflection to a reduced aileron deflection. The model is linear in parameters with this reduced aileron.

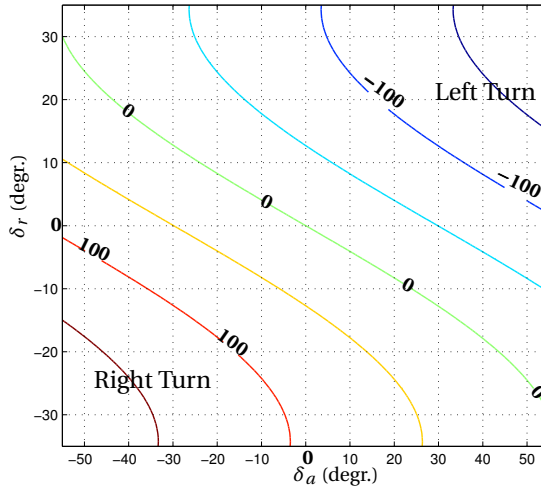


Figure 3.3: Available initial roll rate acceleration in  $\text{degr./s}^2$ , for PA-34 with gear and flaps up. No thrust asymmetry, 85 KTAS and altitude 300m. (Positive control deflection is left rudder and left aileron.)

## 3

zero until maximum rudder deflection is reached, and roll angle  $\phi$  is adjusted to maintain heading as long as enough aileron is available. When the speed is below the airspeed at which maximum aileron is needed, the aircraft is no longer in trim but would start a continuous roll. The calculations are, however, continued below this speed to determine the effect on  $\beta$ . The condition presented is with maximum power on the left engine and the right engine off and feathered at an altitude of 300m and  $\gamma$  adjusted to maintain airspeed. This figure is particularly useful for showing the velocity at which  $\beta = 0^\circ$  can not be maintained. This is also the point where the required aileron to maintain level flight will increase rapidly. Furthermore, and as can be seen in Fig. 3.5b, the lateral control is lost at a higher airspeed than directional control.

#### DEFINING LATERAL CONTROL SPEED

While Fig. 3.5a might be useful for the engineer, it is not yet useful to the pilot. Firstly, he should not be alerted to the speed where lateral control is lost, but to the speed where just enough lateral control is available. Secondly, the lateral control limit is not the same type of limit as the stall limit, which depends mainly on  $C_{L_{max}}$  and the available elevator control. Lateral control depends on multiple parameters. The pilot can influence the roll performance, and the minimum velocity for a certain roll performance, by using differential power or by applying additional rudder. Therefore the basic question arises as to what minimum lateral control velocity must be presented to the pilot. The required roll performance can be realized with different combinations of rudder, asymmetric thrust, aileron and spoiler deflections. The next list gives some of the different possibilities for the presentation of the minimum lateral control velocity:

- Adequate roll control is available while using only aileron, maintaining the present

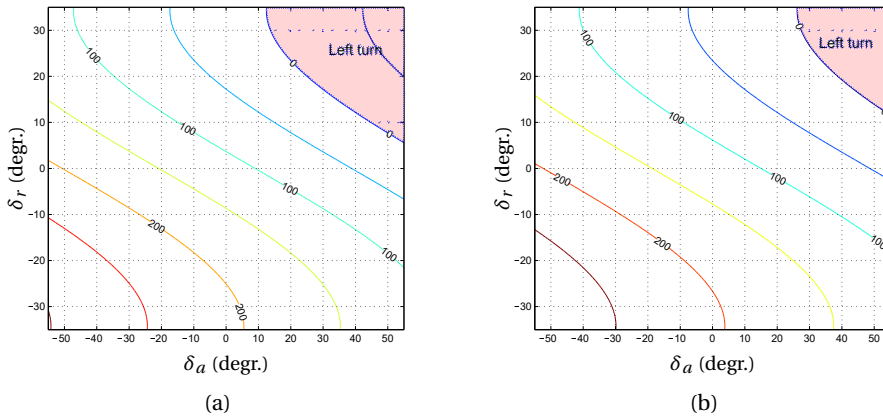


Figure 3.4: Effect of airspeed on roll performance; Available initial roll rate acceleration in  $degr./s^2$ , for PA-34 with gear and flaps up. Left engine maximum power right engine feathered. (a) 85 KTAS, (b) 80 KTAS.

rudder and present thrust;

- Adequate roll control is available with aileron while maintaining zero  $\beta$  with rudder and present thrust;
- Adequate roll control is available using full rudder and aileron maintaining present thrust;
- Adequate roll control is available while using only aileron, maintaining the present rudder and selecting maximum asymmetric thrust;
- Adequate roll control is available with aileron while maintaining zero  $\beta$  with rudder and selecting maximum asymmetric thrust; and
- Adequate roll control is available using full rudder and aileron and selecting maximum asymmetric thrust.

It is obvious that considering six different speeds will not help the pilot to quickly regain aircraft control and that a choice has to be made. It seems reasonable, also from a performance point of view, to maintain zero  $\beta$  for as long as possible. However, what if the pilot does not maintain zero  $\beta$ ? If we want to give the pilot feedback on his control inputs it is better to calculate the  $V_c$  for the actual  $\beta$ . However, we have to adjust for the fact that, when there is asymmetric thrust, this  $\beta$  can not be maintained below a certain speed because rudder will reach its maximum deflection.

A similar reasoning goes for the power setting. We could present the pilot with the speed necessary to maintain lateral control with maximum asymmetric power, but then we would not give feedback on the effect of power adjustments. Therefore we prefer presenting the minimum control velocity based on the present power. However, we have to

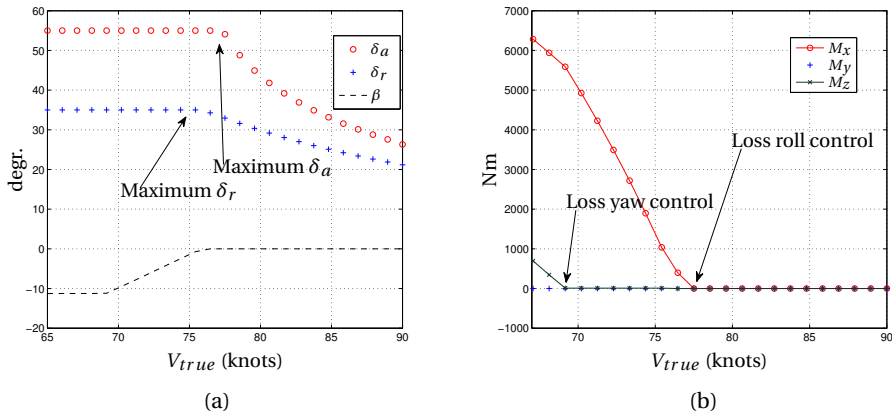


Figure 3.5: Trim conditions PA-34.  $\beta = 0$  until maximum  $\delta_r$  is reached,  $\phi$  is adjusted to maintain heading as long as enough aileron is available. Flap=25°; Gear up; Trimmed for maximum climb with right engine failed; (a) Control deflections (b) Aerodynamic moments in body coordinate system.

adjust for the change in thrust with velocity under constant power conditions.

3

Our initial choice was to base  $V_c$  on available aileron deflection, current  $\beta$ , current thrust or power, and corrected for thrust changes due to airspeed change and for reaching the rudder limit. After the initial test, described in Chapter 7 it was found that it was advantageous to give the pilots feedback on roll performance available with maximum rudder. Therefore a second  $V_c$  indication was added based on the available aileron using present engine thrust and maximum rudder deflection, where the engine thrust was again corrected for the change in airspeed.

If we would limit ourselves to calculating the  $V_c$  for engine failures, we could find a parametric solution based on simulations with the non-linear model of the PA-34. However, if we would like to incorporate all conceivable failure conditions, we have to take an approach based on physics and determine the aircraft model parameters. Based on these parameters we can then calculate the  $V_c$ . Therefore two steps are required. First we have to find the proper model to predict lateral and directional control, this will be discussed in Chapter 5. The second step is to find a method to derive control velocity from the model parameters, which will be discussed later in this chapter.

### 3.4. ONE ENGINE INOPERATIVE AND $V_{mca}$

In order to discuss the 'One Engine Inoperative' (OEI) situation we will first recapitulate the equations needed for static equilibrium. Because the  $V_{mca}$  condition is a special form of a 'Steady Heading Side Slip' we will discuss the general case first and then move to  $V_{mca}$ . In the treatment of  $V_{mca}$ , special attention is given to the relation of engine power and airspeed with controllability because these relations are needed later for the derivation of the lateral control velocity.

### 3.4.1. FORCES, MOMENTS AND REFERENCE FRAMES

In this section we will explain the reference frames and variables that we use, based on [2, Ch. 4], [18, Ch. 6], [3, Ch. 3]. We will present the results of the derivations of these references only, except where we have to deviate from the assumptions used.

#### ASSUMPTIONS

All equations are derived under the following assumption: the aircraft is a rigid body with constant mass and inertia tensor, the earth is flat and the effect of rotating masses (e.g., propellers) are ignored. Under the assumption of a flat non-rotating earth, the  $C_G$  coordinate system, with a fixed reference point can be used as an inertial reference frame, while the rigid body with fixed mass and inertia tensor allows for the use of the standard (Newton) based equations of motion for a rigid body in a rotating reference frame.

#### FORCES AND MOMENTS

The contributions to forces and moments on the aircraft originate from three sources: aerodynamics, thrust and gravity. Forces and moments can be expressed in different reference coordinate systems and have to be transformed to a single coordinate system to be added. The coordinate system of choice for this addition is  $C_B$ . The aerodynamic forces: Lift (L), Drag (D) and side force (C)<sup>17</sup> are expressed in the  $C_A$  coordinate system. Because of the standard signs used for lift and drag, the aerodynamic forces in the ( $C_A$ ) coordinate system are:  $[-L \quad -C \quad -D]^T$ , where the  $-C$  is chosen by [18] to make it a right handed system. When rotated to the body axis coordinate system the forces are labelled  $[X \quad Y \quad Z]^T$ . The thrust forces are also defined in  $C_B$ , the force of gravity  $Mg$  is defined along the Z axis of  $C_G$  and also has to be transformed to  $F_B$ .

Moments are only expressed in the body coordinate system, primarily because the inertia tensor is defined in this coordinate system. The different moments around their respective axes are named  $[L \quad M \quad N]^T$ . When expressed in relation to the c.g., only the aerodynamic forces and thrust will contribute to these moments, but gravity will not. However, when the c.g. is not known, as could be the case for a damaged aircraft, and another reference point is used, then the effects of gravity on the moments must be included. We will derive the equations for an arbitrary reference point later on in this chapter.

#### NORMALIZATION

Forces and moments are normalized by dividing all forces by  $qS$ , the rolling and yawing moments by  $qSb$  and the pitch moment by  $qS\bar{c}$  where  $q$  is the dynamic air pressure  $\frac{1}{2}\rho V^2$ ,  $S$  is the wing area,  $b$  is the wingspan and  $\bar{c}$  is the mean aerodynamic chord. The result of this normalization is that forces and moments become non-dimensional, independent of airspeed and size, only dependent on other non-dimensional parameters such as  $\alpha$ ,  $\beta$ , Mach number, non-dimensional turn rates and control deflections. The non-dimensional coefficients are denoted with  $C$  and a subscript identifying axis of the forces and moments. This gives:

<sup>17</sup>C is arbitrary chosen in accordance with [18], normally seldom used.

- Aerodynamic forces in the  $C_A$  coordinate system  $[L \ D \ C]^T$  will be modified to  $[C_L \ C_D \ C_C]^T$ ;
- Forces in the  $C_B$  coordinate system  $[X \ Y \ Z]^T$  become  $[C_X \ C_Y \ C_Z]^T$ ;
- Moments in the  $C_B$  coordinate system  $[L \ M \ N]^T$  become  $[C_l \ C_m \ C_n]^T$ ;
- Instead of using mass, we use the non-dimensional form for lateral and directional motions  $\mu_b$ , which is defined as  $\mu_b = \frac{m}{\rho S b}$ ;
- Instead of using inertia moments we use the non-dimensional radii  $K_{xx}^2 = \frac{I_{xx}}{mb^2}$ ,  $K_{yy}^2 = \frac{I_{yy}}{m\bar{c}^2}$  and  $K_{zz}^2 = \frac{I_{zz}}{mb^2}$ ;
- The cross products of inertia  $I_{xy}$ ,  $I_{xz}$  and  $I_{yz}$  are normalized in the same way and labelled  $J_{xy}$ ,  $J_{xz}$  and  $J_{yz}$  respectively.

The independent variables on which the coefficients depend are normalized in the following manner:

- the roll rates  $[p \ q \ r]^T$  become  $[\frac{pb}{2V} \ \frac{q\bar{c}}{V} \ \frac{rb}{2V}]^T$ ;
- All angles like  $\alpha$ ,  $\beta$  and the deflections of the control surfaces elevator ( $\delta_e$ ), aileron ( $\delta_a$ ) and rudder ( $\delta_r$ ) are expressed in radians and are already non-dimensional;
- A special case is the engine thrust output. Several engine parameters can be used as a measure of thrust, for example the engine fuel flow, rpm and torque. But, as will be shown later, there is also a large difference between propeller and turbojet aircraft. This will be discussed in more detail in the section about  $V_{mca}$ . For now we only state the results that for turbojet aircraft using the normalized fuel flow  $\frac{ff}{V^2}$  works well [19] and for propeller aircraft  $\frac{Torque}{V^3}$  can be used.

To get a linear approximation of the non-dimensional forces and moments, the partial derivatives of the coefficients to the independent variables are determined. The most important independent variables for lateral-directional motion are:  $\phi$ ,  $\beta$ ,  $\frac{pb}{2V}$ ,  $\frac{rb}{2V}$ ,  $\delta_a$ ,  $\delta_r$ ,  $\delta_{TL}$  and  $\delta_{TR}$ , where the last two variables are the normalized engine inputs for left and right engine. The partial derivatives are denoted with a second subscript indicating to what variable the derivative was taken.

### STATIC LATERAL-DIRECTIONAL EQUILIBRIUM

For the lateral static equilibrium equations we assume that all accelerations:  $\dot{p}$ ,  $\dot{q}$ ,  $\dot{r}$ ,  $\dot{u}$ ,  $\dot{v}$  and  $\dot{w}$  are zero. Furthermore we assume that all control inputs are fixed. The aircraft can be in a constant turn, consequently  $q$  and  $r$  can be non-zero but the roll angle is constant hence  $p = 0$ . Furthermore, the side slip is not necessarily zero but is constant. If we assume that  $\theta$  is small, the following relations exist in a turn [2, p. 446] (see Fig. 3.6):

- The component of the gravity force along the Y-axis is:  $Mg \sin \phi$ . In non-dimensional form, divided by  $qS$  this gives:  $\frac{mg}{qS} \sin \phi$ . Under the assumption that  $\phi$  is small and there is no substantial side force due to  $\beta$ , this expression can be changed to  $C_L \phi$ , using the fact that in this condition  $C_L = \frac{mg}{qS}$ . However, as shown in Fig. 3.6, when the side force due to side slip is substantial, it carries part of the weight and  $C_L$  becomes less than  $\frac{mg}{qS}$ . Because our intent is to also investigate the larger side slips and roll angles, we will use  $\frac{mg}{qS}$  instead of  $C_L$ .
- The centripetal force in the  $X_B Y_B$  plane of the aircraft is the sum of  $\frac{mg}{qS} \sin \phi + C_{Y\beta} \beta$ . This is equal, but opposite in sign, to the reaction force, the centrifugal acceleration  $Vr$ , multiplied by the aircraft mass  $m$ . We can make the reaction force non-dimensional and a function of the non-dimensional roll rate  $\frac{rb}{2V}$ . This gives:  $\frac{-Vr m}{qS} \frac{b}{b} = \frac{-m}{\rho S b} \frac{rbV}{0.5V^2}$  which gives  $4\mu_b \frac{rb}{2V}$ .

Using the relationships derived above, and assuming that aileron and engines do not contribute to the side force ( $C_{Y\delta_a}$ ,  $C_{Y\delta_{TL}}$ , and  $C_{Y\delta_{TR}}$  are 0), the lateral static equilibrium equation becomes:

$$\begin{bmatrix} \frac{mg}{qS} & C_{Y\beta} & -4\mu_b & 0 & C_{Y\delta_r} & 0 & 0 \\ 0 & C_{l\beta} & C_{l_r} & C_{l\delta_a} & C_{l\delta_r} & C_{l_{TL}} & C_{l_{TR}} \\ 0 & C_{n\beta} & C_{n_r} & C_{n\delta_a} & C_{n\delta_r} & C_{n_{TL}} & C_{n_{TR}} \end{bmatrix} \cdot \begin{bmatrix} \sin \phi \\ \beta \\ \frac{rb}{2V} \\ \delta_a \\ \delta_r \\ \delta_{TL} \\ \delta_{TR} \end{bmatrix} = 0 \quad (3.3)$$

For the discussion of steady heading side slip and  $V_{mca}$  Eq. 3.3 is sufficient because they are both cases of static equilibrium. For the dynamic response we also need the equations for linear and rotational acceleration of a rigid body in a rotational frame. These equations will be discussed in Section 4.2 where we need them to derive the equations for the calculation of  $V_c$ .

### 3.4.2. STEADY HEADING SIDE SLIP

The steady heading side slip is a static condition where a combination of  $\beta$  and  $\phi$  results in a steady heading, or  $\dot{\psi} = 0$ . To achieve this equilibrium in the lateral-directional equations, as presented in [2, p. 453], we set  $\dot{\beta}$ ,  $\dot{p}$ ,  $\dot{q}$ ,  $\dot{r}$  and  $\dot{r}$  to zero. Furthermore, we assume that using the same power setting for the left and the right engine will cancel the engine effect on roll, yaw and side slip. With these assumptions Eq. 3.3 can be simplified to the following equation:

$$\begin{bmatrix} \frac{mg}{qS} & C_{Y\beta} & 0 & C_{Y\delta_r} \\ 0 & C_{l\beta} & C_{l\delta_a} & C_{l\delta_r} \\ 0 & C_{n\beta} & C_{n\delta_a} & C_{n\delta_r} \end{bmatrix} \begin{bmatrix} \sin \phi \\ \beta \\ \delta_a \\ \delta_r \end{bmatrix} = 0 \quad (3.4)$$

Two things differ in Eq. 3.4 with the way this equation is presented in [2, p. 453]. First,  $\frac{mg}{qS}$  is normally replaced by  $C_L$  and in non side slipping flight  $\frac{mg}{qS} = C_L$ , but in steady

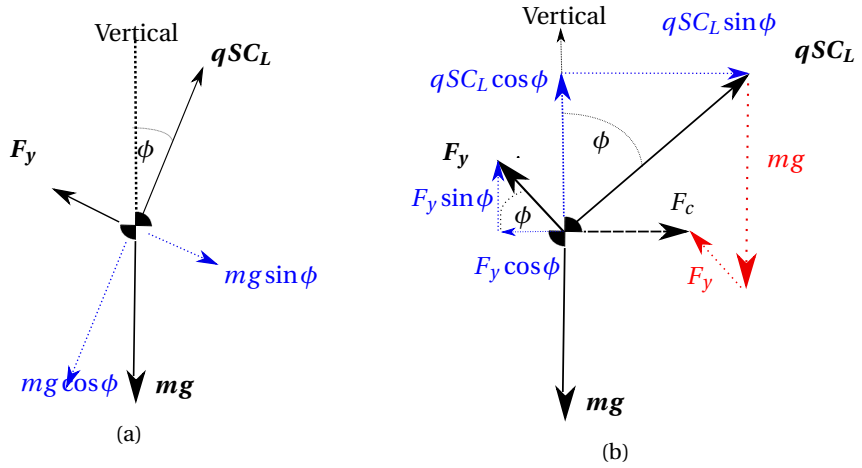


Figure 3.6: Aircraft with side force due to  $\beta$ ; Aircraft  $X_B$  axis is pointing into the paper and  $\theta = 0$ ; (a) In a Steady Heading Side Slip and (b) In a turn where the sum of Lift,  $mg$  and  $F_y$  results in a centripetal force  $F_c$ . In red the laterally displaced vectors, in blue the vector components as a function of  $\phi$ .

heading side slip situations the  $C_L$  depends on the roll angle going to zero in the ultimate case of  $\phi = 90^\circ$ , as illustrated in Fig. 3.6a. In this special case the aerodynamic side force completely compensates the aircraft weight, while the lift force has to be zero in order to maintain heading. This ultimate case of steady heading side slip with  $\phi = 90^\circ$  (while maintaining altitude) is not purely theoretical. This manoeuvre is called the 'knife edge' and performed on a regular basis during air displays. Secondly, instead of using  $\phi$  as variable we use  $\sin \phi$ , so we don't have to limit ourselves to small roll angles.

In this discussion and drawings we assume  $\theta = 0$  and  $\alpha$  is small; in Fig. 3.6a and 3.6b the  $X_B$  axis is pointing into the page. By using  $mg \cos \theta$  instead of  $mg$  and using  $qSC_L \cos \theta$  in stead of  $qSC_L$ , this derivation can be extended to all values of  $\theta$ . However, when  $\theta$  is small, which is typical for one-engine-out situations,  $\cos \theta \approx 1$ . If the engine thrust angle with the velocity vector is significant, the component of the thrust parallel to the lift must be added to the lift vector. In our derivation we assume this effect to be negligible.

A convenient way to solve this equation is to first determine the relationship between  $\delta_r$ ,  $\delta_a$  and  $\beta$  from rows 2 and 3 of Eq. 3.4. Given a rudder deflection of  $\delta_r$  it is easy to calculate the required aileron deflection and  $\beta$  to have a zero roll rate and yaw rate, so we modify this equation to:

$$\begin{bmatrix} \beta \\ \delta_a \end{bmatrix} = \begin{bmatrix} C_{l\beta} & C_{l\delta_a} \\ C_{n\beta} & C_{n\delta_a} \end{bmatrix}^{-1} \begin{bmatrix} C_{l\delta_r} \\ C_{n\delta_r} \end{bmatrix} \delta_r \quad (3.5)$$

It is interesting to note that the relation between  $\delta_r$ ,  $\delta_a$  and  $\beta$  is independent of speed. Next we derive  $\phi$  using the first row of Eq. 3.4 :

$$\phi = \arcsin \left( \frac{-qS(C_{Y\beta} \cdot \beta + C_{Y\delta_r} \cdot \delta_r)}{mg} \right) \quad (3.6)$$

The angle  $\phi$  turns out to be dependent on dynamic pressure  $q$ , and thus on airspeed. With Eq. 3.6 we can also determine the speed required to perform the ‘knife edge’ (neglecting thrust contribution). As illustrated in Fig. 3.6a, there is no resulting horizontal force and therefore the heading is constant. It is important to note that the side slip ( $\beta$ ) is not dependent on the roll angle but only on  $\delta_r$  and  $\delta_a$ . This is of course a direct result of the fact that the side force due to  $\phi$ , ( $mg \sin \phi$ ), acts on the c.g. and consequently does not generate a moment. Therefore a change in  $\phi$  does not lead to a change in  $\beta$ , and we can assume a constant side force due to  $\beta$  when we investigate the effect of changing  $\phi$  and turning. This will be discussed next.

### TURNING WITH $\beta$

It is important for the discussion on engine failure to investigate the effect of a steady turn while there is a substantial side force. This situation is depicted in Fig. 3.6b, from this figure the following relations are evident:

$$qSC_L \cos \phi + F_Y \sin \phi = -mg, \quad (3.7)$$

or the required lift to make a level turn is:

$$qSC_L = (-mg - F_Y \sin \phi) / \cos \phi, \quad (3.8)$$

and the resulting centripetal force  $F_c$  is then<sup>18</sup>:

$$F_c = qSC_L \sin \phi + F_y \cos \phi \quad (3.9)$$

The next step is to investigate the difference between a right and a left turn. In the following example we assume that  $F_y = 0.1mg$  and to the left. Next we divide all forces by  $mg$  in order to change from forces to the non-dimensional load factor  $n$  where  $n_y = \frac{F_y}{mg}$ ,  $n_z = \frac{F_z}{mg}$  and  $n_c = \frac{F_c}{mg}$ . The used side force of  $0.1mg$  is not uncommon, as we can see in Fig. 3.7, where the required  $n_z$  and the resulting centripetal load factor  $n_c$  are given for this situation and compared to the situation without any aerodynamic side force. We notice that the steady heading side slip point is at  $\phi = +5.7^\circ$ ; this is a common amount of roll angle in a ‘wing low approach’ in side slip.

From Fig. 3.7 it is clear that the  $n_y$  due to side slip only gives an offset in the relation between  $\phi$  and turn rate. The  $\phi$  for zero heading change is now  $5.7^\circ$  and a change in  $\phi$  from this position, gives almost the same side force and consequently the same turn rate as a turn with  $\phi = 25^\circ$  without side slip. Table 3.4 gives the values of  $n_y$  and  $n_z$  (for a  $25^\circ$   $\phi$  change left and right from the neutral position of  $5.7^\circ$  right). It shows that the required  $n_z$  and  $n_y$ , for a  $25^\circ$  displacement from the steady heading side slip situation to the right

<sup>18</sup>Note that the depicted  $F_y$  in Fig. 3.6b is negative, the positive  $Y_B$  axis is to the right.

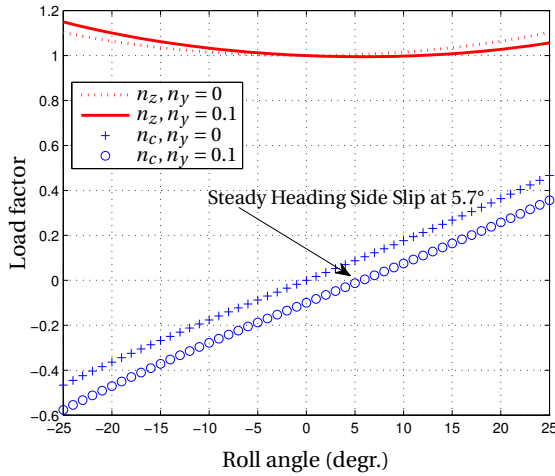


Figure 3.7: Effect of roll angle on lift and centripetal force with a constant side force due to  $\beta$  that is  $0.1mg$ , based on Eq. 3.9.

Table 3.4: Effect of  $25^\circ$  change in  $\phi$  left and right from neutral steady heading side slip position at  $5.7^\circ$ , compared to  $\phi = 25^\circ$  without side slip.

	With side slip $\phi = 5.7^\circ - 25^\circ = -19.3^\circ$	With side slip $\phi = 5.7^\circ + 25^\circ = 30.7^\circ$	No side slip Right: $\phi = 25^\circ$
$n_y$	-0.455	0.478	0.423
$n_z$	1.094	1.104	1.103

and to the left, shows very little difference. Based on these data it is clear that for the pilot not much has changed, the turn performance to the right and to the left requires almost the same  $n_z$ , there is just a 1% difference, and the lateral acceleration left and right differs only 5%. The only thing the pilot has to realize is that the neutral position is  $5.7^\circ$  right roll angle. However, we have not yet evaluated the effect of  $r$  on required aileron and rudder. This will be discussed next.

### THE EFFECT OF TURN RATE

In a steady turn there will be a small lift difference between the wing on the outside and on the inside of the turn, due to the velocity difference. This causes a roll moment that tends to increase the roll angle. Another source for a roll moment in a steady turn is the vertical tail [2, p. 344]. The curved airflow around the aircraft gives a side slip angle on the vertical tail. This effect tends to increase the roll angle as well. Both effects are accounted for in the parameter  $C_{l_r}$ . To compensate for this effect, an additional aileron deflection is needed in a steady turn, which can be derived from Eq. 3.10. Assuming that rudder deflection is kept constant this gives:

$$C_{l_r} \frac{r p}{2V} + C_{l_{\delta_a}} \delta_a = 0 \quad (3.10)$$

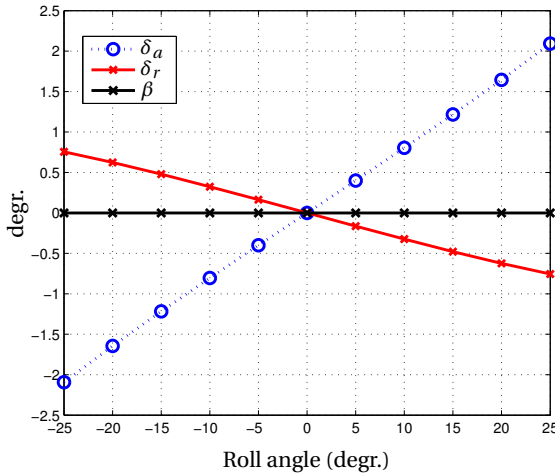


Figure 3.8: Required aileron en rudder deflection to maintain a level turn for the PA-34 at zero side slip angle, flying at 80 KTAS.

In a steady level turn we can write  $r$  as a function of roll angle. Realizing that  $\psi = \frac{V}{g} \tan \phi$ , that  $r = \psi \cos \phi$  and combining this with Eq. 3.10 we can determine the required additional aileron deflection to maintain a constant  $\phi$  in a level turn.

$$\Delta \delta_a = -\frac{C_{l_r}}{C_{l_{\delta_a}}} \frac{bg}{2V^2} \sin \phi \quad (3.11)$$

Eq. 3.11 shows that the required aileron deflection increases with wing-span<sup>19</sup> and roll angle, and is largest at low airspeeds. Furthermore, the contribution of the vertical tail area to  $C_{l_r}$  is decreasing with increasing angle of attack [2, p. 344]. This will slightly reduce this effect at low speed. However, if we look at the simulation with the non-linear model of the PA-34 at 80 knots TAS, which is shown in Fig. 3.8, we see that the combined effect, even at this low airspeed, is small. Two degrees of additional aileron deflection is needed to maintain a steady turn when  $\phi = 25^\circ$  and the effect is linear with  $\phi$ .

When the available control deflection is limited, for instance in the event of an engine failure, it is important to know how the roll angle direction will influence the available control. Therefore, we repeated the previous simulation, but now with a fixed side slip of  $+10^\circ$ . The results are presented in Fig. 3.9.

We see that with side slip from the right, a large negative aileron deflection is needed. The absolute aileron deflection needed in a left turn is slightly higher than to the right. So, while it is much easier to start a left roll because of the large deflection available, it is slightly harder to stop because the deflection to the right is less. There is an even smaller

<sup>19</sup>Assuming that  $C_{l_{\delta_a}}$  remains the same despite the wingspan change.

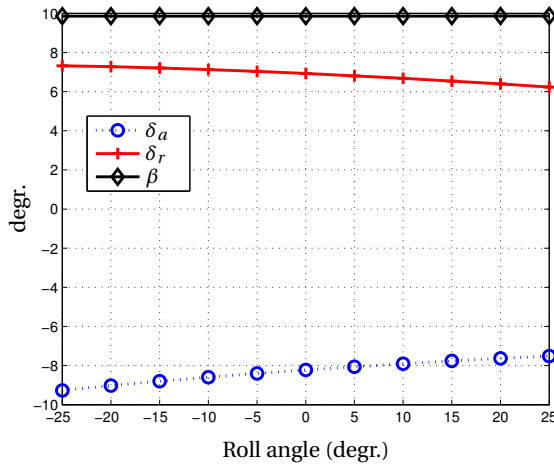


Figure 3.9: Required aileron and rudder deflection to maintain a level turn with  $10^\circ\beta$  for a PA-34 80 KTAS.

change in  $\delta_r$  that is caused by the adverse yaw effect ( $C_{n\delta_r}$ ). So while we initially stated that roll angle will not cause a side slip, there is a secondary effect from the turn rate  $r$  that requires additional aileron input, and this additional aileron input can cause a side slip because of the adverse yaw. However, this effect of the turn rate is very small. We will now start the discussion of  $V_{mca}$  and engine failures and use the findings above later to evaluate turning with a failed engine.

### 3.4.3. ONE ENGINE OUT AND $V_{mca}$

$V_{mca}$  is the standard measure for lateral-directional controllability in flight, for the situation where the most critical engine has failed. Because this measure is often the only lateral-directional control measure that is presented to the pilot,<sup>20</sup> it is appropriate to investigate the strong and weak points of this measure.  $V_{mca}$  is normally determined in flight tests, and is applicable for one configuration: gear down, flaps set for take off or approach, the failed engine feathered if an automatic feathering is installed, aft c.g. and the lightest gross-weight [20], [4]. Together, these constitute the most restrictive configuration. For our further evaluation, this configuration is assumed.

#### ENGINE FAILURE

The effect of an engine failure is determined by the type of engine. The simplest case is the turbojet engine, which delivers thrust that is almost constant over a considerable speed range [21] and causes hardly any induced flow over the wing that generates an additional roll moment. The more interesting case is the propeller driven aircraft. Here thrust increases with decreasing airspeed, there is induced flow over the wing and over the tail, causing additional roll and yaw moments. Also, for twin engine propeller aircraft the propeller size requires the engines to be installed further away from the fuse-

<sup>20</sup>The only one for air operations, there is also a measure for directional control on the ground.

lage, while twin engine jet aircraft can even use fuselage mounted engines, consequently in propeller aircraft, the engine thrust typically has a larger arm. We will discuss these elements first before going to the derivation of the  $V_{mca}$ .

#### PROPELLER INDUCED FLOW EFFECTS

In order to determine the lateral controllability of propeller-aircraft a good understanding of propeller induced flow effects is needed. Many studies like [22], [23], [24], [25] and [26] have investigated these effects with numerical analysis and with wind-tunnel experiments. The following studies [27] and [13] evaluated these effects during actual flight tests. An analysis of these studies is made in Appendix A. Furthermore an additional study was done on the relation between thrust and airspeed using a propeller model described in Appendix B. The results of this evaluation are also presented in Appendix A. The main results of this analysis are presented here:

- The simulation with the propeller model showed that, while the thrust dependence on airspeed was less than  $\frac{1}{V}$  at low airspeeds, this was a fair approximation above the aircraft stall speed.
- The effect of the induced flow on roll showed to change with  $\frac{1}{V^2}$  instead of  $\frac{1}{V}$  as is normally used in analysis.
- The induced cross flow over the vertical, in case of an engine failure, increases the yaw moment. The magnitude of the induced flow depends on wing position, engine position and the propeller turn direction, where the effect of the 'Inboard Up' (IU) turning propeller is stronger than that of the 'Outboard Up' (OU) turning propeller. Generally the cross-flow is accounted for by multiplying the direct thrust moment with a constant. However, flight tests show that this effect is less linear and the effect decreases at low airspeed.

#### $V_{mca}$ AND SIDE FORCE

In the previous paragraphs we found that the thrust for propeller driven aircraft is dependent on the aircraft velocity; a rough approximation (Fig. A.1) is  $\frac{P}{V}$  where  $P$  is the constant power and  $V$  the true airspeed. The thrust coefficient  $T_c$ , which is defined as  $\frac{Thrust}{qS}$  then becomes a function of  $V^{-3}$  or  $T_c = \frac{P}{0.5\rho SV^3}$ . Mannée showed that the yaw moment due to the engine  $C_{n_e}$  is larger than  $T_c \times \frac{y_e}{b}$  where  $y_e$  is the moment arm of the engine in relation to the c.g. This increase can be approximated by a linear constant  $k$  for an OU turning propeller but is dependent on the  $T_c$  value for the IU turning propeller. This dependency of  $k$  on  $T_c$  also forms an additional dependency on  $V$ . Furthermore, dependencies on AoA as described by [26] further complicate velocity dependency. Calculating the roll moment (Fig. A.2) we found that the additional lift can be approximated by  $\frac{a}{V^2}$  where  $a$  is a constant. This would imply that the engine roll moment coefficient  $C_{l_e}$  can be approximated by  $C_{l_e} = \frac{(a)y_e}{0.5\rho V^4 Sb}$ . However, as described by [26], AoA effects will also affect the lift distribution behind the propeller, changing the effective arm ( $y_e$ ) as a function of AoA.

In the following derivations we will assume a  $V^{-3}$  relation for  $T_c$ ,  $C_{n_e}$  and for the side force generated by the engine  $C_{Y_e}$  due to the cross flow. For  $C_{l_e}$  we will assume  $V^{-4}$ . This rough approximation is only sufficient to explain the relation between  $V_{mca}$  and roll angle. For an accurate calculation the exact velocity dependency of  $T_c$  and  $C_{N_e}$  must be established experimentally. If we now modify Eq. 3.4 by adding the effect of one engine inoperative and the other one at maximum power while the rudder is at its maximum deflection, we get the following equation:

$$\begin{bmatrix} \frac{mg}{qS} & C_{Y\beta} & 0 & C_{Y\delta_r} \\ 0 & C_{l\beta} & C_{l\delta_a} & C_{l\delta_r} \\ 0 & C_{n\beta} & C_{n\delta_a} & C_{n\delta_r} \end{bmatrix} \begin{bmatrix} \sin\phi \\ \beta \\ \delta_a \\ \delta_{rmax} \end{bmatrix} + \begin{bmatrix} 0 \\ \frac{k_1 P_{max} Y_e}{0.5\rho V^4 S b} \\ \frac{k_2 P_{max} Y_e}{0.5\rho V^3 S b} \end{bmatrix} = 0, \quad (3.12)$$

where  $k_1$  and  $k_2$  are the appropriate scaling constants.

If we first solve rows 2 and 3, we may rewrite Eq. 3.12 to:

$$\begin{bmatrix} \beta \\ \delta_a \end{bmatrix} = \begin{bmatrix} C_{l\beta} & C_{l\delta_a} \\ C_{n\beta} & C_{n\delta_a} \end{bmatrix}^{-1} \left( - \begin{bmatrix} C_{l\delta_r} \\ C_{n\delta_r} \end{bmatrix} \delta_{rmax} - \begin{bmatrix} \frac{k_1 P_{max} Y_e}{0.5\rho V^4 S b} \\ \frac{k_2 P_{max} Y_e}{0.5\rho V^3 S b} \end{bmatrix} \right) \quad (3.13)$$

Comparing Eq. 3.13 with Eq. 3.5 for steady heading side slip shows that the relation between  $\beta$  and  $\delta_r$  has become speed dependent. Solving Eq. 3.13 for different values of  $V$  will give the required aileron deflection and  $\beta$  for each airspeed. With these derived  $\beta$ ,  $\delta_a$ , the first row of Eq. 3.12 can be used to calculate the  $\phi$  that will give a constant heading (Eq. 3.14) as a function of the dynamic pressure  $q$  and aircraft mass:

$$\phi = \arcsin \left( \frac{qS}{mg} \left( -C_{Y\beta} \beta - C_{Y\delta_r} \delta_r \right) \right) \quad (3.14)$$

This calculation was done for the PA-34 using the aircraft data from [28]. For the aircraft thrust, the same  $\frac{1}{V}$  approximation was used as in Fig. A.1 and for the roll moment the delta lift  $\frac{1}{V^2}$  approximation was the same as in Fig. A.2. The calculations were made for a right engine failure with the left engine operating at maximum power while the rudder was fully deflected to the left<sup>21</sup>. This combination of maximum rudder and maximum asymmetric thrust at all velocities, while adjusting  $\phi$  to maintain heading, is not the way a pilot will operate his aircraft but is very instructive for showing the available lateral control. The result is presented in Fig. 3.10.

For the control of an aircraft with one engine inoperative there are five velocity points that are important. They are labelled in Fig. 3.10.

1. The velocity where  $\beta = 0$ . This point minimizes the drag due to side slip. A further decrease in airspeed will cause an unfavourable  $\beta$  that will increase the re-

<sup>21</sup>The PA-34 has counter-rotating propellers and a low wing, which both minimize the cross flow effect. In the model [28] no constant is used to account for cross flow.

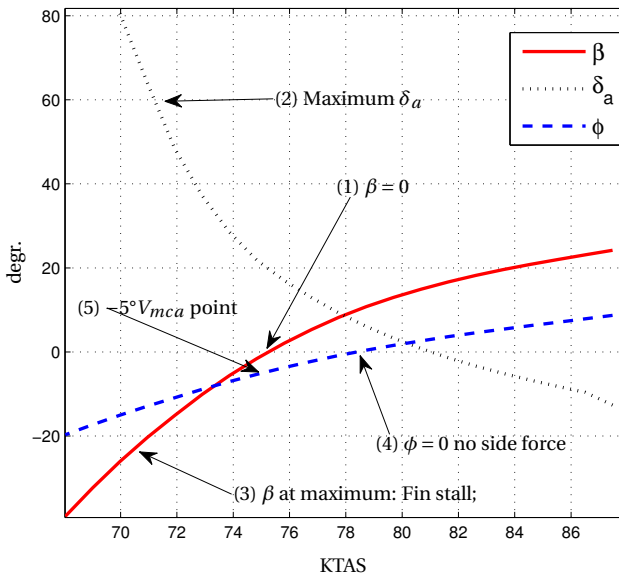


Figure 3.10: PA-34 Right Engine Inoperative, Left Engine Maximum Power and Rudder Full Left.

quired aileron deflection. At airspeeds above this velocity a favourable  $\beta$  is possible, which will decrease the required aileron deflection.

2. The velocity where  $\delta_a$  reaches its maximum value. Below this speed roll control will be lost.
3. The velocity where  $\beta$  reaches its maximum value. At lower speeds the aircraft fin will stall causing a yaw departure.
4. The velocity where  $\phi = 0$ . At this velocity the side force generated by  $\beta$  cancels out the side force generated by the rudder and the engine. This is the lowest velocity that enables the pilot to maintain heading with  $\phi = 0$ . Below this velocity a certain roll angle is required to cancel out the side forces and maintain heading.
5. The velocity where  $\phi = -5^\circ$ . This is the maximum roll angle allowed for the determination of the  $V_{mca}$ . The manufacturer can choose a smaller value, e.g., the velocity where  $\beta = 0$ . For the PA-34 with this mass (1901 kg) these points are very close to each other.

One of the most interesting points that can be found in Fig. 3.10 is the proximity of the different points. There is just 3.5 knots difference between the standard  $V_{mca}$  and the point where aileron deflection reaches its maximum value.

### $V_{mca}$ AND TURNS

The last issue regarding  $V_{mca}$  is the effect of turning. First of all, we have to realize that  $V_{mca}$  is not defined in a turn, by definition it is a steady heading side slip. So arguments that  $V_{mca}$  increases or decreases in a turn can not be made. However, in a similar manner as with steady heading side slip, we can evaluate what the changes are in moments and forces when, starting from the  $V_{mca}$  steady heading side slip condition, a turn is made.

The result is surprisingly simple, because neither the engine forces and moments, nor the rudder moments depend on  $\phi$ ; we have exactly the same situation as with a steady heading side slip. Consequently, the effects are also similar: If we have a left engine failure we have to use right rudder to maintain side slip at zero. Right rudder will give a side force to the left, this situation is similar in sense, but not in magnitude, as with the steady heading side slip situation depicted in Fig. 3.9. This implies that a steady left turn into the 'dead' engine requires slightly more right aileron and slightly less left rudder than a steady turn in the opposite direction. But again, these effects are small. The situation in Fig. 3.9 is for a PA-34 with  $10^\circ$  of side slip. The rudder deflection needed to generate a similar side force is  $34^\circ$  or within  $1^\circ$  of the maximum rudder deflection. In other words, the situation depicted in Fig. 3.9 is comparable to having a failed left engine, maximum rudder deflection to the right and zero side slip.

While the steady turn away or towards the dead engine requires almost equal control inputs, it is of course clear that the maximum roll rate into the dead engine is far greater than away from it, and that there is a risk of over-banking, which requires all roll inputs to be made carefully, but it does not limit a turn in either direction.

### CONCLUSION ON $V_{mca}$

After this discussion on  $V_{mca}$  a few points should be clear.  $V_{mca}$  is a steady heading side slip point with the most critical engine inoperative. It is not linked to an aerodynamic limit like  $\beta = 0$ . As shown in Fig. 3.10 it may be close to the point where  $\beta$  is zero, but it is not necessarily the same. It may give adequate roll performance but the fact that this point is stable only guarantees that there is some roll performance and not that the roll performance is sufficient. It may not even guarantee that the side slip can be made zero. Because  $V_{mca}$  does not classify as a control limit, it is hard to predict what will happen when the aircraft is flown below  $V_{mca}$ . Because the rudder is already at its maximum deflection, it is evident that adverse  $\beta$  will occur and will increase rapidly. This increase will limit roll performance and the most important question is whether the aircraft will first depart in yaw, or whether the roll control limit will be reached first. For the PA-34 it is clear from Fig. 3.10 that the roll limit will be reached first.

### COMPARISON BETWEEN $V_c$ AND $V_{mca}$

In the first part of this chapter we derived the control limits for directional and lateral control. For directional control we showed that the minimum airspeed that enables the pilot to maintain zero  $\beta$  under the condition of maximum asymmetric power is a practical limit. This limit is often close to the  $V_{mca}$ , but a more exact requirement that enables to minimize the drag due to side slip. However, an additional airspeed to guarantee sufficient roll control,  $V_c$ , is also needed. For certification purposes we believe that this

combination of the airspeed for zero  $\beta$  and the  $V_c$ <sup>22</sup>, is a better requirement than the  $V_{mca}$ .

### 3.5. CONCLUSIONS

In developing a lateral-directional control limit that can advise pilots to which airspeed sufficient lateral-directional control is available, while this limit adjusts for damage and thrust asymmetry, we have reached the following conclusions:

- Starting with the NASA definition for controllability, namely the capability to change attitude, we can derive practical limits for sufficient control expressed in AoA, airspeed and side slip angles.
- Directional control limits should be based on side slip with as standard limit the ability to maintain zero side slip with maximum asymmetric thrust moment. In case of aircraft damage, a non-zero side slip situation will constitute a performance problem and may cause roll problems but will generally not lead to a yaw departure because roll limits will be reached first.
- Roll limits should be defined as the capability to make a minimum roll angle change over time, which is in line with Military Specifications (MIL-F-8785C).
- The requirement for a minimum roll angle change and the ability to maintain zero side slip under the condition of maximum asymmetric thrust is a more precise limit than  $V_{mca}$ . The  $V_{mca}$  requirement, in its pure form, is a steady heading side slip requirement which is close to the zero side slip point but not exactly the same. The additional roll requirements for  $V_{mca}$  in the FAR are less specific than the roll requirements in the Military Specifications.
- Because roll limits are typically reached before yaw limits we should present the pilot with the speed where the roll authority limit is reached.
- In case of asymmetric thrust, the effect of roll angle direction (into or away from the dead engine) on roll control is small, for the evaluated PA-34 it equates to a maximum 2° reduced aileron deflection when the roll angle is 25°. This does not minimize the risk of over-banking but indicates that a steady bank angle into the dead engine can be maintained.
- For the determination of the available roll control of a damaged aircraft, a model is necessary where the c.g. can be shifted away from the standard reference point. In our derived model the c.g. shift can be determined by the effect of aircraft motion on changes in the load factor, while the c.g. shift will not affect the standard aerodynamic and thrust moments.
- The pilot should be presented with a realistic  $V_c$ . Therefore the choice was made to base the  $V_c$  on current engine setting and the current side slip. However, the  $V_c$  is

<sup>22</sup>For certification purposes the  $V_c$  should be based on on the condition of maximum asymmetric power and the optimum use of rudder. This should not be confused with the dynamic  $V_c$  we will derive in the next

adjusted for the change in engine thrust due to the change from current airspeed to  $V_c$ . Furthermore, if in the deceleration to  $V_c$  the maximum rudder deflection is reached, the change in side slip will be accounted for.

- It was found that the effect of propeller on directional and lateral control differed. Generally, it is assumed that thrust from propeller aircraft is  $\frac{P}{V}$  which makes the normalized thrust moment dependent on  $\frac{1}{V^3}$ . It was found that the directional effect due to thrust moment and cross flow was slightly less than  $\frac{1}{V^3}$  while the roll effect was close to  $\frac{1}{V^4}$ .

## REFERENCES

- [1] E. L. Duke, R. F. Antoniewicz, and K. D. Krambeer, *NASA Reference Publication 1207, Derivation and Definition of a Linear Aircraft Model*, Tech. Rep. (NASA, 1988).
- [2] J. A. Mulder, J. C. van der Vaart, and M. Mulder, *Atmospheric Flight Dynamics* (Technical University Delft, Faculty LR, 2007).
- [3] P. H. Zipfel, *Modeling and Simulation of Aerospace Vehicle Dynamics* (AIAA, 2007).
- [4] H. Horlings, *Staying Alive With a Dead Engine*, in *Proceedings - European Aviation Safety Seminar, EASS, Athens, Greece March 13-15* (2006).
- [5] P. Le Blaye, *Agility: History, Definitions and Basic Concepts*, Tech. Rep. (NATO, 2000).
- [6] H. Allen editor, *Dictionary of Technical Terms for Aerospace Use. NASA SP-7* (NASA, 1965).
- [7] Anon., *Volume II Flying Qualities Chapter 1: Introduction to Flying Qualities* (USAF TPS, Edwards AFB CA, 1991).
- [8] J. C. Gibson, *The Definition, Understanding and Design of Aircraft Handling Qualities*, Tech. Rep. Report LR-756 (TUDelft, 1995).
- [9] K. N. Hossain, V. Sharma, M. B. Bragg, and P. G. Voulgaris, *Envelope Protection and Control Adaptation in Icing Encounters*, in *41st Aerospace Sciences Meeting and Exhibit, Reno, NV; USA; Jan. 6-9* (2003).
- [10] T. L. J. Lombaerts, S. Schuet, D. Acosta, J. Kaneshige, K. Shish, and L. Martin, *Piloted Simulator Evaluation of Maneuvering Envelope Information for Flight Crew Awareness*, in *Proc. of the AIAA Guidance, Navigation, and Control Conference 2015, MGNC 2015 - Held at the AIAA SciTech Forum 2015, Kissimmee, USA* (2015).
- [11] Anon., *T.O.-1C-135(K)* (The Boeing Company, 2002).
- [12] H. J. Koolstra and M. M. van Paassen, *Investigation in the Boundaries of Thrust Based Longitudinal Control*, TBD (To be published).
- [13] L. P. Trottier, H. J. Koolstra, G. K. Bruce, T. H. Thacker, J. P. P., and H. H. Reda, *Limited Static Air Minimum Control Speed Testing using the Thrust-Moment-Coefficient Method*, Tech. Rep. (USAF TPS, Edwards AFB, CA, 1985).
- [14] Anon., *Flight Manual F16A/B* (LMTAS, 1996).
- [15] V. Stepanyan, K. Krishnakumar, and N. Nguyen, *Adaptive Control of a Transport Aircraft Using Differential Thrust*, in *Proc. of the AIAA Guidance, Navigation, and Control Conference and Exhibit, Chigago, USA, Aug. 10-13* (2009).
- [16] Anon., *Aviation-Safety-Database*, Aviation Safety Network website (1985), [/http://aviation-safety.net/database/record.php?id=19850812-1](http://aviation-safety.net/database/record.php?id=19850812-1).

- [17] Anon., *Aviation-Safety-Database*, Aviation Safety Network website (2014), <http://www.aviation-safety.net/database/dblist.php?Event=WXT>.
- [18] W. C. Durham, *Aircraft Dynamics and Control* (Virginia Polytechnic Institute and State University Blacksburg, Virginia, 2002).
- [19] H. J. Koolstra, H. J. Damveld, and J. A. Mulder, *Envelope Determination of Damaged Aircraft*, in *Proc. of the AIAA Guidance, Navigation, and Control Conference 2012, Minneapolis, USA, Aug. 13-16* (AIAA, 2012).
- [20] Anon., *Volume II, Flying Qualities Phase, Chapter 8, Engine-Out Operations* (USAF TPS, Edwards AFB, CA, 1988).
- [21] Anon., *Performance Theory and Flight Test Techniques* (USAF TPS, Edwards AFB, CA, 1979).
- [22] G. J. D. Zondervan, *A Review of Propeller Modelling Techniques Based on Euler Methods* (Delft University Press, 1998).
- [23] J. Manné, N.L.L. *Rapport A 1508 A; Windtunnel Onderzoek naar de Invloed van de Vliegtuigconfiguratie op Gier- en Rolmoment ten Gevolge van het Uitvallen van een Motor Bij een Tweemotorig Schroefvliegtuig*, Tech. Rep. (NLR, 1962).
- [24] J. Manné, N.L.L. *Rapport A 1508 B; Windtunnel Investigation on the Influence of the Aircraft Configuration on the Yawing and Rolling Moment of a Twin Engined, Propeller-Driven Aircraft with one Engine Inoperative*, Tech. Rep. (NLR, 1963).
- [25] M. J. T. Schroiijen, L. L. M. Veldhuis, and R. Slingerland, *Propeller Empennage Interaction Effects on Vertical Tail Design of Multiengine Aircraft*, *Journal of Aircraft* **47**, 1133 (2010).
- [26] L. L. M. Veldhuis, *Propeller Wing Aerodynamic Interference*, Ph.D. thesis, Technical University Delft (2005).
- [27] M. J. T. Schroiijen and R. Slingerland, *Propeller Slipstream Effects on Directional Aircraft Control with One Engine Inoperative*, in *Collection of Technical Papers - 45th AIAA Aerospace Sciences Meeting, Reno, USA, January 8-11*, Vol. 18 (2007) pp. 12592-12604.
- [28] R. J. de Muynck and M. Van Hesse, *The A-Priori Simulator Software Package of the Piper PA34 Seneca III*, Tech. Rep. (TU Delft, 1990).

# 4

## DESIGN OF THE $V_c$ -ALGORITHM



## 4.1. INTRODUCTION

In the previous chapter we have defined the limits for sufficient lateral control. In this chapter we will derive a state-space model that can be used for an aircraft that is damaged and, consequently, may have an unknown inertia tensor and c.g. location. This model will be used for model parameter identification as well as for the prediction of the lateral control limit. Based on the parameters of this model, we will derive the algorithm to estimate the  $V_c$ . This algorithm is based on the standard roll performance equations, but we need to apply six corrections in order for the algorithm to work properly.

## 4.2. DERIVATION OF STATE SPACE MODEL AROUND AN ARBITRARY REFERENCE POINT

When an aircraft is damaged, its c.g. location, its mass and the inertia tensor may not be known. This means that our parameter identification as well as the calculation of the  $V_c$  should somehow take all these uncertainties into account. For this purpose we derive the State Space lateral-directional model around an *arbitrary* reference point. We follow the same notation as the author of [1], which implies the following rules:

- Frames are physical entities in which the problem is defined. We typically use the Body frame and the Inertial frame. Coordinate systems are the enumeration of the Euclidean space and may or may not coincide with a reference frame or have a fixed orientation in respect to a reference frame. Coordinate system are chosen to fit the problem.
- Square brackets denote the coordinate systems.  $[\mathbf{x}]^B$  means that  $\mathbf{x}$  is expressed in body coordinates.
- For vectors we use bold lower case, for matrices bold upper case and for scalars normal script.
- For points we use subscripts:  $\mathbf{s}_{BA}$  is the displacement vector from B to A.
- The superscript denotes which frame is involved.  $\mathbf{v}^I$  is the velocity vector  $\mathbf{v}$  in the inertial frame; and  $[\mathbf{v}^I]^B$  expresses this vector in body coordinates or  $[u \ v \ w]^T$ ;
- $T^{BA}$  is the transformation from coordinate system A to coordinate system B.
- The 'over bar'  $\overline{[\ ]}$  is used to indicate the transpose.
- $\mathbf{\Omega}$  is the skew symmetric matrix form of the rotation vector  $\boldsymbol{\omega}$  that transforms the cross product  $\boldsymbol{\omega} \times \mathbf{x}$  to the matrix multiplication  $\mathbf{\Omega}\mathbf{x}$ .  $[\boldsymbol{\omega}^{BI}]^B$  denotes the rotation vector of the body reference frame with respect to the inertia frame, expressed in body coordinates. In a similar way, the displacement vector  $\mathbf{s}_{BA}$  is written as  $\mathbf{S}_{BA}$  when used in a vector multiplication, e.g., the moment of gravity is  $\mathbf{s} \times m\mathbf{g} = \mathbf{S}_{BA}m\mathbf{g}$
- $m$  denotes the mass,  $m^B$  is the mass of body B.

- $\mathbf{I}_{B_r}^B$  is the inertia tensor in the body frame around point  $B_r$ .
- $[D^I]$  is the rotational time derivative, which is, in this case, expressed in the inertial frame. For a rank 1 tensor  $\mathbf{x}$  it is defined as:

$$[D^I \mathbf{x}]^B = \left[ \frac{d\mathbf{x}}{dt} \right]^B + [T]^{BI} \overline{\left[ \frac{dT}{dt} \right]^{BI}} [\mathbf{x}]^B \quad (4.1)$$

For the derivation of the equations two transformations are required, the Euler transformation and the Grubin transformation. The Euler transformation is used to change the reference frame of the rotational time derivative. Typically, Newton's laws are expressed in an inertia frame but measurements are often in the body frame. The Euler transformation is defined in [1, p 111]:

$$D^A \mathbf{x} = D^B \mathbf{x} + \boldsymbol{\Omega}^{BA} \mathbf{x}, \quad (4.2)$$

where  $\mathbf{x}$  is an arbitrary vector and  $\boldsymbol{\Omega}^{BA}$  the skew rotation matrix, that expresses the rotation of frame  $B$  with respect to frame  $A$ .

The Grubin transformation is used to correct for the additional forces that are experienced in a reference point  $B_r$  which is dislocated from the c.g.  $B_c$ . These forces are the centrifugal force and the force due to angular acceleration. For translational dynamics Newton's second law can be expressed as [1, p 153]:

$$m^B D^I \mathbf{v}_{B_r}^I = \mathbf{f} - m^B (\boldsymbol{\Omega}^{BI} \boldsymbol{\Omega}^{BI} \mathbf{s}_{B_c B_r} + D^I \boldsymbol{\Omega}^{BI} \mathbf{s}_{B_c B_r}) \quad (4.3)$$

where  $\mathbf{s}_{B_c B_r}$  is the vector from the body c.g. to the arbitrary reference point,  $m^B$  is the body mass,  $\mathbf{f}$  represents the forces at  $B_r$  and the before last and last terms represent, respectively, the correction to the forces due to centrifugal acceleration and angular acceleration. For rotational dynamics the Grubin transformation gives the following correction on the moment equation [1, p 188]:

$$D^I (\mathbf{I}_{B_r}^B \boldsymbol{\omega}^{BI}) = \mathbf{m}_{B_r} - m^B \mathbf{S}_{B_c B_r} D^I \mathbf{v}_{B_r}^I \quad (4.4)$$

Here  $\mathbf{m}_{B_r}$  is the moment around  $B_r$  and the last term is the additional Grubin term. Comparing this additional term with Eq. 4.3 shows that this correction is equal to Eq. 4.3 vector multiplied with  $\mathbf{S}_{B_c B_r}$ . Because the forces experienced in  $B_r$ , and corrected for the Grubin acceleration, are equivalent to the forces experienced in the c.g.  $B_c$ , we can also state that the correction for the moment equation is equal to the forces at the c.g. vector multiplied by  $\mathbf{S}_{B_c B_r}$ .

We start our derivation with the following two equations [1, p. 160] which relate angular and linear acceleration in the rotating body coordinate systems (B), with moments and forces in the body coordinate systems.

$$[\mathbf{f}]^B = m^B [\dot{\mathbf{v}}_B^I]^B + m^B [\boldsymbol{\Omega}^{BI}]^B [\mathbf{v}_{B_r}^I]^B \quad (4.5)$$

$$[\mathbf{m}]^B = \mathbf{I}_{B_c}^B [\dot{\boldsymbol{\omega}}^{BI}]^B + [\boldsymbol{\Omega}^{BI}]^B \mathbf{I}_{B_c}^B [\boldsymbol{\omega}^{BI}]^B \quad (4.6)$$

From these two equations the complete set of dynamic equations can be derived. There are two different uses for this set of equations: First they can be used for parameter identification. If the mass and the inertia tensor are known, the terms of the equation on the right-hand side of the equal sign are known or can be measured and are used to solve the left-hand side. The coefficients on the left-hand side can be solved, given that independent variables are known. The second use is to determine the aircraft trajectory based on inputs, aerodynamic coefficients, the inertia tensor, mass and aircraft state. In this situation the equations have to be rearranged to solve for  $\dot{\mathbf{v}}$  and  $\dot{\boldsymbol{\omega}}$ :

$$[\dot{\mathbf{v}}_B^I]^B = \frac{1}{m^B} [\mathbf{f}]^B - [\boldsymbol{\Omega}^{BI}]^B [\mathbf{v}_{B_c}^I]^B \quad (4.7)$$

$$[\dot{\boldsymbol{\omega}}^{BI}]^B = (\mathbf{I}_B^B)^{-1} ([\mathbf{m}]^B - [\boldsymbol{\Omega}^{BI}]^B \mathbf{I}_B^B [\boldsymbol{\omega}^{BI}]^B) \quad (4.8)$$

These equations are sufficient for many applications, however, in case of a damaged aircraft, the inertia tensor, mass and c.g. location might not be known. In that case a reference point  $B_r$  has to be used, for example the position of the IMU where the accelerations and rotations are measured<sup>1</sup>. This approach will give a new set of equations that can be used under all circumstances. We will first derive the equation for side force and then for the yaw and roll moments.

#### SIDE FORCE

The translational dynamic equation for a rigid body with mass  $m^B$  and inertial velocity  $\mathbf{v}_{B_r}^I$  at the reference point  $B_r$ , which is dislocated from the c.g.  $B_c$  [1, p. 187] was already presented in Eq. 4.3 and is repeated here for clarity:

$$m^B D^I \mathbf{v}_{B_r}^I = \mathbf{f} - m^B (\boldsymbol{\Omega}^{BI} \boldsymbol{\Omega}^{BI} \mathbf{s}_{B_c B_r} + D^I \boldsymbol{\Omega}^{BI} \mathbf{s}_{B_c B_r})$$

where  $\mathbf{f}$  represents all the external forces and  $\mathbf{s}_{B_c B_r}$  is the vector from  $B_r$  to the c.g.  $B_c$ . The last two terms represent the Grubin corrections. To express all forces and accelerations in the body frame, the Euler transformation [1] has to be applied to the rotational derivative; expressing all elements in body coordinates gives:

$$m^B \left( \left[ \frac{d\mathbf{v}_{B_r}^I}{dt} \right]^B + [\boldsymbol{\Omega}^{BI}]^B [\mathbf{v}_{B_r}^I]^B \right) = [\mathbf{f}]^B - [m^B (\boldsymbol{\Omega}^{BI} \boldsymbol{\Omega}^{BI} \mathbf{s}_{B_c B_r} + D^I \boldsymbol{\Omega}^{BI} \mathbf{s}_{B_c B_r})]^B, \quad (4.9)$$

which can be elaborated as:

<sup>1</sup>If the IMU is part of an INS, it is able to give the inertial accelerations, otherwise it measures specific forces that must be reduced to accelerations.

$$\begin{aligned} \frac{[\mathbf{f}]^B}{m^B} &= \begin{bmatrix} \dot{u} \\ \dot{v} \\ \dot{w} \end{bmatrix} + \begin{bmatrix} 0 & -r & q \\ r & 0 & -p \\ -q & p & 0 \end{bmatrix} \begin{bmatrix} u \\ v \\ w \end{bmatrix} + \\ &+ \begin{bmatrix} 0 & -r & q \\ r & 0 & -p \\ -q & p & 0 \end{bmatrix} \begin{bmatrix} 0 & -r & q \\ r & 0 & -p \\ -q & p & 0 \end{bmatrix} \begin{bmatrix} \Delta x \\ \Delta y \\ \Delta z \end{bmatrix} + \begin{bmatrix} 0 & -\dot{r} & \dot{q} \\ \dot{r} & 0 & -\dot{p} \\ -\dot{q} & \dot{p} & 0 \end{bmatrix} \begin{bmatrix} \Delta x \\ \Delta y \\ \Delta z \end{bmatrix} \quad (4.10) \end{aligned}$$

When we express the sum of the aerodynamic and propulsive forces as  $\mathbf{f} = \overline{[X \ Y \ Z]}$  and move the gravity to the right-hand side, Eq. 4.10 can be rewritten for the side force  $Y$  as:

$$Y = m^B ((\dot{v} + ru - pw) + (pq + \dot{r})\Delta x - (p^2 + r^2)\Delta y + (qr - \dot{p})\Delta z - g \cos\theta \sin\varphi) \quad (4.11)$$

Dividing by  $m^B$  and  $V$ , and recognizing that  $\frac{u}{V} = \sin\alpha$ ,  $\frac{v}{V} = \cos\alpha$ ,  $\frac{w}{V} = \sin\beta$  we can rewrite the equation to:

$$\dot{\beta} = \frac{Y}{Vm} - r \cos\alpha + p \sin\alpha + \frac{g \cos\theta \sin\varphi}{V} - \frac{(pq + \dot{r})\Delta x - (p^2 + r^2)\Delta y + (qr - \dot{p})\Delta z}{V} \quad (4.12)$$

Changing to non-dimensional roll rates and non-dimensional mass ( $\mu_b = m/\rho S b$ ) and recognizing that  $Y = \frac{1}{2}\rho C_y S V^2$  gives:

$$\begin{aligned} \dot{\beta} &= \frac{C_y \cdot \frac{1}{2} \rho V^2 S}{V \mu_b \rho S b} - \frac{rb}{2V} \left( \frac{2V}{b} \cos\alpha \right) + \frac{pb}{2V} \cdot \left( \frac{2V}{b} \cdot \sin\alpha \right) + \frac{g \cos\theta \sin\varphi}{V} + \\ &\quad - \left( \left( \frac{pb}{2V} \right) \left( \frac{qb}{2V} \right) + 0.5 \left( \frac{\dot{r} b^2}{2V^2} \right) \right) \left( \frac{4V\Delta x}{b^2} \right) + \\ &\quad + \left( \left( \frac{pb}{2V} \right)^2 + \left( \frac{rb}{2V} \right)^2 \right) \left( \frac{4V\Delta y}{b^2} \right) + \\ &\quad - \left( \left( \frac{qb}{2V} \right) \left( \frac{rb}{2V} \right) + 0.5 \left( \frac{\dot{p} b^2}{2V^2} \right) \right) \left( \frac{4V\Delta z}{b^2} \right) \quad (4.13) \end{aligned}$$

Multiplying by  $\frac{b}{V}$  removes velocity dependencies from all the dependent variables and expresses the derivatives in non-dimensional time. Moving all measured fractions to the left gives:

$$\begin{aligned} \frac{b\dot{\beta}}{V} + \frac{rb}{2V} 2 \cos(\alpha) - \frac{pb}{2V} 2 \sin(\alpha) - \frac{bg \cos(\theta) \sin(\varphi)}{V^2} &= \frac{C_y}{2\mu_b} - \frac{4\Delta x}{b} \left( \frac{pb}{2V} \frac{qb}{2V} + 0.5 \frac{\dot{r} b^2}{2V^2} \right) + \\ &+ \frac{4\Delta y}{b} \left( \left( \frac{pb}{2V} \right)^2 + \left( \frac{rb}{2V} \right)^2 \right) - \frac{4\Delta z}{b} \left( \frac{qb}{2V} \frac{rb}{2V} - 0.5 \frac{\dot{p} b^2}{2V^2} \right) \quad (4.14) \end{aligned}$$

The aerodynamic side force  $C_y$  can be expressed as a function of its derivatives. From many textbooks like [2] we know that aerodynamic forces depend on the following variables:  $\alpha$ ,  $\beta$ , Mach, control deflections, roll, yaw and pitch rate and also on higher order

forms, combinations and derivatives of these variables. The optimum number of variables is determined later in Chapter 5. For now we limit ourselves to the most important parameters:

$$C_y = y_\beta \beta + y_p^* \left( \frac{pb}{2V} \right) + y_r^* \left( \frac{rb}{2V} \right) + y_{\delta_c} \delta_c \quad (4.15)$$

where, for shortness of notation,  $\delta_c$  is the input from all controls including the engine inputs. Substituting Eq. 4.15 in Eq. 4.14, and renaming the dependent variables  $y$ , so  $-\frac{4\Delta x}{b} = y_x$ ,  $-\frac{4\Delta y}{b} = y_y$  and  $-\frac{4\Delta z}{b} = y_z$ , the equation to be solved becomes:

$$\begin{aligned} \frac{b\dot{\beta}}{V} + \frac{rb}{2V} 2 \cos(\alpha) - \frac{pb}{2V} 2 \sin(\alpha) - \frac{bg \cos(\theta) \sin(\varphi)}{V^2} = y_\beta \beta + y_p^* \left( \frac{pb}{2V} \right) + y_r^* \left( \frac{rb}{2V} \right) + y_{\delta_c} \delta_c + \\ + y_x \left( \frac{pb}{2V} \frac{qb}{2V} + 0.5 \frac{rb^2}{2V^2} \right) + y_y \left( \left( \frac{pb}{2V} \right)^2 + \left( \frac{rb}{2V} \right)^2 \right) + y_z \left( \frac{qb}{2V} \frac{rb}{2V} - 0.5 \frac{pb^2}{2V^2} \right) \end{aligned} \quad (4.16)$$

Equation 4.16 is the form used for parameter identification with all measured parameters on the left-hand side. For the derivation of the  $V_c$  algorithm later this chapter, we need to move the terms  $\frac{rb}{2V} 2 \cos(\alpha)$ ,  $-\frac{pb}{2V} 2 \sin(\alpha)$  and  $-\frac{bg \cos(\theta) \sin(\varphi)}{V^2}$  to the right. Combining these terms gives:  $y_r = y_r^* - 2 \cos \alpha$  and  $y_p = y_p^* + 2 \sin \alpha$ , while the last term now becomes  $y_\phi \phi$  which gives:

$$\begin{aligned} \frac{b\dot{\beta}}{V} = y_\beta \beta + y_\phi \phi + y_p \left( \frac{pb}{2V} \right) + y_r \left( \frac{rb}{2V} \right) + y_{\delta_c} \delta_c + \\ + y_x \left( \frac{pb}{2V} \frac{qb}{2V} + 0.5 \frac{rb^2}{2V^2} \right) + y_y \left( \left( \frac{pb}{2V} \right)^2 + \left( \frac{rb}{2V} \right)^2 \right) + y_z \left( \frac{qb}{2V} \frac{rb}{2V} - 0.5 \frac{pb^2}{2V^2} \right) \end{aligned} \quad (4.17)$$

#### LATERAL MOMENTS

We start with Eq. 4.8 and apply the Grubin transformation as given in Eq. 4.4. If the displacement vector from the c.g. ( $B_c$ ) to the reference point  $B_r$  is defined as  $\mathbf{s}_{B_c B_r}$  the equation is:

$$[\mathbf{I}_B^B]^B \left[ \frac{\delta \omega^{BI}}{\delta t} \right]^B + [\boldsymbol{\Omega}^{BI}]^B [\mathbf{I}_B^B]^B [\omega^{BI}]^B = [\mathbf{m}_{B_r}]^B - m^B \mathbf{S}_{BR} D^I \mathbf{v}_{B_r}^I \quad (4.18)$$

Using Eq. 4.3 we can express the Grubin correction term  $m^B \mathbf{S}_{BR} D^I \mathbf{v}_{B_r}^I$  as:

$$m^B \mathbf{S}_{BR} D^I \mathbf{v}_{B_r}^I = \mathbf{S}_{BR} (f - m^B (\boldsymbol{\Omega}^{BI} \boldsymbol{\Omega}^{BI} \mathbf{s}_{B_c B_r} + D^I \boldsymbol{\Omega}^{BI} \mathbf{s}_{B_c B_r})) \quad (4.19)$$

This means that the correction is equal to the forces experienced at  $B_r$  minus the additional acceleration forces due to the rotation and rotation acceleration of  $B_r$  relative to the c.g.  $B_c$ , and this result pre-multiplied with  $\mathbf{S}_{B_c B_r}$ . However, if we use the forces at the c.g. the last two terms will vanish. In our simulations, this is the case<sup>2</sup>. But if we

<sup>2</sup>If the accelerations are not measured at the c.g., these measured accelerations, probably close to  $B_r$ , must be corrected to the c.g. To do this the vector  $\mathbf{s}_{B_c B_r}$  must be estimated, this is possible using Eq. 4.17 to find  $y_x$ ,  $y_y$  and  $y_z$ , and these parameters can be transformed to  $\Delta x$ ,  $\Delta y$  and  $\Delta z$ .

want to separate the effect of a c.g. change from these equations we have to realize that the moment  $\mathbf{m}_{B_r}$  also contains the moment due to the shifted c.g. which is  $m^B \mathbf{S}_{B_c B_r} \mathbf{g}$ . Using  $\mathbf{m}_{B_r} = \mathbf{m}_{B_r}^* + m^B \mathbf{S}_{B_c B_r} \mathbf{g}$ , where  $\mathbf{m}_{B_r}^*$  is the moment at  $B_r$  before the c.g. shift, and using the corrected forces measured at the c.g., Eq. 4.18 can be changed to:

$$[\mathbf{I}_{B_c}^B]^B \left[ \frac{\delta \omega^{BI}}{\delta t} \right]^B + [\boldsymbol{\Omega}^{BI}]^B [\mathbf{I}_{B_c}^B]^B [\omega^{BI}]^B = [\mathbf{m}_{B_c}^*]^B - m^B [\mathbf{S}_{B_c B_r}]^B \left( \left[ \frac{\mathbf{f}}{m^B} \right]^B + [\mathbf{g}]^B \right) \quad (4.20)$$

We can either transform  $\frac{\mathbf{f}}{m^B}$  and  $\mathbf{g}$  separately to body coordinates, which is done for example in [3] or realize that  $(\frac{\mathbf{f}}{m^B} + \mathbf{g})$  is equal to the total acceleration sensed at the c.g. We take the second approach, now Eq. 4.20 expressed in the body frame simplifies to:

$$[\mathbf{I}_{B_c}^B]^B \left[ \frac{\delta \omega^{BI}}{\delta t} \right]^B + [\boldsymbol{\Omega}^{BI}]^B [\mathbf{I}_{B_c}^B]^B [\omega^{BI}]^B = \begin{bmatrix} m_x^* \\ m_y^* \\ m_z^* \end{bmatrix}^B - m \begin{bmatrix} 0 & -\Delta z & \Delta y \\ \Delta z & 0 & -\Delta x \\ -\Delta y & \Delta x & 0 \end{bmatrix} \begin{bmatrix} a_x \\ a_y \\ a_z \end{bmatrix} \quad (4.21)$$

With this restructuring of the equation we have achieved a situation where the c.g. shift parameters are directly linked with the acceleration variables which are readily available in flight. In addition, it represents a more compact description than traditional ones as for example given in [3]. On top of that, all aerodynamic and thrust moments are still related to the standard reference point and will not be affected by a c.g. change. We expect that this formulation will simplify our parameter identification. Using this last form, the moment equations for roll and yaw can be derived from Eq. 4.21 and give:

$$m_x = I_{xx} \dot{p} + I_{xz} \dot{r} + I_{xy} \dot{q} - I_{yx} r p - I_{yy} r q - I_{yz} r^2 + I_{zx} q p + I_{zy} q^2 + I_{zz} q r - m \Delta z a_y + m \Delta y a_z, \quad (4.22)$$

and:

$$m_z = I_{zx} \dot{p} + I_{zz} \dot{r} + I_{zy} \dot{q} - I_{xx} q p - I_{xy} q^2 - I_{xz} q r + I_{yx} p^2 + I_{yy} p q + I_{yz} p r - m \Delta y a_x + m \Delta x a_y \quad (4.23)$$

For ease of further manipulation we group all terms that do not involve  $\dot{p}$  or  $\dot{r}$  in R1 and R2:

$$R1 = I_{xy} \dot{q} - I_{yx} r p - I_{yy} r q - I_{yz} r^2 + I_{zx} q p + I_{zy} q^2 + I_{zz} q r - m \Delta z a_y + m \Delta y a_z \quad (4.24)$$

$$R2 = I_{zy} \dot{q} - I_{xx} q p - I_{xy} q^2 - I_{xz} q r + I_{yx} p^2 + I_{yy} p q + I_{yz} p r - m \Delta y a_x + m \Delta x a_y \quad (4.25)$$

Now the equations can be rewritten to:

$$\begin{aligned} m_x &= I_{xx}\dot{p} + I_{xz}\dot{r} + R1 \\ m_z &= I_{zx}\dot{p} + I_{zz}\dot{r} + R2 \end{aligned} \quad (4.26)$$

Solving these equations for  $\dot{p}$  and  $\dot{r}$  gives:

$$\dot{p} \left( 1 - \frac{I_{xz}I_{xz}}{I_{xx}I_{zz}} \right) = \frac{m_x}{I_{xx}} - \frac{I_{xz}m_z}{I_{xx}I_{zz}} + \frac{I_{xz}R2}{I_{xx}I_{zz}} - \frac{R1}{I_{xx}} \quad (4.27)$$

and:

$$\dot{r} \left( 1 - \frac{I_{xz}I_{xz}}{I_{xx}I_{zz}} \right) = \frac{m_z}{I_{zz}} - \frac{I_{xz}m_x}{I_{xx}I_{zz}} + \frac{I_{xz}R1}{I_{xx}I_{zz}} - \frac{R2}{I_{zz}} \quad (4.28)$$

Moving to our goal to express  $\dot{p}$  and  $\dot{r}$  in relation to the coefficients  $C_l$  and  $C_n$  we move to non-dimensional units. Using the following relations for the inertia tensor elements:  $I_{xx} = mb^2K_{xx}^2$ ,  $I_{zz} = mb^2K_{zz}^2$ ,  $I_{zx} = mb^2J_{zx}$ , the inverse of  $\left( 1 - \frac{I_{xz}I_{xz}}{I_{xx}I_{zz}} \right)$  can be expressed as  $\left( \frac{K_{xx}^2K_{zz}^2}{A} \right)$ , where  $A = \left( K_{xx}^2K_{yy}^2 - (J_{zx})^2 \right)$ . Applying this in Eq. 4.27 and 4.28 gives:

$$\dot{p} = \left( \frac{K_{zz}^2}{A} \right) \left( \frac{m_x}{mb^2} \right) - \left( \frac{J_{zx}}{A} \right) \left( \frac{m_z}{mb^2} \right) + \left( \frac{J_{zx}}{A} \right) \frac{R2}{mb^2} - \left( \frac{K_{zz}^2}{A} \right) \left( \frac{R1}{mb^2} \right) \quad (4.29)$$

and:

$$\dot{r} = \left( \frac{K_{xx}^2}{A} \right) \left( \frac{m_z}{mb^2} \right) - \left( \frac{J_{zx}}{A} \right) \left( \frac{m_x}{mb^2} \right) + \left( \frac{J_{zx}}{A} \right) \frac{R1}{mb^2} - \left( \frac{K_{xx}^2}{A} \right) \left( \frac{R2}{mb^2} \right) \quad (4.30)$$

Next we use that the mass  $m$  can be expressed as  $m = \rho S b \mu_b$ ,  $m_x = q S b C_l$  and  $m_z = q S b C_n$ . Consequently  $\frac{m_x}{mb^2}$  changes to  $\frac{0.5\rho V^2 S b C_l}{\rho S b \mu_b b^2}$  or  $\frac{2V^2}{4\mu_b b^2} C_l$ , and in a similar way  $\frac{m_z}{mb^2}$  changes to  $\frac{2V^2}{4\mu_b b^2} C_n$ :

$$\dot{p} = \left( \frac{K_{zz}^2}{4\mu_b A} \right) \left( \frac{2V^2}{b^2} \right) C_l - \left( \frac{J_{zx}}{4\mu_b A} \right) \left( \frac{2V^2}{b^2} \right) C_n + \left( \frac{J_{zx}}{A m b^2} \right) R2 - \left( \frac{K_{zz}^2}{A m b^2} \right) R1, \quad (4.31)$$

and:

$$\dot{r} = \left( \frac{K_{xx}^2}{4\mu_b A} \right) \left( \frac{2V^2}{b^2} \right) C_n - \left( \frac{J_{zx}}{4\mu_b A} \right) \left( \frac{2V^2}{b^2} \right) C_l + \left( \frac{J_{zx}}{A m b^2} \right) R1 - \left( \frac{K_{xx}^2}{A m b^2} \right) R2 \quad (4.32)$$

Now we multiply Eq. 4.31 and 4.32 by  $\frac{b^2}{V^2}$  which removes the velocity dependence from the first two terms on the right hand side and restores the non-dimensional relationship in the aerodynamic derivatives. This gives:

$$\frac{\dot{p}b^2}{2V^2} = (K_{zz}^2 C_l - J_{zx} C_n) \frac{1}{4A\mu_b} + \left(\frac{b^2}{2V^2}\right) \left(\frac{J_{zx}}{Amb^2}\right) R2 - \left(\frac{b^2}{2V^2}\right) \left(\frac{K_{zz}^2}{Amb^2}\right) R1 \quad (4.33)$$

Similarly, Eq. 4.32 will transform to:

$$\frac{\dot{r}b^2}{2V^2} = (K_x^2 C_n - J_{zx} C_l) \frac{1}{4A\mu_b} + \left(\frac{b^2}{2V^2}\right) \left(\frac{J_{zx}}{Amb^2}\right) R1 - \left(\frac{b^2}{2V^2}\right) \left(\frac{K_{xx}^2}{Amb^2}\right) R2 \quad (4.34)$$

$C_l$  and  $C_n$  are the standard roll and yaw moment coefficients that are dependent on  $\frac{pb}{2V}$ ,  $\frac{rb}{2V}$ ,  $\beta$ , the control deflections  $\delta_a$ ,  $\delta_r$  and the normalized thrust moments for left and right engine  $\delta_{TL}$  and  $\delta_{TR}$ . The here derived stability derivatives in state space form for an aircraft with an unknown c.g. and inertia tensor, are all linear combinations of the well known  $C_l$  and  $C_n$  derivatives.

It is interesting to note that some publications [2, p. 152] don't use the non-dimensional accelerations  $\frac{\dot{p}b^2}{2V^2}$  and  $\frac{\dot{r}b^2}{2V^2}$  but  $\dot{p}$  and  $\dot{r}$ . The result is that the new state space derivatives are not just linear combinations of the  $C_n$  and  $C_l$  derivatives but are also velocity dependent, making this form less suitable for parameter identification.

The next step is to solve for the last two terms, involving  $R1$  and  $R2$ , in both equations. First  $\left(\frac{b^2}{2V^2}\right) \left(\frac{J_{zx}}{Amb^2}\right) R2$  stands for:

$$\left(\frac{b^2}{2V^2}\right) \left(\frac{J_{zx}}{Amb^2}\right) (I_{zy}\dot{q} - I_{xx}qp - I_{xy}q^2 - I_{xz}qr + I_{yx}p^2 + I_{yy}pq + I_{yz}pr - m\Delta y a_x + m\Delta x a_y)$$

using the fact that the inertia moments can be expressed as  $mb^2$  times their non-dimensional form, and moving to non-dimensional rates gives:

$$\begin{aligned} \left(\frac{b^2}{2V^2}\right) \left(\frac{J_{zx}}{Amb^2}\right) R2 = & \left(\frac{J_{zx}}{A}\right) \left(J_{zy} \left(\frac{b^2\dot{q}}{2V^2}\right) - 2K_{xx}^2 \left(\frac{bqbpp}{2V2V}\right) - 2J_{yx} \left(\frac{bq}{2V}\right)^2 - 2J_{zx} \left(\frac{bqbr}{2V2V}\right) + \right. \\ & \left. + 2J_{yx} \left(\frac{bp}{2V}\right)^2 + 2K_{yy}^2 \left(\frac{bpbq}{2V2V}\right) + 2J_{yx} \left(\frac{bpbpr}{2V2V}\right) - \frac{\Delta y}{b} \left(\frac{ba_x}{2V^2}\right) + \frac{\Delta x}{b} \left(\frac{ba_y}{2V^2}\right) \right) \quad (4.35) \end{aligned}$$

In a similar way  $-\left(\frac{b^2}{2V^2}\right) \left(\frac{K_{zz}^2}{Amb^2}\right) R1$  is:

$$-\left(\frac{b^2}{2V^2}\right) \left(\frac{K_{zz}^2}{Amb^2}\right) (I_{xy}\dot{q} - I_{yx}rp - I_{yy}rq - I_{yz}r^2 + I_{zx}qp + I_{zy}q^2 + I_{zz}qr - m\Delta z a_y + m\Delta y a_z)$$

and can be changed to:

$$\begin{aligned} -\left(\frac{b^2}{2V^2}\right) \left(\frac{K_{zz}^2}{Amb^2}\right) R1 = & \left(\frac{-K_{zz}^2}{A}\right) \left(J_{xy} \left(\frac{b^2\dot{q}}{2V^2}\right) - 2J_{xy} \left(\frac{brbpb}{2V2V}\right) - 2K_{yy}^2 \left(\frac{brbq}{2V2V}\right) - 2J_{yz} \left(\frac{br}{2V}\right)^2 + \right. \\ & \left. + 2J_{zx} \left(\frac{bqbpb}{2V2V}\right) + 2J_{zy} \left(\frac{qb}{2V}\right)^2 + 2K_{zz}^2 \left(\frac{bqbr}{2V2V}\right) - \frac{\Delta z}{b} \left(\frac{a_y b}{2V^2}\right) + \frac{\Delta y}{b} \left(\frac{a_z b}{2V^2}\right) \right) \quad (4.36) \end{aligned}$$

and for the yaw equation,  $\left(\frac{b^2}{2V^2}\right)\left(\frac{1_{zx}}{Amb^2}\right)$  R1 is:

$$\left(\frac{b^2}{2V^2}\right)\left(\frac{J_{zx}}{Amb^2}\right)\left(I_{xy}\dot{q} - I_{yx}r p - I_{yy}r q - I_{yz}r^2 + I_{zx}q p + I_{zy}q^2 + I_{zz}q r - m\Delta z a_y + m\Delta y a_z\right)$$

and can be changed to:

$$\begin{aligned} \left(\frac{b^2}{2V^2}\right)\left(\frac{J_{zx}}{Amb^2}\right)R1 = & \left(\frac{I_{zx}}{A}\right)\left(J_{xy}\left(\frac{b^2\dot{q}}{2V^2}\right) - 2J_{xy}\left(\frac{brbp}{2V2V}\right) - 2K_{yy}^2\left(\frac{brbq}{2V2V}\right) - 2J_{yx}\left(\frac{br}{2V}\right)^2 + \right. \\ & \left. + 2(J_{zx})\left(\frac{bqb p}{2V2V}\right) + 2J_{zy}\left(\frac{bq}{2V}\right)^2 + 2K_{zz}^2\left(\frac{bqbr}{2V2V}\right) - \left(\frac{\Delta z}{b}\right)\left(\frac{a_y b}{2V^2}\right) + \left(\frac{\Delta y}{b}\right)\left(\frac{a_z b}{2V^2}\right)\right) \end{aligned} \quad (4.37)$$

and the last term  $-\left(\frac{b^2}{2V^2}\right)\left(\frac{K_{xx}^2}{Amb^2}\right)$  R2 is:

$$-\left(\frac{b^2}{2V^2}\right)\left(\frac{K_{xx}^2}{Amb^2}\right)\left(I_{zy}\dot{q} - I_{xx}q p - I_{xy}q^2 - I_{xz}q r + I_{yx}p^2 + I_{yy}p q + I_{yz}p r - m\Delta y a_x + m\Delta x a_y\right)$$

will change to:

$$\begin{aligned} -\left(\frac{b^2}{2V^2}\right)\left(\frac{K_{xx}^2}{Amb^2}\right)R2 = & \left(\frac{K_{xx}^2}{A}\right)\left(J_{zy}\left(\frac{b\dot{q}}{2V^2}\right) - 2K_{xx}^2\left(\frac{bqb p}{2V2V}\right) - 2J_{xy}\left(\frac{bq}{2V}\right)^2 - 2J_{xz}\left(\frac{bqbr}{2V^2}\right) + \right. \\ & \left. + 2J_{yx}\left(\frac{bp}{2V}\right)^2 + 2K_{yy}^2\left(\frac{bpbq}{2V^2}\right) + 2J_{yz}\left(\frac{bpb r}{2V2V}\right) - \frac{\Delta y}{b}\left(\frac{a_x b}{2V^2}\right) + \frac{\Delta x}{b}\left(\frac{a_y b}{2V^2}\right)\right) \end{aligned} \quad (4.38)$$

We can see that all parameters related to R1 and R2 are dependent on the variables:  $\frac{\dot{q}b^2}{2V^2}$ ,  $\left(\frac{qb}{2V}\right)^2$ ,  $\left(\frac{pb}{2V}\right)^2$ ,  $\left(\frac{rb}{2V}\right)^2$ ,  $\left(\frac{qb}{2V}\frac{pb}{2V}\right)$ ,  $\left(\frac{qb}{2V}\frac{rb}{2V}\right)$ ,  $\left(\frac{pb}{2V}\frac{rb}{2V}\right)$ ,  $\frac{a_x b}{2V^2}$ ,  $\frac{a_y b}{2V^2}$  and  $\frac{a_z b}{2V^2}$ . We can group the parameters for each variable, and these are listed in Table 4.1. It is interesting to note that most terms in lines 2 to 10 of Table 4.1 will be zero if the off-diagonal terms of the inertia tensor are zero. The lines (9 : 11) represent the effect that the reference point is not located in the c.g.

The final form of the State Space equations that we will use is:

$$\begin{aligned} \frac{\dot{p}b^2}{2V^2} = & l_\beta \cdot \beta + l_p \cdot \left(\frac{pb}{2V}\right) + l_r \cdot \left(\frac{rb}{2V}\right) + l_{\delta_a} \cdot \delta_a + l_{\delta_r} \cdot \delta_r + l_{TL} \cdot \delta_{TL} + l_{TR} \cdot \delta_{TR} + \\ & + l_{\dot{q}} \cdot \left(\frac{\dot{q}b^2}{2V^2}\right) + l_{q^2} \cdot \left(\frac{qb}{2V}\right)^2 + l_{p^2} \cdot \left(\frac{pb}{2V}\right)^2 + l_{r^2} \cdot \left(\frac{rb}{2V}\right)^2 + l_{qp} \cdot \left(\frac{qb}{2V}\frac{pb}{2V}\right) + \\ & + l_{qr} \cdot \left(\frac{qb}{2V}\frac{rb}{2V}\right) + l_{pr} \cdot \left(\frac{pb}{2V}\frac{rb}{2V}\right) + l_{ax} \cdot \left(\frac{a_x b}{2V^2}\right) + l_{ay} \cdot \left(\frac{a_y b}{2V^2}\right) + l_{az} \cdot \left(\frac{a_z b}{2V^2}\right) + dF_l \end{aligned} \quad (4.39)$$

and

Table 4.1: Relation between SS parameters and Aerodynamic Coefficients; In line 1 the subscript 'aero' represents all standard partial derivatives for  $C_l$  and  $C_n$  like  $\beta$ ,  $\frac{pb}{2V}$ ,  $\frac{rb}{2V}$ ,  $\delta_a$ ,  $\delta_r$  and  $A = (K_{xx}^2 K_{yy}^2 - (J_{zx})^2)$ . Note that the parameters in lines 2,3,4,5 and 8 will be zero if the off-diagonal terms of the Inertia tensor are zero.

Roll derivatives			Yaw derivatives		
no	name	value	name	value	
1	$l_{aero}$	$(K_{zz}^2 C_{l_{aero}} - J_{xy} C_{n_{aero}}) / (4A\mu_b)$	$n_{aero}$	$(K_{xx}^2 C_{n_{aero}} - J_{zx} C_{l_{aero}}) / (4A\mu_b)$	
2	$l_{\dot{q}}$	$(J_{zx} J_{zy} - K_{zz}^2 J_{xy}) / A$	$n_{\dot{q}}$	$(J_{zx} J_{xy} + K_{xx}^2 J_{zy}) / A$	
3	$l_{q^2}$	$-2(J_{zx} J_{yx} + K_{zz}^2 J_{zy}) / A$	$n_{q^2}$	$2(J_{zx} J_{zy} - K_{xx}^2 J_{xy}) / A$	
4	$l_{p^2}$	$2(J_{zx} J_{yx}) / A$	$n_{p^2}$	$2(K_{xx}^2 J_{yx}) / A$	
5	$l_{r^2}$	$2(K_{zz}^2 J_{yz}) / A$	$n_{r^2}$	$-2(J_{zx} J_{yx}) / A$	
6	$l_{qp}$	$2(J_{zx}(K_{yy}^2 - K_{xx}^2) - K_{zz}^2 J_{zx}) / A$	$n_{qp}$	$2(J_{zx} J_{zx} + K_{xx}^2(K_{yy}^2 - K_{xx}^2)) / A$	
7	$l_{qr}$	$2(-J_{zx} J_{zx} - K_{zz}^2(K_{zz}^2 - K_{yy}^2)) / A$	$n_{qr}$	$2(J_{zx}(K_{zz}^2 - K_{yy}^2) - K_{xx}^2 J_{xz}) / A$	
8	$l_{pr}$	$2(J_{zx} J_{yx} + K_{zz}^2 J_{xy}) / A$	$n_{pr}$	$-2(J_{zx} J_{xy} - K_{xx}^2 J_{yz}) / A$	
9	$l_{ax}$	$(J_{zx}(-\frac{\Delta y}{b})) / A$	$n_{ax}$	$(K_{xx}^2(-\frac{\Delta y}{b})) / A$	
10	$l_{ay}$	$(J_{zx}(\frac{\Delta x}{b}) - K_{zz}^2(-\frac{\Delta z}{b})) / A$	$n_{ay}$	$(J_{zx}(-\frac{\Delta z}{b}) + K_{xx}^2(\frac{\Delta x}{b})) / A$	
11	$l_{az}$	$-(K_{zz}^2(\frac{\Delta y}{b})) / A$	$n_{az}$	$(J_{zx}(\frac{\Delta y}{b})) / A$	

$$\begin{aligned}
\frac{\dot{r}b^2}{2V^2} = & n_{\beta} \cdot \beta + n_p \cdot \left(\frac{pb}{2V}\right) + n_r \cdot \left(\frac{rb}{2V}\right) + n_{\delta_a} \cdot \delta_a + n_{\delta_r} \cdot \delta_r + n_{TL} \cdot \delta_{TL} + n_{TR} \cdot \delta_{TR} + \\
& + n_{\dot{q}} \cdot \left(\frac{\dot{q}b^2}{2V^2}\right) + n_{q^2} \cdot \left(\frac{qb}{2V}\right)^2 + n_{p^2} \cdot \left(\frac{pb}{2V}\right)^2 + n_{r^2} \cdot \left(\frac{rb}{2V}\right)^2 + n_{qp} \cdot \left(\frac{qb}{2V} \frac{pb}{2V}\right) + \\
& + n_{qr} \cdot \left(\frac{qb}{2V} \frac{rb}{2V}\right) + n_{pr} \cdot \left(\frac{pb}{2V} \frac{rb}{2V}\right) + n_{ax} \cdot \left(\frac{axb}{2V^2}\right) + n_{ay} \cdot \left(\frac{ayb}{2V^2}\right) + n_{az} \cdot \left(\frac{azb}{2V^2}\right) + dF_n \quad (4.40)
\end{aligned}$$

In both equations the term  $dF$  represents the additional bias term or off-set from zero. This extra term may be needed in case a damaged aircraft experiences an additional moment (e.g., damaged flap) that is not related to any of the used variables.

### 4.3. BASIC ROLL PERFORMANCE USING A LINEAR MODEL APPROACH

In the previous section the non-linear model was made non-dimensional, linearised, and rewritten in a State Space (SS) form, which will also be used for parameter identification. Our SS presentation differs slightly from the traditional SS presentation as used for example in [2, p. 152]. All rows are multiplied by  $\frac{b}{V}$  to remove all velocity dependencies from the parameters and express the state derivatives in non-dimensional units. The aircraft model parameters are determined over the trajectory flown and are optimized to be independent of  $V$ .<sup>3</sup> If model parameters are not independent of  $V$ , the parameter

<sup>3</sup>But parameters will be dependent on AoA, which is also a velocity dependency. If the model parameter change with AoA is large this may lead to a reset and recalculation of the parameters.

identification model will detect the parameter change after a speed change and reset. For the derivation of the roll performance we can omit all coupled terms because we assume that  $r$  and  $q$  are close to zero. This simplifies Eqs. 4.17, 4.39 and 4.40 to:

$$\frac{b\dot{\beta}}{V} = y_{\beta}\beta + y_{\phi}\phi + y_p\left(\frac{pb}{2V}\right) + y_r\left(\frac{rb}{2V}\right) + y_{\delta_c}\delta_c \quad (4.41)$$

$$\frac{b^2\dot{p}}{2V^2} = l_{\beta}\beta + l_p\left(\frac{pb}{2V}\right) + l_r\left(\frac{rb}{2V}\right) + l_{\delta_c}\delta_c + l_{\delta_{Fn}}\frac{a_z b}{2V^2} \quad (4.42)$$

$$\frac{b^2\dot{r}}{2V^2} = n_{\beta}\beta + n_p\left(\frac{pb}{2V}\right) + n_r\left(\frac{rb}{2V}\right) + n_{\delta_c}\delta_c + n_{\delta_{Fn}}\frac{a_z b}{2V^2} \quad (4.43)$$

In these equations we used the term  $\delta_c$  for compactness, which stands for all applicable control inputs:  $\delta_a$ ,  $\delta_r$ ,  $\delta_{TL}$  and  $\delta_{TR}$ . To correct for the asymmetric c.g., Table 4.1 gave three parameters (line 9-11), for roll control the most important terms in a lateral asymmetry are  $l_{\delta_{Fn}}$  and  $n_{\delta_{Fn}}$  which depend on the vertical acceleration variable or  $\frac{a_z b}{2V^2}$ .

#### METHOD USED

To derive the equations for  $V_c$  we take a two step approach. First, the equation is derived to relate a fixed roll angle change in a specified time to an airspeed based on the available aileron deflection. Second, the available aileron is calculated. In a normal flight situation, the available aileron will be constant with velocity. However if, for example, the aircraft has an engine failure, part of the available aileron travel will be needed to counteract the effects of the asymmetry, and the remaining aileron travel for manoeuvring is limited. Since the required aileron excursion for counteracting asymmetries varies with speed, the available aileron will also change with velocity. The following corrections will therefore be applied:

1. Correct for current roll and roll acceleration. This correction is necessary because the aileron may not be in the 'neutral' position.
2. Correct for engine failure. With decreasing airspeed the engine effect on roll and yaw moments increases, requiring more rudder and aileron.
3. Correct for asymmetric mass. The mass moment is constant but the moment of the aileron to correct for the asymmetry depends on velocity, therefore more aileron is required at lower velocities.
4. Correct for the available rudder. This correction is needed to calculate the roll performance if maximum rudder is used.
5. Correct for adverse yaw. The calculations are based on the concept that  $\beta$  is maintained. However, when rudder control is limited or rudder is already at its maximum deflection,  $\beta$  can not be kept constant and adverse yaw will occur, reducing the available roll performance.
6. Correct for roll coupling. Even with good autopilots, no change of  $\phi$  is performed without some changes in AoA and side slip. These corrections are used to compare data from simulations with the calculated  $V_c$ .

### USE OF DIFFERENT $V_c$ VALUES, $V$ AND $V_0$

In the following derivations we use different  $V_c$  values;

- $V_{c1}$  is the limit speed to achieve a minimum roll performance using maximum aileron, while rudder is used to maintain  $\beta$  constant.
- $V_{c2}$  is the limit speed to achieve a minimum roll performance using maximum aileron and rudder.
- $V_{cL}$  is the  $V_c$  for a left roll and  $V_{cR}$  is the  $V_c$  for a right roll.

The subscripts are used in a limiting way, e.g., if  $V_{c1}$  is used it is valid for both left and right roll and  $V_{cR}$  is valid for both maximum aileron roll and roll with maximum rudder and aileron. Note that  $V_c$  is to be computed with knowledge on the current velocity  $V_0$ , further note that this calculation depends on the velocity  $V$ .  $V_c$ ,  $V_0$  and  $V$  are all expressed in  $m/s$ .

#### 4.3.1. DERIVATION BASIC $V_c$ EQUATIONS

Starting with Eqs. 4.41, 4.42 and 4.43, the roll equation with  $\beta = 0$ ,  $r = 0$  and with constant load factor and engine settings is:

$$\frac{\dot{p}b^2}{2V^2} = l_p \frac{pb}{2V} + l_{\delta_a} \delta_{a,av}, \quad (4.44)$$

where  $\delta_{a,av}$  is the total available aileron input. This formula can be rearranged into:

$$\dot{p} = \frac{V}{b} l_p p + \frac{2V^2}{b^2} l_{\delta_a} \delta_{a,av} \quad (4.45)$$

This differential equation can be expressed as a function of maximum roll rate and lag time constant. Defining:

$$p_{max} = -\frac{2V}{b} \frac{l_{\delta_a}}{l_p} \delta_{a,av} \quad (4.46)$$

and:

$$\tau = \frac{-b}{V l_p} \quad (4.47)$$

The roll rate in time is derived by solving Eq. 4.45:

$$p(t) = \left(1 - e^{-\frac{t}{\tau}}\right) p_{max} \quad (4.48)$$

This can be integrated to the roll angle change in time, with  $p = 0$  at  $t = 0$  to:

$$\varphi(t) = \left(\tau e^{-\frac{t}{\tau}} + t - \tau\right) p_{max} \quad (4.49)$$

Because the required roll performance is defined as a certain roll angle change  $\varphi_{req}$  per fixed time  $T$ , the following relationship exists:

$$\varphi_{req} = \left( \tau e^{-\frac{T}{\tau}} + T - \tau \right) p_{max} \quad (4.50)$$

This equation is the basis from which to calculate at what velocity the minimum roll performance is reached.  $p_{max}$  is directly related to  $V$  but the relationship of  $(\tau e^{-\frac{T}{\tau}} + T - \tau)$  with  $V$  is more complicated. Fortunately, the dependence of  $\tau$  on  $V$  is low and close to linear. Therefore a first order approximation is used based on the present velocity  $V_0$ :

$$f(\tau) = \tau e^{-\frac{T}{\tau}} + T - \tau, \quad (4.51)$$

which can be modified to:

$$f(V) = \frac{-b}{Vl_p} e^{\frac{TVl_p}{b}} + T + \frac{b}{Vl_p} \quad (4.52)$$

Taking the first derivative to  $V$  of this function is then:

$$\frac{\delta f(V)}{\delta V} = \frac{-b}{V^2 l_p} e^{\frac{TVl_p}{b}} + \frac{-b}{Vl_p} \frac{Tl_p}{b} e^{\frac{TVl_p}{b}} + \frac{-b}{V^2 l_p} \quad (4.53)$$

Numeric analysis for realistic values of  $l_p$ ,  $V$  and  $b$ <sup>4</sup> reveals that the first two terms are very small, consequently the derivative can be approximated by the last term only. Defining:

$$f'(V_0) \approx \frac{-b}{V_0^2 l_p} = \frac{\tau}{V_0} = C_2 \quad (4.54)$$

and

$$C_1 = f(V_0) - V_0 C_2 = \tau \left( e^{-\frac{T}{\tau}} - 2 \right) + T \quad (4.55)$$

Eq. 4.50 can be approximated by:

$$\varphi_{req} = (C_1 + C_2 V) \frac{-2V}{b} \frac{l_{\delta_a}}{l_p} \delta_{a,av}, \quad (4.56)$$

which establishes the required relationship between the required roll performance ( $\varphi_{req}$ ), the found stability derivatives, the available aileron deflection ( $\delta_{a,av}$ ) and the velocity ( $V$ ). The most practical way is to calculate a minimum roll speed in both directions and choose the most limiting value. Therefore we will make two equations. Using the convention [2], that positive control deflections give a nose-down pitch, a left roll and a left yaw, we can combine the roll with control deflection. Defining the required roll angle change to the right as  $\varphi_{req,max}$  and to the left as  $\varphi_{req,min}$  and maximum aileron to the left as  $\delta_{a,max}$  and to the right as  $\delta_{a,min}$ , the equation for maximum right roll is:

<sup>4</sup>Using the values for the PA34:  $b = 12m$  and  $l_p = -0.76s$  for the situation  $T = 1.5s$  and  $V = 40m/s$  shows that the first two components contribute to 6% of the value of  $f'(V)$ ; The means that if the  $V_c$  differs 20m/s with  $V_0$ , the value of  $(\tau e^{-\frac{T}{\tau}} + T - \tau)$  changes less than 1%.

$$\varphi_{req,max} = (C_1 V + C_2 V^2) \left( \frac{-2l_{\delta_a}}{bl_p} \right) (\delta_{a,min} - \delta_{a,av}) \quad (4.57)$$

Replacing  $\varphi_{req,max}$  and  $\delta_{a,min}$  by  $\varphi_{req,min}$  and  $\delta_{a,max}$ , respectively, will give the equation for maximum left roll. Finally, we have to establish the aileron deflection available. In the normal situation, where the aircraft is straight and level in non-accelerated flight without power asymmetry, full aileron should be available. In other cases the available aileron can be limited. We noted six different situations that require a correction on the available aileron deflection, these six corrections are discussed next.

#### CORRECTION 1: CORRECTING FOR ROLL RATE AND ACCELERATION

The first correction is the delta aileron deflection needed to stop the present roll rate and roll acceleration. This correction can be derived from Eq. 4.45 and is:

$$C_3 = \left( \dot{p} - \frac{V}{b} l_p p \right) \cdot \frac{1}{l_{\delta_a}} \cdot \frac{b^2}{2V_0^2} \quad (4.58)$$

This correction, while speed-dependent, is only applied at the present speed ( $V_0$ ) and is a fixed correction, because we don't yet know the cause of this roll rate and acceleration, which may or may not be speed-dependent. For instance, if the present roll rate and roll acceleration are pilot commanded, they do not restrict the roll rate but must be taken into account to correctly determine the roll rate available.

#### CORRECTION 2: CORRECTING FOR ASYMMETRIC THRUST

Before correcting for asymmetric thrust, the proper definition and normalization of engine control inputs are required. The engine inputs can be in torque, Engine Pressure Ratio (EPR) or fuel flow, depending on the type of engine. During our research, simulations were carried out using the Cessna Citation 500 model (where fuel flow is the best indicator for engine thrust) and the PA-34 model, where torque was used. The thrust and the moments were normalized, so fuel flow was divided by  $V^2$  and torque by  $V^3$ . This normalization is essential for calculating the effect of speed changes on thrust.

One can argue that engine control derivatives are known parameters that can be calculated from engine performance data. Consequently, they can be included in the model and can be omitted from parameter identification. However, there are some rare occasions where engine fuel/thrust relation can change. An example is the open nozzle failure for the PW F100 engine (installed in the F-15 and F-16). In that particular situation the fuel flow/thrust relation changes dramatically. In our simulations we have, for that reason, treated engine parameters as parameters to be estimated.

The asymmetric thrust can either be completely countered by rudder, or by a combination of rudder and  $\beta$  and even by  $\beta$  alone if the rudder has failed. We start the derivation by assuming that  $\beta = 0$  can be maintained and make corrections for limited rudder capability thereafter. The required rudder and aileron to maintain  $\dot{\beta} = 0$ ,  $\dot{p} = 0$  and  $\dot{r} = 0$

is derived next. Defining:

$$A1 = \begin{bmatrix} y\delta_a & y\delta_r \\ l\delta_a & l\delta_r \\ n\delta_a & n\delta_r \end{bmatrix}, \quad (4.59)$$

the effect of differential thrust is given by:

$$Y1 = \begin{bmatrix} y\delta_{TL} & y\delta_{TR} \\ l\delta_{TL} & l\delta_{TR} \\ n\delta_{TL} & n\delta_{TR} \end{bmatrix} \begin{bmatrix} \Delta\delta_{TL} \\ \Delta\delta_{TR} \end{bmatrix} \quad (4.60)$$

The change in rudder and aileron can now be calculated using a standard least squares approximation:

$$\begin{bmatrix} \Delta\delta_a \\ \Delta\delta_r \end{bmatrix} = (A1^T A1)^{-1} A1^T Y1 \quad (4.61)$$

From the required  $\Delta\delta_r$ , three different scenarios develop. Firstly the special case where the required rudder at present velocity already exceeds the available rudder, secondly the case where the required rudder at the minimum control velocity exceeds the rudder available and thirdly the case where maximum rudder is not required. Therefore we first have to calculate the predicted rudder at the estimated  $V_c$  to check if it exceeds the available rudder. This has to be calculated for left and right rolls. The equation for predicted available right rudder ( $\delta_{r,predR}$ ) at  $V_c$  is:

$$\delta_{r,predR} = \delta_{r_{min}} - \delta_r - \Delta\delta_r \left( \frac{V_0^2}{V_{cR}^2} - 1 \right) - (\delta_{a_{min}} - \delta_a + C_3) \frac{-n\delta_a}{n\delta_r}; \quad (4.62)$$

where  $(\delta_{r_{min}} - \delta_r)$  is the available right rudder at present velocity,  $\Delta\delta_r(V_0^2/V_{cR}^2 - 1)$  is the increase in required rudder to counter the asymmetric moment and the last term is the rudder required to counter the adverse yaw effect of the application of maximum available right aileron. By changing  $\delta_{r_{min}}$  and  $\delta_{a_{min}}$  to  $\delta_{r_{max}}$  and  $\delta_{a_{max}}$  and replacing  $V_{cR}$  by  $V_{cL}$ , the equation for predicted left rudder is obtained.

#### SCENARIO 1; SUFFICIENT RUDDER TO MAINTAIN $\beta = 0$

When the maximum predicted rudder does not exceed the rudder available, the effect of asymmetric thrust on the required change in aileron deflection  $\Delta\delta_a$  can be derived from Eq. 4.61. This correction is labelled  $C_4$  or:

$$\begin{bmatrix} C_4 \\ .. \end{bmatrix} = (A1^T A1)^{-1} A1^T Y1 \quad (4.63)$$

Because of the normalization of thrust, the correction is velocity-dependent. The reduction in available aileron at  $V_{cR}$ :

$$\Delta\delta_a = C_4 \left( \left( \frac{V_0}{V_{cR}} \right)^n - 1 \right) \quad (4.64)$$

The parameter  $n$  in this equation depends on the type of engine as explained in Section A. For propeller aircraft  $n = 3$  and for turbo jet aircraft  $n = 2$ .

**SCENARIO 2;  $\delta_{r,req} > \delta_{r,av}$** 

The second scenario is where the required rudder is more than the available rudder. In this situation the aircraft can not maintain zero  $\beta$ . Here we first convert the rudder deficit into a side slip angle  $\beta$  and then calculate the required aileron to counteract the roll due to side slip. For a right roll this occurs when  $\delta_{r,predR} > 0$ , and for a left roll when  $\delta_{r,predL} < 0$ . This gives an additional correction that we label  $C_{10R}$  and  $C_{10L}$ . Because it is calculated with the actual  $V_c$ , it does not need a velocity correction:

$$C_{10R} = -\delta_{r,predR} \frac{n_{\delta_r} l_{\beta}}{n_{\beta} l_{\delta_a}}; \quad (4.65)$$

**SCENARIO 3;  $\delta_{r,req} > \delta_{r,current}$** 

In the last scenario, maximum rudder deflection is already achieved at the present velocity. In that case Eq. 4.61 can not be used. Also in cases where the rudder has failed<sup>5</sup>, and consequently  $n_{\delta_r}$ ,  $l_{\delta_r}$  and  $y_{\delta_r}$  are zero, the matrix A1 is unusable. We then have to calculate the expected further increase in side slip, as rudder is either completely used or unusable, and the required aileron to counteract the further growth in  $\beta$ . This gives the following equations:

Defining:

$$A2 = \begin{bmatrix} y_{\delta_a} & y_{\beta} \\ l_{\delta_a} & l_{\beta} \\ n_{\delta_a} & n_{\beta} \end{bmatrix}, \quad (4.66)$$

the effect of differential thrust is given by:

$$Y1 = \begin{bmatrix} y_{\delta_{TL}} & y_{\delta_{TR}} \\ l_{\delta_{TL}} & l_{\delta_{TR}} \\ n_{\delta_{TL}} & n_{\delta_{TR}} \end{bmatrix} \begin{bmatrix} \Delta\delta_{TL} \\ \Delta\delta_{TR} \end{bmatrix} \quad (4.67)$$

The change in  $\beta$  and  $\delta_a$  can now be calculated using a least squares approximation:

$$\begin{bmatrix} \Delta\delta_a \\ \Delta\beta \end{bmatrix} = (A2^T A2)^{-1} A2^T Y1 \quad (4.68)$$

The correction  $\Delta\delta_a$  is the aileron deflection required to counter the present  $\beta$  due to the thrust moment. It is the correction  $C_4$  that is dependent on  $V_c$ . In this situation, the corrections  $C_{10R}$  and  $C_{10L}$  are of course zero.

**CORRECTION 3: CORRECTING FOR AVAILABLE RUDDER**

The normal situation is when the rudder is used to maintain zero  $\beta$ . However, roll performance can be increased by applying additional rudder generating proverse yaw, which is needed for the calculation of  $V_{c2}$ . From the equations in Subsection 4.3.1 the available rudder that can be transformed into an equivalent aileron deflection is known. This is

<sup>5</sup>The rudder does not have to be failed in the neutral position; if it is failed in another position the rudder effect may carry over to the bias parameter.

the correction  $C_5$  that is required if we want to calculate the  $V_c$  with maximum rudder assistance. For a right rudder this is:

$$C_{5R} = -\delta_{r,predR} \frac{n_{\delta_r}}{n_\beta} \frac{l_\beta}{l_{da}} \quad (4.69)$$

This equation is identical to Eq. 4.65. However, in that situation there was a deficit in right rudder that had to be corrected, in this case there is a surplus of right rudder.

#### NO CORRECTION NEEDED FOR ASYMMETRIC DRAG

Structural damage may cause an additional and asymmetric drag that causes a lateral or directional moment. While many types of structural damage may occur, and the effects of the damage may vary widely, the fact that these disturbances are caused by aerodynamic forces will make the effect proportional to dynamic pressure, similar to the effect of control surfaces. In order to model these correctly, they should not be part of the control and stability parameters but rather act as a bias to these parameters. These bias factors, already incorporated in the model are referred to as:  $y_F$ ,  $l_F$  and  $n_F$ . In case of damage these parameters might change, however, we do not have to account for these parameters in the control velocity calculation. The effect of the asymmetric drag is already accounted for in the actual aileron position, roll rate and roll acceleration and this correction is expected to remain constant with velocity change.

#### CORRECTION 4: CORRECTING FOR ASYMMETRIC LIFT AND MASS

Asymmetric lift can be a result of the loss of part of a wing or for example be due to a split flap situation. A split flap situation can be regarded as a bias in the control deflection and will show up in the bias parameters. For loss of part of the wing, the situation is different but quite similar to an asymmetric mass distribution. The roll moment generated by an asymmetric mass distribution is:  $L = mgy_{cg}n_z$ . Given a constant mass ( $m$ ) and arm ( $y_{cg}$ ) the moment only depends on  $n_z$ . The moment generated by loss of part of a wing can be estimated to be  $L = \Delta S b_d C_{L\alpha} \alpha q$ , where  $\Delta S$  is the missing part of the wing and  $b_d$  the average distance to the  $X_B$ -axis. This can be rewritten in  $L = \frac{\Delta S b_d}{S} m g n_z$ , which makes both failures a function of  $n_z$ .

Similarly, the effect of asymmetric mass distribution can be seen as a function of AoA. Choosing whether to couple with  $n_z$  or AoA, normally the accelerations can be measured with less noise than angle of attack, making it prudent to couple with  $n_z$ . These parameters are therefore named  $l_{\delta_{Fn}}$ ,  $n_{\delta_{Fn}}$  and  $y_{\delta_{Fn}}$ . To calculate this effect we start with the roll equation:

$$\frac{\dot{p}b^2}{2V^2} = l_\beta \delta \beta + l_p \frac{pb}{2V} + l_r \frac{rb}{2V} + l_{\delta_a} \delta_a + l_{\delta_r} \delta_r + l_{\delta_{TL}} \delta_{TL} + l_{\delta_{TR}} \delta_{TR} + l_{\delta_{Fn}} \delta_{Fn} + l_{\delta_F} \delta_F \quad (4.70)$$

Asymmetric mass distribution and lift effect will cause the parameter  $l_{\delta_{Fn}}$  to appear. This parameter is multiplied by  $\delta_{Fn}$ , the normalized load factor ( $\frac{a_z b}{2V^2}$ ), which is velocity-dependent. Keeping  $p$  and  $r$  at zero and disregarding asymmetric thrust, which is already accounted for, all other speed dependent parameters will vanish. The change of

$\delta_{Fn}$  by velocity must be compensated by a change in aileron deflection. The equation for asymmetric lift or mass is:

$$\Delta\delta_a = -\frac{l_{\delta_{Fn}}}{l_{\delta_a}} \delta_{Fn} \left( \left( \frac{V_0}{V} \right)^2 - 1 \right) \quad (4.71)$$

Defining  $C_6 = -\frac{l_{\delta_{Fn}}}{l_{\delta_a}} \delta_{Fn}$ , the correction for asymmetric mass distribution is then:

$$\Delta\delta_a = C_6 \left( \left( \frac{V_0}{V} \right)^2 - 1 \right) \quad (4.72)$$

#### CORRECTION 5: CORRECTING FOR ADVERSE YAW AND SIDE SLIP

When either the rudder is at its maximum deflection or the rudder effectiveness is reduced, zero  $\beta$  can not be maintained and the aircraft will be sensitive to adverse yaw. This will reduce the roll performance of the aircraft and is also subject to a Dutch roll that can not be suppressed any more due to the lack of rudder authority. Several ways were investigated to account for this Dutch Roll effect. One can estimate the Dutch roll damping and frequency and calculate the effect of the excited Dutch Roll on the roll angle change. It was found that the most accurate results were obtained by a numeric simulation using a Runge-Kutta integration. The numeric solution was achieved with the following steps:

- Based on the initial estimate of  $V_c$ , the available aileron deflection ( $\delta_{a,av}$ ) is calculated. There are two possible causes for a change in available aileron with air-speed: asymmetric power and asymmetric mass. These corrections were calculated above in Eqs. 4.64, 4.65, 4.68 and 4.72.
- A Runge-Kutta integration was made over the time period of the required roll using Eqs. 4.41, 4.42 and 4.41, using as sole input the available aileron deflection at  $V_c$ . Furthermore the constant  $l_{\delta_a}$  was set to zero to isolate the adverse yaw effect from the normal roll response.
- The achieved roll angle change must now be transformed into an equivalent aileron input ( $\Delta\delta_a$ ). This can be achieved by using Eqs. 4.47, 4.46 and 4.48 for, respectively, the roll time constant  $\tau$ , the maximum roll rate  $p_{max}$  and the roll angle change  $\Delta\phi$ . This gives the following adverse yaw correction:

$$p_{max} = \Delta\phi(t) \left( \tau e^{-\frac{t}{\tau}} + t - \tau \right)^{-1}, \quad (4.73)$$

and:

$$\Delta\delta_a = p_{max} \frac{-b}{2V} \frac{l_p}{l_{\delta_a}}, \quad (4.74)$$

and this  $\delta_a$  becomes the adverse yaw correction  $C_{11}$ .

- Finally the correction is different for right and left roll because the available aileron in both directions can differ and the  $V_c$  values for right and left roll can also differ, therefore we have a  $C_{11R}$  and  $C_{11L}$ , which are already calculated at the value of  $V_{cR}$  and  $V_{cL}$  respectively.

#### CORRECTION 6: CORRECTING FOR AERODYNAMIC ROLL COUPLING

This correction is different from other corrections. We do not need it for prediction but if we want to compare the actual roll with the predicted roll we have to account for the fact that the actual roll is not always a perfect roll around the velocity vector and this correction must be applied. Due to the inertia of the aircraft, an interchange between  $\alpha$  and  $\beta$ , called aerodynamic roll coupling may occur. The actual roll coupling depends on the controls applied during the roll motion. If the (auto)-pilot maintains a constant  $\alpha$  and  $\beta$  in the roll, no coupling will take place. However, when  $\alpha$  and  $\beta$  are controlled less stringently in a roll, an interchange of  $\alpha$  and  $\beta$  can take place. The change from  $\alpha$  to  $\beta$  will decrease the roll rate when  $\alpha$  is positive. The effect of  $\beta$  to  $\alpha$  interchange is especially important in the case of a rudder-assisted roll and the effect is an increase in load factor when the turn is away from the  $\beta$  angle. With lateral asymmetries, this increase in load factor will decrease the roll performance if the turn is away from the asymmetry (meaning a turn to the left when the c.g. is displaced to the right).

We have developed two different procedures to correct for this coupling. The first procedure assumes that the aircraft  $X_B$  axis retains its orientation during the roll, this will give the maximum amount of coupling. A second procedure that we developed is based on the measured change in load factor and  $\beta$  during the roll and uses these to calculate the effect on the roll authority. This second method uses partly the same derivations but the first steps can be omitted. We will indicate where the second method starts. The importance of this second method is that we can compare test data with the calculated  $V_c$  as done in Chapter 6.

The effect of roll coupling is calculated for left and right roll separately, and for the  $\alpha$  and  $\beta$  at  $V_{c1}$  and  $V_{c2}$ , respectively. If the (estimated)  $V_{c1}$  and  $V_{c2}$  are known, the roll time constant  $\tau$  can be calculated with Eq. 4.47:  $\tau = \frac{-b}{I_p V_c}$ . Because the required roll angle change ( $\phi_{req}$ ) and required time ( $T$ ) are given (this is the required roll control), the maximum roll rate is:

$$p_{max} = \phi_{req} \left( T + \tau \left( e^{-\frac{T}{\tau}} - 1 \right) \right) \quad (4.75)$$

Next we need  $\phi(t)$ , which was already derived in Eq. 4.49 and is repeated here:

$$\phi(t) = p_{max} \left( t + \tau \left( e^{-\frac{t}{\tau}} - 1 \right) \right)$$

The estimated  $\alpha$  at  $V_{c1}$  and  $V_{c2}$  is:  $\alpha_{est} = \alpha(t) \left( \frac{V(t)}{V_c} \right)^2$ , for the estimated  $\beta$  the present  $\beta$  is used but corrected for rudder-assisted roll by the  $\Delta\beta$  derived from Eq. 4.69. The alpha and beta interchange during the roll is then:

$$\Delta\beta(t) = \alpha_{est} \sin\phi(t) + \beta_{est} (\cos\phi(t) - 1) \quad (4.76)$$

$$\Delta\alpha(t) = -\beta_{est} \sin\phi(t) + \alpha_{est} (\cos\phi(t) - 1) \quad (4.77)$$

The change in  $\alpha$  can be transformed into a change in load factor  $\Delta N_z(t) = \frac{\Delta\alpha(t)}{\alpha_{est}} N_z(t)$ . Here we have reached the point where we can either use this predicted load factor and  $\beta$  change, or start with the measured change in load factor and  $\beta$ .

To transform the time-varying effect of  $\Delta\beta(t)$  and  $\Delta N_z(t)$  to a fixed aileron correction, two steps are taken. Firstly we transform the time effect of  $\Delta\beta(t)$  and  $\Delta N_z(t)$  to fixed changes in  $\beta$  and  $N_z$  that have the same effect; we will label these as  $\Delta\beta_{eff}$  and  $\Delta N_{z_{eff}}$ . We tried to use the average change, however, this leads to an overestimation of the effect. When we realized that we can regard  $\Delta\beta(t)$  and  $\Delta N_z(t)$  as an input in the roll response, it is more accurate to convolute these inputs with the first order roll response and compare this to a step input of  $\beta$  and  $N_z$  in the roll response. This convolution is done by numerical integration. The ratio between the numerical integration and the step input determines the effective  $\beta$  and  $N_z$ , or:

$$\beta_{eff} = \frac{\text{Convoluted } \beta(t) \text{ with roll response}}{\text{Convoluted Step } \beta \text{ with roll response}} \quad (4.78)$$

Secondly,  $\Delta\beta_{eff}$  and  $\Delta N_{z_{eff}}$  have to be converted to the change in available aileron. This can be done simply by using Eq. 4.42. This gives:

$$0 = l_\beta \beta_{eff} + l_{\delta_a} (\Delta\delta_a) + l_{\delta_{Fn}} \frac{N_{z_{eff}}}{V_c^2} \quad (4.79)$$

The value of  $\Delta\delta_a$  is the required correction which we label  $C_9$ . If  $\Delta\beta_{eff}$  and  $\Delta N_{z_{eff}}$  are derived from a right roll,  $C_{9R}$  is:

$$C_{9R} = -\Delta\beta_{eff} \left( \frac{l_\beta}{l_{\delta_a}} \right) - \frac{l_{\delta_{Fn}}}{l_{\delta_a}} \left( \frac{N_{z_{eff}}}{V_c^2} \right), \quad (4.80)$$

and for  $C_{9L}$  the same equation is used, however,  $\Delta\beta_{eff}$  and  $\Delta N_{z_{eff}}$  must then be derived from a left roll.

#### TOTAL AVAILABLE AILERON DEFLECTION

The available aileron deflection ( $\Delta\delta_a$ ) as a function of airspeed can now be calculated for left and right roll and with and without the use of rudder. Defining the present aileron deflection as  $\delta_{a,V_0}$ , the available aileron deflection as a function of  $V$  is:

$$\Delta\delta_a(V) = \delta_{a,min} - \delta_{a,V_0} + C_3 - C_4 \left( \frac{V_0^n}{V^n} - 1 \right) - C_6 \left( \frac{V_0^2}{V^2} - 1 \right) - C_{5R} - C_{9R} - C_{10R} - C_{11R} \quad (4.81)$$

If we combine Eq. 4.81 with Eq. 4.57 we have an equation depending on  $V$ , solving for  $V$  will give the appropriate  $V_c$ , which will be either  $V_{c1L}$ ,  $V_{c1R}$ ,  $V_{c2L}$  or  $V_{c2R}$ , depending on the constants and corrections used.

Table 4.2: Constants and corrections used in  $V_c$  calculations.

Constant	Function and Remarks
$C_1$	Roll constant at $V = 0$ $f(T, \tau)$
$C_2$	Change of roll constant with $V_{true}$
$C_3$	Correction $\delta_{a,av}$ for present $\dot{p}$ and $p$
$C_4$	Correction $\delta_{a,av}$ for thrust asymmetry dependent on $V^2$
$C_5$	Correction $\delta_{a,av}$ for use of max. rudder
$C_6$	Correction $\delta_{a,av}$ for asymmetric mass
$C_9$	Correction $\delta_{a,av}$ for roll coupling
$C_{10}$	Correction $\delta_{a,av}$ for maximum $\delta_r$ reached in OEI
$C_{11}$	Correction $\delta_{a,av}$ for adverse yaw

$$0 = -\varphi_{req,max} + (C_1 \cdot V + C_2 V^2) \left( \frac{-2l\delta_a}{bl_p} \right) \times \left( \delta_{a,min} - \delta_{a,V_0} + C_3 - C_4 \left( \frac{V_0^n}{V^n} - 1 \right) - C_6 \left( \frac{V_0^2}{V^2} - 1 \right) - C_{5R} - C_{9R} - C_{10R} - C_{11R} \right) \quad (4.82)$$

A damped and limited Newton method was used to solve this equation. In the simulations that follow, this equation was solved at every time step, using the estimated aircraft stability derivatives, the actual control deflections and the updated corrections for the available aileron.

#### DEMONSTRATION OF $V_c$ ALGORITHM

To demonstrate the working of the  $V_c$  algorithm, a non-linear model of the Piper Seneca (PA-34) [4] was used. With this model the trim positions were calculated for two failure conditions at 80 KTAS in level flight.

The first failure condition is an engine failure combined with different levels of rudder and aileron effectiveness, simulating a (partial) damaged rudder and aileron. From these trim points the  $V_c$  was calculated for a 10 degree roll angle change in 1s. The effect is shown graphically in Fig. 4.1a. Interesting to note is the bend in the  $V_c$  lines. This is the point where maximum rudder is just capable of maintaining zero  $\beta$ . If the rudder effectiveness is further reduced side slip will develop and the  $V_c$  will increase for the same aileron effectiveness. This bend is a sharp point as correctly depicted in the  $V_c = 60m/s$  line. However, due to the interpolation routine from Matlab, a slightly rounded bend is depicted in the other  $V_c$  curves. Fig. 4.1b shows the same situation for a rudder assisted roll. Because the rudder is now at its maximum deflection there is no bend and the  $V_c$  lines show a linear relation between rudder and aileron effectiveness. It should be noted that the  $V_c$  lines are closer together at the lower rudder and aileron efficiencies, showing the non-linear relation between  $V_c$  and rudder and aileron effectiveness.

The second demonstration involves a lateral asymmetry where different asymmetric moments are combined with normal rudder and different aileron effectiveness levels,

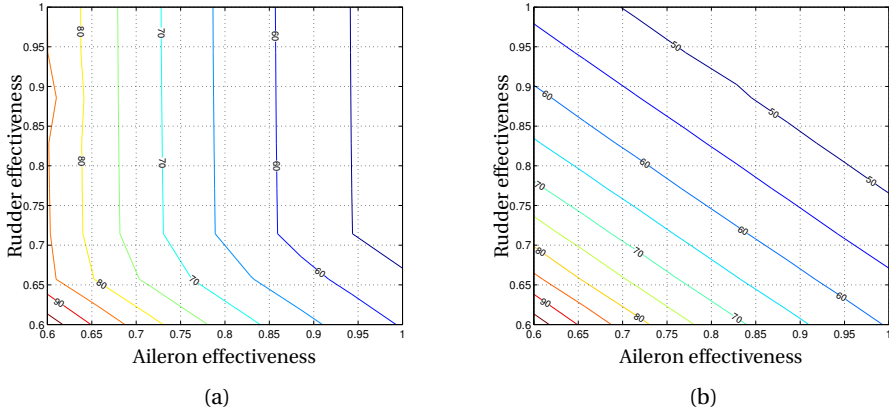


Figure 4.1: Effect of rudder effectiveness levels combined with and right engine failure on  $V_c$  (KTAS) (a)  $V_{c1}$  and (b)  $V_{c2}$ .

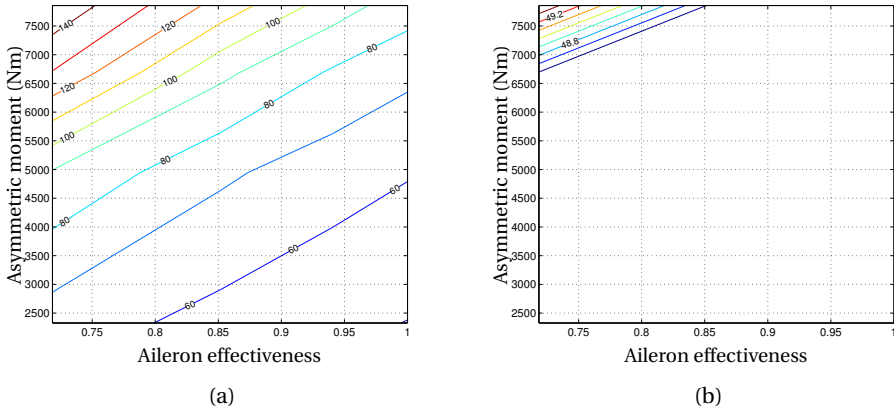


Figure 4.2: Effect of rudder effectiveness levels combined with and right engine failure on  $V_c$  (KTAS) (a)  $V_{c1}$  and (b)  $V_{c2}$ ; effect of lateral asymmetry combined aileron effectiveness levels on  $V_c$  (KTAS): (c)  $V_{c1}$  and (d)  $V_{c2}$

simulating a partial failure of the aileron. The  $V_c$  is again calculated for a trim point at 80 KTAS and for a 10 degree roll angle change in 1s. Fig. 4.2a shows the  $V_{c1}$  for this situation, and Fig. 4.2b shows the  $V_{c2}$ . Fig. 4.2a shows an almost linear relation between asymmetric moment and aileron effectiveness for a given  $V_c$ , which was to be expected. When the asymmetric moment increases, or the aileron effectiveness decreases the  $V_c$  lines are closer together, showing the non-linear relation.

Fig. 4.2b shows the same condition for  $V_{c2}$ . The additional rudder is so effective that the  $V_{c2}$  is lower than the stall speed for most conditions. These points below the stall speed can not be calculated accurately with the model and are also of little practical value. Consequently they are omitted, and the  $V_c$  lines are restricted to the upper left corner of the graph where the asymmetric moment is high and the aileron efficiency low.

But the essence for the pilot will be that just two velocities are shown: The minimum velocity needed for the required roll performance with maximum aileron and the velocity needed for the required roll performance with maximum aileron *and* rudder. Both are based on the current power settings.

#### 4.4. CONCLUSIONS

In this chapter we have developed a model for an aircraft with an unknown c.g. location and inertia tensor. This model can be used for damaged aircraft where these parameters may be unknown. We have created a set of equations to enable  $V_c$  calculation. The  $V_c$  gives the minimum airspeed for the required roll performance, using either maximum aileron deflection roll ( $V_{c1}$ ), or maximum aileron and rudder ( $V_{c2}$ ). This algorithm is designed to account for any combination of damage and asymmetric thrust level.

Corrections were derived to account for disturbing effects such as present roll rates and accelerations as well as adverse yaw. Special attention was given to velocity dependent corrections related to asymmetric engine power and asymmetric weight distribution.

In the next chapters we will evaluate this model in off-line simulations using failure scenarios in realistic conditions. The first step is to optimize the model size. Our aircraft model with an unknown c.g. location and inertia tensor has many parameters, in the next chapter we will evaluate if this model size can be optimized in such a way that the parameter identification is fast, and that the parameters are accurate enough to predict the roll performance of the aircraft at low speed.

## REFERENCES

- [1] P. H. Zipfel, *Modeling and Simulation of Aerospace Vehicle Dynamics* (AIAA, 2007).
- [2] J. A. Mulder, J. C. van der Vaart, and M. Mulder, *Atmospheric Flight Dynamics* (Technical University Delft, Faculty LR, 2007).
- [3] B. J. Bacon and I. M. Gregory, *General Equations of Motion for a Damaged Asymmetric Aircraft*, in *Proc. of the AIAA Atmospheric Flight Mechanics Conference, Hilton Head, USA, Aug. 20-23*, Vol. 1 (2007) pp. 63–75.
- [4] R. J. de Muynck and M. Van Hesse, *The A-Priori Simulator Software Package of the Piper PA34 Seneca III*, Tech. Rep. (TU Delft, 1990).

# 5

## MODEL SELECTION

*Since all models are wrong the scientist cannot obtain a "correct" one by excessive elaboration. On the contrary, following William of Occam he should seek an economical description of natural phenomena. Just as the ability to devise simple but evocative models is the signature of the great scientist so over-elaboration and over-parametrization is often the mark of mediocrity.*

George E. P. Box (1976)

**The contents of this chapter are based on:**

**Paper title** The effect of model size for prediction of control effectiveness  
**Authors** Herman J. Koolstra, Coen C. de Visser, and J.A. (Bob) Mulder  
**Published in** Proceedings of the AIAA Guidance, Navigation, and Control Conference, the AIAA SciTech Forum, January 2015, Kissimmee, USA

## 5.1. INTRODUCTION

The first step towards an on-line calculation and presentation of the aircraft lateral manoeuvrability limits was the development of a model for an aircraft with an unknown mass, c.g. location and inertia tensor, and an algorithm for the calculation of  $V_c$  based on the model parameters in Chapter 4. We intend to apply an on-line estimation of the parameters of this model in flight, and then use these parameters to also calculate the  $V_c$ , for cases where the aircraft has an engine failure or sustained other damage. The question posed in this chapter is: what is the optimum model size for the prediction?

An adequate model should have enough parameters to enable a correct envelope prediction, but should also avoid over-fitting, since the addition of too many parameters could delay the calculation, or degrade the solution. Methods presented in literature for model size selection are primarily intended for determining the number of parameters required for a model to fit the data. Here, the purpose of the model is the prediction of a single value,  $V_c$ . This calculated  $V_c$  can be a velocity outside the speed range where the data is collected, and be based on control deflections smaller than the maximum deflections used for the calculation of  $V_c$ . The suitability of the different model selection methods for this purpose will be evaluated. Why prediction is so important here will be illustrated with the following two examples.

### ILLUSTRATING THE PROBLEM

The first is the IAF F-15 accident [1], in which the aircraft lost a large part of its right wing due to an in-flight collision. The accident caused the aircraft to depart in roll, and it started to spiral down to the ground while the airspeed was increasing. Fortunately, there was enough altitude available, and the pilot was able to regain aircraft control at a certain speed. In this specific example, determining the usable lateral control envelope would have been almost trivial for the pilot, because he had just experienced the airspeed and g-level at which roll control could be regained. The same would also be true for a parameter identification method. Instead of predicting the minimum control speed for roll control, it can present the speeds based on the parameters measured at and beyond the control boundary, with the added value that the envelope prediction method can also nicely establish the relationship between g-level and roll authority.

The second example is the Saab 340 accident at Schiphol Airport (April 4, 1994) [2]. Here, the aircraft experienced a problem with one engine. Instead of feathering the engine, the approach was made with the suspected engine in idle. This was initially uneventful, but when an overshoot was performed, the added drag of the idle engine caused loss of control. Pilots were unaware of the limited controllability until the go-around manoeuvre was initiated.

The question for an envelope prediction method in this case is the following:

*Can we use the model developed in Chapter 4 to estimate the model parameters with data gathered in flight, while still being well within the flight envelope, and use it to predict the edges of the control envelope?*

In order to be able to predict  $V_c$  for damaged aircraft, we developed a model in Chapter 4 that does not depend on a known mass, c.g. location and inertia tensor. The challenge of this model is that it has more parameters than a model with known mass, c.g. and inertia tensor. Furthermore, some of these model parameters show a high level of collinearity, others seem to be of limited importance. Therefore the sufficiency question is raised:

*What parameters are needed to make an adequate lateral envelope prediction, when using a model with freedom in mass and mass distribution?*

#### APPROACH

The approach to select the ‘best’ model for  $V_c$  prediction is based on simulations with a non-linear model of the Piper Seneca (PA-34). With this model, 48 runs with different failure scenarios were made. To select the best model, as well as the best model selection criteria for our situation, each scenario was evaluated with an increasing number of model parameters. The addition of parameters stopped when there was no statistically significant improvement possible, according to the selection method used. To verify the prediction capability of the statistical selection method, the selected model parameters were used to predict a maximum roll manoeuvre at low speed using a Runge-Kutta integration. This maximum roll manoeuvre was executed at the end of the run and was not part of the data used for the model parameter’ determination. Using this procedure we could simulate how well the model parameters, determined in the part of the run that did not involve extreme manoeuvres, could predict this maximum manoeuvre. This maximum manoeuvre is also the manoeuvre for which the  $V_c$  is determined. The process is graphically depicted in Fig. 5.1. We will now explain each step in detail.

## 5.2. EXPERIMENT SET-UP

### 5

#### AIRCRAFT MODEL

The test data were derived using a non-linear model of the PA-34. This model is well suited for studying lateral control problems because it is a twin propeller aircraft that has many interesting features, such as adverse yaw, differences in engine settings that cause large moments around the Z-axis and significant lift differences between right and left wing that cause additional strong roll moments at low airspeed. This model was originally a FORTRAN based model written for ATC Flight Simulators in Switzerland [3]. The model was re-hosted to a Matlab Simulink environment and one addition was made. The initial model did account for lift difference caused by different power settings, however this difference was not used to compute a roll moment when there was a thrust difference between the right and left engines. Therefore the model was changed to calculate the lift from right and left wing separately and calculate the additional roll moment. For this it was assumed that the lift difference arm was equal to the lateral distance of the propeller axis to the aircraft centre-line.

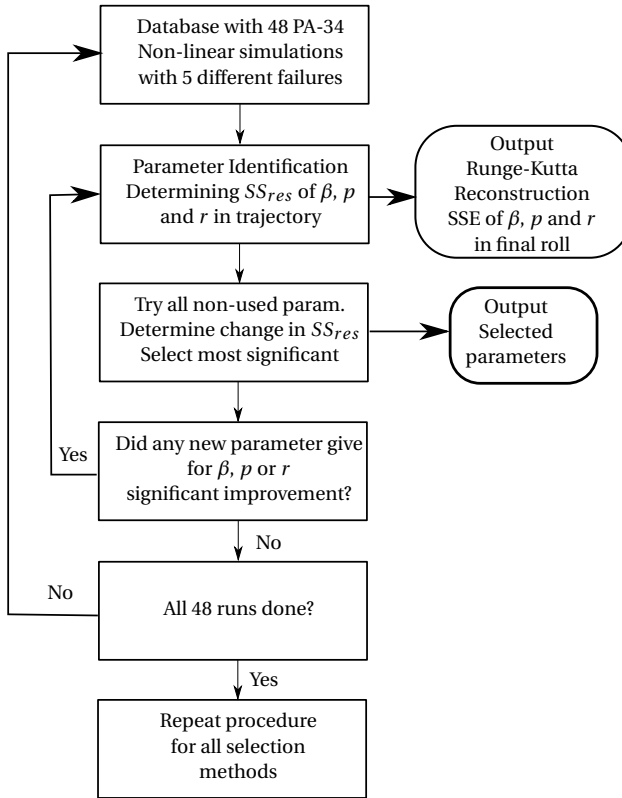


Figure 5.1: Overview of the selection process

### TEST PROFILE

A typical profile is shown in Fig. 5.2. The simulation started with an undamaged model in straight and level flight that accelerated from 120 KTAS to a fast cruise of 160 KTAS (82.3 m/s). After 30 seconds a failure was inserted, thereafter a controllability check was initiated that consisted of consecutive small sinusoidal inputs in roll, pitch, yaw and power that should enable the parameter identification. Subsequently, a climb was initiated and velocity was reduced to 120 KTAS (61.7 m/s). In order to assess if the level of control inputs would influence the solution, 50% of the runs used a single set of control inputs and the other 50% used a double set of control inputs as is shown in Fig. 5.3b. Near the end of the run the bank was changed to 25 degrees and at 170 seconds a maximum deflection roll was made, reversing the bank angle (Fig. 5.3a). For engine failures, rudder hard-overs and lateral asymmetries, the roll was always made to the most limiting side (e.g., with a right rudder hard-over the final roll was to the left) for all other runs turns were made to both sides.

The aircraft control was done by a programmable auto pilot that was based on a PID controller modified to inject control inputs into the model and to follow a scripted tra-

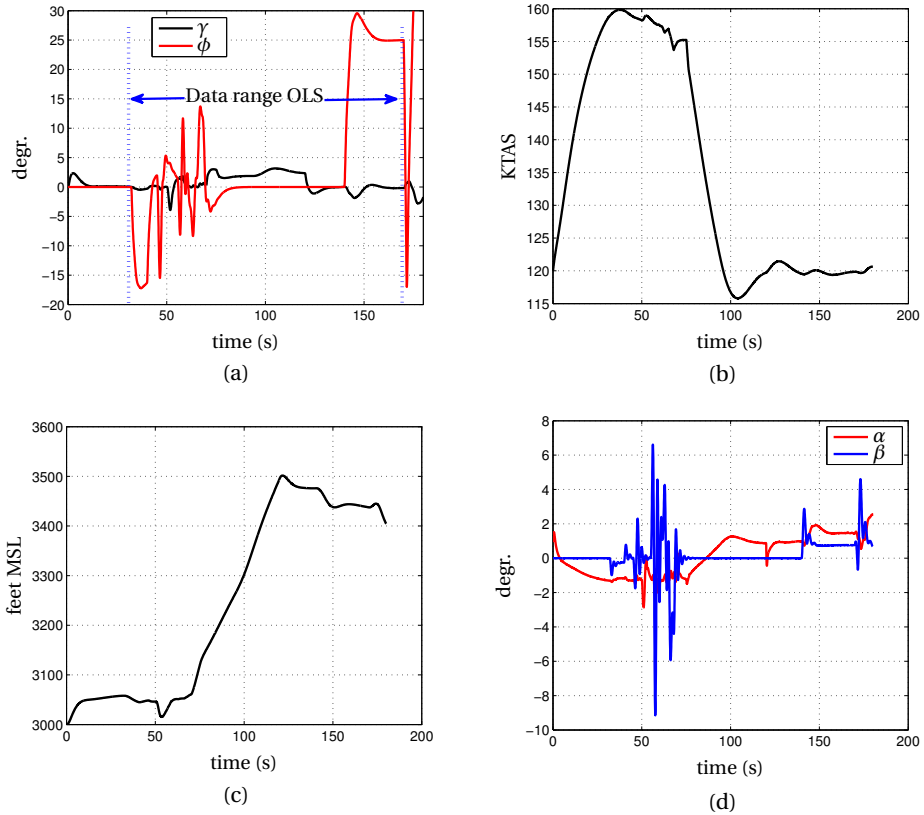


Figure 5.2: Flight profile used, failure injected at 30 seconds and maximum deflection roll at 170 seconds; (a) roll angle and climb angle (b) *KTAS* (c) Altitude (feet) (d)  $\alpha$  and  $\beta$  in degrees. The run is a 50% aileron failure, in smooth flying conditions with a single set of inputs.

## 5

jectory. These runs were done in smooth flying conditions and repeated in turbulent flying conditions. Turbulence was generated using the Dryden model as presented in MIL-F-8785C. This model uses an altitude-dependent scale length and a wind velocity dependent intensity. The experienced turbulence<sup>1</sup> is presented in Table 5.1

The failures and final manoeuvres are shown in Table 5.2. With each failure type, eight different runs were created, four runs in smooth flying conditions and four in turbulent flying conditions. From each set of four, two runs had a single set of control inputs and the other two had a double set of control inputs. From the two runs, one had a maximum roll to the right and the other to the left.

<sup>1</sup>This was determined by subtracting the smoothed  $\alpha$ ,  $\beta$  and  $V$  from the measured values.

Table 5.1: Generated turbulence levels

Parameter	Standard Deviation	Units
Vtas	0.57	knots
$\alpha$	0.18	degrees
$\beta$	0.12	degrees

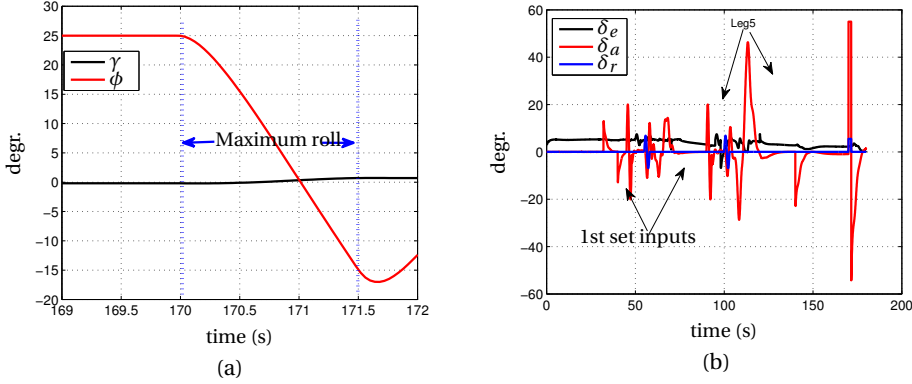


Figure 5.3: Flight profile used, (a) the maximum rate roll at 170 sec, used as evaluation criterion, (b) inputs from a run with a double set of inputs. In runs with a single set of inputs the second set, starting at 90 sec. is omitted.

### MODEL USED

The model used for parameter estimation is the model for the asymmetric motions of the aircraft developed in Chapter 4. This model calculates  $\frac{b\dot{\beta}}{V}$ ,  $\frac{b^2\dot{p}}{2V^2}$  and  $\frac{b^2\dot{r}}{2V^2}$  and is repeated below:

$$\frac{b\dot{\beta}}{V} = y_{\beta}\beta + y_{\phi}\phi + y_p\left(\frac{pb}{2V}\right) + y_r\left(\frac{rb}{2V}\right) + y_{\delta_a}\delta_a + y_{\delta_r}\delta_r + y_{TL}\delta_{TL} + y_{TR}\delta_{TR} + y_x\left(\frac{pb}{2V}\frac{qb}{2V} + 0.5\frac{\dot{r}b^2}{2V^2}\right) + y_y\left(\left(\frac{pb}{2V}\right)^2 + \left(\frac{rb}{2V}\right)^2\right) + y_z\left(\frac{qb}{2V}\frac{rb}{2V} - 0.5\frac{\dot{p}b^2}{2V^2}\right) + y_F\delta_F, \quad (5.1)$$

and:

$$\frac{\dot{p}b^2}{2V^2} = l_{\beta}\beta + l_p\left(\frac{pb}{2V}\right) + l_r\left(\frac{rb}{2V}\right) + l_{\delta_a}\delta_a + l_{\delta_r}\delta_r + l_{TL}\delta_{TL} + l_{TR}\delta_{TR} + l_{\dot{q}}\left(\frac{\dot{q}b^2}{2V^2}\right) + l_{q^2}\left(\frac{qb}{2V}\right)^2 + l_{p^2}\left(\frac{pb}{2V}\right)^2 + l_{r^2}\left(\frac{rb}{2V}\right)^2 + l_{qp}\left(\frac{qb}{2V}\frac{pb}{2V}\right) + l_{qr}\left(\frac{qb}{2V}\frac{rb}{2V}\right) + l_{pr}\left(\frac{pb}{2V}\frac{rb}{2V}\right) + l_{ax}\left(\frac{a_xb}{2V^2}\right) + l_{ay}\left(\frac{a_yb}{2V^2}\right) + l_{az}\left(\frac{a_zb}{2V^2}\right) + l_F\delta_F, \quad (5.2)$$

and:

Table 5.2: Failure types and associated final manoeuvres

Failure	Final Manoeuvre	Number of runs
No failure	left and right rolls	8
50% loss of aileron	left and right rolls	8
100% loss of rudder	left and right rolls	8
Left engine Failure	right roll	4
Right engine Failure	left roll	4
Asymmetry left wing heavy	right roll	4
Asymmetry right wing heavy	left roll	4
Rudder hard-over to the left	right roll	4
Rudder hard-over to the right	left roll	4

$$\begin{aligned}
\frac{\dot{b}^2}{2V^2} = & n_{\beta} \cdot \beta + n_p \cdot \left(\frac{pb}{2V}\right) + n_r \cdot \left(\frac{rb}{2V}\right) + n_{\delta_a} \cdot \delta_a + n_{\delta_r} \cdot \delta_r + n_{TL} \cdot \delta_{TL} + n_{TR} \cdot \delta_{TR} + \\
& + n_{\dot{q}} \cdot \left(\frac{\dot{q}b^2}{2V^2}\right) + n_{q^2} \cdot \left(\frac{qb}{2V}\right)^2 + n_{p^2} \cdot \left(\frac{pb}{2V}\right)^2 + n_{r^2} \cdot \left(\frac{rb}{2V}\right)^2 + n_{qp} \cdot \left(\frac{qb}{2V} \frac{pb}{2V}\right) + \\
& + n_{qr} \cdot \left(\frac{qb}{2V} \frac{rb}{2V}\right) + n_{pr} \cdot \left(\frac{pb}{2V} \frac{rb}{2V}\right) + n_{ax} \cdot \left(\frac{a_x b}{2V^2}\right) + n_{ay} \cdot \left(\frac{a_y b}{2V^2}\right) + n_{az} \cdot \left(\frac{a_z b}{2V^2}\right) + n_F \delta_F \quad (5.3)
\end{aligned}$$

This model is linear in its unknown parameters, thus an Ordinary Least Squares (OLS) method can be used to estimate the parameters. Because the aircraft state is treated as an input, the rows become independent and consequently each row can be solved separately. Initially the smallest size of the Eqs. 5.1, 5.2 and 5.3 were used with only the basic set of parameters as depicted in Table 5.3. This minimum set of independent variables was based on earlier research with a small business jet model [4]. The first twelve additional independent variables were derived in Section 4.2 and two variables,  $\beta^2$  and non-linear aileron ( $\delta_a$ )<sup>3</sup>, were added later to account for possible higher order aerodynamic effects. These additional variables are also presented in Table 5.3.

### MODEL SIZE SELECTION

A graphical representation of the model selection process is given in Fig. 5.4, which shows the standard statistical method that is discussed here, as well as the alternate selection method that will be discussed later this chapter. Starting with the smallest set of independent variables (the basic set in Table 5.3), the aircraft model parameters were calculated with the OLS, using the data from the moment of failure until the moment just before the maximum roll manoeuvre. Furthermore, the Sum Squared of the Residue Error ( $SS_{res}$ ) was determined, which is the cumulative squared error between the data and the regression model over the analysed trajectory. The  $SS_{res}$  is an important input for the statistical model selection criteria, which will be discussed in the next section.

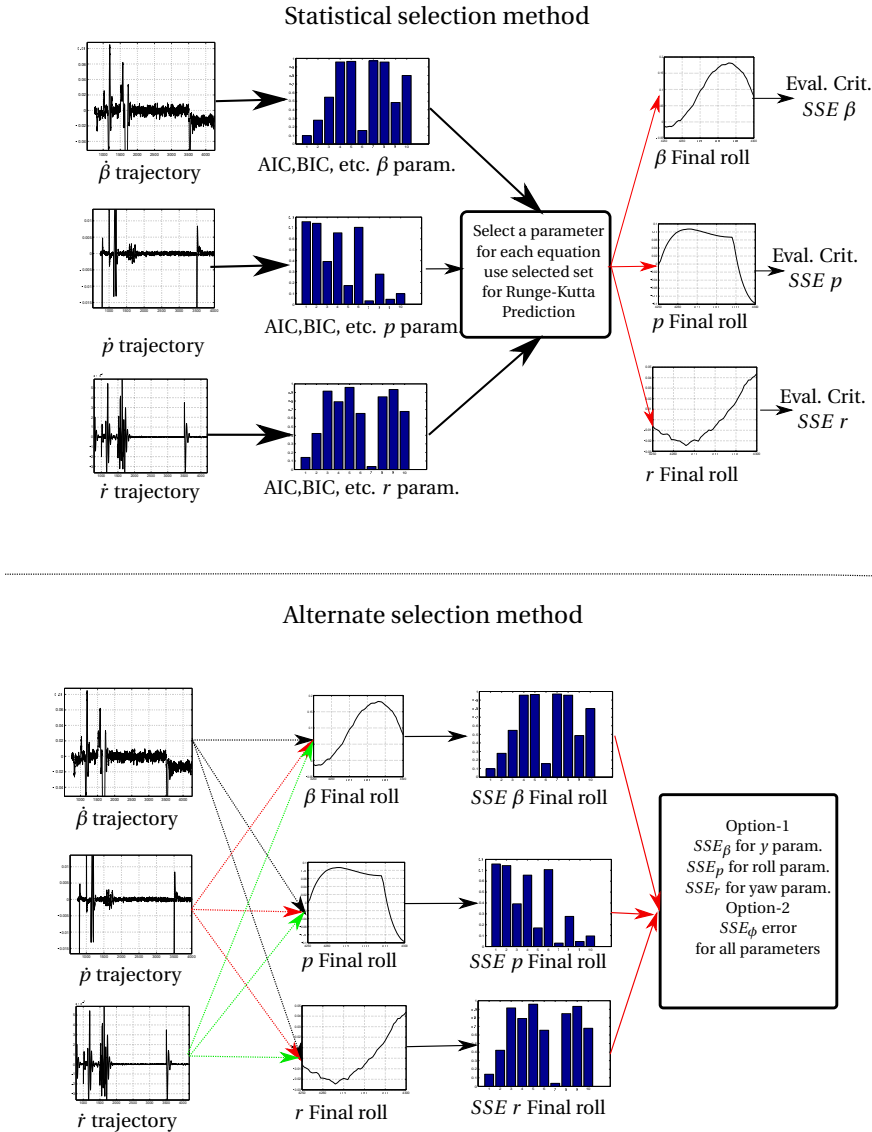


Figure 5.4: Comparison between normal and alternate selection process.

Next, for  $\frac{\hat{\beta}b}{V}$ ,  $\frac{\hat{p}b^2}{2V^2}$  and  $\frac{\hat{i}b^2}{2V^2}$  separately, all yet unused independent variables of Table 5.3 were tried sequentially to measure their effect on the change in the value of the selection criterion. This required the recalculation of the model parameters and the recalculation of the  $SS_{res}$ . After all unused independent variables were tried for the  $\beta$ , roll and yaw equations, the optimum parameter for addition for each equation was determined and added to the basic set. If no candidate variable could further improve the selection criteria, the optimum for that equation was reached.

Table 5.3: List of independent variables examined.

Basic set of variables				
No	Independent variable	Dependent parameters		
		$\beta$	roll	yaw
B1	$\beta$	$y_\beta$	$l_\beta$	$n_\beta$
B2	$\phi$	$y_\phi$	$l_\phi$	$n_\phi$
B3	$\frac{pb}{2V}$	$y_p$	$l_p$	$n_p$
B4	$\frac{rb}{2V}$	$y_r$	$l_r$	$n_r$
B5	$\delta_a$	$y_{\delta_a}$	$l_{\delta_a}$	$n_{\delta_a}$
B6	$\delta_r$	$y_{\delta_r}$	$l_{\delta_r}$	$n_{\delta_r}$
B7	$\delta_{TL}$	$y_{\delta_{TL}}$	$l_{\delta_{TL}}$	$n_{\delta_{TL}}$
B8	$\delta_{TR}$	$y_{\delta_{TR}}$	$l_{\delta_{TR}}$	$n_{\delta_{TR}}$
B9	$\frac{a_z b}{2V^2}$	$y_{\delta_{az}}$	$l_{\delta_{az}}$	$n_{\delta_{az}}$
B10	$\delta_F$	$y_{\delta_F}$	$l_{\delta_F}$	$n_{\delta_F}$
Additional variables examined				
1	$\frac{pb}{2V} \frac{rb}{2V} - 0.5 \frac{\dot{b}^2}{2V^2}$	$y_x$	-	-
2	$\left(\frac{pb}{2V}\right)^2 + \left(\frac{rb}{2V}\right)^2$	$y_y$	-	-
3	$\frac{qb}{2V} \frac{rb}{2V} - 0.5 \frac{\dot{p}b^2}{2V^2}$	$y_z$	-	-
4	$\frac{\dot{q}b^2}{2V^2}$	-	$l_{\dot{q}}$	$n_{\dot{q}}$
5	$\frac{pb}{2V} \frac{qb}{2V}$	-	$l_{pq}$	$n_{pq}$
6	$\frac{qb}{2V} \frac{rb}{2V}$	-	$l_{qr}$	$n_{qr}$
7	$\frac{pb}{2V} \frac{rb}{2V^2}$	-	$l_{pr}$	$n_{pr}$
8	$\left(\frac{qb}{2V}\right)^2$	-	$l_{q^2}$	$n_{q^2}$
9	$\left(\frac{rb}{2V}\right)^2$	-	$l_{r^2}$	$n_{r^2}$
10	$\left(\frac{pb}{2V}\right)^2$	-	$l_{p^2}$	$n_{p^2}$
11	$\frac{ba_x}{V^2}$	-	$l_{\delta_{ax}}$	$n_{\delta_{ax}}$
12	$\frac{ba_y}{V^2}$	-	$l_{\delta_{ay}}$	$n_{\delta_{ay}}$
13	$(\delta_a)^3$	$y_{(\delta_a)^3}$	$l_{(\delta_a)^3}$	$n_{(\delta_a)^3}$
14	$\beta^2$	$y_{\beta^2}$	$l_{\beta^2}$	$n_{\beta^2}$

With this new set of independent variables and model parameters, a Runge-Kutta integration was performed to make a prediction of the roll, yaw and side-slip in the final manoeuvre. The Sum of Squared Errors (SSE) in the prediction of  $\beta$ ,  $p$  and  $r$  in this maximum roll manoeuvre became the measures to determine how well the revised model was also able to predict the maximum performance roll. If these errors started to increase, this would be an indication that the addition of parameters had become counter-productive. After the new variables were selected, the process restarted with the revised set of parameters. This process continued until the selection criterion value could not be

decreased any further by adding an additional parameter in any of the three equations.

Because the optimum number of parameters was determined separately for each row, the final outcome could be a set of chosen parameters that differed for each row. This process was repeated for each of the 48 runs. Thereafter the whole process was repeated for the next model selection criterion.

It should be noted that while each equation is independently optimized, in the following Runge-Kutta integration the state is based on the initial state at the start of the prediction and propagated by the estimated model, and the coupling between the three equations is restored. For the selection method to work satisfactorily, the improvement in the selection criterion value should also coincide with a decrease in the prediction errors in the final manoeuvre. Having three measures to rate the performance of each selection criterion, one can argue that a weighted average between the three measures is needed. However, because our main objective is to have a good prediction of the roll performance, we should favour the improvement of the roll performance when we have to choose between selection criteria.

### 5.3. STATISTICAL MODEL SIZE SELECTION METHODS

Many statistical methods for model selection exist. Research [5] based on Monte Carlo simulations has shown that there is no single method or criterion able to handle all known cases. Model size, structure, collinearity and signal-to-noise ratio of the measured and control signals may influence the result. Furthermore, there is a basic difference between the selection of the correct model from a set of possible solutions (checking for consistency), and the selection of an adequate model based on the assumption that the real model has infinite parameters (looking for efficiency).

In this evaluation of the different methods we limit ourselves to establishing a common parameter that is indicative of the way the selection method works. This common parameter is based on the assumption that, by using the OLS method, the residual error will have a normal distribution. Two variables are important in the comparison of the model selection methods: firstly the number of parameters already in the model ( $k$ ) and secondly, the number of data points ( $N$ ).

In aircraft parameter identification, the number of data points is usually high, so we are more interested in how the model criteria behave with a large number of samples ( $N$ ). While all criteria are different, we will show that it is possible to rework them in such a way, that the *relative reduction in the prediction error variance for the addition of one additional parameter* becomes the common parameter with which we can compare these selection methods. This common parameter will prove to be dependent on the present number of parameters ( $k$ ) and the number of samples ( $N$ ).

#### DEFINITIONS

If we have a linear regression model  $y_i = x_i \beta^T + \epsilon$  where  $\epsilon$  is a zero-mean random error,  $\beta$  is the matrix with model parameters,  $x_i$  is the input (row)vector from sample  $i$  with

the independent variables and  $y_i$  is the measurement row vector from sample  $i$ . We can use the OLS method [6] to calculate the estimate of  $\beta$ :  $\hat{\beta} = (X^T X)^{-1} X^T Y$ , where  $X$  is the matrix containing  $N$  input row vectors with length  $k$ , and  $Y$  is the matrix containing  $N$  measurements of the  $j$  rows. We further define:

$$f_i = x_i \hat{\beta}^T \quad (5.4)$$

$$\bar{y} = \frac{1}{N} \sum^i y_i \quad (5.5)$$

$$SS_{tot} = \sum^i (y_i - \bar{y})^2 \quad (5.6)$$

$$SS_{reg} = \sum^i (f_i - \bar{y})^2 \quad (5.7)$$

$$SS_{res} = \sum^i (f_i - y_i)^2 \quad (5.8)$$

#### COEFFICIENT OF DETERMINATION

The coefficient of determination  $R^2$  [7] is a standard tool to compare different models and is defined as:

$$R^2 = \left( 1 - \frac{SS_{res}}{SS_{tot}} \right) \quad (5.9)$$

When the sum of the residual error is zero, which is the case using OLS<sup>2</sup>, the following relation is true:

$$SS_{reg} + SS_{res} = SS_{tot}, \quad (5.10)$$

and consequently  $R^2$  can also be expressed as  $\frac{SS_{reg}}{SS_{tot}}$  or  $\frac{SS_{reg}/N}{SS_{tot}/N}$ , which explains why it is called a measure of the explained variance.  $R^2$  is a useful measure for ordering the candidate parameters. However,  $R^2$  will always increase with a larger number of parameters in the regression, unless a parameter does not explain any variation at all.  $R^2$  can thus not be used as a criterion for determining the model order. To do that, we used the corrected  $R^2$ , written as  $\bar{R}^2$ , that is defined in [7] as:

$$\bar{R}^2(k) = 1 - (1 - R^2) \frac{N-1}{N-k-1} \quad (5.11)$$

Using Eq. 5.9 in Eq. 5.11 gives:

$$\bar{R}^2(k) = 1 - \left( \frac{SS_{res}}{SS_{tot}} \right) \left( \frac{N-1}{N-k-1} \right) \quad (5.12)$$

<sup>2</sup>The residual error must be zero because the bias parameter should cancel the residual error.

While the  $\bar{R}^2$  clearly penalizes the increase in the number of parameters, it is also evident from the last equation that the penalty will decrease rapidly when  $N$  is large. This is however typically the case when estimating aircraft model parameters; the number of samples is several orders of magnitude larger than the number of parameters.

To be able to compare the different model selection criteria, we compared how much relative residue variance decrease is necessary for adding one model parameter as a function of the present number of parameters  $k$  and the number of samples  $N$ . If  $\sigma_k^2$  and  $\sigma_{k+1}^2$  are the error variances for respectively  $k$  and  $k + 1$  parameters, the relative residue variance decrease is:  $\frac{\sigma_{k+1}^2}{\sigma_k^2}$ . Furthermore, the relation between  $SS_{res}$  and  $\sigma^2$  is:  $\frac{SS_{res}}{N-1} = \sigma^2$ . We use these relations to transform  $\bar{R}^2$ . Using the  $\bar{R}^2$  criterion, a parameter should only be added if  $\bar{R}^2$  increases, or:

$$\bar{R}^2(k+1) > \bar{R}^2(k) \quad (5.13)$$

Using Eq. 5.12 and realizing that  $SS_{res}$  is dependent on  $k$ , but  $SS_{tot}$  is independent of  $k$  we can write:

$$1 - \left( \frac{SS_{res(k+1)}}{SS_{tot}} \right) \left( \frac{N-1}{N-k-2} \right) > 1 - \left( \frac{SS_{res(k)}}{SS_{tot}} \right) \left( \frac{N-1}{N-k-1} \right) \quad (5.14)$$

Multiplying by  $-1$  (Changing from  $<$  to  $>$ ), adding 1 to both sides, multiplying both sides by  $\frac{SS_{tot}}{(N-1)^2}$ , rearranging the fractions and realizing that  $\frac{SS_{res}}{N-1} = \sigma^2$  brings this equation in the required form. Eq. 5.15 expresses the required decrease in residue variance needed to add another parameter based on the  $\bar{R}^2$  criterion:

$$\frac{\sigma_{k+1}^2}{\sigma_k^2} < \frac{N-k-2}{N-k-1} \quad (5.15)$$

#### PARTIAL F TEST

Another well-known model test [7] is the Fisher or  $F$  test. In the  $F$  test, two models are compared: Model one with  $k_1$  parameters and a regression sum of squares  $SS_{reg_1}$  and model two with  $k_2$  parameters and a regression sum of squares  $SS_{reg_2}$  ( $k_2 > k_1$ ). The  $F$  value is defined as:

$$F = \frac{\frac{SS_{reg_2} - SS_{reg_1}}{k_2 - k_1}}{\frac{SS_{res_2}}{N - k_2}} \quad (5.16)$$

Rewriting this equation for the addition of a single parameter and using  $SS_{reg_k} = SS_{tot} - SS_{res_k}$ , realizing that  $SS_{tot}$  is the same for  $k$  and  $k + 1$ , the model yields:

$$F = \frac{SS_{res_1} - SS_{res_2}}{SS_{res_2}} (N - k_2) \quad (5.17)$$

This clearly shows that the  $F$  value will almost linearly increase with  $N$ . On the other hand, if we look at the statistical tables for the *required*  $F$  value to accept the extra parameter, the  $F$  value decreases quickly if  $N$  increases and will be almost constant for  $N > 100$ .

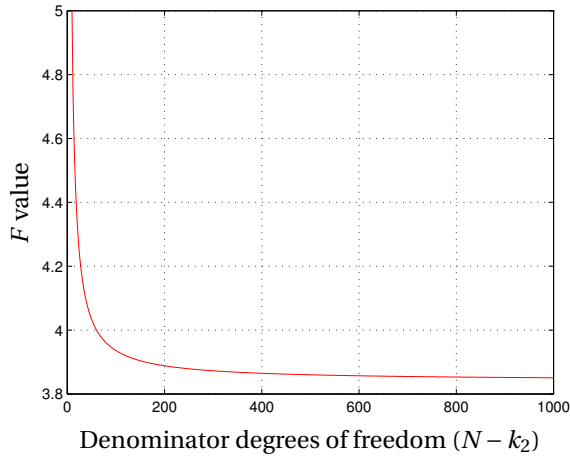


Figure 5.5: Relation between F value and  $(N - k_2)$  for a probability of 95% and  $k_2 - k_1 = 1$ .

For a 95% confidence level, meaning that the chance of incorrectly adding a parameter is not more than 5%, the  $F$  value for  $N = 100$  is 3.95 and for  $N \rightarrow \infty$  it is 3.84.

Similar as with  $\bar{R}^2$  we assume an initial  $k$  parameters, and investigate the case of adding one parameter, hence  $k_2 - k_1 = 1$ . For a given  $F$  value based on  $N$  and the required confidence level, Eq. 5.17 can be rewritten for the required change in the error variance:

$$\frac{\sigma_{k+1}}{\sigma_k} < \frac{N - (k + 1)}{F + N - (k + 1)} \quad (5.18)$$

## 5

### AKAIKE INFORMATION CRITERION

In 1974, Akaike developed a new criterion for model selection [8], the Akaike Information Criterion (AIC). This is derived from the 'Kullback Leibner distance', which in turn is based on the concept of statistical entropy. The AIC is defined as:

$$AIC = -\ln(L) + 2k, \quad (5.19)$$

where  $L$  represents the likelihood of the distribution. We can solve this log likelihood ratio. The likelihood of a realisation with the parameters  $(x_i, \dots, x_n)$  that is normally distributed with the mean  $\mu$  and the standard deviation  $\sigma$  is given by the product of each probability or:

$$L = \prod_{i=1}^N \frac{1}{\sigma\sqrt{2\pi}} \exp\left(-\frac{(x_i - \mu)^2}{2\sigma^2}\right) \quad (5.20)$$

This equation can be rewritten to:

$$L = \frac{(2\pi)^{-\frac{N}{2}}}{\sigma^N} \exp \left[ -\frac{\sum (x_i - \mu)^2}{2\sigma^2} \right] \quad (5.21)$$

Now we can solve for the log likelihood ratio:

$$\ln(L) = -\frac{1}{2} N \ln(2\pi) - N \ln(\sigma^2) - \frac{\sum (x_i - \mu)^2}{2\sigma^2} \quad (5.22)$$

Because for our application we have no means to differentiate between the variance of our realisation  $\frac{\sum (x_i - \mu)^2}{N-1}$  and the population variance  $\sigma^2$ , the last term in this equation can be rewritten to  $\frac{1}{2}N$ . This implies that the first and last terms on the right-hand side are constants (for a given  $N$ ), and the AIC can be rewritten as:

$$AIC = N \ln(\sigma^2) + 2k + C, \quad (5.23)$$

where  $C$  is an arbitrary constant. We look again at the condition that will give a decrease in  $AIC$  for one additional parameter:

$$AIC_{(k+1)} < AIC_k, \quad (5.24)$$

or:

$$N \ln(\sigma_{(k+1)}^2) + 2(k+1) < N \ln(\sigma_k^2) + 2k, \quad (5.25)$$

which after some manipulation can be written in the required form:

$$\frac{\sigma_{(k+1)}^2}{\sigma_k^2} < e^{-\frac{2}{N}} \quad (5.26)$$

This AIC should only be used when  $k < \sqrt{N}$ , and in that particular case the criterion becomes independent of  $k$ . When this criterion can not be met, AIC corrected ( $AIC_c$ ) should be used, which is:

$$AIC_c = AIC + \frac{2N(k+1)}{N-k-2} \quad (5.27)$$

In a similar way as for AIC this can be rewritten to a change in  $\sigma^2$  required for one additional parameter:

$$\frac{\sigma_{(k+1)}^2}{\sigma_k^2} < e^{\left( \frac{-2}{N} - \frac{2(k+2)}{N-1-k} + \frac{2(k+1)}{N-k-2} \right)} \quad (5.28)$$

### PREDICTED SQUARE ERROR

The Predicted Squared Error (PSE) was introduced by Barron [9] as a method for the determination of model size and was used in [10] for designing control systems for damaged aircraft. The PSE is based on the concept of estimating the future error based on the training error. It is proven in [9] that the future error  $\sigma_f^2$  can be estimated based on the training error  $\sigma_t^2$ , the training input  $T$  and future input  $F$  by:

$$\sigma_f^2 = \sigma_t^2 + \frac{1}{N_f} \sigma_t^2 \text{trace} \left( \frac{\overline{FF}}{\overline{TT}} \right), \quad (5.29)$$

where the subscript  $f$  is used for the future data and  $t$  for the training data and  $\overline{F}$  is the transpose of  $F$ . In the special case where the training input and the future input are similar  $\frac{\overline{FF}}{\overline{TT}}$  is a unit matrix of size  $k$ , hence the trace is  $k$ . Furthermore because  $N_f = N_t$  we can now use the term  $N$  instead. Based on this identity Barron developed the PSE, which is defined as:

$$PSE = TSE + 2\sigma_p^2 \frac{k}{N}, \quad (5.30)$$

where TSE is the training variance (or  $\sigma^2$ ) and  $\sigma_p^2$  is defined by Barron as: A prior estimate of the true signal error variance that does not depend on the particular model being considered. In [9] it is suggested to use half the covariance of the output<sup>3</sup> as the value for  $\sigma_p^2$ . It is clear from Eq. 5.30 that when parameters are added,  $\sigma^2$  will decrease but the fraction  $\frac{k}{N}$  will increase with  $k$ . Next we derive the relative improvement needed to add one single parameter:

$$PSE(k+1) < PSE(k), \quad (5.31)$$

or:

$$\sigma^2(k+1) + 2\sigma_p^2 \frac{k+1}{N} < \sigma^2(k) + 2\sigma_p^2 \frac{k}{N}, \quad (5.32)$$

which after some manipulation can be written as:

$$\frac{\sigma_{k+1}^2}{\sigma_k^2} < 1 - \frac{\frac{2\sigma_p^2}{\sigma_k^2}}{N} \quad (5.33)$$

PSE is our first measure that is relative to the strength of the signal value ( $\sigma_p^2$ ). We can not compare it with the other criteria unless we assume a certain value for  $\frac{\sigma_p^2}{\sigma_k^2}$ . In Figs. 5.6a and 5.6b we use two different values  $\frac{\sigma_p^2}{\sigma_k^2} = 5$  and  $\frac{\sigma_p^2}{\sigma_k^2} = 2$  to enable a comparison.

### BAYESIAN INFORMATION CRITERION

In 1978 Schwartz developed the Bayesian Information Criterion (BIC)[11]. The BIC is defined as:

$$BIC = -2 \ln(L) + k \ln(N) - k \ln(2\pi), \quad (5.34)$$

Where  $L$  again stands for the likelihood of the distribution. In most applications the last term is omitted because it is considered of less importance at large  $N$ . However,

<sup>3</sup>Defined as  $\frac{\overline{YY}}{N}$  where  $Y$  is the multi row ( $r$ ) output with dimensions  $(N, r)$ .

when it is used, AIC and BIC become quite similar at small values of  $N$ . Because we are more interested in large  $N$  we will also omit the last term. Using again the likelihood of the normal distribution as given in Eq. 5.22, or  $\ln(L) = -N \ln(\sigma^2) + C$ , the relative improvement needed to add one single parameter using the BIC criterion is:

$$BIC_{(k+1)} < BIC_k, \quad (5.35)$$

or:

$$-2 \ln L(k+1) + (k+1) \ln(N) < -2 \ln L(k) + k \ln(N) \quad (5.36)$$

Using  $\ln L = -N \ln(\sigma^2) + C$  we get:

$$2N \ln(\sigma_{k+1}^2) + C + (k+1) \ln(N) < 2N \ln(\sigma_k^2) + C + k \ln(N), \quad (5.37)$$

subtracting  $C + k \ln N$  from both sides gives:

$$2N \ln(\sigma_{k+1}^2) + \ln(N) < 2N \ln(\sigma_k^2), \quad (5.38)$$

rearranging the terms gives:

$$2N \ln(\sigma_{k+1}^2) - 2N \ln(\sigma_k^2) < -\ln(N), \quad (5.39)$$

or:

$$\ln \left( \frac{\sigma_{k+1}^2}{\sigma_k^2} \right)^{2N} < \ln(N^{-1}), \quad (5.40)$$

which after some manipulation gives:

$$\frac{\sigma_{k+1}^2}{\sigma_k^2} < N^{-\frac{1}{2N}} \quad (5.41)$$

### COMPARISON AND DISCUSSION

On the condition that the errors have a Gaussian distribution, we can now compare all standard methods by calculating the value of  $\frac{\sigma_{k+1}^2}{\sigma_k^2}$  that is required to add one additional model parameter. The values are plotted in Figs. 5.6a and 5.6b. The interesting points are firstly that not only PSE, BIC and AIC are constants, which we saw from the derived equations, but that for larger values of  $N$  all criteria approach constant values. The second, and surprising conclusion is the great similarity between the criteria, especially at larger values of  $N$ . Generally speaking, if at larger values of  $N$  an extra model parameter decreases the variance by more than 1%, this new parameter will be accepted.

While this may be statistically correct, it is not what we want from an engineering perspective. If we want to find an adequate model, we also want to make accurate predictions. This means that the prediction error should not exceed certain predetermined values. However, based on this relative measure we can have a situation in which ten

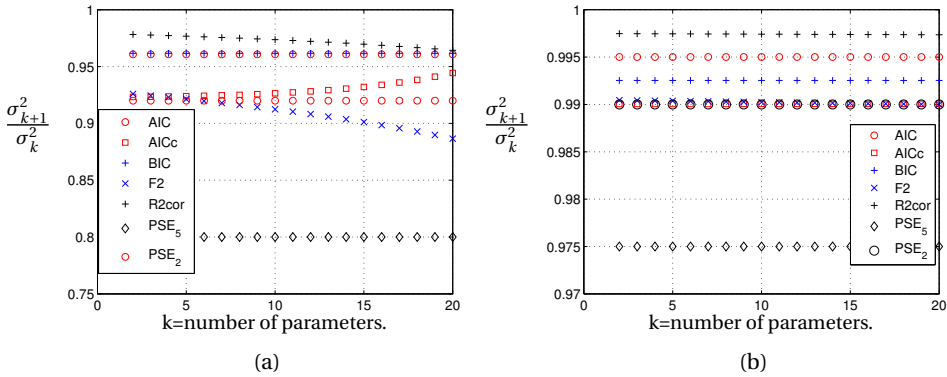


Figure 5.6: Comparing the different model selection criteria for (a) N=50 and (b) N=400

model parameters were added that each decreased the standard error by one percent, giving a total reduction of only 9.56%, as well as a situation where each parameter decreased the standard error by 90%, giving a total reduction of  $10^{-10}$ . Or in other words, the model that is statistically relevant may or may not meet our engineering requirement.

A special case is PSE, Figs. 5.6a and 5.6b clearly show that PSE is also changing linearly with  $N$ , however it is the only criterion that is related to the variance of the signal ( $\sigma_p^2$ ). A more practical way to rewrite PSE is:

$$\sigma_{k+1}^2 - \sigma_k^2 > \frac{\sigma_p^2}{N} \tag{5.42}$$

This clearly shows that when using PSE, there is a minimum fixed amount of improvement needed for each step.

5

In the next step we will design an alternate method to select the best model that is not based on a statistical criterion but on the improvement of the model prediction of the final roll.

ALTERNATE METHOD

It will be shown later in the results section, that the statistical model selection systems all had a tendency to over-fit, which was experimentally verified by the fact that the addition of the parameters was continued beyond the point where the best prediction accuracy of the final roll manoeuvre was reached and even to the extent that the prediction error became larger than it was before any additional parameter was added. We will use the term ‘initial error’ for the prediction error in the final roll manoeuvre with the basic set of parameters. A new selection method was developed in this thesis to prevent this over-fitting, which was based on the effect of the added parameters on the prediction accuracy of the maximum performance manoeuvre. The new method is graphically depicted in Fig. 5.4 and uses the following steps:

1. First the collinearity of the candidate independent variable was checked against the independent variables already included in the model. In this check, the OLS was used to check to what extent the new variable could be composed from the inputs of the parameters already included. If the  $R^2$  of this OLS was larger than 0.95, the new parameter was omitted from the list of candidate parameters.
2. The set with the new independent variable was used to recalculate the estimates of the model parameters and their uncertainty. This was based on the trajectory from the failure until just before the final roll manoeuvre.
3. Using Runge-Kutta integration, the effect of the added model parameter on the prediction error of the final manoeuvre was calculated for the nominal values of the added model parameter and for the values one standard deviation above and below the nominal value. Through this procedure, the uncertainty in the model parameter was transformed to an uncertainty error in the prediction.
4. If the decrease in the prediction error due to the addition of the model parameter was smaller than the uncertainty of the error discussed above, the candidate was omitted.
5. Finally, a limit was set on the required accuracy. The decrease in the sum of absolute errors during the maximum performance roll had to be significant in relation to the sum of the absolute value of the output. This limit was set to 1%. In our model three output values  $\dot{\beta}$ ,  $\dot{p}$  and  $\dot{r}$  were evaluated separately on this 1% criterion.

This alternate method was loosely based on the PRESS<sup>4</sup> [10] method. We also used the check for collinearity and checked for uncertainty in the parameters as was done in the PRESS method. However, instead of using the PSE method for selection, which employs a relative improvement as explained above, we used an absolute measure for the error. Another important difference is that this alternate method can never be used in a real-time selection environment, which is feasible with the other methods. It is a selection method that assumes that the final manoeuvre is known and compares what parameters contribute most to a good prediction. The consequence is that findings with the alternate method are only relevant if they encompass a large spectrum of flight situations.

The selection of the best candidate for incorporation in the model was based on the largest reduction in the SSE in the final manoeuvre. Here we have an infinite number of possibilities. One option is that we use the SSE of  $\beta$ , to select the  $\beta$  parameters, the SSE in roll to select the roll parameters and the SSE in yaw for the yaw parameters. However, we can also base the choice of all parameters on the reduction of one SSE. Because we are interested in the achieved roll angle change over time we also selected the SSE of  $\phi$ . We investigated both options, the first is labelled 'AM' and the second 'AM- $\phi$ '. A concern with this last method is that we might sacrifice physical reality to mitigate errors.

---

<sup>4</sup>PRESS is Predicted Residual Sum of Squares.

## 5.4. RESULTS

### INITIAL RESULT

The differences between the selection models can be seen from Tables 5.4, 5.5 and 5.6, which show the percentage of runs (out of 48) in which that additional model parameter was selected.

Table 5.4: Selected additional model parameters by method for  $\beta$  row;

param.	Percentage of times selected from 48 runs						
	AICC	BIC	PSE	R2	F2	AM	AM $-\phi$
1	68.8	37.5	58.3	72.9	77.1	0.0	0.0
2	50.0	25.0	58.3	62.5	77.1	20.8	18.8
3	64.6	41.7	58.3	75.0	77.1	0.0	0.0
13	72.9	52.1	58.3	72.9	77.1	22.9	25.0
14	54.2	27.1	58.3	66.7	77.1	14.6	16.7
Mean	62.1	36.7	58.3	70.0	77.1	11.7	12.1

For the optimization of the  $\beta$  prediction, the F2 method selected the largest number of extra model parameters, while the alternate method selected the fewest. The most restrictive ‘classical’ method was BIC. It might initially seem surprising that some selection mode shows identical figures for the all parameters, e.g., PSE and F2 that choose each  $\beta$  parameter respectively, in 58.3% and 77.1% of all cases. This only implies that these parameters are ‘required’ by similar scenarios. We should also note that for the statistical selection method the percentage for the other methods does not differ much. For example the difference between the highest and lowest value for the R2 method is 12.5%, or 6 out of the 48 scenarios where one parameter was selected and the other not.

For the  $p$  prediction, again the F2 method selected the largest number of extra model parameters, while the alternate method selected the fewest. The most restrictive classical method again was the BIC.

For the  $r$  prediction, the R2 method selected the largest number of extra model parameters, while the alternate method selected the fewest. The most restrictive classical method was now the PSE method.

Table 5.7 shows the number of ‘successful’ runs, where the final Sum Squared Error (SSE) of the Runge-Kutta prediction is smaller than the initial SSE. For all statistical methods the result was disappointing. The last column gives the number of runs in which the initial error was larger than the final error for all three rows ( $\beta$ ,  $p$  and  $r$ ).

It was further investigated whether these failures could be attributed to certain scenarios, turbulent conditions, lack of inputs or certain failure scenarios. Table 5.8 shows

Table 5.5: Selected additional model parameters by method for roll row.

param.	Percentage of times selected from 48 runs						
	AICC	BIC	PSE	R2	F2	AM	AM- $\phi$
4	56.3	20.8	50.0	68.8	91.7	0.0	0.0
5	91.7	68.8	54.2	93.8	91.7	12.5	12.5
6	75.0	50.0	52.1	79.2	91.7	0.0	0.0
7	64.6	43.8	50.0	85.4	91.7	6.3	6.3
8	70.8	29.2	50.0	81.3	91.7	2.1	2.1
9	66.7	29.2	52.1	89.6	91.7	8.3	8.3
10	85.4	56.3	52.1	93.8	91.7	31.3	31.3
11	93.8	68.8	66.7	95.8	97.9	4.2	4.2
12	77.1	52.1	54.2	87.5	91.7	4.2	4.2
13	97.9	85.4	77.1	97.9	93.8	2.1	2.1
14	75.0	56.3	56.3	87.5	91.7	4.2	4.2
Mean	77.7	50.9	55.9	87.3	92.4	6.8	6.8

Table 5.6: Selected additional model parameters by method for yaw row.

param.	Percentage of times selected from 48 runs						
	AICC	BIC	PSE	R2	F2	AM	AM- $\phi$
4	25.0	8.3	18.8	45.8	10.4	10.4	4.2
5	52.1	47.9	33.3	64.6	47.9	37.5	33.3
6	52.1	33.3	33.3	60.4	39.6	22.9	22.9
7	50.0	41.7	27.1	62.5	41.7	25.0	25.0
8	47.9	25.0	31.3	58.3	27.1	14.6	12.5
9	45.8	35.4	25.0	54.2	35.4	22.9	25.0
10	56.3	45.8	39.6	66.7	47.9	41.7	35.4
11	62.5	52.1	35.4	66.7	54.2	0.0	0.0
12	58.3	37.5	37.5	68.8	37.5	8.3	6.3
13	50.0	41.7	25.0	54.2	43.8	18.8	29.2
14	58.3	45.8	22.9	64.6	45.8	20.8	22.9
Mean	50.8	37.7	29.9	60.6	39.2	20.3	19.7

that the Alternate Method seems to work better in smooth flying conditions than in turbulence and the aileron failures showed the lowest number of successes. The success rate with the other methods was too low to make any conclusion on the scenario.

A further examination was done to establish whether the final prediction error was also the minimum achieved in the successive parameter addition. These results are presented in Table 5.9 and show that in almost every run (except for the AM) the addition of parameters was continued after the minimum prediction result was reached.

The results of Tables 5.7 and 5.9 clearly show that the Alternate Method has the lowest tendency to increase the error. However, it is still surprising that a method that is based on the reduction of that error can still over-fit. This feature is the result of the fact that selection of an additional parameter was done per row, but then the combined effect of all three rows is integrated into a single simulation using a Runge-Kutta integration; this

Table 5.7: Number of successful runs out of 48, where the final error  $<$  initial error, for the three different equations (roll,  $\beta$  and yaw). The last column gives the number of runs in which the final error was smaller than the initial error in all three equations.

Final error $<$ Initial error Successful runs out of 48				
Method	$\beta$	roll	yaw	All
AICC	5	4	4	0
BIC	4	2	2	0
PSE	9	6	7	1
R2	8	6	7	0
F2	7	5	7	0
AM	37	39	41	27
AM- $\phi$	35	38	40	26

Table 5.8: Division of successful runs; presented values are the number of successful runs per test condition. The number of runs for each test condition is presented in the second column.

Test Condition	No runs	AICC	BIC	PSE	R2	F2	AM	AM- $\phi$
Turbulence	24	0	0	0	0	0	7	6
Smooth conditions	24	0	0	1	0	0	20	20
Limited inputs	24	0	0	1	0	0	14	13
Extra inputs	24	0	0	0	0	0	13	13
Non Failure runs	8	0	0	1	0	0	5	5
50% Aileron failure	8	0	0	0	0	0	2	2
100% Rudder failure	8	0	0	0	0	0	6	6
Engine failures	8	0	0	0	0	0	6	5
Rudder hardover	8	0	0	0	0	0	3	3
Lateral asymmetry	8	0	0	0	0	0	5	5

## 5

combined effect does often lead to a small increase in error.

Graphically this effect on  $\beta$  is demonstrated in Figs. 5.7a and 5.7b. The effect on the roll is demonstrated in Figs. 5.7c and 5.7d. These figures show the results of a run in smooth flying conditions with a lateral asymmetry. When comparing the  $\beta$  errors before the addition of model parameters, (Fig. 5.7a) and after, (Fig. 5.7b), we see that the addition of parameters caused an increase in SSE, and this increase happens in the last 0.7 second of the manoeuvre. Adding model parameters for the roll response shows a similar behaviour, an increase in SSE after the addition of 10 parameters, Fig. 5.7d, but now the increase in SSE starts directly at the beginning of the manoeuvre.

To get an insight into how each added model parameter affected the final outcome, plots were made of the SSE error in the final roll manoeuvre as a function of the number of added parameters, see Fig. 5.8. The figure shows that the error in  $\beta$  and  $r$ —after an initial increase— starts to decrease. The optimum is reached after the addition of the fourth parameter, however, both continue beyond this optimum, and the  $\beta$ -SSE even exceeds

Table 5.9: Number of successful runs out of 48, where the final error is the minimum error, for the three different equations (roll,  $\beta$  and yaw). The last column gives the number of runs in which the final error was the minimum error in all three equations.

Final error is the minimum error				
Successful runs out of 48				
Method	$\beta$	roll	yaw	All
AICC	1	0	0	0
BIC	1	0	0	0
PSE	2	2	0	0
R2	2	2	0	0
F2	1	1	0	0
AM	31	26	40	18
AM- $\phi$	30	26	38	17

the initial value. For  $p$  and  $\phi$ , the situation in this run is even worse, the SSE increases up to the addition of the sixth parameter and although after this the SSE decreases it remains well above the initial value.

We now want to compare these results with the results of a run using the same failure, but in turbulent flying conditions. Comparing Fig. 5.9 with 5.8 shows that in turbulent conditions all the SSE values rise above the initial value, and the optimum for  $\beta$  and yaw is now reached after the addition of a second parameter.

## 5.5. ADDITIONAL SIMULATIONS

The previous results were also presented in [12]. They were based on a failure that occurred at 160 KTAS while the maximum roll manoeuvre was performed at 120 KTAS. However, because the actual approach speed of the PA-34 is much lower, it was interesting to also investigate what the results would be at an approach speed of around 80 KTAS. These simulations, close to the manoeuvre limits of the model, required an adaptation of the autopilot that was not functional when the first results were presented. The new profile started at an airspeed of 120 knots at a low altitude of 300 feet and used a final velocity of 80 - 85 knots. The same failures and identification manoeuvres of the initial tests were used. The results are presented in Table 5.10.

If we compare these results with Tables 5.7 and 5.8 we see the same trend: all selection methods lead to over-fitting and the number of successful runs is very small except in the alternate methods. There are small differences between the two sets of simulations in the exact number of additional model parameters added, but these results confirm our earlier conclusions that the standard methods lead to over-fitting.

Finally, we compared the increase in SSE due to the over-fitting for the different selection methods. For this evaluation we summed the SSE over all 48 runs for each selection method and compared these with the initial SSE before any additional model parameter

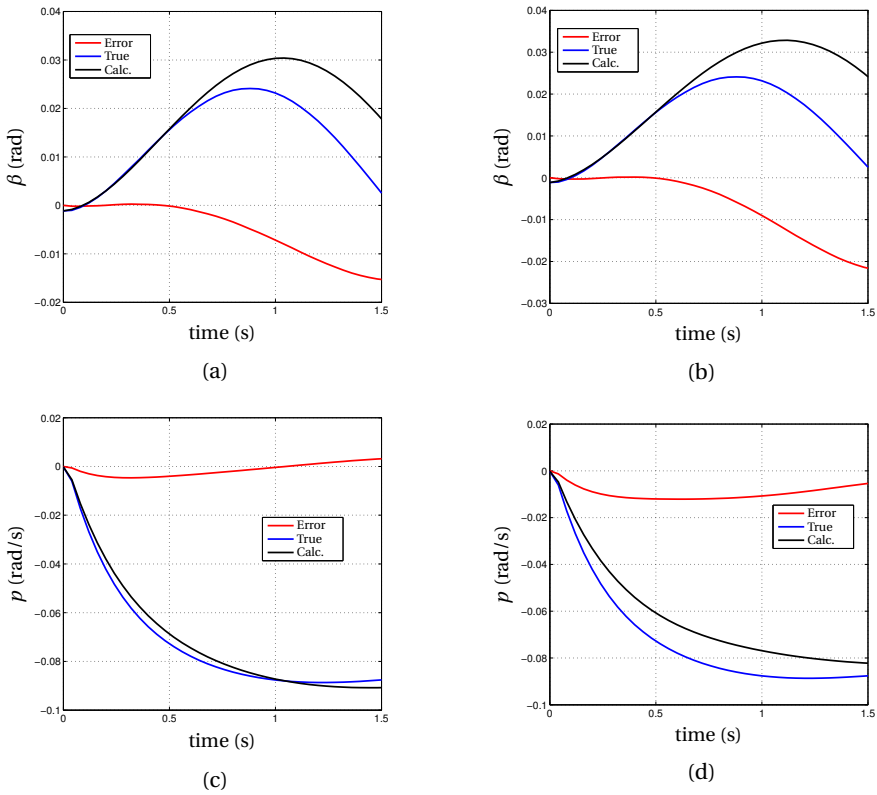


Figure 5.7: Comparison between the calculated  $\beta$  and  $p$  in the final roll manoeuvre, based on the derived model parameters, using a Runge Kutta integration and the actual  $\beta$  and  $p$  values. The chosen run is a lateral asymmetry in smooth flying conditions; (a) initial  $\beta$  errors, (b) final  $\beta$  errors after 5 additional model parameters were added, (c) initial  $p$  errors (d) final  $p$  errors after 10 additional model parameters were added. The AICC criterion was used for selecting additional model parameters.

was added. These results are presented in Tables 5.11 and 5.12 for the initial set of 48 runs, and the second set based on the lower final velocity.

The results show an almost explosive increase in the SSE due to the addition of extra parameters, especially in the SSE of  $\beta$ . Comparing the results from smooth flying conditions with flights in turbulence shows that the largest increase occurs in turbulence, however, the increase in SSE in smooth conditions is also considerable.

The results for flights at lower speed differ significantly. While the initial errors are the same order of magnitude, the error increase due to the addition of parameters is much smaller. Furthermore, the runs in turbulent conditions show an even smaller increase than in smooth conditions. Apparently the prediction from data at high speed is more difficult than from data at a lower speed. While the quantitative effect may be dif-

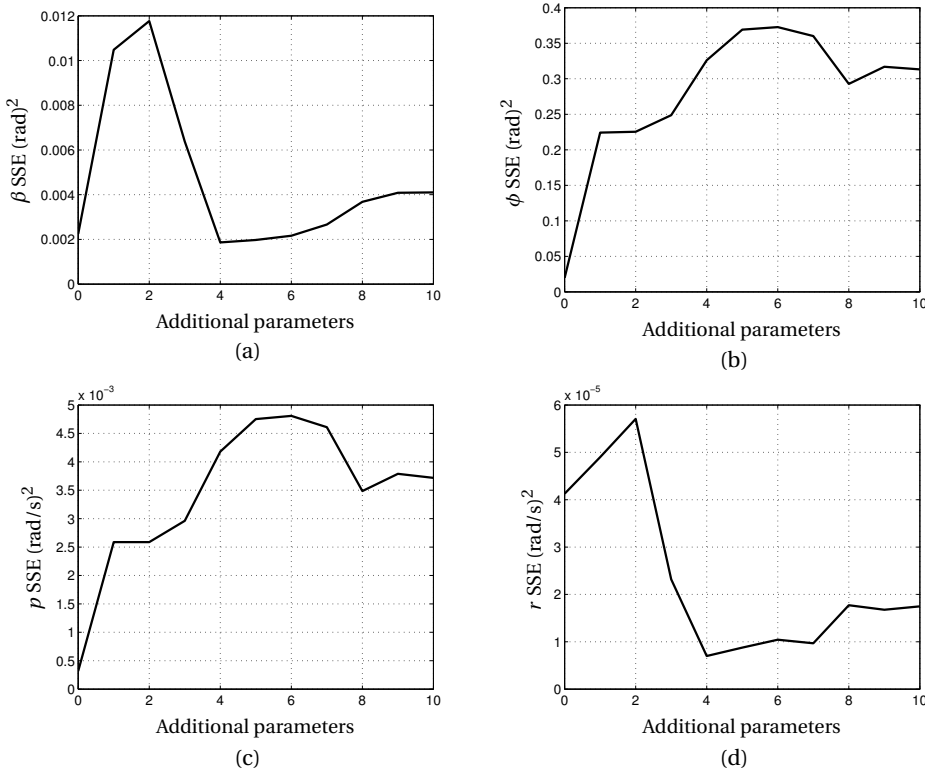


Figure 5.8: SSE error of  $\beta$ ,  $\phi$ ,  $p$  and  $r$ , in the final roll manoeuvre, as function of added model parameters; shown is run 177, a lateral asymmetry in smooth flying conditions.

ferent, the common fact is that all standard model selection criteria are adding too many parameters to enable an accurate prediction.

#### CONCLUSION ON SELECTION METHODS

The results show that the classical methods investigated added too many parameters, which increased the SSE of the predicted final manoeuvre to above the initial value. This similar behaviour of the statistical methods was to be expected from the theoretical analysis, which showed the large similarity of these methods.

Both Alternate Methods worked well, even if there was an increase in the SSE, this increase was small. These methods were the only methods with a positive effect in the summed SSE over all runs, as can be seen in Tables 5.11 and 5.12. From these data it is evident that we should base our model on the results of the Alternate Method. Choosing between the two models we opt for the standard model, not based on  $\phi$  optimization, because an optimization of  $\beta$ , roll and yaw will give a more physically correct model. Later this chapter we try to find the cause(s) of over-fitting of standard statistical methods.

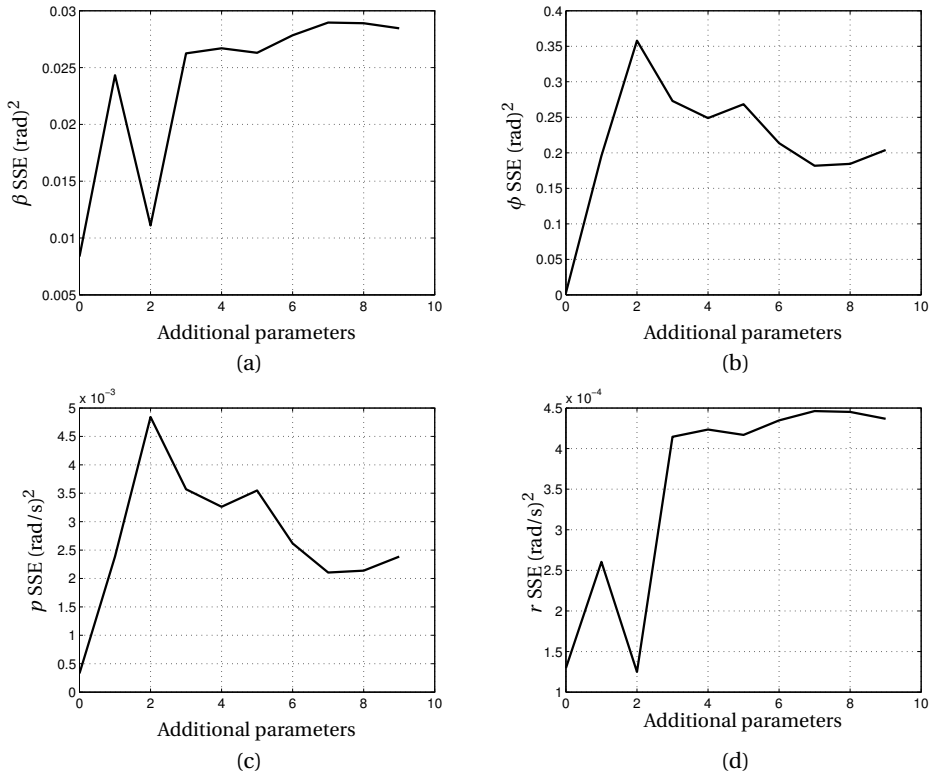


Figure 5.9: SSE error in final roll as function of added model parameters in run 181, lateral asymmetry in turbulent flying conditions; (a)  $\beta$ , (b)  $\phi$ , (c)  $p$ , and (d)  $r$ .

## 5

### OPTIMUM MODEL

If one of the statistical methods would have given a favourable result we could have adapted the model in flight based on the failure condition. However, the alternate method can only be used in off-line simulations, we need the information of the final roll manoeuvre, and therefore the model will be fixed. In the previous simulations, the optimum model was derived for each scenario, but now we must select one optimum model and investigate the effect on all scenarios. Unfortunately, the parameters chosen by the Alternate Method (Tables 5.4, 5.5 and 5.4) differ considerably depending on the failure. The highest percentage for a single parameter is 41.7%, indicating that using this parameter is favourable in 41.7% of the scenarios, but may have a yet unknown, negative effect in the remaining 58.3%. To investigate this effect we added the three most often chosen additional parameters i.e. 2, 5 and 10, to the basic model and compared the results of this model with the results of the basic model. These results are presented in Table 5.13.

The results of Table 5.13 show that the overall effect of adding these parameters is an increase in the SSE. The increase in SSE is much lower than the increase caused by

Table 5.10: New evaluation at 80 KTAS; Percentage of successful runs out of 48 where the final error < initial error for the three different rows (roll,  $\beta$  and yaw). The last column gives the number of runs where the final error was smaller for roll,  $\beta$  and yaw.

Final error < initial error Successful runs out of 48				
Method	$\beta$	roll	yaw	All
AICC	22	6	14	2
BIC	29	21	5	1
PSE	20	3	12	1
R2	20	3	4	1
F2	28	12	15	5
AM	31	41	47	29
AM- $\phi$	33	41	46	30

Table 5.11: Initial and final SSE of the final roll reconstruction for the different selection methods. The top three rows present the SSE over all 48 simulations, the three middle rows show the contribution of the 24 runs in smooth flying conditions, and the bottom three rows show the contribution of the 24 runs in turbulent conditions to the SSE. All runs were with the final roll manoeuvre at 120 KTAS.

param.	INITIAL	AICC	BIC	PSE	R2	F2	AM	AM- $\phi$
Results all flying conditions (48 runs)								
$\beta$	0.445	731.16	713.03	590.18	574.11	1154.20	0.3494	0.3762
roll	0.023	15.00	14.42	11.96	11.84	20.97	0.0160	0.0167
yaw	0.013	14.98	13.74	13.59	14.09	20.33	0.0077	0.0089
Results smooth flying conditions (24 runs)								
$\beta$	0.162	1.49	1.54	1.42	1.70	1.51	0.0802	0.0607
roll	0.010	0.13	0.14	0.09	0.14	0.13	0.0049	0.0045
yaw	0.005	0.04	0.04	0.05	0.05	0.05	0.0028	0.0036
Results turbulent flying conditions (24 runs)								
$\beta$	0.283	729.67	711.49	588.76	572.41	1152.69	0.2692	0.3155
roll	0.012	14.86	14.28	11.88	11.70	20.84	0.0111	0.0121
yaw	0.008	14.94	13.70	13.54	14.05	20.28	0.0049	0.0053

the addition based on the other selection methods as presented in Tables 5.11 and 5.12, but it is still an increase. This suggests that the basic model might be the better choice. Because we have only investigated the reconstruction error and not the effect on the accuracy of the  $V_c$  prediction, we will use the basic model as well as the model with three added parameters in the next chapter, where we optimize the  $V_c$  prediction.

## 5.6. INVESTIGATING POSSIBLE CAUSES OF OVER-FITTING

### OVERVIEW

The results favour a much smaller model than standard model selection criteria suggest. Three possible reasons why the standard selection methods do not perform well were further investigated. The first reason could be collinearity. With a high number of variables, collinearity may exist. Therefore an additional test was performed to check if setting a collinearity limit would improve the standard methods. A second reason could

Table 5.12: Initial and final SSE of the final roll reconstruction for the different selection methods. The top three rows present the SSE over all 48 simulations, the three middle rows show the contribution of the 24 runs in smooth flying conditions, and the bottom three rows show the contribution of the 24 runs in turbulent conditions to the SSE. For all simulations the final roll was made at an airspeed between 80 to 85 KTAS.

param.	INITIAL	AICC	BIC	PSE	R2	F2	AM	AM- $\phi$
Results all flying conditions (48 runs)								
$\beta$	0.22	3.77	3.09	3.35	4.19	3.59	0.200	0.189
roll	0.04	0.66	0.41	0.67	0.80	0.59	0.021	0.022
yaw	0.02	0.38	0.21	0.33	0.40	0.24	0.010	0.010
Results smooth flying conditions (24 runs)								
$\beta$	0.13	2.84	2.37	2.42	2.85	2.67	0.097	0.096
roll	0.02	0.32	0.31	0.36	0.32	0.29	0.009	0.009
yaw	0.01	0.19	0.17	0.18	0.21	0.19	0.006	0.006
Results turbulent flying conditions (24 runs)								
$\beta$	0.10	0.93	0.72	0.93	1.34	0.92	0.104	0.093
roll	0.02	0.34	0.10	0.31	0.48	0.30	0.012	0.013
yaw	0.01	0.19	0.04	0.15	0.19	0.05	0.004	0.004

Table 5.13: The sum of the SSE in the final roll reconstruction over 48 scenarios. Comparing the results of the basic model and the model with three added parameters, i.e 2, 5 and 10.

parameter	Basic model	Model with 3 added variables
	SSE	SSE
$\beta$	0.44528	1.0528
$p$	0.02261	0.0719
$r$	0.01268	0.0211
$\phi$	0.88701	2.6994

## 5

be that the number of samples gives an exaggerated indication of information content. Typical pilot inputs have a low frequency content, unless pilots are engaged in a high gain tracking task. Consequently the information content may be low. To investigate this hypothesis the effect of adding more data on the set with the maximum number of input parameters (24) was investigated. The rationale for using the model with the largest number of parameters is as follows: All parameters are legitimate candidates that originate directly from the model derivation in Chapter 4. If the lack of data is the contributing factor, then this effect may be different for each parameter, but by using the maximum number of variables the visibility of this effect is the greatest. Finally it was investigated whether the linearisation of higher order parameters, needed for our linear regression analysis, contributed to over-fitting.

## METHOD

We investigated these plausible causes on one specific run. If that would give an improvement, the method could be applied on all runs. However, if there was no improvement there would be no need to test it on all runs. The run we chose was Run 177, a

lateral asymmetry in smooth flying conditions. This run was chosen because many of the additional parameters are non-zero and theoretically needed.

#### COLLINEARITY

To investigate the effect of collinearity, an extra step was added to the selection method. Before an additional independent variable was investigated for incorporation into the model, it was checked for collinearity with the already incorporated independent variables. As measure for collinearity the Variation Inflation Factor (VIF) [13, p. 408] is often used, which is defined as:

$$VIF = \frac{1}{1 - R^2}, \quad (5.43)$$

where  $R^2$  is the coefficient of determination (Eq. 5.9) of the new input variable against the input variables incorporated. However, it is more intuitive to just use the  $R^2$  value, which implies that 1 is complete collinearity and zero is none; and therefore we use  $R^2$ . In the following evaluation we checked if the AICC method in run 177 would improve if we set collinearity limits of 0.90 and 0.80. In run 177 the failure simulated was a lateral asymmetry.

Figs. 5.10a, 5.10b, 5.10c and 5.10d depict the effect of collinearity limits on the SSE of  $\beta$ ,  $p$ ,  $r$  and  $\phi$ , measured over the final roll manoeuvre. The results show an almost random behaviour. Not adding variables with a collinearity higher than 0.9 worked unfavourably for  $\beta$  but favourably for yaw. When the collinearity limit was set to 0.8 the difference disappeared. For  $p$  and  $\phi$  the 0.9 limit showed the least increase in SSE while setting the limit to 0.8 gave similar results to having no limit. However, the important point is that the adding of parameters still increased the SSE in roll and yaw and therefore we should rule out collinearity as the cause of over-fitting.

#### INCREASE IN DATA POINTS

The second experiment investigated the effect of an increase in data points. Four different runs with exactly the same failure, a partial loss of aileron, but with different control inputs and different turbulence levels, were combined. This was done by using a recursive least squares in the following way: It started in the first run without any knowledge about the model parameters and their covariance. In the second run the final values of the model parameters and their covariance of the first run were used as input values. This continued in the same fashion for the third and fourth run. In these multiple runs the final maximum roll manoeuvre was initially excluded because we preferred to investigate the capability to predict this final roll, however, later in this chapter we will include this effect and note the differences.

From the derived model parameters and the inputs, the normalized  $\beta$ ,  $p$  and  $r$  accelerations were reconstructed for each run and compared with the measured values to calculate the SSE. Fig. 5.11 shows the change in SSE per run, Fig. 5.11a shows the SSE from the trajectory up to the final roll, while Fig. 5.11b displays the SSE of the final roll. We notice a positive effect of the multiple runs on the decrease of the SSE in the final roll manoeuvre and a slightly smaller positive effect on the SSE over the measured trajectory.

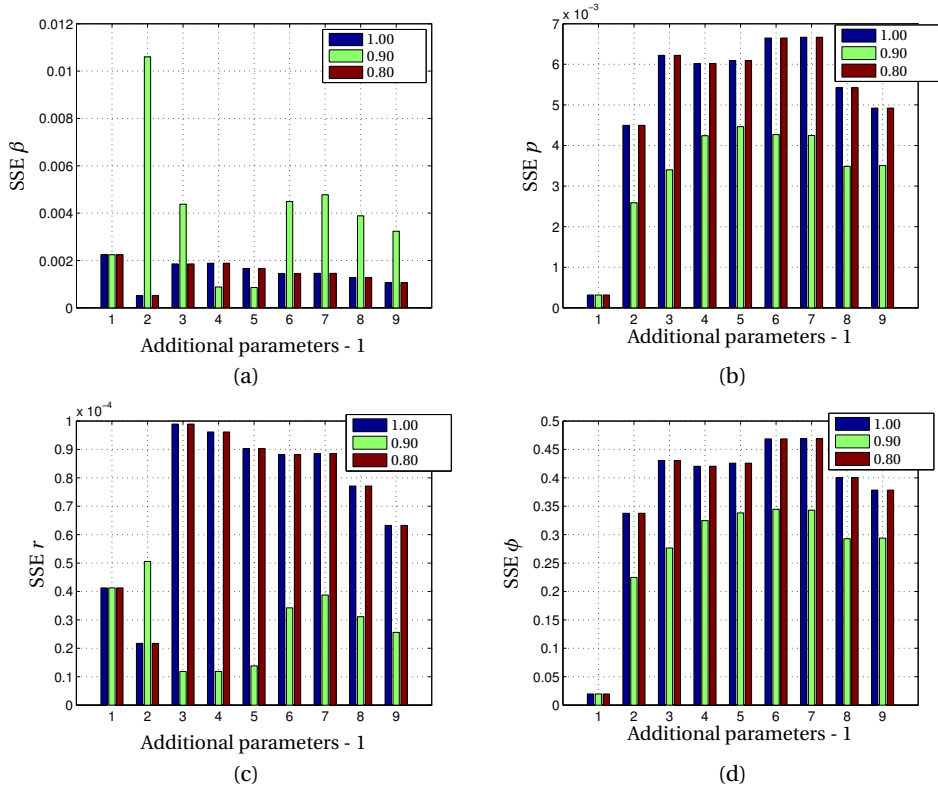


Figure 5.10: The effect of adding a collinearity check on the AICC method. The chosen run (177) is a lateral asymmetry in smooth flying conditions; Three limits were investigated: 1.0, which equates to no limit, 0.9 maximum collinearity and 0.8 maximum collinearity. The figures present the SSE of the final roll as function of additional parameters. Figure (a) is SSE  $\beta$ , (b) is SSE  $p$  and (c) is SSE  $r$  and (d) is SSE  $\phi$  over the complete run.

## 5

To value this positive effect on the SSE in the final roll manoeuvre we have to compare these data with the SSE data achieved with the smallest model.

When we compare the SSE over the trajectory up to the final roll, using 10 and 24 independent variables (Fig. 5.12), we note that the large set with 24 input variables in general<sup>5</sup> has a lower SSE than the 10 variable set. This is in line with theory and would suggest that the 24 variable set has a higher accuracy. The surprising fact is, however, the difference in prediction accuracy.

Fig. 5.13 shows the SSE of the prediction of the maximum roll. It is clear that using 10 independent variables gives a much higher prediction accuracy. In short, the more

<sup>5</sup>Using give a lower SSE over the complete trajectory. But here we are using RLS and the SSE is the value over the last run. Consequently, the SSE of the larger model might sometimes be slightly higher but should converge to a lower value.

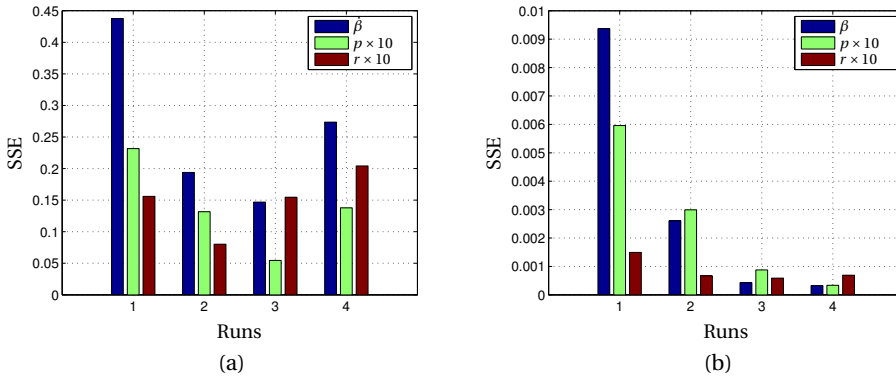


Figure 5.11: Effect of data size (multiple runs) on SSE for 24 parameter model. The multiple runs do not include data from the final roll. Runs are for a partial aileron failure in smooth and turbulent conditions with different types of inputs. (a) is SSE for trajectory up to the final roll and (b) is the SSE of the predicted final roll.

accurate reconstruction of the past is no guarantee for a better prediction of the future. This underlines and confirms what we already noticed before, and proves that the size of the data set was not an issue.

Further research was conducted into why the large model showed a larger SSE. In the next analysis the prediction method was changed. Instead of basing the prediction on the measurements until the final roll, the maximum roll data were incorporated as follows: The model parameters at the start of the run were based on the analysis of the complete previous run including the maximum deflection roll. Of course, the prediction of the present run was made based on the data up to but not including the final roll. The effect of this change is shown in Fig. 5.14a.

Of course, this can be seen as a trivial test, because, if we include data about the maximum deflection roll, the model parameters must be better suited to predict it. But it also confirms that the parameter identification worked correctly and this inaccuracy to predict the maximum roll should be completely attributed to the amount of manoeuvring in the initial part of the simulation. Another remarkable fact is that the SSE, using the model based on 10 independent variables and not based on the data including the maximum roll (marked by 10\*), has a similar accuracy as the model using 24 independent variables and based on the complete data set including the maximum performance roll.

The manoeuvring before the final roll is, however, far from benign, as can be seen in Fig. 5.14b. This run not only has the standard small inputs for heading changes but also deliberate control checks. In the case of the aileron deflection, this incorporated a deflection to 40% of the maximum range. Based on these results, we suspect that the higher order model parameters that are linearised for the least squares estimation can not be estimated accurately, unless large excitations are used. We will further investigate these ‘non-linear effects’ in the next section.

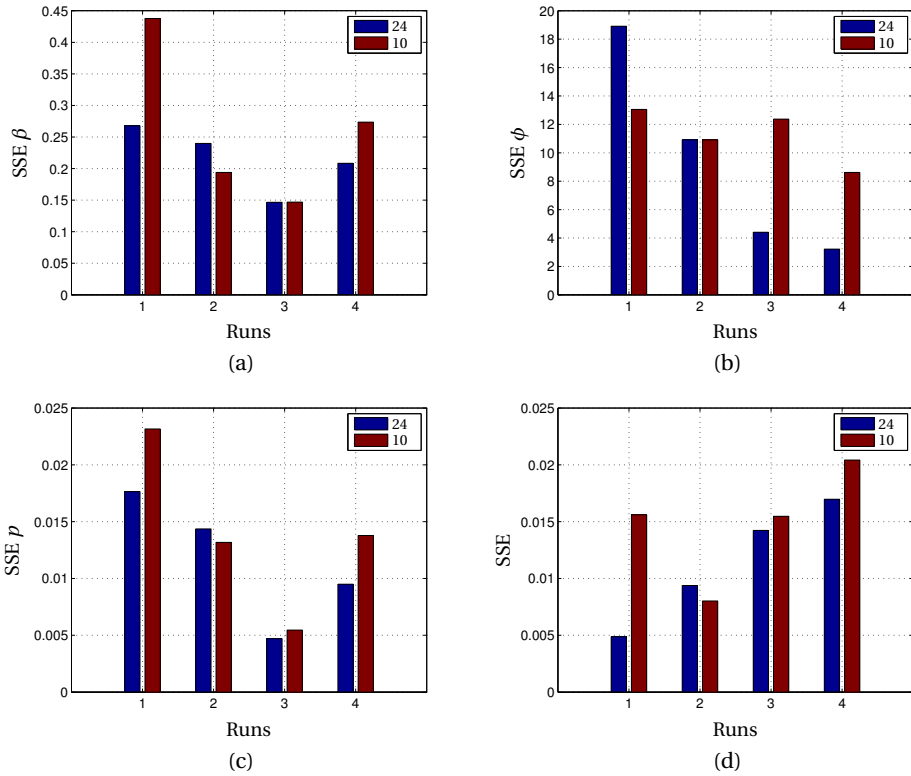


Figure 5.12: Comparing the minimum model size with the maximum size (10 and 24 independent variables) for the SSE over the trajectory up to the final roll. The failure is a partial loss of aileron.

## 5

### NON-LINEAR EFFECTS

The identification model is linear in the parameters, but the system itself is not linear. Typically, the additional independent variables are higher order, like:  $\left(\frac{pb}{2V}\right)^2$ ,  $\left(\frac{pr}{2V}\right)^2$  and  $\beta^2$ . In limited manoeuvring the squared inputs are small and consequently the accuracy of the model parameters related to these inputs will be lower. However, finding these higher order model parameters could be of the utmost importance in manoeuvres at the control limits. Here, we will investigate, as an example, the aileron behaviour of the PA-34. The actual aileron performance of the PA-34 used in the model is non-linear, as shown in Fig. 5.15. Because this non-linear behaviour was known, it was incorporated into the parameter identification process using:

$$\delta_{a,red} = \delta_a - 0.3778(\delta_a)^3 \quad (5.44)$$

With this new  $\delta_{a,red}$  the linearity in parameters was restored, which facilitated system identification. However, assuming that this non-linear behaviour was not standard but a result of damage, we wanted to identify this non-linear behaviour during the OLS

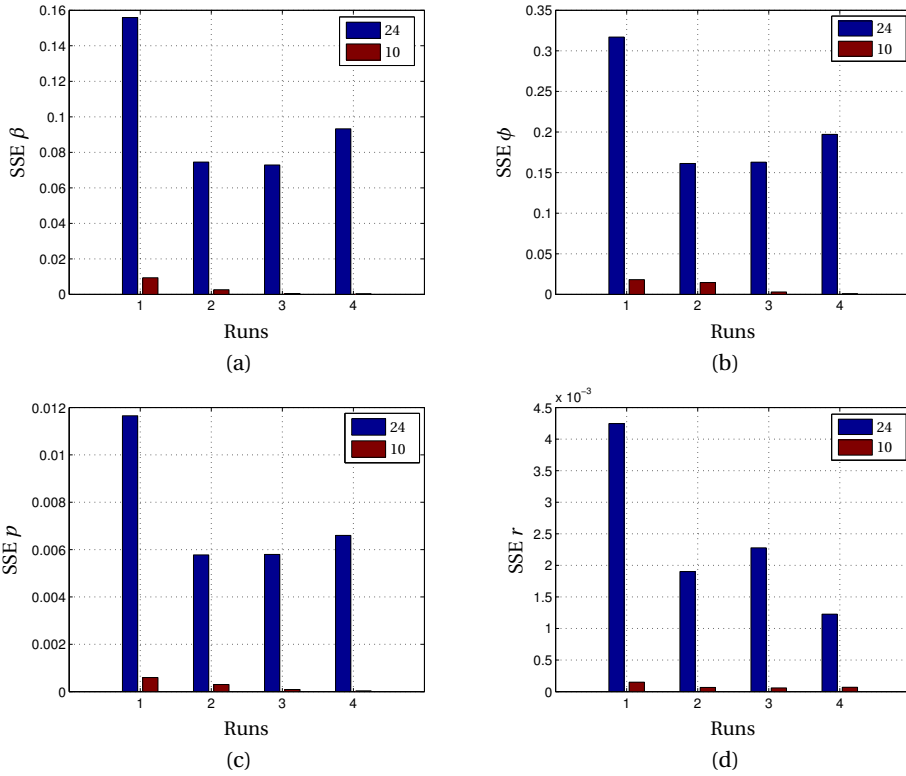


Figure 5.13: Difference in SSE of the predicted roll for both the 10 and 24 parameter model.

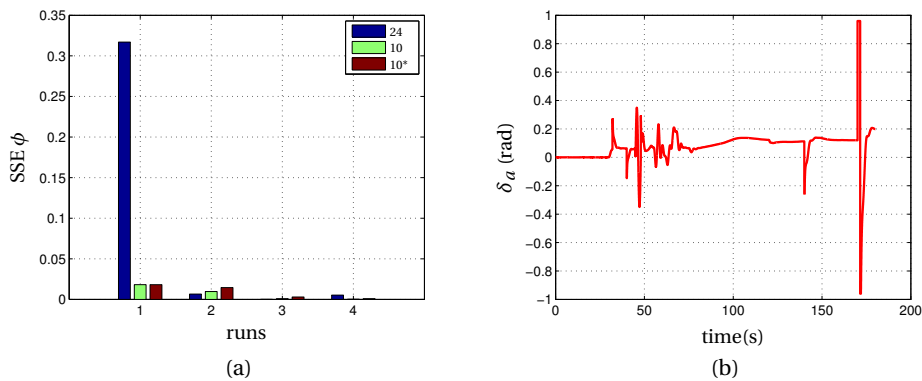


Figure 5.14: Figure (a) shows the SSE of  $\phi$  for the predicted roll using the 24 and 10 independent variables. The final roll is included in the first two data sets. For comparison the SSE of  $\phi$  without the final roll, using the 10 parameter set is included and marked as 10\*. Figure (b) shows typical aileron inputs used in each run.

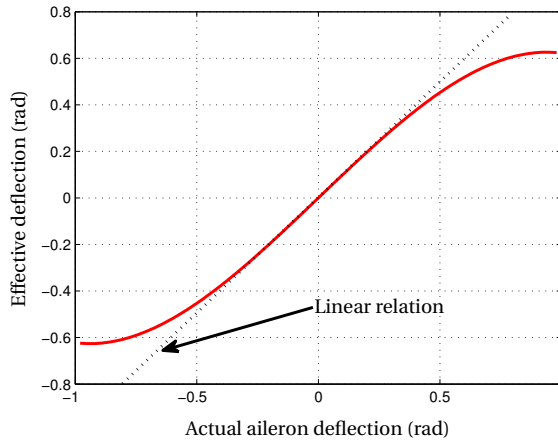


Figure 5.15: Aileron effectiveness PA-34 based on Eq. 5.44.

trajectory. So, we removed the rule to transform the aileron deflection and investigated the effect of this removal on the SSE. Now the independent variable  $(\delta_a)^3$ , and the related parameters  $y_{(\delta_a)^3}$ ,  $l_{(\delta_a)^3}$  and  $n_{(\delta_a)^3}$  are needed to correct for the non-linear aileron. As can be seen in Table 5.3 the aileron deflection to the third power is already incorporated into the additional variables.

If we look at the result of this data analysis in Fig. 5.16, three different cases are compared. Firstly the effect of the 10-variable set with the linearised aileron, secondly the effect of the non-linear aileron with the 24-variable set and thirdly the same set with the final roll incorporated into the parameter identification process (after the first run). Fig. 5.16a shows the normal view, and Fig. 5.16b an expanded view because of the small size of the SSE for the 10-variable model. It is obvious that the non-linear prediction, based on the data before the roll, has an order of magnitude larger errors than the linearised model. This confirms the difficulty in making envelope predictions using non-linear parameters. When we base our envelope predictions on data including the maximum roll, the non-linear aileron will have smaller errors than the standard set, which is to be expected. However, we should not call this the prediction of the envelope because it is more a confirmation of the measurements.

## 5.7. CONCLUSION

Our investigation regarding the right model for envelope prediction showed that standard model selection methods are not well suited for the determination of the model order, if this model is used to predict manoeuvres requiring larger inputs than are used for PID. An alternative method, designed to focus on the aircraft behaviour in manoeuvring at the edge of the envelope, proved to be more robust and was less prone to increase the prediction error. Another conclusion is that the continuous adaptation of a model, as for example done in [10] may not be the preferred method for performing envelope

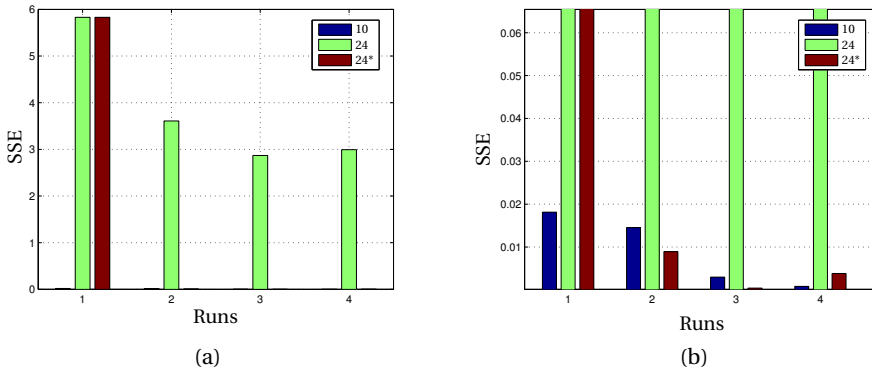


Figure 5.16: Prediction accuracy in SSE ( $\phi$ ). Comparing (1) the 10 parameter model using the linearised aileron, with (2) the 24 parameter model and the non linear aileron and (3) the same set as (2) but with incorporation of the final roll in the parameter estimation. Figure (a) shows the normal view and Figure (b) shows the expanded view.

prediction, at least not when using the selection methods we evaluated.

The model order selection was based on an empirical dataset, with a number of representative failures and for expected flight conditions. Since the selection was based on a limited number of cases, we had to ensure that we covered all possible lateral envelope limiting cases to prevent us from developing a model that is only capable of handling a subset of all possible lateral control problems. The selected subset was based on our experience with lateral failures that have occurred over the years, as well as on the fact that an aircraft is a physical system with limited possibilities to affect the lateral control.<sup>6</sup>

Higher order independent variables have a detrimental effect on the accuracy of the prediction. In order to estimate these model parameters related to the higher order variables correctly, large control deflections are necessary. For throttle inputs, these larger inputs are easily done, because maximum throttle excursion will not generate excessive loads on the aircraft. However, a pilot faced with a damaged aircraft will normally fly his aircraft carefully and refrain from large aileron, elevator and rudder inputs, especially at high speed where these inputs may cause high roll and g-loads. A possible work-around is to continue with control checks when the speed is reduced and controls can be more easily deflected close to the maximum range without excessive loads. Even after that, if we make a model-based envelope prediction, the pilot must be aware of its limitations and his or her crucial roll in achieving accurate results.

In this chapter we have evaluated model size based on the reconstruction accuracy of the final roll manoeuvre. Based on these findings we can limit the number of models for further investigations. The models chosen are the basic model and with three added

<sup>6</sup>If we limit ourselves to manual control and exclude failures of autopilot and advanced control systems.

parameters as shown in Table 5.13. In the next chapter we will evaluate the effect of model size and other variables such as PID method, normalization and pre-set values on the accuracy of the  $V_c$  prediction.

## REFERENCES

- [1] J. Easley, *No Wing F15*, USS BENNINGTON CREW'S STORIES (2015), <http://www.uss-bennington.org/phz-nowing-f15.html>.
- [2] Anon, *Accident Description*, Aviation Safety Network (2016), <http://aviation-safety.net/database/record.php?id=19940404-1>.
- [3] R. J. de Muynck and M. Van Hesse, *The A-Priori Simulator Software Package of the Piper PA34 Seneca III*, Tech. Rep. (TU Delft, 1990).
- [4] H. J. Koolstra, H. J. Damveld, and J. A. Mulder, *Envelope Determination of Damaged Aircraft*, in *Proc. of the AIAA Guidance, Navigation, and Control Conference 2012, Minneapolis, USA, Aug. 13-16* (AIAA, 2012).
- [5] M. Coenen and T. Huls, *Modelselectie: AIC en BIC*, Tech. Rep. (Radboud Universiteit Nijmegen, 2008).
- [6] G. Strang, *Linear Algebra and its Applications* (Academic Press, INC, 1980).
- [7] Anon, *NIST/SEMATECH e-Handbook of Statistical Methods* (NIST, 2013) <http://www.itl.nist.gov/div898/handbook/>.
- [8] H. Akaike, *A new Look at the Statistical Model Identification*, IEEE Transactions on Automatic Control **19**, issue **6**, 716–723 (1974).
- [9] A. Barron, *Self-Organizing Methods in Modeling* (Marcel Dekker, New York, 1984) p. 87:103.
- [10] T. J. J. Lombaerts, *Fault Tolerant Flight Control*, Ph.D. thesis, Technical University Delft (2010).
- [11] G. Schwartz, *Estimating the Dimension of a Model*, The Annals of Statistics **6**, 461 (1978).
- [12] H. J. Koolstra, C. C. de Visser, and J. A. Mulder, *Effective Model Size for the Prediction of the Lateral Control Envelope of Damaged Aircraft*, in *Proc. of the AIAA Guidance, Navigation, and Control Conference, the AIAA SciTech Forum 2015, Kissimee, USA* (2015).
- [13] M. H. Kutner, C. J. Nachtsheim, J. Neter, and W. Li, *Applied Linear Statistical Models* (McGraw-Hill, 2004).



# 6

## CONFIGURATION CHOICES AND PREDICTION ACCURACY



## 6.1. INTRODUCTION

In the previous chapters we developed the equations needed to calculate the minimum lateral control velocity, based on the derived parameters of our state space model, and we determined the optimal model size based on the prediction capability of the maximum roll manoeuvres. In this chapter, we design the  $V_c$  Prediction System (VPS) that will be used for the pilot-in-the-loop testing described in Chapters 7 and 8. In the design of the VPS we have several configuration options, these options include the choice of parameter identification method, the choice of normalization of the independent variables and the choice in initial model parameter values. Furthermore, in this chapter we will again use several model size options, but now the emphasis lies on evaluating the effect of model size on the  $V_c$  prediction. We will first discuss the design of the VPS and explain the different configuration options. Based on the configuration options, a set of 48 different combinations was used in the subsequent  $V_c$  evaluation. For this evaluation we used failure scenarios, which were generated off-line with the non-linear model of the Piper Seneca. In the  $V_c$  evaluation the aim is to find the combination that accurately and timely predicts  $V_c$ . We will also develop some refinements in the VPS routine to further improve accuracy.

## 6.2. CONFIGURATION CHOICES FOR VPS

### 6.2.1. VPS DESIGN

In this paragraph we present an overview of the different modules used in the VPS. Detailed information on each module is given in the specific sections. A diagram of the VPS is presented in Fig. 6.1. The first module is the Parameter Identification (PID) that uses the aircraft state and the control inputs to derive the aircraft parameters. The second module is the error detection, that measures the differences between the predicted and measured aircraft responses. If this, time averaged, error exceeds a pre-determined threshold, this serves as an indication that some aircraft parameters are in error, which might be caused by aircraft damage. On error detection the PID is reset. This reset is required because the PID is normally ‘averaging’ all available data, past and present. The reset will cause the PID to forget the past data and to use only the data gathered after the error detection. This will enable a quicker convergence to the new parameter values. The error detection method used is described in Appendix C. In the third module the  $V_c$  is calculated based on aircraft parameters and a required roll angle change in a pre-defined time period. In the last module the  $V_c$  value is integrated in the Primary Flight Display (PFD).

There are four configuration options involved with the PID. The first option is the model size as discussed in Chapter 5. There we showed that the small model had a better prediction capability than the larger models. Based on the results we selected three model sizes to be further evaluated here. The first model is the smallest model, with 10 independent variables. Because we use three rows to calculate slip angle rate, roll acceleration and yaw acceleration, expressed as  $\frac{b\dot{\beta}}{V}$ ,  $\frac{b\dot{p}}{2V}$ , and  $\frac{b\dot{r}}{2V}$ , the total number of aircraft parameters is 30. The second model size used adds three independent variables, namely:

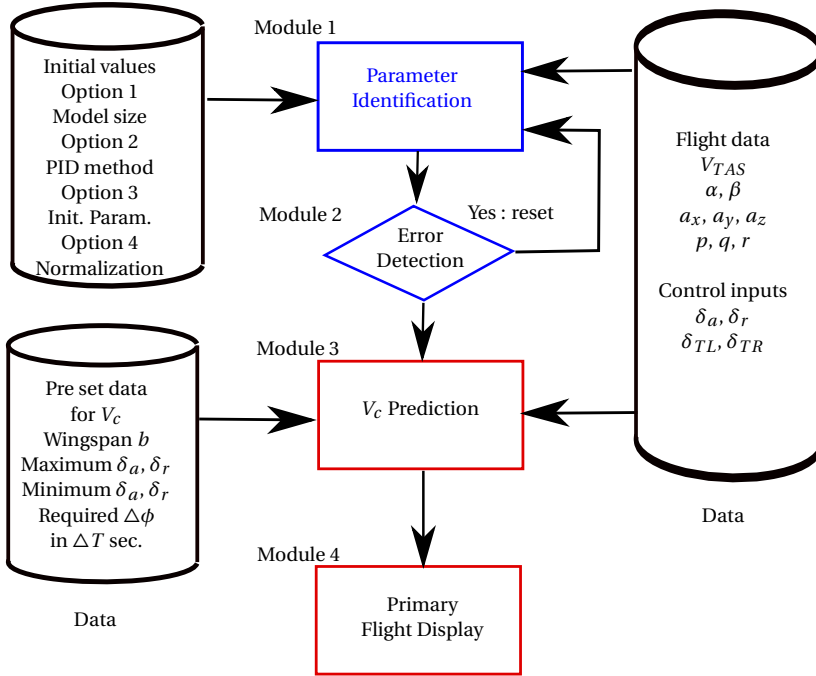


Figure 6.1: Graphic representation of the VPS. The black boxes contain the initial parameter values and flight information used. The blue boxes contain the chosen PID system and error detection system. The red boxes include the models designed in this thesis.

$\left(\left(\frac{pb}{2V}\right)^2 + \left(\frac{rb}{2V}\right)^2\right)$ ,  $\left(\frac{pb}{2V} \frac{qb}{2V}\right)$  and  $\left(\frac{pb}{2V}\right)^2$ . These parameters were selected because the alternate selection method of Chapter 5 chose these parameters most frequently. Finally, we also used the full model with 22 independent variables. According to our findings in Chapter 5, the second model should perform best, but by including the two other models in this evaluation, we hope to confirm the findings of Chapter 5 and also quantify the effect on the  $V_c$  prediction.

## 6

The second option is the PID method used. An important choice is whether the PID should use a reset, as explained above, or use a Forgetting Algorithm (FA) that favours the recent data over the old. We will evaluate two types of FA and two PID methods with resets in detail in Section 6.2.2, and will also make some configuration choices to optimize the forgetting algorithms.

The third option concerns which initial parameter values should be used in the model. Initial model parameter values are necessary for two reasons: firstly, with initial model parameter values the VPS can start right away with the  $V_c$  prediction and no time is wasted. Secondly, normal flight conditions are not ideal for PID. For example, in normal flight the pilot will not use asymmetric thrust, which makes it hard to assess the

effect of engine thrust on roll and yaw. By using a proper initial model parameter set, adequate default values are provided for those model parameters that cannot be identified sufficiently accurately from normal flight. Therefore, we will select two different speeds for which a set of initial model parameter values will be determined and used. How the initial values are derived and what initial values are used is further described in Section 6.2.3.

The fourth option is the normalization used. As discussed in Chapter 3, the aircraft roll due to the induced propeller flow was not proportional to the thrust, but proportional to  $\frac{T}{V TAS}$ . From the initial model parameter values derived in Section 6.2.3 we learn that more independent variables can benefit from a changed normalization, resulting in a smaller parameter change over the speed range. This will be discussed in more detail in Section 6.2.3 as well. In our further evaluation of the  $V_c$  prediction accuracy we will use this new normalization, as well as the more commonly used normalization.

The total combination of options is 48: three model sizes, four PID methods, two different set of initial values and two normalization methods. All these combination are evaluated using a set of simulations, coincidentally numbering also 48, with the non-linear model of the Piper Seneca. This set of simulations is similar, but not identical, to the set used in Chapter 5 and is further described in Section 6.3. Apart from these simulations, special runs were made to derive the initial values, these runs are described in Section 6.2.3. We will first discuss the four PID methods in more detail and thereafter the options for initial model parameter values.

## 6.2.2. PARAMETER IDENTIFICATION OPTIONS

For our parameter estimation we propose the proven two-step method [1], which is a fast and simple method for parameter estimation. In the first step, a state estimation is performed, normally using extended Kalman Filtering. In the second step, the Recursive Least Squares (RLS) is used to estimate the system parameters. In our off-line simulation we used the non-linear aircraft model of the Piper Seneca to generate the data, therefore the data are not polluted by measurement noise and we can restrict ourselves to the second step. However, for the implementation in a real aircraft both steps are required.

There are different forms of RLS methods. The main choice is between standard RLS or an Forgetting Algorithm (FA). The standard RLS method uses a reset after the detection of a failure, as explained above, while FA methods constantly adapt and don't need a reset. The constant adaptation of the FA method normally comes at the price of reduced stability in the estimated parameter values. The Forgetting Algorithm with Damping (FAD), as developed by [2], can provide improved stability over the standard FA methods. Both the standard FA and the FAD method were used in our evaluation.

Damping is normally not required for RLS methods, except after a reset when parameter values show large excursions. An RLS method with damping was developed by Mayne [3] and named the Modified Kalman Method. This method is not a standard Kalman filter but an RLS method, which uses a noise matrix  $R$  in a similar way as the

Kalman filter. This  $R$  matrix has a dampening effect on parameter change, particularly when the number of samples is still low. We will now discuss the different methods in more detail.

### RLS METHOD

Defining the measurement vector as  $Z$ , the input vector as  $H$  and the (unknown) model parameter vector as  $\beta$ , the system can be defined as:

$$Z = \beta H + v, \quad (6.1)$$

where  $v$  is the white noise vector. The RLS method as described by [3] uses the following two equations to solve for  $\beta$ :

$$\hat{\beta}_{n+1} = \hat{\beta}_n + P_n H_n (Z_n - H_n^T \hat{\beta}_n) \quad (6.2)$$

$$P_{n+1} = P_n - P_n H_n (1 + H_n^T P_n H_n)^{-1} H_n^T P_n, \quad (6.3)$$

where  $P^{-1} = \sum_1^n H H^T$  and  $\hat{\beta}$  is the estimated value of  $\beta$ .

The system is initiated with a  $P$  matrix with large values and  $\beta$  set to the expected value or zero when no reference is known. For later comparison with the MKM method we like to point out that  $P_n H$  can be seen as the 'gain' of the RLS method because in Eq. 6.2, the residue is multiplied by  $P_n H$  to update  $\beta$ .

Defining the variance of the residue as  $R_v$ , the covariance matrix of  $\beta$  is defined as:

$$\text{cov}(\beta) = R_v P \quad (6.4)$$

### MODIFIED KALMAN

The MKM [3] developed by Mayne solves the same problem as RLS via a procedure that resembles the Kalman filtering update. The main difference is that this method uses the measurement noise variance matrix  $R$ . Starting with the state space definition of a linear time-invariant system:

$$\dot{x} = Ax + Bu; y = Cx + Du + v, \quad (6.5)$$

where  $x$  is the state,  $y$  is the observation,  $u$  is the control input and  $v$  is the noise input and  $A$ ,  $B$ ,  $C$  and  $D$  are the matrices defining the system. In our situation we have a fully observable state  $x$ , and  $D$  is the zero matrix. For parameter identification this system can now be modified by augmenting the system matrix and state.

$$\dot{\hat{x}} = [AB] \begin{bmatrix} x \\ u \end{bmatrix} \quad (6.6)$$

In the modified Kalman method [3] the known extended state and the unknown model parameters are interchanged. The model parameters are collected in a single column vector  $\beta$ , while the extended state parameter vector  $[x^T u^T]$  becomes the row vector  $\hat{x}$ . Equation 6.6 can be reformulated as:

$$\dot{x} = M\beta, \quad (6.7)$$

where  $M$  is a matrix with the same number of rows as  $[AB]$  and repeated blocks of the augmented state vector  $\hat{x}$ :

$$M = \begin{bmatrix} \hat{x} & 0 & 0 & 0 \\ 0 & \hat{x} & 0 & 0 \\ 0 & 0 & \hat{x} & 0 \\ 0 & 0 & 0 & \hat{x} \end{bmatrix} \quad (6.8)$$

The standard Kalman filter approach is now used to solve for  $\beta$ . The Kalman gain  $K$  is defined as:

$$K = PkM^T(MPkM^T + R)^{-1}, \quad (6.9)$$

where  $Pk$  is the covariance of  $\beta$  and  $R$  is the noise measurement variance. Initially  $Pk$  is set at an arbitrary high level and  $Pk$  is updated with the equation:

$$Pk_{k+1} = (I - KM)Pk_k \quad (6.10)$$

The  $R$  matrix might be initially unknown but can be estimated based on the measured residue. In our realization  $R$  was updated with a slow forgetting algorithm:

$$R = 0.995R + 0.005(ee^T), \quad (6.11)$$

where  $e$  is the innovation vector. By the incorporation of  $R$  this method becomes damped, with more conservative updates of the estimate when  $R$  is large, which would, for example, be appropriate when flying in turbulence. If  $R$  would be set to zero, this method would be identical to the RLS method as shown below.

### COMPARING RLS AND MKM

An easy way to compare both methods is first to rewrite RLS and the MKM method in individual equations per row. The block diagonal matrix  $M$  shows that rows are treated independently so it can be done for the MKM method, while for RLS working by row is already quite common [4]. If we evaluate by row, the noise matrix  $R$  becomes a scalar and a single row  $M$  reduces to  $\hat{x}$ , which is similar to the  $H^T$  vector used in RLS. We can now rewrite the gain and  $Pk$  update equations to:

$$K = PkH(H^T PkH + R)^{-1} \quad (6.12)$$

Furthermore,  $Pk$  is the variance of  $\beta$ , if we now use the covariance of  $\beta$  as derived by the RLS method (Eq. 6.4)  $Pk = R_v P$ . The gain can be written as:

$$K = R_v PH(H^T R_v PH + R)^{-1} \quad (6.13)$$

This indicates that as the measured variance of the residue  $R_v$  of the RLS method equals the predicted variance  $R$  of the MKM method, the gain can be written as:

$$K = PH(H^T PH + 1)^{-1} \quad (6.14)$$

Because  $H^T P H$  will decrease over time, the denominator will approach 1 and the gain will approach  $P H$ , which is similar to the RLS gain. This explains why the results of the MKM and RLS are very close except for the first samples, or the first samples after a system reset.

Doing the same exercise for the comparison of the  $P k$  and  $P$  update and starting with equation 6.10:

$$P k_{n+1} = (I - K M) P k_n \quad (6.15)$$

Using  $P k = R_\nu P$ :

$$P_{n+1} R_\nu = (I - K M) P_n R_\nu \quad (6.16)$$

$$P_{n+1} = (I - K H^T) P_n \quad (6.17)$$

Replacing  $K$  with equation 6.14:

$$P_{n+1} = P_n - P_n H_n (H_n^T P_n H_n + 1)^{-1} H_n^T P_n, \quad (6.18)$$

which is identical to equation 6.3. From this we can conclude that the  $P k$  and  $P$  update are similar if the  $R_\nu = R$ .

#### ILLUSTRATING THE DIFFERENCE BETWEEN RLS AND KF

The difference between RLS and MKM can be illustrated with a simulation of parameter identification in a noisy environment. In this simulation the unknown augmented system matrix is  $\begin{bmatrix} 1 & 3 \\ 4 & -1 \end{bmatrix}$ . Halfway through the simulation at 15 seconds, the model

matrix parameters are changed to  $\begin{bmatrix} 1 & 0.5 \\ 4 & -2 \end{bmatrix}$ .

As augmented input we used  $u = \begin{bmatrix} \sin(t) \\ \sin(3.4t + 5) \end{bmatrix}$  and white noise is added to the system output with a signal to noise ratio of 0.5. Both the RLS and the MKM system start with the estimated model parameters set at zero. When the model parameters are changed, it is assumed that this change is detected and the  $P$  matrix of the RLS method and the  $P_k$  Matrix of the MKM method are both reset to their initial (large) values. Fig. 6.2 presents the results of this simulation.

Comparing the RLS method depicted in Fig. 6.2a with the MKM method in Fig. 6.2b, we notice that the reset of the RLS method gives initially a spike in the value of the model parameters but after a few seconds this error diminishes and RLS and MKM converge. This dampening effect of MKM is useful during system resets. In Fig. 6.2b the  $R$  value of the MKM was constantly adapted by the measured error using a forgetting algorithm. Instead of using the measured error to determine  $R$ , one can also set  $R$  to a fixed value. As explained before, the  $R$  value has a dampening effect, in Fig. 6.2c  $R$  is set to 100 times the actual noise, which dampens the change of parameters. In Fig. 6.2d the  $R$  value was

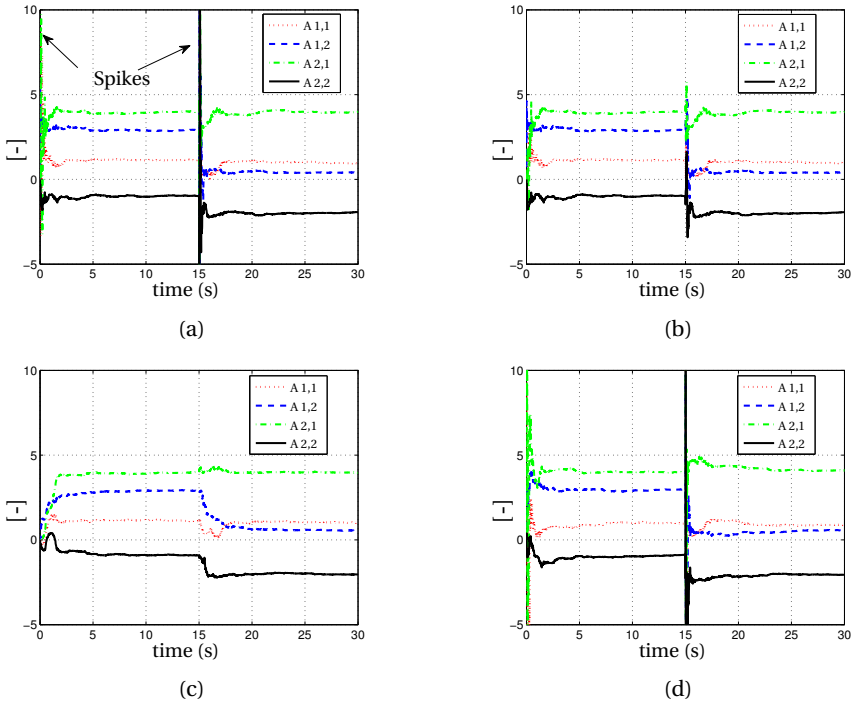


Figure 6.2: Comparison of RLS and MKM PID method when system A changes at 15 sec. in a high noise environment  $S/N=0.5$ . In (a) RLS response; in (b) MKM with adaptive  $R$ ; in (c) MKM with very large  $R$ , which causes heavy damping and in (d) MKM with small  $R$  that becomes identical to RLS.

set to a very low value 0.01 of the actual noise variance. The effect is that the difference with the RLS method disappears, as was also shown in the analysis above.

**CONCLUSION MKM**

Using the MKM method instead of the RLS method can be useful when large transients must be avoided, or when there is a lot of measurement noise. Starting with an incorrect  $R$  value does not influence the final results because the  $R$  value can be adapted with the measured error.

**THE STANDARD FORGETTING ALGORITHM**

The standard Forgetting Algorithm (FA) [5], [6] uses a forgetting factor  $\lambda$  ( $0 < \lambda < 1$ ) that is used to adjust the  $P$  value. While  $P$  is defined as  $P_i^{-1} = \sum H_i H_i^T$  the FA is using the following steps where  $\beta_i$  is the model parameter vector and  $H_i$  the input vector.

$$\text{The prediction is given by: } Y_i = \beta_i H_i \tag{6.19}$$

$$\text{The prediction error is given by: } \epsilon = Z_i - Y_i \tag{6.20}$$

$$\text{The gain is: } k = \lambda^{-1} P_i H_i^T / (1 + \lambda^{-1} H_i P_i H_i^T) \quad (6.21)$$

$$\text{The update is: } \beta_{i+1} = \beta_i + k\epsilon \quad (6.22)$$

$$\text{The adaptation of } P \text{ is: } P_i^{-1} = \lambda P_{i-1}^{-1} + H_i H_i^T \quad (6.23)$$

By using an FA, the influence of the older inputs is reduced, the  $P$  matrix values remain higher and the adjustments of the model parameters are quicker. The challenge with the FA method is to find a  $\lambda$  that balances the quick adaptation to the new situation with sufficient stability of the solution. In Fig. 6.3 the effect of different  $\lambda$  values is illustrated for a run using the PA-34 model with a lateral asymmetry in turbulent flying conditions. This run is part of the set used to evaluate the VPS and is described in Section 6.3. The figure displays the calculated  $V_c$  as a function of time, the asymmetry error is introduced at 30 seconds into the run and the correct value for  $V_{cL}$  after the failure is  $44\text{ m/s}$ . This figure shows that the setting  $\lambda = 0.9925$  does not stabilize well, the setting  $\lambda = 0.995$  shows a much better stabilization and improves further when  $\lambda = 0.9975$ , but here the final error is larger. A further increase in  $\lambda$  to 0.9995 shows that the convergence to the correct value is much slower. Based on this and similar runs it was found that for asymmetry problems  $\lambda = 0.9945$  worked best while for all other failures  $\lambda = 0.9985$  was preferable. As a compromise  $\lambda$  was set to 0.9975.

#### FA WITH DAMPING

One of the known problems of the FA method is that the adjustments might be too fast. In [2] a new forgetting algorithm was introduced that employed a damping algorithm. For this damped forgetting algorithm we use the acronym (FAD). For an exact description of how this damping was incorporated in the RLS we refer to the source paper [2]. The goal of the authors of [2] was to combine adaptability and stability. In their paper the authors used a forgetting factor  $\lambda = 0.999$  and a damping factor  $\delta = 10$ . In an earlier investigation [7] involving error detection, it turned out that these settings were not optimum for calculating the  $V_c$ . It was shown that the optimum settings were failure-dependent and a compromise had to be made. The settings used for the evaluation in this chapter were  $\lambda = 0.995$  and  $\delta = 200$ .

## 6

### 6.2.3. INITIAL MODEL PARAMETER VALUES AND NORMALIZATION PROFILES

As mentioned in this chapter's introduction sections, there are two reasons to use initial model parameter values in the PID. Firstly to enable the  $V_c$  calculation to start directly and secondly, normal flight conditions are not sufficient to determine all required aircraft parameters. Pilots will normally not use excessive manoeuvring with large side slips nor apply asymmetric power, which are both required to determine accurate model parameters for these conditions. To calculate the initial model parameter values we used sixteen scenarios, eight with a right or left engine failure and eight without an engine failure. Both sets of eight runs were divided evenly in runs in turbulent conditions and in smooth flying conditions. The scenarios included a maximum performance roll at the

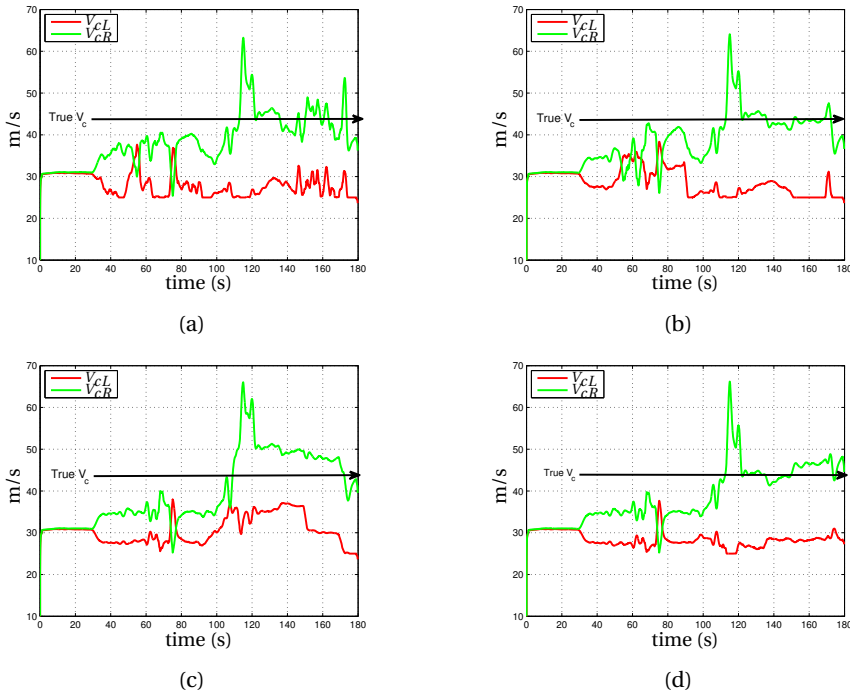


Figure 6.3: Comparison of different  $\lambda$  values for the FA method; The run is done with a PA-34 in turbulent flying conditions with an asymmetry failure at 30 seconds in the flight. The run details are described in Section 6.3. The true  $V_c$  value after the failure is 44 m/s. In red the  $V_c$  for a left roll ( $V_{cL}$ ) and in green  $V_{cR}$  for a right roll. (a)  $\lambda = 0.9925$ ; (b)  $\lambda = 0.995$ ; (c)  $\lambda = 0.9975$  (d)  $\lambda = 0.9995$ .

end of the profile. During the runs, inputs were given on all controls separately. The profile of a typical scenario is depicted in Fig. 6.4 and the inputs used in that scenario are in Fig. 6.5. Each profile lasted 3 minutes, giving a total of 48 minutes of flight time on which the initial model parameter values were based, giving ample opportunity for the model parameters to settle.

The initial parameter values calculated included the aircraft model parameters but also the  $P$  matrix for the RLS method and the  $P_k$  matrix for the MKM method. In this manner the VPS starts in the same condition as if the aircraft was already flying for a considerable amount of time after having performed extensive manoeuvring. It may be self-evident that each model size and normalization requires its own set of initial parameters. We extended the choice by calculating initial model parameters for different airspeeds. We selected the typical approach speeds of 80 and 85 knots, normal cruise 120 knots and fast cruise 160 knots. These different speeds enabled us to assess whether the model parameters are reasonably constant over the speed range, which is important for an accurate  $V_c$  prediction and will be discussed next.

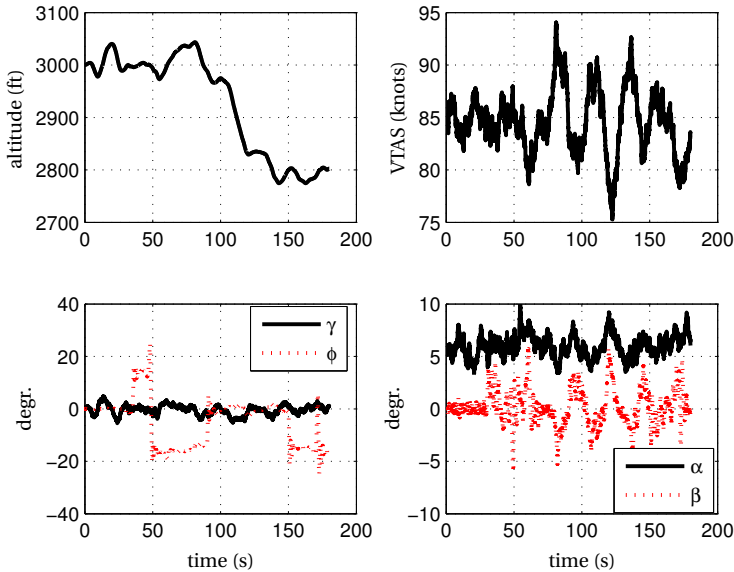


Figure 6.4: Flight profile for determining initial model parameter values. Shown profile is a left engine failure in turbulent conditions at an average true airspeed of 85 knots.

A typical scenario for which we aim to present the  $V_c$  is an aircraft that encounters a problem while flying at cruise speed. After the failure detection and some manoeuvring performed by the pilot, the model parameters are updated and a safe speed is presented to the pilot that can be used for the ensuing approach and landing.

To make an accurate prediction, it is important that the determined model parameters are reasonably constant over the speed trajectory, otherwise the predicted  $V_c$  might be inaccurate and a new reset might be necessary after a speed change. When parameters are not constant, there are two ways to correct. The first, and most common, is the introduction of additional parameters that depend on higher order independent variables such as  $\alpha^2$ ,  $\beta^2$  etc. However, as we have found in Chapter 5, these additional parameters associated with higher order independent variables degraded the prediction accuracy. A second option is to tune the normalization of the independent variable. If the model and normalization are well chosen, runs at different velocities should give the same model parameter values.

For the calculation of the initial model parameter values we restricted ourselves to two PID methods: RLS and MKM. The reason we omitted the two methods based on forgetting algorithms is simple: forgetting algorithms constantly adjust, and the initial model parameter values determined after 16 different scenarios will be biased to the last scenario and not represent the weighted average over all scenarios.

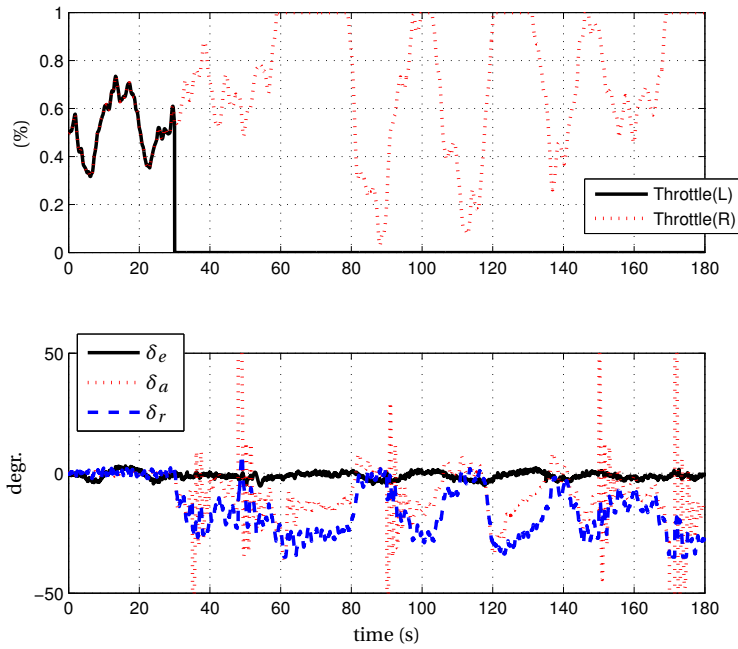


Figure 6.5: Inputs in initial model parameter values profile. The profile shows a left engine failure (Run 111) in turbulent conditions at an average true airspeed of 85 knots.

Table 6.1: The maximum relative difference in the model parameters over the speed range 80 to 160 knots compared to the 120 knots value. The presented value is the fractional change, e.g., 2.00 means a 200% change.

param	MKM			RLS		
	10	13	22	10	13	22
$y_\beta$	0.04	0.04	0.10	0.33	0.33	2.46
$l_\beta$	0.28	0.28	0.82	0.23	0.23	0.99
$l_p$	0.03	0.03	0.23	0.08	0.08	0.20
$l_r$	0.84	0.85	0.38	0.85	0.86	0.53
$l_{da}$	0.02	0.02	0.03	0.03	0.03	0.02
$l_{dr}$	0.11	0.09	1.20	0.12	0.10	1.33
$l_{TL}$	0.75	0.72	0.56	0.68	0.65	1.27
$l_{TR}$	0.69	0.67	0.64	0.62	0.61	0.17
$n_\beta$	0.20	0.19	1.62	0.24	0.23	1.02
$n_p$	5.41	6.11	3.50	3.18	3.55	2.22
$n_r$	0.10	0.09	0.72	0.02	0.02	0.51
$n_{da}$	0.12	0.12	0.11	0.16	0.15	0.14
$n_{dr}$	0.04	0.04	1.18	0.06	0.06	0.77
$n_{TL}$	0.17	0.17	0.15	0.22	0.21	0.18
$n_{TR}$	0.17	0.17	0.19	0.23	0.22	0.24

#### RESULT INITIAL MODEL PARAMETER VALUES WITH STANDARD NORMALIZATION

Table 6.1 presents the results for a selection of model parameters that are important for the  $V_c$  calculation. To enable a quick comparison, the table presents the maximum relative change compared to the 120 knots value. This value was derived in the following way. The parameter values derived at 120 knots were subtracted from the values derived at 80, 85 and 160 knots. The new values were divided by the value for 120 knots, and the maximum absolute value is presented in the table. Consequently, a zero value indicates that there is no velocity influence at all. These simulations did not yet include failures, because we first wanted to establish the effect of velocity on the model parameters of the undamaged aircraft. Some of these parameters are very small or still zero, however, PID methods will find small values for these parameters that are actually noise, but the relative change in these noise parameters can be quite high. Therefore, we omitted these noise parameters from the table.

From Table 6.1 it can be concluded that the important roll performance parameters  $l_{\delta_a}$  and  $l_p$  do not change much over the speed trajectory. However, there is a significant velocity dependency for the parameters  $l_\beta$ ,  $l_r$ ,  $n_p$  and the roll parameters due to the engine  $l_{TR}$  and  $l_{TL}$ . We will address all these parameters individually.

- The  $n_p$  parameter is the parameter with the largest relative increase of 6.11 when we use the 13 variable model.  $n_p$  is the yaw due to roll and this is caused by the drag difference between the “up going” and the “down going” wing. The induced drag difference is of course more pronounced at high angles of attack. The actual value changes from -0.0185 at 80 knots to +0.01 at 160 knots. However, we can

improve the velocity independence  $\frac{pb}{2V}$  by changing its associated variable from  $\frac{pb}{2V}$  to  $\frac{pb}{2V^2}$ .

- The parameter  $l_\beta$ , or the effective dihedral, changes from -0.24 at 80 knots to -0.17 at 160 knots. The effect of the change in this parameter on the  $V_c$  accuracy will be significant in all situations where zero side slip can no longer be maintained. Thus, when the parameter is updated or derived at high speed, the roll performance of the aircraft could be overestimated, leading to a  $V_c$  estimate that is too low.
- The parameter  $l_r$  changes from 0.42 at 80 knots to 0.21 at 160 knots. This roll due to yaw is caused by the velocity difference between the forward and aft going wing and is directly related to airspeed. To compensate for this effect we can change the normalization of its associated variable from  $\frac{nb}{2V}$  to  $\frac{nb}{2V^2}$ .
- Finally the parameters  $l_{TL}$  and  $l_{TR}$ . As explained in Chapter 3 for propeller aircraft the engine power is commonly normalized by dividing the power by  $V^3$ , however it was also shown that the effect of power on roll, due to the lift difference over the wing, was even stronger and requires a  $V^4$  normalization. However, using a  $V^4$  normalization did not lower the change in the model parameter value over the complete speed range, especially the deviation at 160 knots became large. Further investigation revealed that an optimum normalization of engine power was achieved by dividing the power by  $V^{3.45}$ . However, even with this normalization, there remains a considerable value change over the speed range as illustrated in Table 6.2. Fortunately, the model parameter change due to airspeed is much less from the cruise speed to the minimum speed of 80 knots.

#### RESULTS INITIAL MODEL PARAMETER VALUES WITH IMPROVED NORMALIZATION

In our analysis both normalizations, the standard and the modified, were used to assess the effect on prediction accuracy. The effect of this new normalization on the model parameters is presented in Table 6.2. As can be seen, the velocity dependency of the engine parameters is much smaller but still present.

Another interesting finding is that parameters of the largest size model (22 independent variables) have the largest airspeed dependency, confirming the findings of Chapter 5, while the airspeed dependency of models with 10 and 13 parameters is almost identical. New is the fact that the performance of the two PID methods differs. The fact that the MKM method uses an additional damping with the  $R$  matrix explains this difference, however, we have not yet established what the effect is on the  $V_c$  determination.

#### SELECTED OPTIONS

We have considered several options for VPS, which particularly affect the PID. Firstly, for the initial conditions we limit ourselves to the most common airspeeds 85 and 120 KTAS. Secondly, we use two normalization options, the standard normalization as discussed in Chapter 3 and the improved normalization for  $l_{le}$ ,  $l_{re}$ ,  $l_r$  and  $n_p$ . Thirdly, we evaluate three different model sizes with 10, 13 and 22 independent variables and fourthly we use four different PID methods. This gives a total of 48 different configurations that will be evaluated for  $V_c$  prediction accuracy and convergence speed in next section.

Table 6.2: The maximum relative difference of the model parameters over the speed range 80 to 160 knots compared to the 120 knots value with new normalization for  $l_{TL}$ ,  $l_{TR}$ ,  $l_r$  and  $n_p$ .

param	MKM			RLS		
	10	13	22	10	13	22
$y_\beta$	0.04	0.04	0.10	0.33	0.33	2.46
$l_\beta$	0.25	0.26	0.95	0.22	0.23	1.24
$l_p$	0.03	0.03	0.23	0.08	0.08	0.21
$l_r$	0.15	0.16	0.35	0.21	0.21	0.49
$l_{da}$	0.05	0.05	0.05	0.03	0.03	0.03
$l_{dr}$	0.15	0.15	1.37	0.15	0.14	1.74
$l_{TL}$	0.26	0.26	0.23	0.64	0.62	1.04
$l_{TR}$	0.21	0.21	0.26	0.60	0.58	0.30
$n_\beta$	0.19	0.19	1.18	0.24	0.23	0.98
$n_p$	3.28	3.74	3.88	1.81	2.05	2.02
$n_r$	0.10	0.09	0.31	0.02	0.02	0.45
$n_{da}$	0.11	0.12	0.11	0.16	0.15	0.14
$n_{dr}$	0.04	0.04	0.70	0.06	0.05	0.71
$n_{TL}$	0.17	0.17	0.15	0.21	0.21	0.19
$n_{TR}$	0.17	0.17	0.19	0.23	0.22	0.24

### 6.3. LATERAL CONTROL VELOCITY PREDICTION

#### TEST OBJECTIVES AND STEPS

The overall objective of the simulations was to investigate whether the VPS could predict the roll control velocities accurately and timely. As explained in Chapter 3, the roll performance at the present velocity can relatively easily be calculated from aileron power ( $l_{\delta_a}$ ), roll damping ( $l_p$ ) and available aileron deflection with adjustments for the adverse yaw effect if zero side slip cannot be maintained. However, to predict the roll performance at a lower speed, corrections must be made for asymmetric weight and asymmetric thrust. Furthermore, we have to determine whether at that lower speed the required rudder exceeds the available rudder. If this situation occurs, we have to correct for the  $\beta$  that will develop. The prediction of the roll performance at lower velocity is important to give the pilot of a damaged aircraft guidance during his deceleration to a safe approach and landing velocity. The profile used was designed to evaluate this particular situation.

#### EVALUATION METHOD

To be able to precisely test a large number of different failures under different conditions we reversed the test process. In the normal situation, as used for the pilot-in-the-loop test, the required  $\Delta\phi$  in a predetermined  $\Delta t$  is an input in the VPS. If in this situation the pilot wants to verify the  $V_c$ , he has to slow the aircraft speed to  $V_c$  and perform a maximum aileron roll. Next the difference between the required roll angle change and the achieved roll angle change can be measured. This difference has then to be reduced to an error in the  $V_c$  prediction.

However, by reversing the procedure, the  $\Delta V_c$  can be measured directly. In this procedure, the flight profile always ends with a maximum performance roll at a low airspeed. This measured roll angle change is used as reference input in the VPS. When the VPS is now evaluating the flight data, it is constantly calculating the  $V_c$  for this roll and we can evaluate how quickly the calculated  $V_c$  converges to the measured  $V_c$ . This measured  $V_c$  is the measured average airspeed during the roll. Another benefit of this reversal of the procedure is that different types of failures are all tested at the same low speed.

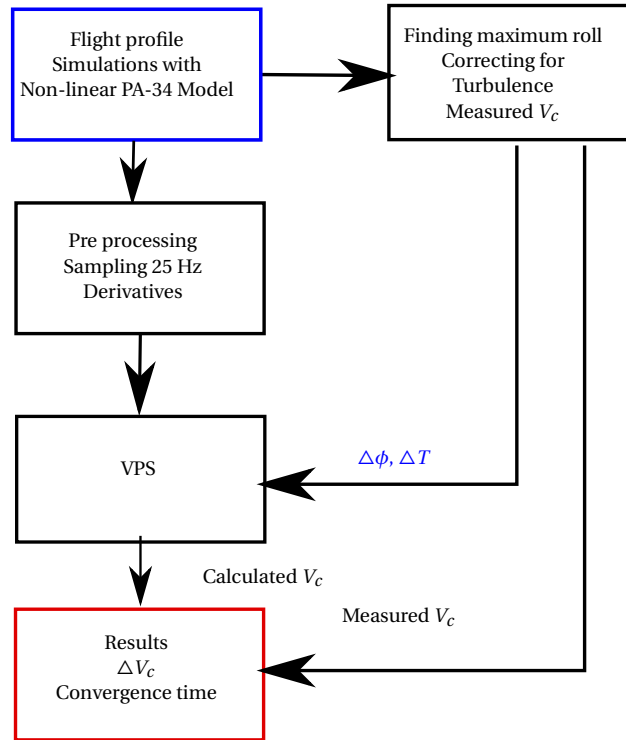
A graphic representation of the evaluation method is given in Fig. 6.6. An overview of the steps is given here and discussed in more detail below.

1. The input data are based on off-line simulations of failure profiles with the non-linear model of the PA-34
2. The maximum roll at the end of the profile is measured and used as VPS input, the measured average airspeed during the roll is used as measured  $V_c$  and used for determination of the  $V_c$  prediction error.
3. The flight data are pre-processed for the VPS. This involves a re-sampling from 100 to 25 Hz and numerically taking the derivatives of  $p$ ,  $r$  and  $\beta$ . The combination of 25 Hz and using three point derivatives was used to limit noise in the derivatives. It was verified that this procedure did not affect the prediction accuracy.
4. Next the  $V_c$  is calculated over the complete trajectory based on the model parameters and the required roll performance.
5. In the final analysis the calculated  $V_c$  is compared to the measured  $V_c$ , which is the mean of the airspeed at the start of the roll and the airspeed at the end of the roll.

#### FLIGHT PROFILES

The flight profiles started in straight and level flight at a cruise speed of 125 knots TAS; the failures were initiated after 30 seconds, subsequently identification inputs were given in pitch, roll and yaw, and engine inputs were made with each throttle separately. After these inputs, the aircraft was decelerated to approach velocity. At this final velocity the maximum deflection aileron roll was performed for 1.5 seconds to provide values for the reference roll as described above.

In the simulations of engine failures and asymmetries, the roll was always made to the most limiting side, while for control failures the roll was opposite to the actual initial roll angle, e.g., if the aircraft was in a right turn the roll was to the left. A typical failure profile is presented in Fig. 6.7 and the control inputs for this profile are presented in Fig. 6.8. Runs were made with turns in both directions and both with and without turbulence. Turbulence was generated using the Dryden spectrum [8]. The turbulence intensity and characteristic length were set using the altitude dependent Mil. Spec. 1797 models [9]. The final turbulence outputs were multiplied by 0.5 to achieve a turbulence level that was acceptable for an aircraft with a low wing loading, such as the Piper Seneca.

Figure 6.6: Graphic representation of the  $V_c$  test.

The resulting variations in  $\alpha$ ,  $\beta$  and velocity for the initial airspeed and the approach velocity are presented in Table 6.3.

Control inputs are essential for the identification of the change in the model parameters. Different techniques are available to identify parameters. Experimental test pilots [10] are trained to perform frequency sweeps to find the frequency of the aircraft eigen motions and subsequently use doublets at the previously-determined frequency to measure damping. One special advantage of this technique is that even without any data collection system, the frequency and damping can be determined by simple observations and a stopwatch. Other methods employed use step inputs based on the fact that a step contains information at all frequencies. In [11] a comparison was made of more

Table 6.3: Effect of turbulence on the standard deviation of  $\alpha$ ,  $\beta$  and  $V_{tas}$ .

	120 kts	85 knots
$V_{tas}$ (m/s)	0.25	0.22
$\alpha$ (degr.)	0.28	0.55
$\beta$ (degr.)	0.18	0.25

advanced flight test manoeuvres and their usability for parameter identification. However, we have decided not to use these optimized flight test manoeuvres as determined in this study. The reason is that we consider it unrealistic to expect the average pilot of a damaged aircraft to be acquainted with flight test techniques. It may well be that the natural reaction of that pilot will be to return to land as quickly as possible, without performing any identification manoeuvres.<sup>1</sup> In our simulation a single sine shape input is sequentially made in pitch, roll yaw and on each throttle. We expect that this type of manoeuvre can be performed by a pilot who has been given the instruction to make a quick input with each control separately.

To further analyse the effect of control inputs, two different types of runs were made: the first type used a single set of control inputs at cruise velocity just after the failure, while the second set added an extra set of inputs during the deceleration to approach speed.

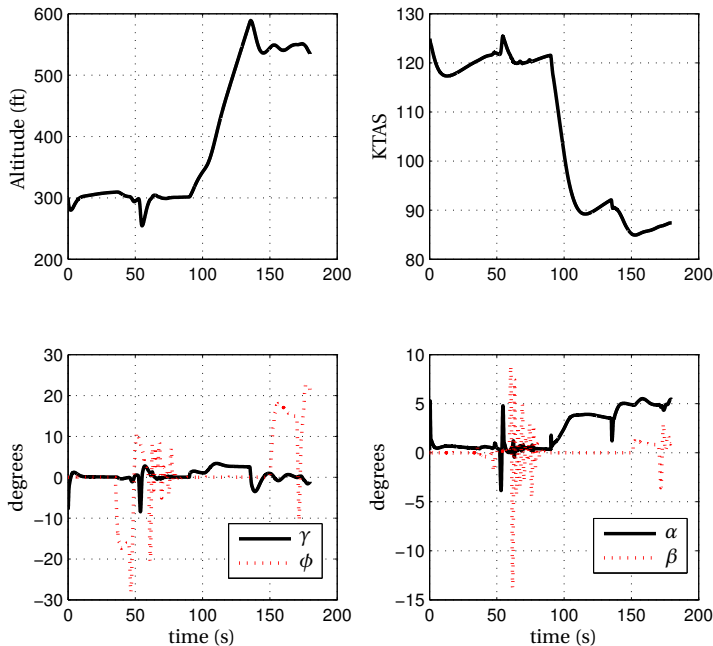


Figure 6.7: Typical Failure profile; 50% Aileron Failure in smooth flying conditions.

Five different types of failures were investigated:

- Partial aileron failures simulated by a reduction of 50% in aileron effectiveness;

<sup>1</sup>As was the case in the El Al accident in Amsterdam in 1992 [12]

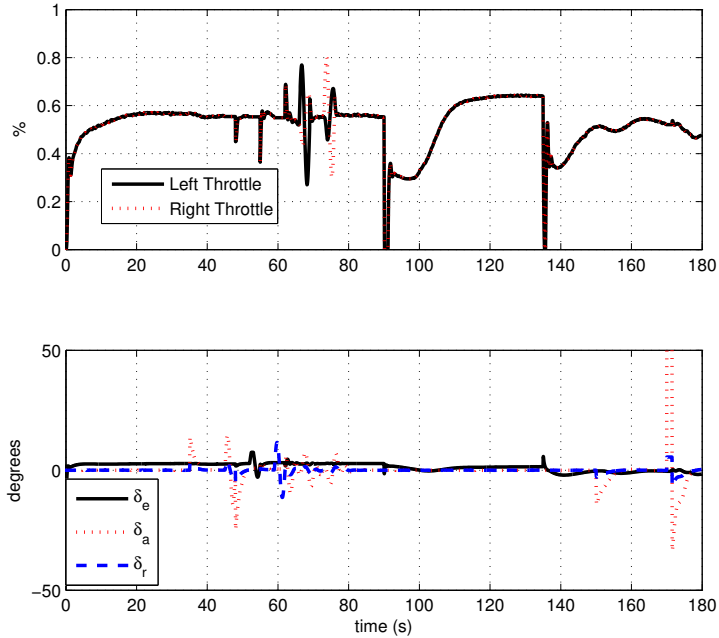


Figure 6.8: Control inputs during failure profile. Shown profile is a partial (50%) aileron failure

- Rudder failures simulated by the reduction of rudder effectiveness to zero;
- Lateral asymmetries caused by a lateral weight imbalance;
- Rudder hard-over, simulated by a fixed deflection on the rudder without the capability to change it. The rudder was not completely deflected because in the PA-34 this situation always results in an uncontrollable roll;
- Engine failures; these failures differ from the other failures because the engine performance is part of the model, therefore no change in model parameters occurs when asymmetric power is either selected by the pilot or evolves from an engine failure. For this reason the engine failures are treated separately.

### CORRECTIONS

Two corrections are required to make an accurate comparison between the actual velocity at which the final roll is made and the predicted velocity for this roll performance. The first correction adjusts for the fact that the predicted roll is calculated for a constant load factor and a constant  $\beta$ . In reality, aerodynamic coupling and controller response delays will prevent that these conditions are precisely met. Therefore a (small) correction is

made for these ‘not-perfect’ rolls. This correction is described in detail in Section 4.3.1. In summary, the error is approximated in the following manner:

- Based on the velocity during the roll, the roll time constant can be approximated by:  $\tau = \frac{-b}{I_p V_c}$ , and based on the achieved roll rate the maximum roll rate can be estimated,  $p_{max} = \phi_{req} / \left( T + \tau \left( e^{\frac{-T}{\tau}} - 1 \right) \right)$ . Based on  $p_{max}$  and  $\tau$ , the estimated first order approximation of the roll can be made (Eq. 4.49), which is repeated below:

$$\phi(t) = p_{max} \left( t + \tau \left( e^{\frac{-t}{\tau}} - 1 \right) \right)$$

- Next the measured change in  $\beta$  and  $N_z$  during the roll is numerically convoluted with Eq. 4.49; which is allowed because  $\beta$  and  $N_z$  also produce roll responses<sup>2</sup>. This calculated response is compared with the effect of a step input (Eq. 4.78) to calculate  $\beta_{eff}$  and  $N_{z_{eff}}$ , which stand for the effective  $\beta$  and  $N_z$ , or the step inputs that will generate the same response as the time varying measured change in  $\beta$  and  $N_z$ . Eq. 4.78 is repeated below.

$$\beta_{eff} = \frac{\text{Convoluted } \beta(t) \text{ with roll response}}{\text{Convoluted Step } \beta \text{ with roll response}}$$

- The last step is to convert  $\beta_{eff}$  and  $N_{z_{eff}}$  to an equivalent aileron deflection that generates the same roll response, this is done by using Eq. 4.42. And this generates the aileron deflection correction  $C_9$ , which is used in Eq. 4.82 to calculate the  $V_c$ .

This first correction corrects the  $V_c$  for the additional inputs in  $\beta$  and  $N_z$  that can increase as well as decrease the roll performance.

The second correction is required to address measurement errors due to turbulence. Turbulence can cause the aircraft to already have a roll rate at the start of the roll. If the initial roll is in the opposite direction of the intended roll, a simple interpolation is made to the point where the roll rate is zero and this point is used as the updated start time for the roll, so the time to achieve the required roll angle change is adjusted and the measured roll angle change is measured from this time to the end of the roll. If the aircraft already had a roll rate in the intended direction, the first 50 data points were used to estimate the maximum roll rate and the time constant assuming a first order roll response. With this estimated maximum roll rate and the roll time constant the extra time is calculated to achieve the roll rate at the start of the manoeuvre and this extra time is added to the measured roll time. Additionally, the achieved roll angle change in this additional time period is added to the measured roll angle change.

#### EVALUATION CRITERIA

In the evaluation of the different model sizes and the parameter identification methods, two criteria are used:

<sup>2</sup>  $\beta$  will always cause a roll and  $N_z$  in case of a lateral asymmetry.

- The *accuracy* of the predicted speed ( $V_c$ ) for the measured roll angle change, compared to the actual measured speed in the roll. For the latter value the mean of the speeds at the start and at the end of the roll is used. The start of the roll is determined by measuring the point where the aileron deflection is above 95% deflection minus half of the time used for aileron step input. The end of the roll is either determined by a fixed time period, e.g., 1 second or the time where the aileron deflection has decreased 0.5% below the maximum value. The presented error in the tables is the mean absolute error expressed in  $m/s$ .
- The *time* it takes for the  $V_c$  prediction to converge to the final value. As measured, the time is used where the predicted  $V_c$  comes within  $5m/s$  of the actual speed at the final roll and stays within  $5m/s$ . Because the predicted  $V_c$  changes, quite correctly, during the identification manoeuvres, specifically by rudder and asymmetric power inputs, the following correction had to be made. For the convergence time calculation the predicted  $V_c$  was supposed to change linearly in the period from the value at the start of the rudder input to the end of the last throttle input. The presented time in the tables is the average time (in seconds) from the start of the profile. This time should be seen in relation with the start of the failure, always at 30 seconds into the profile, and the end of the first control input sequence, which is at 75 seconds.

#### DETECTION AND RESET

For the performance of the RLS and the MKM parameter identification methods it is important what error detection method is used. Common error detection methods look at the mean of the residue, its change in variance or the auto-correlation of the residue. In early investigations [13] and [7] it was shown that these methods had severe drawbacks and a new error detection method was developed. This new method is described in Appendix C. After a detection, the covariance matrix of the MKM was reset to a higher value and for the RLS method the  $P$  matrix was set to a new starting value.

### 6.3.1. RESULTS $V_c$ CALCULATION

#### GENERAL

In Table 6.4 the results of all failure profiles on  $V_c$  accuracy and convergence are presented. The following conditions are compared:

- Three different model sizes, using 10, 13 and 22 independent variables;
- Two types of normalization (I and II) as discussed in paragraph 6.2.3;
- Two different sets of initial model parameter values, the first based on 120 knots, which had the smallest reconstruction error, and the second based on 85 knot, because the low speed manoeuvrability is most crucial;
- The four different PID methods.

The accuracy of the  $V_c$  prediction and its standard deviation is based on the predicted value of  $V_c$  0.5 second before the roll was initiated and the actual velocity during

Table 6.4: Effect of model size, initial model parameter values and normalization on accuracy  $V_c$  prediction in  $m/s$  and Conv. time (s) for all failures in turbulence and smooth flying conditions. Mean is the mean value of the absolute  $V_c$  error.

Preset	Size	Normalized		RLS	FAD	MKM	FA	
85 kts	10	I	Mean (m/s)	2.0	2.9	2.2	3.4	
			St. Dev. (m/s)	2.3	3.1	2.9	3.5	
			Conv. time (s)	80.7	111.4	94.6	142.4	
	13	I	Mean (m/s)	2.0	2.9	2.2	3.3	
			St. Dev. (m/s)	2.2	3.1	2.9	2.9	
			Conv. time (s)	80.8	108.6	85.8	140.5	
	22	I	Mean (m/s)	5.3	2.8	2.0	11.3	
			St. Dev. (m/s)	6.6	3.1	2.7	13.9	
			Conv. time (s)	127.7	115.8	86.3	145.3	
	120 kts	10	II	Mean (m/s)	2.1	2.9	1.9	3.4
				St. Dev. (m/s)	2.4	3.1	2.1	3.6
				Conv. time (s)	84.8	117.6	83.4	145.2
		13	II	Mean (m/s)	2.0	2.9	1.9	3.3
				St. Dev. (m/s)	2.3	3.1	2.1	2.9
				Conv. time (s)	83.9	116.3	83.4	142.4
22		II	Mean (m/s)	3.9	3.0	2.6	12.1	
			St. Dev. (m/s)	4.7	3.3	3.4	14.6	
			Conv. time (s)	113.9	126.4	103.2	146.5	
120 kts	10	I	Mean (m/s)	2.1	3.0	2.2	2.8	
			St. Dev. (m/s)	2.3	3.3	2.3	2.7	
			Conv. time (s)	87.7	106.4	93.4	131.1	
	13	I	Mean (m/s)	2.0	3.0	2.2	2.9	
			St. Dev. (m/s)	2.1	3.3	2.3	2.5	
			Conv. time (s)	87.2	106.1	94.5	130.1	
	22	I	Mean (m/s)	5.6	15.0	5.4	7.9	
			St. Dev. (m/s)	7.4	8.2	6.3	10.8	
			Conv. time (s)	141.4	169.0	134.3	148.7	
	120 kts	10	II	Mean (m/s)	2.2	3.0	2.1	2.8
				St. Dev. (m/s)	2.6	3.2	2.4	2.8
				Conv. time (s)	90.8	101.7	87.3	132.8
		13	II	Mean (m/s)	2.2	2.9	2.2	2.9
				St. Dev. (m/s)	2.4	3.2	2.6	2.5
				Conv. time (s)	88.9	101.7	93.4	131.8
22		II	Mean (m/s)	4.7	11.5	3.2	8.5	
			St. Dev. (m/s)	5.7	6.4	3.8	11.7	
			Conv. time (s)	131.1	164.9	127.2	150.3	

Table 6.5: The effect of model size on accuracy and convergence of the  $V_c$ .

Size		RLS	FA D	MKM	FA
10	Mean (m/s)	2.1	3.0	2.1	3.1
	St. Dev. (m/s)	2.4	3.2	2.4	3.1
	Conv. time (s)	86.0	109.3	89.7	137.9
13	Mean (m/s)	2.1	2.9	2.1	3.1
	St. Dev. (m/s)	2.3	3.2	2.5	2.7
	Conv. time (s)	85.2	108.2	89.3	136.2
22	Mean (m/s)	4.9	8.1	3.3	9.9
	St. Dev. (m/s)	6.1	4.6	7.9	12.7
	Conv. time (s)	128.5	144.0	112.7	147.7

the roll. This value depends primarily on how accurately the roll parameters,  $l_p$  and  $l_{\delta_a}$ , are determined, and to a lesser extent on the accuracy of the adverse yaw parameters,  $n_{\delta_a}$ ,  $n_r$  and  $l_\beta$ . We expect that the accuracy will depend on model size and PID method.

For the convergence of the  $V_c$  more parameters are important. Especially all engine and asymmetry related parameters, because the influence of these parameters increases with the decrease of velocity. This is caused by the increase in magnitude of their corresponding independent variables. Until the engine and asymmetry parameters are accurately determined, it is difficult to predict the controllability at velocities other than the actual velocity. It is expected that the different PID methods, the model size and the type of normalization will affect the accuracy of these parameters and the time needed for convergence of these parameters.

#### EFFECT OF MODEL SIZE ON $V_c$

To assess the effect of model size, the results of Table 6.4, for all initial model parameter values and normalizations are combined in Table 6.5. For every PID method the effect of model size is similar, there is hardly any difference in  $V_c$  error and convergence time between the 10 and 13 independent variable models. However, the model with 22 independent variables gives a large increase in  $V_c$  error, standard deviation and also causes a delayed convergence. Based on the reconstruction results in Chapter 5, this result on the  $V_c$  was to be expected. Furthermore, it confirms the expectation that larger models converge more slowly. However, the addition of only the most important model parameters, based on the reconstruction error as derived in Chapter 5 does not equate to smaller errors in  $V_c$  nor in significant changes in convergence time.

#### EFFECT OF NORMALIZATION ON $V_c$

In Table 6.6 the results of Table 6.4 are combined to assess the effects of changed normalization on the convergence of the  $V_c$ . For the MKM and RLS methods, there is a small average improvement in convergence time with the new normalization; only for the MKM method based on 10 variables the improvement is substantial. The effect for the two forgetting algorithms is even negative, however, this effect was to be expected, PID methods that constantly adapt have less need for parameters that are constant over

Table 6.6: Effect of normalization on convergence time of  $V_c$  in seconds.

Normalization	Size	RLS	FAD	MKM	FA
I	10	84.2	108.9	94.0	136.8
	13	84.0	107.3	90.2	135.3
	22	134.6	142.4	110.3	147.0
II	10	87.8	109.7	85.4	139.0
	13	86.4	109.0	88.4	137.1
	22	122.5	145.7	115.2	148.4
Mean(I-II)		2.0	-1.9	1.8	-1.8

Table 6.7: Best combinations for each PID method

PID	Size	Init.Val.	Norm.	mean (m/s)	St.Dev. (m/s)	conv. time (s)
RLS	13	85	I	2.0	2.2	80.8
KF	10	85	II	1.9	2.1	83.4
FAD	10	85	II	2.9	3.1	117.6
FA	13	120	I	2.9	2.5	130.1

the speed trajectory. Based on these results we can conclude that the effect of improved normalization on  $V_c$  prediction is small.

#### BEST COMBINATIONS AND EFFECT OF FAILURES

Based on the previous results, the optimum combinations for the different PID methods were determined and these are presented in Table 6.7. The table shows that the resetting methods RLS and MKM produce similar results, the MKM method being slightly better, but both are considerably better than both forgetting methods.

The intention of these simulations is to find the best combination that works in turbulent as well as smooth air conditions. However, it is also important to see how turbulence affects the accuracy and convergence time of  $V_c$ . Therefore, the best combinations as depicted in Table 6.7, are presented for turbulence and smooth air conditions separately in Table 6.8. For both the RLS and the MKF PID method the difference in  $V_c$  and convergence time is small. However, for both the FAD and FA method,  $V_c$  in turbulent air conditions is slightly higher and for the FAD method the conversion time is considerably higher in turbulent air conditions.

#### 6.3.2. ENGINE FAILURES

Engine failures have to be evaluated differently. Firstly, engine parameters are an integral part of the model, consequently, resets are not required for the MKM and RLS PID method, nor are identification manoeuvres necessary. Secondly, the  $V_c$  value is dynamic, constantly adjusting to the actual power setting and  $\beta$ . Therefore, we can only assess the convergence of the  $V_c$  value if the power setting and  $\beta$  are kept constant<sup>3</sup>. In the profile

<sup>3</sup>As explained in Chapter 3 the  $V_c$  calculation does correct for the change in  $\beta$  when the  $\beta = 0$  condition can no

Table 6.8: Effect of turbulence on best combinations.

		RLS	FAD	MKM	FA
Turbulence	mean (m/s)	2.0	3.3	2.0	3.0
	St.dev. (m/s)	2.0	3.5	2.5	2.6
	Conv. time. (s)	83.9	127.7	84.0	128.7
Smooth	Mean (m/s)	2.0	2.6	1.9	2.8
	St.Dev. (m/s)	2.4	2.8	1.7	2.4
	Conv. time (s)	77.7	107.4	82.9	131.5

Table 6.9: The effect of model size on  $V_c$  accuracy (m/s) for engine failure; standard deviation (m/s) and Conv. time (s).

Size		RLS	FA D	MKM	FA
10	Mean (m/s)	1.6	2.3	1.6	2.7
	St. Dev. (m/s)	0.3	3.2	0.3	2.9
	Conv. time (s)	36.1	70.0	36.1	84.6
13	Mean (m/s)	1.6	2.4	1.6	2.6
	St. Dev. (m/s)	0.3	3.5	0.3	3.0
	Conv. time (s)	36.1	70.0	36.1	84.6
22	Mean (m/s)	2.0	1.0	2.3	4.7
	St. Dev. (m/s)	0.6	0.4	0.6	5.7
	Conv. time (s)	34.1	34.0	40.7	139.5

used, the engine is failed at 30 seconds, thereafter a climb is started with full asymmetric power that will give a slowly decreasing airspeed. At the end of the run a roll is made to the most limiting side, which is into the working engine. The results of these runs are presented in Table 6.10.

#### EFFECT OF MODEL SIZE

The effect of model size is different for engine failures than for other types of failures. The larger model predicts more accurately than the smaller model as can be seen in Table 6.9. This effect is quite logical, the model is already accurate, because it is based on extensive simulations with engine failures and large roll manoeuvres. The convergence is also direct. After the failure at 30 seconds the engine power is advanced and the  $V_c$  value is immediately within 5 m/s of the final value. The only exception is the FA method. The constant adaptation causes large errors in the  $V_c$  estimate and, consequently, also leads to a late convergence.

For one run, a right engine failure in turbulent flying conditions, the  $V_c$  calculations, using different PID methods, are presented in Fig. 6.9. The PID methods used the large model with 22 independent variables and the modified normalization. It is clear that

longer be maintained with full rudder.

Table 6.10: Effect of model size, initial model parameter values and normalization on accuracy  $V_C$  prediction in  $m/s$  and convergence in seconds, for engine failures in turbulence and smooth flying conditions. Mean is the mean value of the absolute  $V_C$  error.

Preset	Size	Normalized		RLS	FA damped	MKM	FA	
85 kts	10	I	Mean (m/s)	1.7	2.0	1.7	6.3	
			St. Dev. (m/s)	0.3	2.9	0.3	10.3	
			Conv. time (s)	36.4	70.2	36.4	93.4	
	13	I	Mean (m/s)	1.7	2.4	1.7	6.2	
			St. Dev. (m/s)	0.3	3.6	0.3	10.3	
			Conv. time (s)	36.4	70.2	36.4	93.5	
	22	I	Mean (m/s)	2.2	0.9	2.6	1.9	
			St. Dev. (m/s)	0.3	0.4	0.2	3.4	
			Conv. time (s)	36.0	36.9	36.1	143.6	
	120 kts	10	II	Mean (m/s)	1.6	2.0	1.6	1.3
				St. Dev. (m/s)	0.3	2.6	0.3	0.6
				Conv. time (s)	35.9	70.2	35.9	83.2
		13	II	Mean (m/s)	1.7	2.3	1.6	1.2
				St. Dev. (m/s)	0.3	3.3	0.3	0.7
				Conv. time (s)	35.9	70.2	35.9	83.2
22		II	Mean (m/s)	1.8	1.0	2.9	9.9	
			St. Dev. (m/s)	0.3	0.3	0.2	11.4	
			Conv. time (s)	35.9	37.1	65.3	154.2	
120 kts	10	I	Mean (m/s)	1.6	2.6	1.5	1.6	
			St. Dev. (m/s)	0.3	3.8	0.3	0.4	
			Conv. time (s)	36.5	69.9	36.5	80.5	
	13	I	Mean (m/s)	1.6	2.6	1.5	1.5	
			St. Dev. (m/s)	0.3	3.7	0.3	0.5	
			Conv. time (s)	36.5	69.9	36.5	80.5	
	22	I	Mean (m/s)	3.2	1.5	2.8	5.1	
			St. Dev. (m/s)	1.0	0.5	1.2	5.9	
			Conv. time (s)	33.4	31.0	30.6	165.2	
	120 kts	10	II	Mean (m/s)	1.5	2.5	1.4	1.6
				St. Dev. (m/s)	0.3	3.5	0.3	0.4
				Conv. time (s)	35.8	69.5	35.8	81.4
		13	II	Mean (m/s)	1.5	2.4	1.4	1.5
				St. Dev. (m/s)	0.2	3.5	0.3	0.5
				Conv. time (s)	35.8	69.6	35.8	81.4
22		II	Mean (m/s)	0.9	0.6	1.2	1.8	
			St. Dev. (m/s)	0.8	0.4	0.9	2.2	
			Conv. time (s)	30.9	31.2	31.0	95.1	

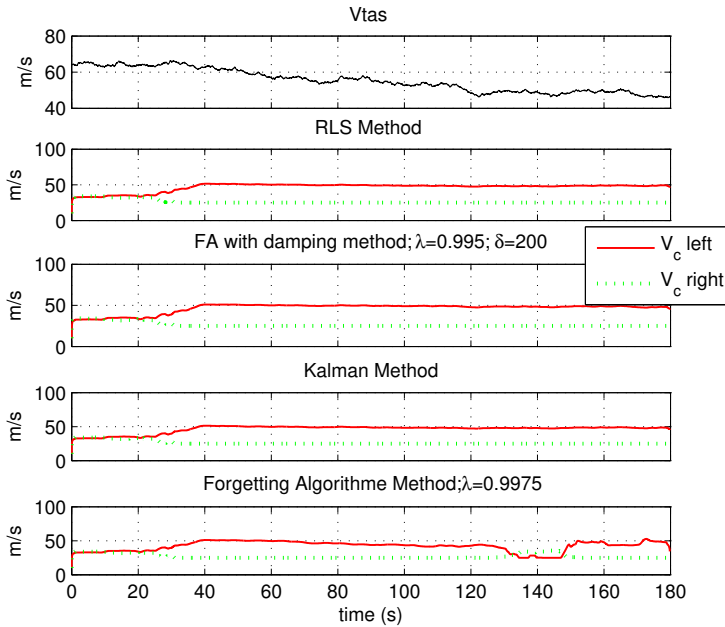


Figure 6.9: Engine failure, comparing different PID methods for run 143 in turbulence conditions, model with 22 variables, initial parameter values based on 120 knots and modified normalization.

the FA method in this simulation is the exception, at time 130s it starts to deviate, which causes an error and also destroys the convergence.

**NORMALIZATION**

The change in normalization was specifically needed because the roll due to thrust ( $l_{TL}$  and  $l_{TR}$ ) is not a function of  $\frac{1}{V^3}$  but  $\frac{1}{V^{3.45}}$ . To investigate this effect the runs were analysed with different normalizations. In Fig. 6.10 the effect of different normalization on the  $V_c$  error during the deceleration from 120 to 85 knots is shown. As can be seen the new normalization makes  $V_c$  independent of airspeed, but the effect is small, not more than 1 m/s. The PID used in this simulation is the MKM method but the RLS method has similar results. The initial model parameter values used were based on 85 knots, consequently the two errors converge at the end where the airspeed is 85 knots. As can be seen in Table 6.11, the positive effect of normalization disappears when the model with 22 variables is used, it works even counter productive because the variance is even larger with the improved normalization.

In Table 6.11 the results of all engine failures with the three different model sizes are combined. The calculation was done with the RLS PID method and the initial model parameter values set of 85 knots. It is clear from these results that the modified normalization (2) has a smaller mean error and standard deviation, however, the effect is rather small.

Table 6.11: Mean  $V_c$  error and standard deviation of  $V_c$  error during the deceleration with full power. The MKM PID method was used with the initial model parameter values set of 85 knots

Normalization	Size	Mean (m/s)	St. Dev.
1	10	-2.3067	0.31459
1	13	-2.3228	0.31259
1	22	-2.6159	0.33275
2	10	-2.0066	0.22825
2	13	-2.0153	0.227
2	22	-3.1784	0.94942

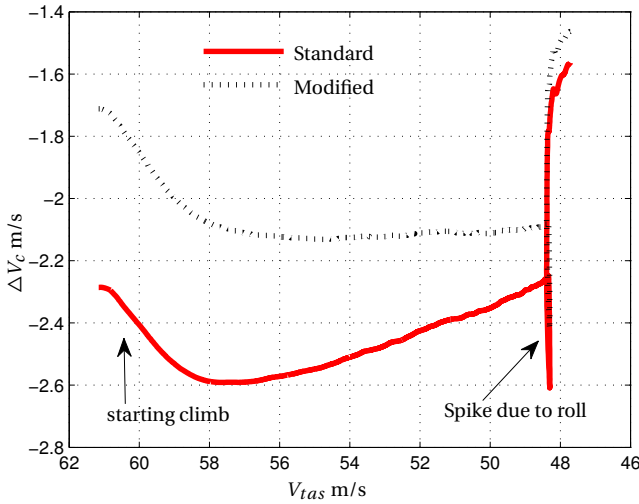


Figure 6.10: Engine failures, error in  $V_c$  comparing the normal and modified normalization for the model with 10 variables; Right engine failure in smooth flying conditions. The 'spike' at low airspeed is caused by the roll carried out at that speed.

INITIAL CONCLUSION

Combining the results of all failures we can conclude that the small model sizes, with 10 or 13 independent variables, give the best results. The difference between 10 and 13 independent variables is small, while increasing to the full model with 22 independent variables decreases accuracy and delayed convergence. Furthermore, the new normalization was better, but the difference was small. When the RLS PID method was used the effect of the improved normalization was not visible. The optimum initial model parameter value set was different for each PID method. MKM, RLS and FAD worked best with the 85 knots initial model parameter value set, while FA had smaller errors with the 120 knots set, but the differences were also small. Comparing the PID methods showed that the reset methods, RLS and MKM were more accurate than the two forgetting algorithms and FAD performed better than FA. In Table 6.12 the results for the different types of failures are presented for all PID methods. For each PID method the best combination of

Table 6.12:  $V_c$  accuracy in (m/s) and convergence time in seconds for different failures and PID methods. For every PID the best initial model parameter set and normalization was used. Mean is the mean value of the absolute  $V_c$  error.

	Initial Values	85	85	85	120
	Size	13	10	10	13
	Normalization	I	II	II	II
Failure		RLS	FAD	MKM	FA
Aileron	Mean (m/s)	2.0	2.4	2.1	1.3
50% loss	Std. Dev. (m/s)	0.5	0.8	0.6	1.6
	time (s)	47.8	111.6	46.9	144.4
Rudder	Mean (m/s)	2.1	2.8	2.0	4.5
loss	Std. Dev. (m/s)	2.5	3.2	0.5	1.0
	time	50.9	97.5	77.6	125.4
Lateral	Mean (m/s)	0.7	2.9	0.5	1.6
Asymetry	Std. Dev. (m/s)	0.8	1.2	0.7	1.8
	time 9s)	103.5	134.2	103.6	116.8
Rudder	Mean (m/s)	3.2	3.5	3.2	4.1
Hard-over	Std. Dev. (m/s)	3.4	3.9	3.6	0.8
	time (s)	121.0	126.9	105.7	140.5
Engine	Mean (m/s)	1.7	2.0	1.6	1.5
Failure	Std. Dev. (m/s)	0.3	2.6	0.3	0.5
	time (s)	36.4	70.2	35.9	81.4

initial model parameter set, number of variables and normalization is used.

Although we have established the most accurate model, initial model parameter set, normalization and PID method, the overall accuracy is rather disappointing. A good accuracy would be less than 1 knot or  $0.5m/s$ , that would make the error as large as the display accuracy of the airspeed indicator. The result is also disappointing when compared to earlier research [14] with  $V_c$  prediction based on the model of the Cessna Citation where accuracies better than  $1m/s$  for  $V_{c1}$ , were achieved for most failures. Based on the difference with this earlier result it was assumed that the specific differences between these two types of aircraft were a probable cause. Because the propeller effect was already accounted for in the model, different causes were investigated. Further research showed that the difference was caused by adverse yaw, which is far more prominent in the Piper Seneca than in the Cessna Citation. This problem will be discussed next.

## 6

### 6.3.3. ADVERSE YAW

In a well executed roll manoeuvre, adverse yaw will not be present. However, when rudder power is limited or not available, adverse yaw is unavoidable. These conditions occur during rudder failures, rudder hard-overs and during engine failures where maximum rudder was used to counter the asymmetric thrust. It was indeed with the simulation of these failures that the initial  $V_c$  calculation had large errors. These could be traced back to an inaccurate calculation of the adverse yaw parameters that was not seen during the

$V_c$  calculation with the Citation model. Looking at the change in yaw parameters during a rudder hard-over in Fig. 6.11 it is clear that the parameters  $n_{\delta_r}$  and  $n_{\delta_F}$  reset correctly. However, if we look at Fig. 6.12 it shows that the parameters  $n_p$  and  $n_r$  also show large deviations, while these parameters are not affected by the failure, and these two parameters are critical for the calculation of the Dutch roll damping.

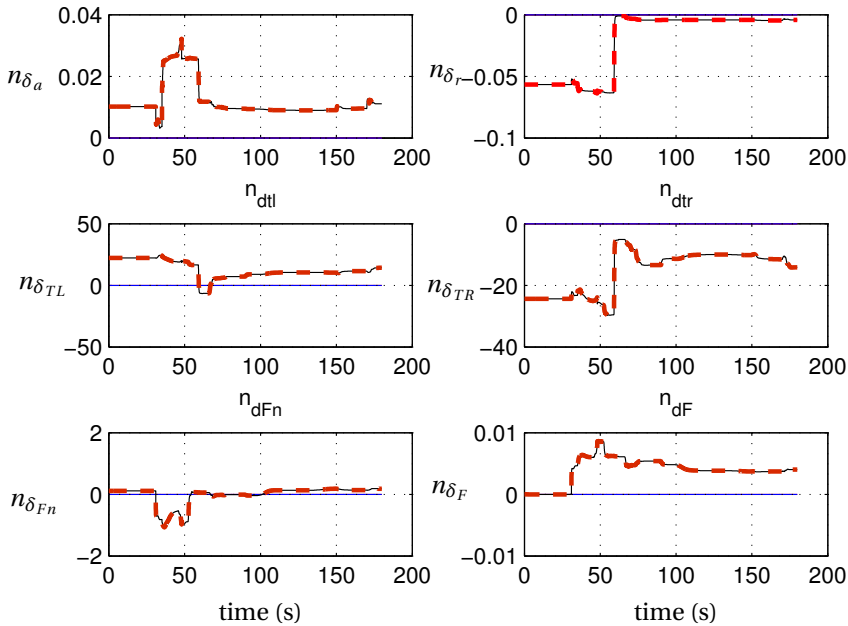


Figure 6.11: PID result state parameters during a Rudder Hard-over; MKM method; resetting by multiplying the covariance matrix by 10,000.

A small improvement could be achieved with the MKM PID method by making a more intelligent reset of the covariance matrix after a failure had been detected. The covariance reset was initially done by multiplying the covariance by 10,000, which worked well for most failures. However, based on physical considerations, one can set a maximum value on the covariance of most model parameters. If we take as example the initial value of the rudder power ( $n_{\delta_r}$ ), it is possible that this value will go to zero, but a change larger than its initial value is not to be expected. This same reasoning is true for most model parameters except for the parameters depending on  $\delta_{Fn}$  and  $\delta_F$ . These parameters are zero when no failure is present. Therefore, the new covariance reset was done by setting the diagonal covariance values to 0.25 times the squared initial value of the model parameter, which equates to assuming that the standard deviation of these parameters is half their initial value. The covariance of the parameters dependent on  $\delta_{Fn}$  and  $\delta_F$  were set to 10 and 1, respectively, which was based (with a considerable margin)

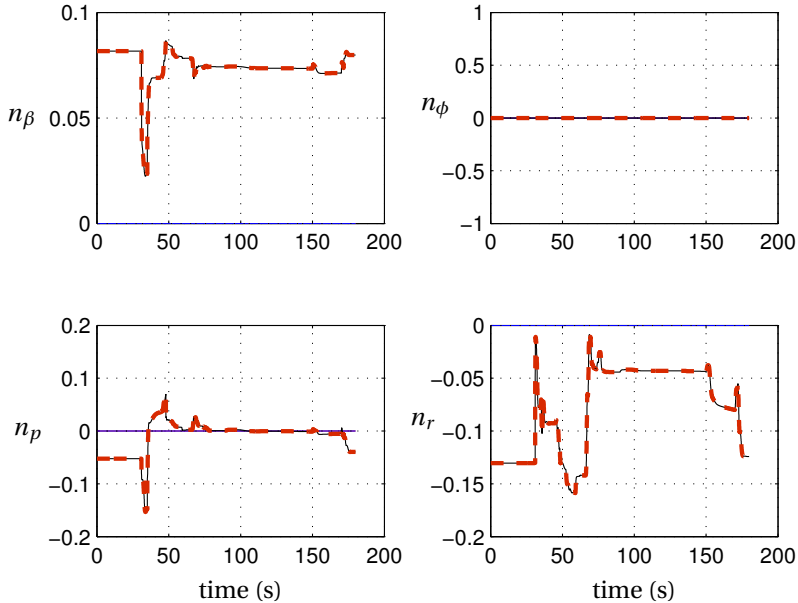


Figure 6.12: PID result model parameters during a Rudder Hard-over; MKM method; resetting by multiplying the covariance matrix by 10,000.

on possible values for asymmetries ( $\delta_{Fn}$ ) and rudder hard-overs ( $\delta_F$ ) respectively. The effect of this improvement can be seen in Fig. 6.13.

But even this correction left a considerable error in the  $V_c$  calculation, which could be as high as  $6m/s$ . If we look at the reconstruction accuracy of the final roll angle change when a rudder hard over is experienced, as depicted in Fig. 6.14, we notice that the initial part of the roll is accurate but that the error starts building up after 0.75 second. This difference is due to the inaccuracy of the Dutch roll parameters, or as can be seen in Fig. 6.14, the late convergence of these parameters. The actual convergence occurs after the final roll, when the large side slips are experienced. The effect of these errors is that the adverse yaw increases more than predicted and both the side slip ( $\beta$ ) and the maximum roll rate will be lower than predicted.

There are a few possible solutions to this problem. One solution is to make control inputs with large deflections to excite large yaw and roll rates. This will enhance the accurate prediction of the parameters  $n_p$  and  $n_r$ . However, considering the fact that the pilot of a damaged aircraft is more inclined to make small inputs, in order to minimize additional loads on the aircraft, this solution is not very practical. Another solution is to limit ourselves to the prediction of the initial roll angle change. As can be seen in Fig. 6.14, the error is small in the initial phase of the roll. Initially we used a fixed roll

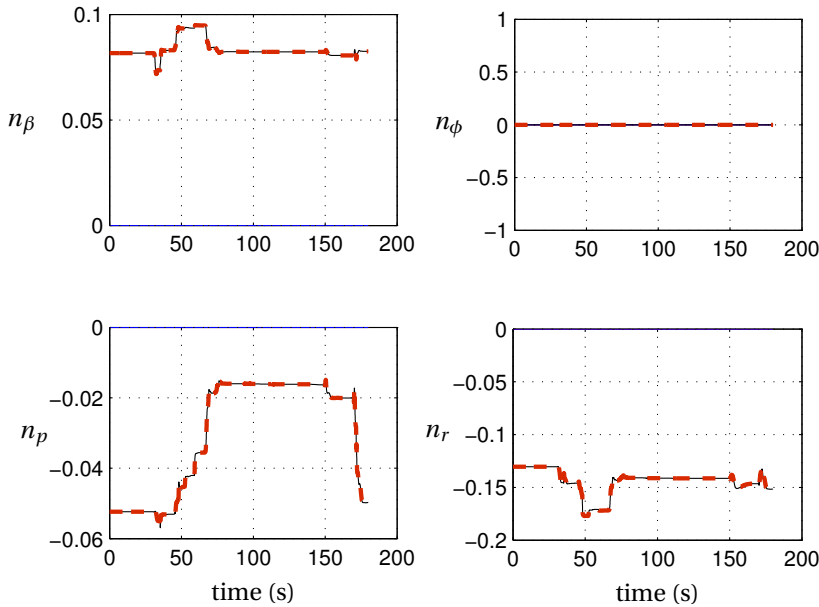


Figure 6.13: Determination of roll control parameters during a Rudder Hardover; MKM method; resetting by setting covariance matrix to fixed values.

angle change in 1.5 seconds, based on certification requirements from Mil. Spec. 1797 [9]. But for controllability we can also use a shorter time period. When we change the time period to 0.75s, the errors in  $V_c$  become more acceptable.

#### 6.3.4. THE FINAL RESULTS

Based on a maximum rate roll angle change in 0.75s, a new analysis was made. In Table 6.13 the best combinations of initial model parameter set, normalization and PID method are presented. The optimum combinations are the same as before (see Table 6.7) but the errors are now much smaller and the convergence time is much faster. The performance of the RLS, MKM and FAD PID methods are now quite close, with the MKM method as the overall best. The standard FA method performance is clearly inferior, not only in terms of accuracy but also in convergence.

With the same best combinations, an overview is made of the  $V_c$  prediction errors per type of failure, also based on the roll angle change in 0.75 seconds. The results are presented in Fig. 6.14. These accuracies are not all within the one knot reading accuracy of the pilot that we hoped to achieve. However, being able to predict a safe manoeuvre velocity with a standard deviation of  $0.9m/s$  or 1.75 knots in a situation where previously no guidance was available, is still a desirable improvement.

Table 6.13: Best combinations for each PID method. Mean is the mean value of the absolute  $V_c$  error.

PID	Size	Init.Val.	Norm.	Mean (m/s)	St. Dev. (m/s)	Conv. time (s)
RLS	13	85	I	1.1	0.9	60.6
KF	10	85	II	1.0	0.9	59.7
FAD	10	85	II	1.7	1.7	80.5
FA	13	120	I	1.9	1.6	93.9

Table 6.14:  $V_c$  accuracy (m/s) and convergence in seconds, based on prediction of the roll angle change in 0.75 second; Results presented for different failures and PID methods. Best combinations of number of variables, initial parameter set and normalization is used for each PID method. Mean is the mean value of the absolute  $V_c$  error.

Failure		Init.Val.	85	85	85	120
		Size	13	10	10	13
	Normalization		I	II	II	II
			RLS	FAD	MKM	FA
Aileron	Mean (m/s)	0.8	1.2	1.3	1.2	
	St. Dev. (m/s)	0.9	1.0	1.1	1.4	
	Conv. time (s)	46.1	50.3	39.7	125.8	
Rudder	Mean (m/s)	0.8	1.5	0.6	2.1	
	St. Dev. (m/s)	0.9	0.7	0.6	0.8	
	Conv. time (s)	30.0	60.7	30.0	45.4	
Asymmetry	Mean (m/s)	1.0	2.3	0.5	1.2	
	St. Dev. (m/s)	0.8	0.9	0.7	1.4	
	Conv. time (s)	90.0	121.6	93.3	129.7	
Rudder hard over	Mean (m/s)	1.2	1.7	1.4	1.9	
	St. Dev. (m/s)	0.6	0.3	0.8	0.9	
	Conv. time (s)	76.2	88.9	82.4	72.5	
Engine	Mean (m/s)	1.6	1.3	1.5	1.7	
	St. Dev. (m/s)	0.4	0.4	0.4	0.5	
	Conv. time (s)	35.5	36.8	35.5	82.9	

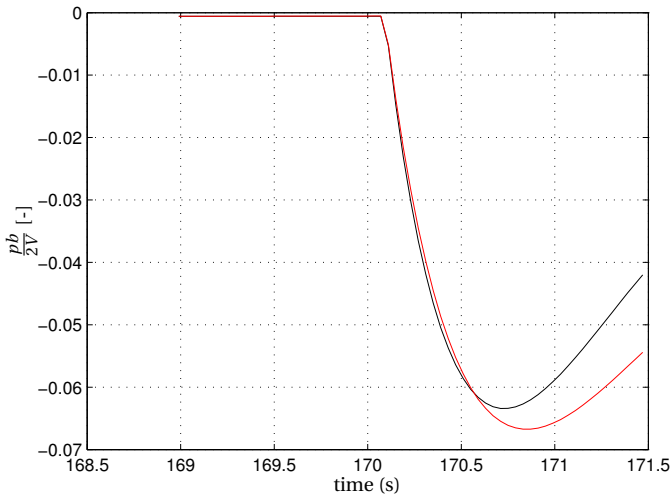


Figure 6.14: Rudder Hardover run 41; Reconstruction of final maximum deflection roll. In red the reconstruction of the roll and in black the actual roll.

#### EFFECT OF INPUTS AND TURBULENCE

Finally we looked at the effect of the extra identification inputs and the effect of turbulence on the  $V_c$  error, its standard deviation and on the convergence time. As can be seen in Table 6.15, turbulence improves the  $V_c$  accuracy of the RLS and MKM method, but decreases the accuracy of both forgetting algorithms. The most visible effect of the additional inputs is the decrease in the  $V_c$  variance. The RLS and FA methods do not improve in mean  $V_c$  error with additional inputs but MKM and FAD do. The improvement in convergence time was large for both forgetting algorithms. We can conclude that forgetting algorithms benefit most from additional inputs while RLS and MKM work best in turbulent flying conditions. These results confirm findings of earlier results [13] that turbulence can enhance the parameter identification.

#### 6.3.5. CONCLUSION

In this chapter we investigated if we could determine the  $V_c$  from a damaged aircraft in a realistic environment. A realistic simulation environment was created by using runs with the model of the Piper Seneca where typical flight manoeuvres plus additional identification manoeuvres were performed. Furthermore, runs were carried out in smooth and turbulent flying conditions and a broad set of failures were used that affected control power of rudder and aileron, added lateral symmetries, rudder hard-overs and engine failures. Different Parameter Identification (PID) methods, different model sizes, and initial model parameter values were investigated.

We can conclude the following:

- The small models, using only 10 or 13 independent variables in each row, gave

Table 6.15: Effect of turbulence and identification inputs on the mean  $V_c$  error, its standard deviation and the mean convergence time. Calculations are made for the optimum combinations of PID, normalization, model size and pre sets.

	PID	RLS	FAD	MKM	FA
	Initial Value	85	85	85	120
	Size	13	10	10	13
	Normalization	I	II	II	II
Turbulence	Mean (m/s)	0.39	0.63	0.72	0.85
	St. Dev. (m/s)	1.02	1.72	0.77	1.65
	Conv. time (s)	52.92	75.30	56.79	87.64
Smooth	Mean (m/s)	0.71	0.57	1.12	0.72
	St. Dev. (m/s)	1.17	1.78	1.02	1.82
	Conv. time (s)	62.78	75.79	60.14	90.92
Ident 1	Mean (m/s)	0.40	0.53	0.92	0.53
	St. Dev. (m/s)	1.25	2.16	1.03	2.08
	Conv. time (s)	56.59	91.43	59.45	112.13
Ident II	Mean (m/s)	0.44	0.50	0.76	0.77
	St. Dev. (m/s)	0.94	1.46	0.85	1.46
	Conv. time (s)	64.57	69.34	63.23	74.55

better results than the large model with 22 independent variables. Because there was hardly any difference between the 10 and 13 variable model it is justified to use the smallest size model;

- The resetting PID methods RLS and MKM performed better than the two forgetting algorithms. MKM achieved the best accuracy and fastest convergence;
- The modified normalization created less variation in the model parameters over the speed trajectory, which enhanced the convergence of the predicted  $V_c$ , however, in absolute terms the improvement is small;
- Different initial parameter sets, representing the model at different speeds, were tested. The results show that the difference between initial parameter sets were small and dependent on the PID method used. For every PID method the optimum initial parameter set was selected;
- A lack of accuracy was discovered in the prediction of the roll angle changes that could be traced back to an inaccuracy of the PID methods to determine two parameters  $n_p$  and  $n_r$ , that are important for calculating the Dutch roll effect. A solution was found by adapting the covariance reset and to restrict the prediction to the roll angle change in the first 0.75 second.
- Forgetting algorithms benefit from additional inputs but decrease in accuracy in turbulence. RLS and MKM improve slightly in accuracy due to turbulent flying conditions, but only MKM improves in accuracy due to additional inputs.

Now we have optimized the  $V_c$  prediction system and have shown that it can predict the remaining roll control for a damaged aircraft with reasonable accuracy, it is time to evaluate its potential using pilot-in-the-loop testing. These tests are described in the next chapters.

## REFERENCES

- [1] J. A. Mulder, J. K. Sridhar, and J. H. Breeman, *AGARD AG-300 Vol.3 Part2* (AGARD, 1994).
- [2] C. Kamali, A. A. Pashilkar, and J. R. Raol, *Evaluation of Recursive Least Squares Algorithm for Parameter Estimation in Aircraft Real Time Application*, *Aerospace Science and Technology* **1**, 165 (2011).
- [3] D. Graupe, *Identification of Systems* (Robert E. Krieger Publishing Company, 1976).
- [4] M. S. Grewal and A. P. Andrews, *Kalman Filtering: Theory and Practice* (John Wiley and Sons, Inc., 2001).
- [5] D. Q. Mayne, *Optimal Non-stationary Estimation of the Parameters of a Linear System with Gaussian Inputs*, *Journal of Electronics and Control* **14**, 101 (1963).
- [6] J. R. Raol, G. Girija, and J. Singh, *Modelling and Parameter Estimation of Dynamic Systems* (Institution of Electrical Engineers, 2004).
- [7] H. J. Koolstra, C. C. de Visser, and J. A. Mulder, *Effective Model Size for the Prediction of the Lateral Control Envelope of Damaged Aircraft*, in *Proc. of the AIAA Guidance, Navigation, and Control Conference, the AIAA SciTech Forum 2015, Kissimee, USA* (2015).
- [8] J. A. Mulder, J. C. van der Vaart, and M. Mulder, *Atmospheric Flight Dynamics* (Technical University Delft, Faculty LR, 2007).
- [9] Anon, *Military Standard, Flying Qualities of Piloted Airplanes; MIL-STD-1797*, Tech. Rep. (DoD, 1987).
- [10] Anon., *Flying Qualities Theory and Flight Test Techniques* (USAF TPS, Edwards AFB, CA, 1984).
- [11] J. A. Mulder, *Design and Evaluation of Dynamic Flight Test Manoeuvres*, Ph.D. thesis, Technical University Delft (1986).
- [12] Anon., *Aviation-Safety-Database*, Aviation Safety Network website (1992), <https://aviation-safety.net/database/record.php?id=19921004-2>.
- [13] H. J. Koolstra, H. J. Damveld, and J. A. Mulder, *An Improved, Turbulence Proof, Reset Mechanism for Parameter Identification after System Change*, in *Proc. of the 2013 AIAA Guidance Navigation and Control Conference, Boston, USA, Aug. 19-22* (2013).
- [14] H. J. Koolstra, H. J. Damveld, and J. A. Mulder, *Envelope Determination of Damaged Aircraft*, in *Proc. of the AIAA Guidance, Navigation, and Control Conference 2012, Minneapolis, USA, Aug. 13-16* (AIAA, 2012).

# 7

## **INITIAL EVALUATION OF PILOT BEHAVIOUR IN SCENARIOS WITH LIMITED ROLL CONTROL**

*No situation is more dangerous than the one  
in which experience gives the wrong solution.*

HJK

## 7.1. INTRODUCTION

Up to now most, if not all, effort in this thesis has been directed towards choosing the correct model, the optimum parameter identification method, the correct failure detection method and to refine the method to calculate the minimum lateral control velocities. But all simulations were done without a pilot in the loop. In October 2014 TU Delft's SIMONA Research Simulator was used to evaluate if pilots could work with a lateral control warning system.

For this test the Primary Flight Display (PFD) was modified to show lateral control limits. This initial test had an exploratory nature, no pilot participant had ever worked with a lateral control warning system before, neither had they ever experienced a reduced lateral control situation during their flight career. Some pilots, however, had been given a  $V_{mca}$  demonstration in the past, but these demonstrations were, for obvious safety reasons, carried out at high altitude where the recovery was done by reducing to idle power and lowering the nose to regain airspeed. Consequently, no experience was gained in how to optimize power and to minimize altitude loss while maintaining lateral control.

In the initial evaluation discussed in this chapter, a total of three scenarios were defined. The first two scenarios are well-known to pilots, namely a one-engine-out traffic pattern and a one-engine-out go-around. In actual flight, these scenarios are flown at the single engine climb speed, which is 90 KIAS for the Piper Seneca. To evoke a situation in which a pilot could unexpectedly enter a roll-limited situation, pilots were asked to make approaches at 80 KIAS. This is above the published  $V_{mca}$ , which is 70 KIAS, just above the minimum lateral control speed. For this test we defined the minimum lateral control speed ( $V_c$ ) to be the speed required to make a  $15^\circ$  roll angle change in 1.5s. A roll-limited situation was indeed encountered in 54 of the 162 experimental runs flown.

The third scenario used was an unfamiliar one: a sudden rudder hard-over. In this scenario, the pilots were instructed to do some manoeuvring in order for the parameter identification system to find the changes in the aircraft stability and control parameters. Thereafter, they were asked to set up for a safe approach and landing using the novel  $V_c$  indication to determine the best velocity.

Flight data, pilot inputs and the  $V_c$  value were collected during the runs. After each run, pilots were asked for comments on the scenario and on the modified PFD. If mistakes were made, pilots were instructed on how they could improve the use of the  $V_c$  indication.

## 7.2. OBJECTIVES

In this exploratory evaluation, the main question was whether a pilot, after some training, could work with the dynamic  $V_c$  display. Stated differently: would the display enhance their recovery from  $V_c$  limited situations, or prevent  $V_c$  limited situations from developing in the first place.

Hence, the experiment had three objectives: The first objective was to investigate if the  $V_c$  display would enhance the handling of engine failures. The handling of engine failures is taught in pilot training and is also part of the yearly qualification for pilots, therefore handling of this failure was familiar to the participants. Engine failures are also the most common cause of limited lateral control<sup>1</sup>. The second objective was to test an experimental side slip display that will be described in more detail below. The third objective was to investigate whether pilots could use the  $V_c$  display to their advantage when they encountered a non engine related lateral control problem.

### 7.3. EXPERIMENTS

In the following, the three different scenarios introduced above will be referred to as separate 'experiments'. All experiments used the same hardware, models, interface and group of participants. Therefore these items are discussed first in this section, then each experiment will be treated separately.

#### 7.3.1. SIMULATOR AND MODELS

##### APPARATUS: SIMONA RESEARCH SIMULATOR

The experiments were performed in the six-degree-of-freedom simulation, SIMONA research simulator (SRS). The SRS has a hydraulic hexapod motion system. Standard wash-out filters were used. Because of the high rates involved in experiments with sudden engine failures, the input signals to the simulator motion system had to be shaped to prevent the simulator from reaching its safety limits. For this shaping, an arctangent filter was designed to shape the roll, roll rate and acceleration outputs of the aerodynamic model before they were passed to the motion system. The effect of the arctangent filter is that inputs up to 1 are passed with limited distortion and that signals from 1 to  $\infty$  are reduced: the maximum absolute value of the output cannot exceed  $0.5\pi$  as can be seen in Equation 7.1 where  $b$  is the breakpoint value,  $A_{air}$  is the aircraft acceleration and  $A_{sim}$  is the acceleration fed into the simulator motion system. The breakpoints (the arctan(1) points) are given in Table 7.1.

$$A_{sim} = b \arctan \frac{A_{air}}{b} \quad (7.1)$$

The hydraulic control loading system generated control forces that were linear with control deflection. The spring constants for the control forces were set to increase linearly with the dynamic pressure, which resulted in control forces that were typical for direct manual control. Control forces were tuned by a research pilot with extensive experience with small twin engine propeller aircraft, including the PA-34 used here.

<sup>1</sup>The most recent, on-line available NTSB database, was over the year 2001 [1]. This database shows that from the 1515 accidents and incidents with two engine general aviation aircraft, engine failure was the initial cause in 408 cases while 4 propeller related accidents in the air make a total of 412 cases where an engine or propeller related lateral-directional asymmetry occurred. All other mechanical failures, which not necessarily all affect the lateral-directional control, account for only 72 cases.

Table 7.1: Breakpoints used for input shaping. The shaping was performed before the inputs were passed to standard wash out filters of the SRS Motion System

parameter	breakpoint
$p, q, r$	0.25 rad/s
$\dot{p}, \dot{q}, \dot{r}$	0.5 rad/s <sup>2</sup>
$a_x, a_y, a_z$	2 m/s <sup>2</sup>

The visual outside display system provides a collimated, 180-degree horizontal by 40-degree vertical field of view. During the experiment, the simulator's right projecting system temporarily broke down, which unfortunately left the pilot with only the left and central display systems. Because a left-hand traffic pattern was used and the pilots occupied the left-hand seat, the effects of this break down were reduced as much as possible.

#### VEHICLE MODEL

The non-linear PA-34 Piper Seneca III aerodynamic model used in the real-time simulation was identical to the model used for all off-line simulations and is described in Chapter 5 and in Reference [2].

#### $V_c$ CALCULATION

The minimum lateral control speed  $V_c$  was calculated in real-time, based on pilot inputs, the aircraft state and the linear aircraft stability and performance parameters that were constantly updated by the parameter identification routine. In a real flight situation the two step method [3] should have been used, but in a simulator the first step, to derive the aircraft state, is not required because the aircraft state is perfectly known. This leaves only the second step, the equation error method. Normally, the recursive least squares (RLS) method would be used for the second step, for this experiment however we applied a modified RLS, the Modified Kalman Filter, described in Chapter 6. Note that the failure detection and reset methods used were based on the Sequential Probability Ratio Test and are described in Refs. [4] and [5]. The failure detection was only required for the third experiment, the rudder hard-over. For engine failures, no detection is required, because engine performance is integrated into the  $V_c$  prediction model.

### 7.3.2. PILOT INTERFACE

#### SIDE SLIP DISPLAY

Side slip indicators have evolved over time. The traditional side slip indicator was the 'ball' indicator as depicted in Fig. 7.1 that was normally combined with a turn indicator in a separate instrument: the 'turn and slip indicator'. Later the slip indicator was often integrated with the attitude indicator and displayed at the bottom of this indicator.

In the present PFDs, the side slip display used is a moving square, mimicking the old 'ball', situated in the top of the attitude indicator, aligned with the bank angle indicator as can be seen in Fig. 7.1. This display has two disadvantages: first, the side slip indicator alignment with the bank angle indicator causes the deflections to be parallel with the

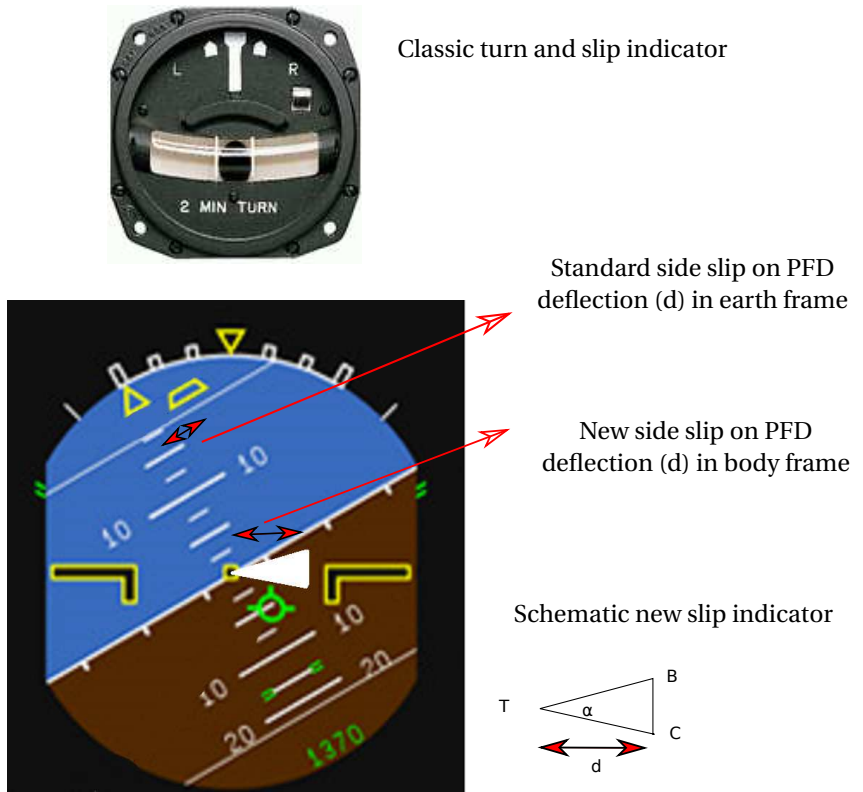


Figure 7.1: Different Side Slip indicators

horizon. However, side slip is defined [6] relative to the aircraft body axis, and deflection should in fact be parallel with the aircraft wing. Consequently, the present display is in error when the aircraft has a bank angle. Second, the available space in the top of the display is limited and, as can be noted in Fig. 7.1, the slip indicator is small. It was therefore not surprising that RNLA Hercules pilots asked to reinstall the old mechanical side slip indicator after the cockpit upgrade, which replaced the old analogue displays with modern integrated PFDs<sup>2</sup>.

The new experimental display, as shown in Fig. 7.1, uses a variable size triangle, with the top (T) of the triangle fixed in the centre of the attitude indicator. The base (BC) of the triangle is deflected linearly with side slip, but now in the body frame. The deflection (d) of this new indicator is equivalent in size to the 'ball' deflection at the top. By using a triangular shape with a fixed angle  $\alpha$  at the top (T), the length of the base (BC) increases linearly with the deflection (d), consequently the presented area is linear with  $d^2$ . This

<sup>2</sup>This information was received when the author tested the RNLA new simulator where this indicator had to be reinstalled.

quadratic increase in area with the side slip makes large side slips far more prominent than the present display, furthermore, the growth (in area) of the side slip indicator is now directly related to the increase in drag that is also a function of  $\beta^2$ .

Both side slip indicators, the conventional one at the top of the PFD and the new one at the display centre were modified to show either the traditional side acceleration ( $\dot{j}$ ) or  $\beta$ . This difference was made clear to the pilot by changing the colour. The traditional side acceleration was presented with a white triangle and a white ball and the colour was changed to yellow when  $\beta$  was displayed. After the tests, it was discovered that the lateral specific force of the model was too low, caused by a programming error in the aerodynamic model. Because of this error only the data based on  $\beta$  were usable and will be discussed in the following sections.

### $V_c$ DISPLAY

A conventional Primary Flight Display (PFD) presents the 1-g stall speed<sup>3</sup> with a standard, red 'barber pole' on the right side of the speed tape. Because it may be confusing for a pilot to have different speed limits displayed at different places across the display, it was decided to use this presentation but with a modified 'barber pole'. The  $V_c$  was not displayed when it was lower than the 1-g stall speed. When it was higher than the stall speed the 'barber pole' was extended in yellow on top of the red barber pole for the stall speed. This is illustrated in Fig. 7.2, where the yellow extension starts above 62 knots. When a failure is detected, the  $V_c$  indication will be inaccurate until the PID system has derived the model parameter values. In order to expedite the identification and to warn the pilot, the warning 'MAN' is splayed in the annunciator window of the PFD, as displayed in Fig. 7.2, to inform the pilot that manoeuvring is required.

### DIFFERENCES WITH THE STANDARD PA-34

Our SIMONA simulation differs from the real PA-34 in several ways. The most important difference is that there was no feathering possibility. Therefore idle thrust was programmed to give little drag as if the propeller was feathered. This enabled the pilot to use this aircraft as if auto-feather was installed. Secondly, only pitch trim was available and no rudder trim. Because most runs were of a short duration, this was not considered a major issue. Finally, colour coding for the new display items was not based on the standard advisory (AC 25-11B Table 5.1) but just to make a clear distinction for the test subjects between the different scenarios as well as to make the new features clearly stand out from the standard PFD items. All displayed speeds in the cockpit were KIAS/KCAS, which are equivalent because there is no position error in the simulator. However, the results, for example  $V_c$  exceedances, are always based on true airspeed.

### 7.3.3. SUBJECTS

Ten pilots participated in the experiments. All pilots had current flight experience on twin or multi-engine aircraft. The flight hours and special qualifications are given in Table 7.2. All pilots were familiar with one-engine-out approaches and go-arounds.

<sup>3</sup>In our simulation the barber pole represents the 1-g stall speed, however, actual mechanization in real aircraft may differ. In some aircraft the barber pole represents the stick shaker speed at the existing load factor.

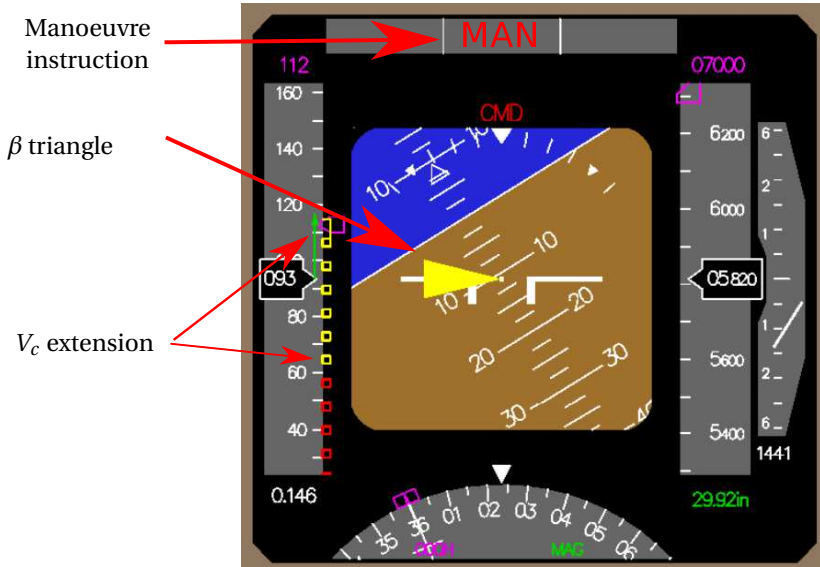


Figure 7.2: The PFD used in the experiments, augmented with (1)  $V_c$  indicator and (2) a centred side slip display that can either display  $\dot{y}$  in white or  $\beta$  in yellow. The Manoeuvre instruction is displayed for 15 seconds after the detection of a failure.

Table 7.2: Subject Pilot background and experience.

Number	Flight. Hrs.	Special Qualifications
4	200-250	Just Graduated Civilian Pilots
1	1,500	Qualified Cessna Citation; Flight instructor
1	3,500	Qualified Cessna Citation
1	3,000	Military Pilot; Qualified C-130H; Experimental Test Pilot
1	800	Military Pilot; Qualified KDC-10;
1	4,000	Qualified twin prop
1	4,500	Qualified 747; Flight Instructor

### INSTRUCTION TO SUBJECTS

For ease of reading the instruction to the subjects are described separately for each experiment.

## 7.4. EXPERIMENT 1; TRAFFIC PATTERN

### 7.4.1. DESIGN AND PROCEDURES

The first experiment was a standard approach to landing with one failed engine, using a traffic pattern that is common in general aviation (see Fig. 7.3). All runs started on the down wind leg, at 800 feet AGL, 125 KIAS and with landing gear and flaps selected up. The traffic pattern was situated at Schiphol airport and was a left-hand pattern for runway 18R, consequently the initial heading on downwind was North and the base leg was oriented to the West. The first task on downwind was to slow down the aircraft to approach speed (80 KIAS), and to reconfigure the aircraft to flaps 25° and gear down when below the gear and flap limit speed of 110 KIAS. When the pilot was given control, one engine was failed as soon as the pilot had stabilized the aircraft in heading and altitude, which was always within in the first 10 seconds of the scenario. At the start of the turn to base leg the descent was started. The aim was to roll out on runway heading (180°) about one mile before the threshold at approximately 300 feet AGL. To reach this point accurately was however difficult, because the field of view of the outside visual would not permit the pilots to see the runway until 90° of the turn was completed. Thereafter the approach was continued to touch down or just before touch down. The actual landing itself was not part of the experiment.

### OBJECTIVES OF THE TEST

The objective of this test was to investigate whether the handling of a roll-limited situation in a standard one-engine out traffic pattern could be improved by adding the new  $V_c$  display and the new side-slip display.

### INDEPENDENT VARIABLE

Two independent variables in this experiment were related to the new indications: the  $V_c$  display and the side slip display, and the third was crosswind. During the familiarization, the  $V_c$  presentation was switched off and the standard side slip display was used in zero wind conditions. Because the 'j' presentation' runs had to be omitted from the evaluation, the only results used are with  $\beta$  displayed in the centre and the  $V_c$  displayed. This left the crosswind as being the only remaining independent variable.

When wind was introduced in the scenario it was always a wind from the East with 15 knots at 10 meters above ground level, increasing logarithmically with increasing height, blowing the aircraft towards the runway. The wind change was used to see whether the decreased space for the turn would tempt pilots to over-bank the aircraft and lose speed, which was a common cause of T-38 accidents<sup>4</sup>.

<sup>4</sup>[http://www.ejection-history.org.uk/Aircraft\\_by\\_Type/t\\_38\\_talon.htm](http://www.ejection-history.org.uk/Aircraft_by_Type/t_38_talon.htm)

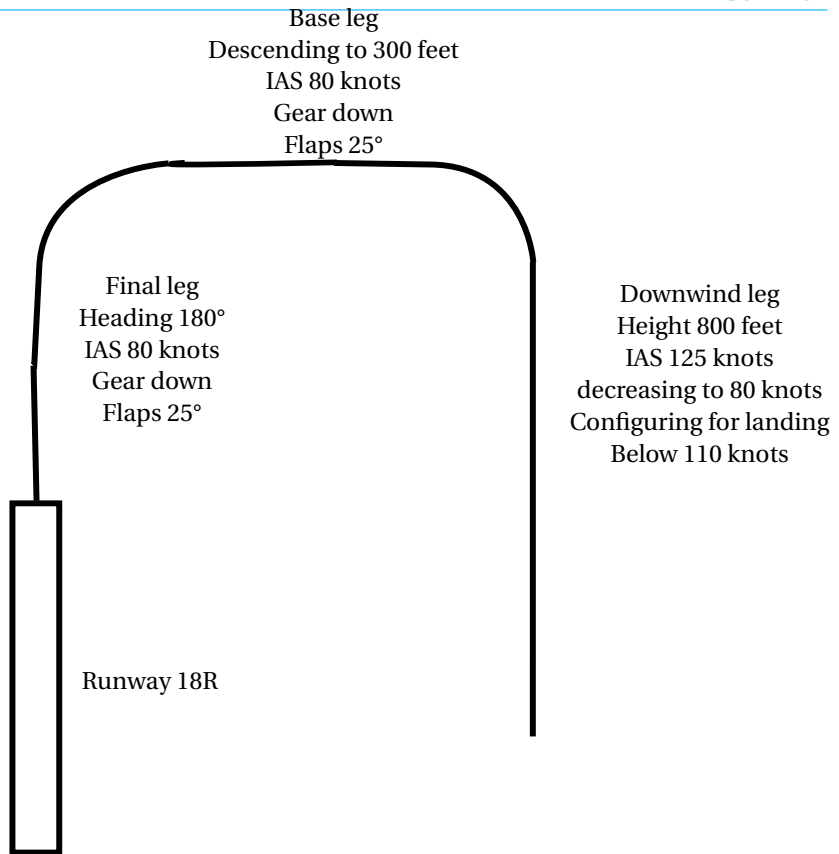


Figure 7.3: General aviation traffic pattern used for runway 18R at Amsterdam Airport (Schiphol)

### PILOT INSTRUCTIONS

Pilots were briefed on the operation of the new  $V_c$  indicator and explained how they could influence this indicator with the amount of asymmetric power and with rudder. The new types of side slip display were explained and shown in the familiarization runs. Pilots were instructed to use the standard techniques and procedures as they were trained to apply in this type of scenario. The only exception was the speed. While normally, in case of an engine failure, the traffic pattern would be flown with the speed that would give optimum single engine climb performance (90 KIAS for the PA-34), here all pilots were instructed to fly this pattern at 80 KIAS to create conditions where the aircraft was closer to the  $V_c$ . However, when the  $V_c$  indication increased above 80 KIAS they were instructed to use the airspeed advised by the  $V_c$  indicator.

### ORDER OF RUNS

The following run sequence was used:

- The first two runs were used to familiarize the pilots with the aircraft and the traffic pattern. Normally, pilots start the turn to base-leg based on their position relative to the runway, but this requires a visual system with a horizontal view of at

least 270 degrees. Therefore, the first two runs were also used by pilots to acquaint themselves with the landmarks to be used for the turn to base-leg.

- The third run was the one-engine-out scenario with the standard (non modified) display.
- The fourth run was the one-engine-out scenario with  $V_c$  indication added and side slip was moved to the centre.
- In the fifth run the side-slip indicator was changed to show  $\beta$ .
- In the sixth run, 15 knots wind from the East was added while the display was similar as in run five.

When pilots experienced difficulties in a run, that run was repeated if time allowed. For the evaluation only the results of runs 5 and 6 were used.

#### OPTIMUM PILOT CONTROL

When we use the term 'optimum pilot control' it is not used in a mathematical sense, as if the pilot would minimize some parameters with a mix of control inputs. Instead we use the term for a stepwise approach, as in a check list, where the most important issues are addressed first. When a pilot has to control an aircraft with one-engine-out, he can come low in airspeed or low on the glide path. In either case he needs more power, but the amount of power he can add depends on the airspeed. If the pilot flies at the recommended speed he can always use full power and lateral control is not an issue. But if, for some reason, the aircraft airspeed is below this recommended speed, the power advance should be limited in order to prevent a lateral departure as explained in Chapter 3. Presently, pilots are not trained in the recovery of one-engine-out aircraft (from this situation) and are only trained to prevent it<sup>5</sup>. Without any  $V_c$  indication, the pilot can only use available aileron and the aircraft roll response, to judge if he is applying too much power.

Using the  $V_c$  indication, the pilot can apply just enough power to move the  $V_c$  indicator to the present airspeed, while using rudder to maintain zero side-slip. In a low airspeed situation, full rudder is normally required for zero side slip, but even when full rudder is not required, it is a good trade-off to use more than the required rudder if that would allow a higher throttle setting. This trade-off is advantageous because the additional thrust is greater than the added drag due to side slip<sup>6</sup>. When power is still insufficient, the nose has to be lowered to increase airspeed and this will enable the use of more power. The worst situation occurs when maximum rudder is already applied and no altitude is available any more to increase airspeed. Applying more power will increase

<sup>5</sup>All participating pilots have had  $V_{mca}$  demonstrations in the past, but all these earlier demonstrations ended before a full lateral control limited situation actually developed.

<sup>6</sup>Without giving a full quantitative analysis, when the rudder distance to the c.g. is greater than the engine distance to the c.g. the required additional aerodynamic side force generated by the rudder is less than the additional engine thrust, and the increased drag of the aircraft due to additional side force is even less.

the  $V_c$  and if the exceedance becomes large, the aircraft could then start an unstoppable roll. An alternative is to raise the gear, reducing the drag and attempt a go-around.

While having discussed the optimum pilot reaction in case of a low airspeed situation with reduced lateral control, it is also important to realize how this situation is created during a one-engine-out traffic pattern. Everything depends on the energy management on the down wind and base leg. When the aircraft is configured for landing with 25° flaps and gear down, level flight can not be maintained with full power on one engine. Consequently a minimum constant descent rate is necessary. When a nice balance is reached between power setting and descent, no lateral control-limited situation will be encountered, however when the power is initially reduced too much, or the initial descent is too steep, energy problems can be encountered. From this description it may be apparent that the optimal recovery from a low airspeed situation in a roll control limited case is more complex than the recovery from a stall. In case of a stall recovery, reducing the angle of attack and applying maximum power will suffice. And as mentioned before, a further complicating factor is that this manoeuvre, of course without the presence of a  $V_c$  indication, is not part of standard pilot training.

#### DEPENDENT MEASURES

Because of the exploratory nature of the test, the emphasis was on collecting subjective comments from the pilots. After each test, pilots were asked if they noticed the new displays and how these affected their actions. In addition, all other subjective comments were collected.

Objective dependent measures were occurrences of excessive bank angles, which are a clear indication of losing lateral control. Furthermore the increase in rudder deflection, the decrease in pitch angle ( $\theta$ ) and also the reduction of power, were objective measures of the proper use of the  $V_c$  display when the  $V_c$  increased above the present airspeed.

#### EXPERIMENT HYPOTHESIS

The first hypothesis was that pilot awareness of available roll control would be enhanced by the  $V_c$  display. This could be verified by pilot comments on the use of the display and the objective measures on the reaction on  $V_c$  exceedances. The second hypothesis was that the position of  $\beta$  in the centre of the new side-slip display would be easier to use for the pilots, which was evaluated only by their subjective comments.

### 7.4.2. RESULTS EXPERIMENT 1

#### GENERAL

The one-engine-out traffic pattern profile that was actually flown differed considerably for each pilot. The fixed points were the starting point, the point from which to turn to base and the position of the threshold. Pilots differed in their initial descent rates in the turn to base leg. Furthermore, some pilots advanced the good working engine directly after the failure and decelerated much slower than others who postponed the power advance until 80 KIAS was reached. The profile did also differ per pilot per run. These variations were however not seen as a drawback, but can actually be seen as a good example of variations that may occur in real situations.

Because of these variations in energy management the roll limited situations occurred at different points in the profile. Typically, a situation with a low airspeed with enough altitude could be countered by dropping the nose, but a situation with low airspeed at low altitude necessitated a power increase that further decreased the lateral control available. Because of the, already mentioned, restriction in the Field of View (FoV) of the simulator, pilots were less aware of their height relative to the threshold in the turn to base. As a consequence, they frequently discovered relatively late that they were low on the glide path and had to adjust power close to the ground and encountered situations where the  $V_c$  exceeded the actual airspeed. The pilot reaction to these  $V_c$  exceedances is discussed in the following paragraph. A rather unexpected result was that some pilots were using less than optimum rudder when the situation did warrant the use of full rudder deflection. Both findings will be discussed in more detail below.

#### EXCEEDING $V_c$

The number of runs made in the first scenario was 74. From these runs, 40 were done with the  $\beta$  side-slip display and used for further analysis. In 20 of these runs  $V_c$  exceedances occurred, the total number of separate exceedances was 43. For the proper definition of a  $V_c$  exceedance we have to cancel noise inputs. If pilots use a power setting that sets the  $V_c$  indication at the present airspeed, or slightly but hardly noticeable above it, this should not be counted as a  $V_c$  exceedance. Also, a short exceedance while setting the power is not critical and can be omitted. To eliminate these exceedances the following criteria were defined to qualify as a true  $V_c$  exceedance:

1.  $(V_c - KIAS) > 2$  knots.
2. The time that  $(V_c - KIAS) > 2$  knots must be more than 2 seconds.

The purpose of the test was to evoke  $V_c$  exceedances, that is why the traffic pattern was flown at 80 KIAS, and to see if proper action was taken. An overview of the results is presented in Table 7.3.

We first look at the causes of the  $V_c$  exceedances:

- In 22 cases the speed at the start of the  $V_c$  exceedance was less than 78 KIAS, more than two knots under the recommended approach speed. This low speed alone will not cause the  $V_c$  exceedance, but an increase in (asymmetric) power, which is the normal reaction in low speed situations, will trigger it. This was an anticipated cause because of the manoeuvring required in the traffic pattern.
- In 27 cases the adverse  $\beta$  was more than  $2^\circ$  at the start of the  $V_c$  exceedance and in 13 cases even more than  $4^\circ$ . This adverse  $\beta$  increased the  $V_c$ . This adverse  $\beta$  was never caused by reaching the rudder limit, because the rudder deflection at the start of the  $V_c$  was in all cases less than the maximum value. This adverse  $\beta$  cause for  $V_c$  exceedance was not expected and indicated that applying correct rudder control in the traffic pattern was somehow difficult for some pilots.

If a  $V_c$  exceedance is noted we expect a proper reaction from the pilot, these reactions might either be a change in pitch angle to increase airspeed, a reduction in asymmetric power, an increase in rudder, or a combination of these reactions. These pilots' actions are shown in Table 7.4. The following reactions were noted:

Table 7.3: Exceedances of  $V_c$  in traffic pattern

Event	no
$V_c$ exceedances total	43
Cumulative Airspeed exceedances	
Airspeed < 78 knots	22
Airspeed < 76 knots	17
Airspeed < 74 knots	12
Airspeed < 72 knots	6
Cumulative $\beta$ exceedances	
Adverse $\beta > 1^\circ$	35
Adverse $\beta > 2^\circ$	27
Adverse $\beta > 3^\circ$	19
Adverse $\beta > 4^\circ$	13
Adverse $\beta > 5^\circ$	8
Average time $V < V_c$	14 sec.
Average $V_c - VTAS$	10.6 knots

Table 7.4: Pilot actions on  $V_c$  exceedance in traffic pattern

Pilot action	No
No corrective action	8
Only corrective rudder	7
Only corrective power	0
Only corrective $\theta$	17
Corrective rudder and power	0
Corrective rudder and $\theta$	2
Corrective power and $\theta$	8
Corrective rudder, power and $\theta$	1

- In 28 cases the nose was lowered. To remove noise a minimum change of  $1^\circ$  was used as threshold value. In 8 cases this pitch change was combined with a reduction in power, and in one case with reduction in power and increase in rudder deflection. Again, to remove noise, a threshold value of 2% was used for the power reduction.
- In 27 cases the rudder deflection was increased (by more than 5%), but only in 10 cases this increase was more than 20%, and these 10 cases are presented in Table 7.4. It is interesting to note that maximum rudder was only used once.
- In 8 cases no sufficient action, or the wrong action was taken. This indicates that the  $V_c$  exceedance was, most likely, not noticed at all. This is also in line with the pilots' comments at the end of the runs, where pilots sometimes commented that they had only glanced at the  $V_c$  display. Initially, most pilots were focused on the outside visual display and had to learn to look inside and to interpret the display.

The major risk during a traffic pattern with one engine out is that sufficient roll control can not be maintained and the aircraft rolls towards the ground. Evaluating the maximum bank angles, we noticed that in one case a bank angle increased to above  $45^\circ$  to  $54.3^\circ$ , which is excessive in a traffic pattern where the maximum bank angle is normally  $30^\circ$ . In two other cases the bank angle was above  $35^\circ$  but still below  $45^\circ$ , indicating a smaller bank excursion. In Fig. 7.4 a typical case is presented where the aircraft becomes low in speed and below the advised  $V_c$  after 65 seconds. The  $\beta$  is fluctuating quite a bit but the average value is maintained at zero. The  $\theta$  is initially fluctuating but decreased at 80 seconds, this initiates the speed increase and the recovery to a speed above  $V_c$ . As can be seen in Fig. 7.4b the pilot uses less than full rudder, which is  $35^\circ$ . If full rudder would have been used, the  $V_c$  would have been lowered and allowed for more power and consequently a faster recovery from the low airspeed situation.

The first conclusion is that this scenario was able to generate ample  $V_c$  exceedances. The second conclusion is that this scenario creates a high workload, and requires pilots to spend most of their time looking outside rather than looking at the instruments. Consequently, seven  $V_c$  exceedances were clearly missed. This might improve by adding an aural alert. Proper action was taken in 36 of a total of 43  $V_c$  exceedances, however, maximum rudder was never used, which will be discussed next.

#### INSUFFICIENT RUDDER APPLICATION

There are several explanations for the finding that pilots did not apply full rudder. First, sometimes the pilot commented that he was using maximum rudder while it was later discovered that he did not. This could have been caused by having positioned the seat too far aft; however, on another run the same pilot used more rudder, which questions if the incorrect position was the real cause. A more probable cause could be that the pilot's perception of maximum rudder is rather imprecise, or that the pilot is using rudder just to maintain zero  $\beta$  and is not considering the use of proverse yaw to further increase roll performance.

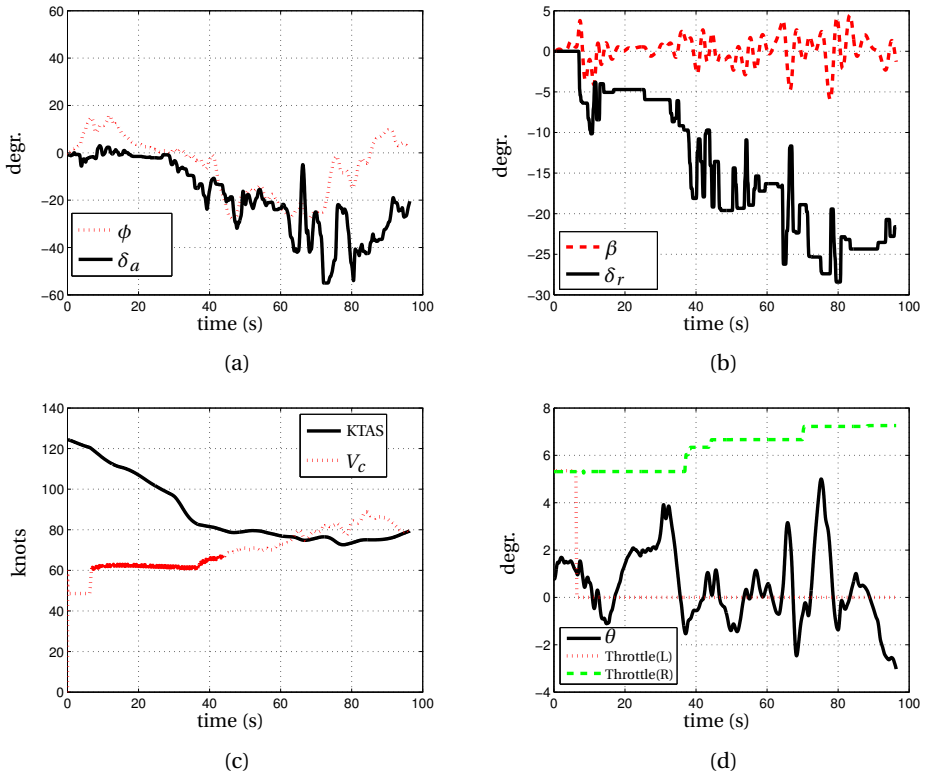


Figure 7.4: Left engine failure with typical  $V_c$  exceedance in traffic pattern scenario (run 9). In (a) roll inputs and response; in (b) Side slip inputs and response; in (c)  $V_c$  and IAS and in (d) throttle positions and  $\theta$ . Full throttle (100%) is at the value of  $10^\circ$ , minimum throttle is at  $0^\circ$ .

As explained in Chapter 3, this technique of maintaining zero  $\beta$  would have worked in a turbojet aircraft, because with zero  $\beta$  there is no significant roll moment left. However, with a twin propeller aircraft there is still a roll moment due to the propeller slipstream and this effect increases with decreasing airspeed. In this case, aileron input is required and roll control can be improved by generating proverse  $\beta$ . However, the test shows that pilots were not intentionally using proverse yaw to increase roll performance. The only pilot who did use proverse yaw did it unintentionally, he said that he did not look at the slip indicator, he was looking outside most of the time and was only checking his airspeed inside.

This last comment initially sounds strange, however, if we check the traces for this pilot (the first 40 seconds in Fig. 7.5), it shows that this pilot is using so much rudder that no aileron deflection is needed when the aircraft has zero bank. Hereby he already maximizes his lateral control and can use more engine power, which more than offsets the additional drag caused by the side slip. So, while the pilot was not checking the  $V_c$  indi-

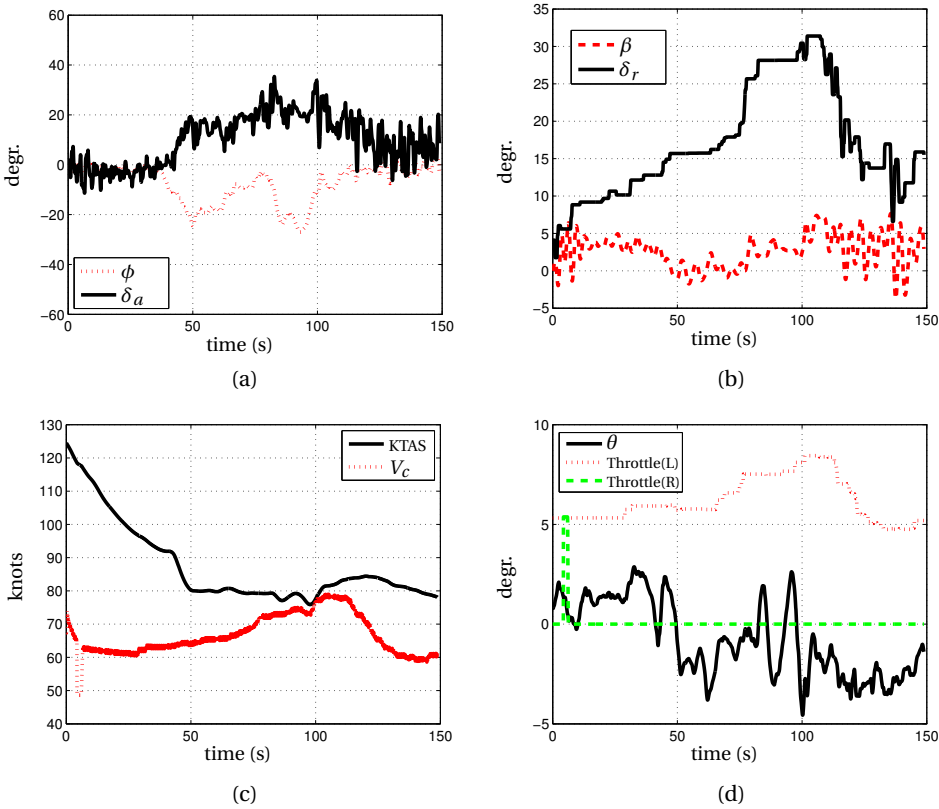


Figure 7.5: Right engine failure in traffic pattern. Typical example of rudder application based on minimizing aileron deflection (run 75). In (a) roll inputs and response; in (b) side slip inputs and response; in (c)  $V_C$  and IAS and in (d) throttle positions and  $\theta$ . Full throttle (100%) is at the value of  $10^\circ$ , minimum throttle is at  $0^\circ$ .

ation at all, the IAS was always above the  $V_C$  as can be seen in Fig. 7.5c. Fig. 7.5b shows that proverse yaw is used almost continuously, and Fig. 7.5d shows the use of power.

From these results, and also from the pilot comments, it became clear that pilots are primarily trained to use rudder to ‘centre the ball’ and not as additional means to improve roll control. Only two out of the ten pilots used a technique to minimize aileron deflection, and by doing so were automatically increasing roll performance. However, this was a personal technique and appeared not to be a common one. As far as energy management is concerned, this technique works well as long as power can be added due to the additional rudder. However, when full power is already applied and enough roll control is available, reducing rudder deflection to zero the  $\beta$  will give the lowest drag and this is the best technique for go-arounds. This technique is however not trained, and can not be trained, because without a  $V_C$  indication it is hard for the pilots to determine when enough roll control is available. Even with the present realisation of the  $V_C$  presentation

it was not clear to the pilots that they were not using enough rudder. Consequently, the display should be modified to provide this information.

## 7.5. EXPERIMENT 2; GO-AROUND

### 7.5.1. EXPERIMENT DESIGN AND PROCEDURES

The second scenario was a go-around from an approach. The approach was made with gear down and flaps 25 degrees at 80 KIAS. The run started at 300 feet AGL, with the aircraft lined up with the runway; the go-around instruction was given at 250 ft AGL. The run was terminated when the aircraft was either in a safe climb, or when an unrecoverable situation developed.

#### INDEPENDENT VARIABLES

In this scenario the position of the slip indicator was changed between runs from top to bottom and from  $\dot{y}$  to  $\beta$ , the  $V_c$  indication was off in the initial runs and later on.

#### PILOT INSTRUCTIONS

Initially, pilots were instructed to use the standard techniques and procedures they were accustomed to, in this scenario. However, it was discovered on the first run that the pilots would raise the gear in a go-around after a positive rate of climb was achieved. While this technique works fine and is safe in a normal take off, it does not work in a one-engine-out go-around because the amount of excess thrust with gear down is limited and often even negative. Therefore, pilots were instructed to raise the gear when initiating the go-around. Further instructions were to delay the raising of the flaps to 85 KIAS and to use 90 KIAS as single engine climb speed.

#### ORDER OF RUNS

For this exploratory test an incremental approach was used. Pilots started with the non-modified display and incrementally new features were added to analyse if these would increase performance. However, due to the already mentioned inaccuracies in the  $\dot{y}$  display, only the runs with the  $\beta$  display are used for analysis and discussed here.

1. The first two runs were familiarization runs, performing the one-engine-out go-around with the standard (non-modified) display;
2. On the next run the  $V_c$  indication was added;
3. Thereafter the side-slip indicator was moved to the centre;
4. Finally the side-slip indicator was changed to show  $\beta$ .

When pilots experienced unexpected difficulties in performing the task, the run was repeated, this happened regularly.

#### OPTIMUM PILOT CONTROL

If this scenario would have been executed at 90 KIAS, which is the standard speed for a one-engine-out approach, the procedure would have been simplified to selecting maxi-

Table 7.5: Exceedances of  $V_c$  in go-around scenario

Event	no
$V_c$ exceedances	20
Cumulative Airspeed exceedances	
Airspeed < 78 knots	5
Airspeed < 76 knots	2
Maximum rudder used	6
Maximum rudder at start $V_c$	3
Average time $V < V_c$	17 sec
Average maximum bank angle	13.8°

mum power, raising gear and flaps and starting to climb while maintaining the airspeed and zero side slip. However, when starting from 80 KIAS (the standard approach speed with all engines working) and failing one engine at this speed, power must be added carefully in order to maintain sufficient lateral control that will be indicated by the increase in the presented  $V_c$  value, and the aircraft pitch attitude should be controlled carefully to prevent the loss of airspeed.

#### DEPENDENT MEASURES

The dependent measures were the  $V_c$  exceedances and the reaction to these exceedances as in experiment one. Additionally, energy management in the go-around was measured. In a properly executed go-around the aircraft energy, which is decreasing slowly in the approach to land, should start to increase as soon as possible after initiation of the go-around. Instead of using total energy, defined as the sum of kinetic and potential energy, we use specific energy (Es), defined as the total energy divided by the mass and has  $(m/s)^2$  as unit.

#### EXPERIMENT HYPOTHESIS

The hypothesis was that pilot awareness of available roll control would be enhanced by the  $V_c$  display.

### 7.5.2. RESULTS EXPERIMENT 2, GO-AROUND

#### GENERAL

A total number of 52 go-arounds were made. Of these 52 runs, 33 were made with the  $V_c$  display activated, the others were familiarisation runs. Of the 33 runs, 23 were made with the correct  $\beta$  display and 10 were made with the side acceleration display. An overview of the results is presented in Table 7.5.

The go-around showed three kinds of problems that delayed the recovery to a safe climb:

1. Using insufficient rudder;
2. Too abrupt power application;

3. Energy management in the go-around.

These problems and the  $V_c$  exceedances will be discussed next.

$V_c$  EXCEEDANCES

In the evaluation of the  $V_c$  exceedances the same noise limits were used as in Experiment one: the exceedance had to be more than 2 knots and had to last at least 2 seconds. In 8 out of the 23 runs with the correct  $\beta$  display, no  $V_c$  exceedance occurred at all, indicating that the pilot was using cautious throttle and enough rudder. An example of such a run is given in Fig. 7.6.

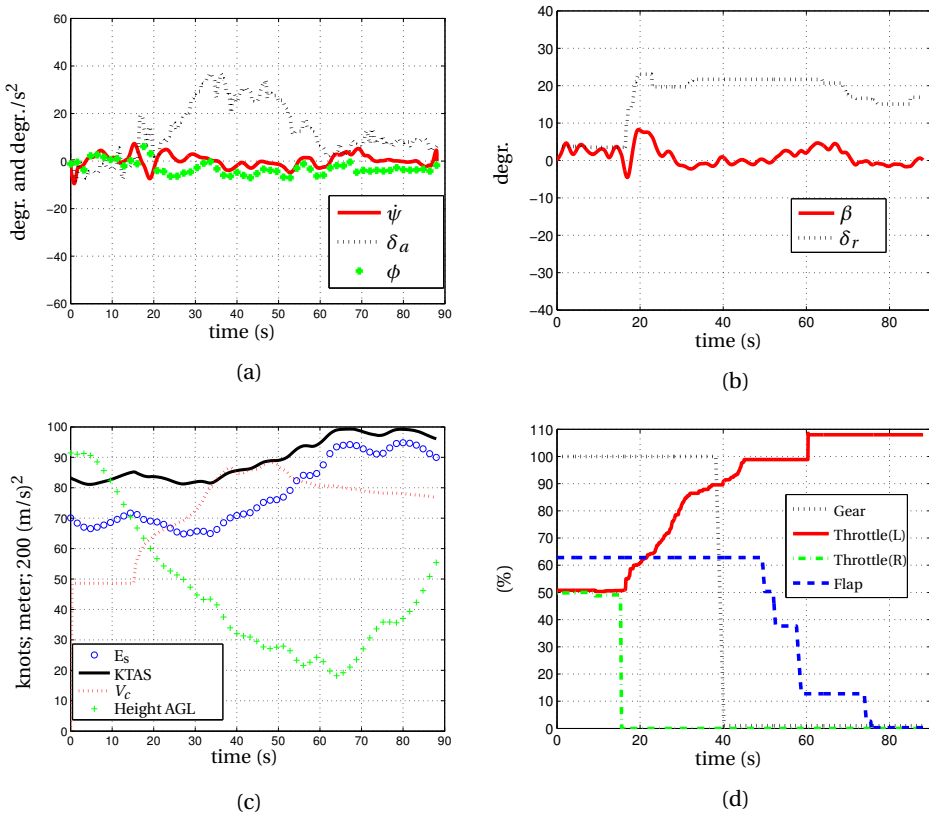


Figure 7.6: Typical well executed go-around with (a) Heading rate, roll angle and roll inputs, (b) side slip and rudder inputs, (c) Energy management with KTAS, height (m) and total specific energy ( $E_s$ ) in units of  $200(m/s)^2$  and (d) Throttles, flap and gear, shown as percentage of their maximum values.

Fig. 7.6d clearly shows that power is added gradually, preventing an overshoot of the  $V_c$  as can be seen in Fig. 7.6c. It is a fair assumption that the  $V_c$  display enabled this precise power application. In Fig. 7.6b we see that  $\beta$  is maintained close to zero while the bank angle excursions and the heading changes are small, as can be seen in Fig. 7.6a.

Table 7.6: Pilot actions on  $V_c$  exceedance in go-around

Pilot action	No
No corrective action	3
Only corrective rudder	0
Only corrective power	2
Only corrective $\theta$	6
Corrective rudder and power	0
Corrective rudder and $\theta$	8
Corrective power and $\theta$	0
Corrective rudder, power and $\theta$	1

While this run is safe, the recovery could have been expedited by raising the gear faster and increasing the power more rapidly.

In the remaining 14 runs with the  $\beta$  display a total of 20  $V_c$  exceedances occurred. When looking at the causes of these exceedances, see Table 7.5, we notice the following:

- There were 5 cases where the speed at the start of the exceedance was less than 78 knots. The low airspeed was either caused by increasing the pitch attitude too early or too much in the go-around, or by not correcting the pitch downward when the engine failure occurred.
- The second cause was not enough rudder, similar to scenario one. Only in three  $V_c$  exceedances full rudder was applied at the start of the exceedance and in only three more instances full rudder was achieved at some point during the time of  $V_c$  exceedance. In other words, in 14 instances rudder was not used at all as a means to improve the lateral control and to lower the  $V_c$ .
- The next cause was an excessive throttle setting for the airspeed. This is a little bit trivial, in all instances the  $V_c$  exceedance could have been prevented by advancing the throttle of the working engine less. However, we can also look into cases where the excessive throttle setting was the only reason. There were only two instances (runs 103 and 194) where a  $V_c$  exceedance occurred while maximum rudder was applied and the speed was above 80 knots. In both instances, full power was applied on the working engine and a small reduction would have prevented the  $V_c$  exceedance.

If we study the pilot responses to the  $V_c$  exceedance in the go-around, see Table 7.6, we notice that:

- Pitch reduction was the most frequent action, in 15 cases, in 6 cases this was the only action and in the other 9 it was combined with rudder (8 times) or power (once);
- In two cases only the throttle was reduced, while still additional rudder was available;

- In three cases no corrective action was taken.

This indicates that in 17 instances a correct action was taken, triggered by the  $V_c$  exceedance, but also that in three events no action was taken. Taking a closer look at these latter three events we notice that:

- In one case (run 31) the pilot applied so much power that he needed almost maximum aileron to maintain zero bank angle. There is definitely no roll performance left and this is a clear  $V_c$  exceedance. However, the  $V_c$  limit gives a roll control margin, and the pilot was consuming this margin to expedite recovery. When this is done cautiously and deliberately, this technique is even better than setting the power so that the  $V_c$  does not exceed the present airspeed, however, this technique requires more pilot skill.
- In one exceedance, the third occurrence in run 49, the exceedance was relatively small, only 3.5 knots, which could either be missed or accepted by the pilot because of the small value.
- In one case (run 195) the  $V_c$  exceedance was caused by raising the nose too high. This high nose attitude was maintained for quite a long time (15 seconds). After those 15 seconds the nose was lowered and the speed increased to above  $V_c$ . Because the average pitch angle during the  $V_c$  exceedance was no more than  $0.5^\circ$  less than the pitch angle at the start of the  $V_c$  exceedance, it does not count as a correct pitch reaction, but it does qualify as a delayed reaction to the  $V_c$  exceedance.

From these results we can conclude that pilots did use the  $V_c$  indication and responded to it in almost all instances. We have to realize that these go-around tests were done after the traffic pattern scenario and that all pilots had already performed go-arounds with the  $\dot{y}$  side slip indication, which were later removed from the evaluation. Consequently, they were getting used to this new indication. At the same time these results confirm the findings of the traffic pattern scenario that full rudder is seldom used.

#### RAPID INPUT

An interesting response occurred once during the trials. In the go-around the pilot applied a rapid throttle input with a delayed rudder input. This immediately led to a large roll excursion and the run was aborted after 25 seconds because an unrecoverable situation had already developed. This run is depicted in Fig. 7.7. As can be seen in Fig. 7.7d, full power is applied at 18 seconds, but rudder (Fig. 7.7b) is hardly increased at that time. Consequently, as can be seen in Fig. 7.7a, the bank angle rapidly increases to more than  $50^\circ$  and  $\dot{\psi}$  to  $40^\circ/s$  while full aileron deflection is applied to counter the roll. The pilot tried to counter the roll by decreasing the power just before the run was stopped. At that moment the gear and flaps were still in their extended positions. The time from full power application (18 seconds) till the abort by the experiment supervisor was only 5 seconds.

While this special event happened only once during the trials, it could happen in real life situations as well. Because the surprise factor in real life emergencies is much

higher, an uncoordinated rapid action could even be more likely. This is, however, hard to prove, because these small twin propeller aircraft don't have flight data recorders that would enable a more thorough accident investigation, which could reveal if there was any delay in the application of full rudder.

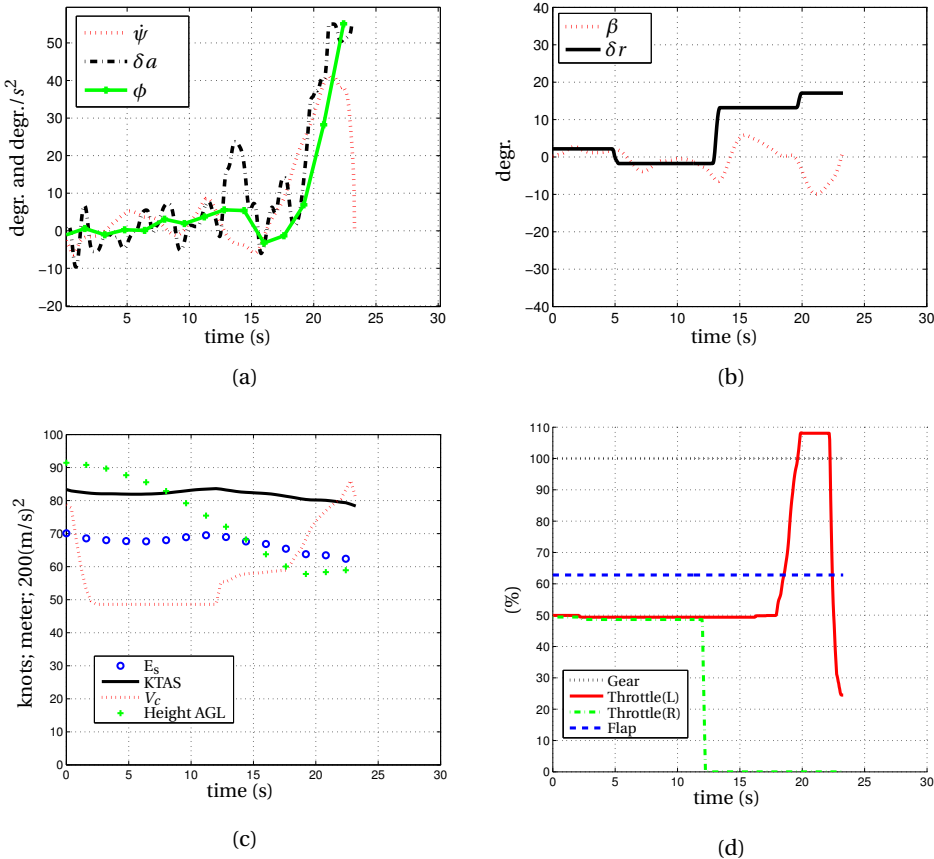


Figure 7.7: Effect of a rapid throttle input with delayed rudder response; (a) Heading rate, roll angle and roll inputs, (b) Side slip and rudder inputs, (c) Energy management with KTAS, height (m) and total specific energy ( $E_s$ ) in units of  $200(m/s)^2$  and (d) Throttles, flap and gear at % of their maximum values

### ENERGY MANAGEMENT IN GO-AROUND

Surprisingly, the major problem during the go-around was not the control of power to prevent  $V_c$  excursions or the control of side-slip. Rather, pilots overestimated the aircraft single engine climb performance. They increased the pitch angle too much when the gear was raised, which led to a fast speed bleed off and often to a reduction well below the initial 80 knots of the approach and also below the present  $V_c$  value. In order to reduce the  $V_c$  below the present speed, a power reduction and a decrease in  $\theta$  was required that delayed the go-around. This problem is not solved by the present display changes

and requires a different approach that will be discussed next.

Another way to study pilot performance in go-around is evaluating the total energy management of the aircraft. When total energy is constantly increasing, the go-around is well executed. Initially, the aircraft is approaching to land and total energy decreases. When the go-around is properly initiated, one should see a constant increase in total energy after the gear is raised and power is added. We measured the development of the specific total energy (the total energy divided by mass) in each of the 52 go-around runs. The starting point was the first increase in total energy, which eliminated the initial descent, and we then measured for how many seconds a decrease in energy was seen. To eliminate short negative periods a limit of 0.4 second was used as threshold value. A histogram of the results is given in Fig. 7.8a.

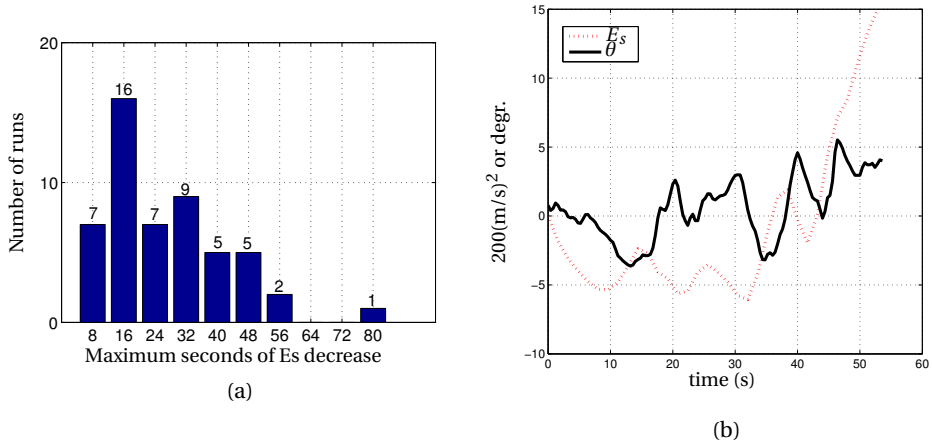


Figure 7.8: (a)Histogram of 52 go-around runs; Total time of energy decrease after initiating go-around and (b) Example of total energy and  $\theta$  control in run 194; The specific total energy is off-set in y-axis for clarity:  $E_s$  at the start of the run is set to 0.

The histogram clearly illustrates that periods with energy decrease were a common problem that affected almost all participating pilots. This decrease in energy was caused by increasing  $\theta$  too much, as can be seen in Fig. 7.8b. For clarity of the picture the specific total energy is off-set down. Every time the pilot increases  $\theta$  the total specific energy starts to drop. This is a logical result: the decrease in airspeed, caused by increasing  $\theta$  too much, will lead to an increase in drag because the aircraft is operating ‘at the back side of the power curve’. Two contributing factors should be noted. Initially, pilots applied the rule that a positive rate of climb is required to raise the gear. If the approach would have been made at a higher speed this is definitely a possibility but, being low in energy and having a low power surplus, it is better to first raise the gear and accelerate before starting the climb. The second contributing factor was, again, that pilots were not inclined to use proverse yaw to enhance the roll control, which would have enabled the use of more power.

## 7.6. EXPERIMENT 3; RUDDER HARDOVER

### 7.6.1. EXPERIMENT DESIGN AND PROCEDURE

The last scenario was a stuck rudder at 15° deflection. As explained in Chapter 6, to get a good parameter identification after a failure, and a subsequent reset of the PID method, pilots inputs are essential. In this scenario the pilots were instructed to perform inputs after the failure and to use the  $V_c$  display to their advantage to derive a safe configuration for approach. This scenario was only flown once per pilot because the surprise effect of an unknown emergency is hard to repeat.

#### INDEPENDENT VARIABLES

There were no independent variables in this scenario.

#### PILOT INSTRUCTIONS

Handling of emergencies is standard for a pilot, and therefore only those instructions were given that were required to make optimum use of the parameter identification method. After the detection of the failure by the fault detection algorithm as explained in Appendix C, a visual warning labelled 'MAN' was displayed in the annunciator window of the PFD, to alert the pilot that manoeuvring was required to enhance the parameter estimation as can be seen in Fig. 7.2. Pilots were briefed that the required manoeuvring could be done by sequential control inputs in each control axis and on each engine. Thereafter, pilots were asked to set the aircraft up for landing, given the  $V_c$  restrictions shown. After this set-up was achieved at a convenient safe altitude, the aircraft was slewed to the downwind position, and pilots were given the opportunity to see that with their chosen aircraft speed and configuration a safe approach could be made.

#### DEPENDENT MEASURES

Because of the exploratory nature of the test the emphasis was on collecting subjective comments from the pilots. Specifically, pilots were asked to give their analysis of the failure, and to determine a safe approach configuration.

#### EXPERIMENT HYPOTHESIS

The hypothesis was that the  $V_c$  indication would be used by the pilots to find a safe approach speed.

#### SCENARIO

The rudder hard-over (RHO) was initiated in a climb at 90 KIAS around 2,000 feet AGL, which gave ample room for recovery. When the RHO occurred, pilots were instructed to level off their aircraft and fly at the standard cruise speed of 120 KIAS to analyse the situation. After the level off, pilots were instructed to execute identification manoeuvres and decide on the best approach configuration and speed. When the aircraft was configured for the approach at the determined approach speed, which was all done at a safe altitude and away from the airport, the simulator was set in hold. To expedite the rest of the scenario, the aircraft position was changed to downwind of runway 18R at Schiphol. From that position the standard traffic pattern was continued to just short of landing, to confirm that a safe approach was feasible with the chosen approach speed based on the  $V_c$  indication.

### 7.6.2. RESULTS RUDDER HARDOVER

Because of the sudden change in  $\beta$ , all pilots were immediately aware of having a control problem, but the exact nature of the problem was, except to one pilot, not directly clear. It was interesting to note that the identification manoeuvres not only improved the parameter estimation but that these also helped pilots in their analysis and to find a solution. Because the pilots had to move the throttles individually, they discovered that the  $\beta$  could be controlled by differential thrust. All pilots realized that landing with differential thrust would be problematic, because the side-slip must be controlled by differential braking when thrust is reduced after landing. This part was intentionally not simulated, as that would have required a more advanced model of the undercarriage. All pilots did find a safe approach speed with the help of the  $V_c$  indication and were able to make a safe approach with the damaged aircraft. Pilots differed in their ability to use the differential thrust to their advantage. Controlling  $\beta$  with differential thrust involved a high mental workload: pilots continuously had to evaluate which throttle had to be advanced or reduced when power changes were required.<sup>7</sup>

### 7.7. DISPLAY COMMENTS AND RUDDER CONTROL

The three chosen scenarios proved to be not the best suited to evaluate the new side slip display in a quantitative fashion. Especially in the go-around, pilots focused most of their attention on the out of the window view. Furthermore, in these scenarios zero  $\beta$  is not always optimum when lateral control is limited. The comments 'I did not look at the  $\beta$  display' or 'I glanced at it once in a while' were noted many times and were made by practically all participants.

Looking at the traces, however, it can be seen that all pilots adjusted rudder constantly, and almost exactly in phase with power changes. To evaluate this numerically for each run, the number of rudder inputs and throttle inputs were determined. If we compare the number of rudder inputs to the throttle inputs, the ratio, for all runs, is 1.01; however, there is large variation between pilots and between runs. The large number of rudder applications, averaging 47 rudder inputs per run, combined with pilot comments, seem to indicate that pilots see the effect of the power application in the movement of the nose and correct that with rudder, instead of using constant reference to the slip indicator. While this practice was evidently working for the pilots in these experiments, it will be much harder to employ this technique in bad weather conditions with limited visibility.

#### PILOT COMMENTS ON SLIP INDICATOR

Out of the ten pilots, eight preferred the new central display, one pilot was indifferent and one preferred the old display at the top. Six pilots commented on the damping of the  $\beta$  display that was considered to be too low. The display was indeed not damped at all which, combined with the adverse yaw tendency of the aircraft, resulted in a rather 'nervous'  $\beta$  display. In future tests some filtering of the displayed slip angle should therefore be applied. All pilots had runs during which they did not look at the slip indicator

<sup>7</sup>The approach is easiest when a long stable straight-in approach is made.

but rather performed the manoeuvre mostly on outside references. Finally, two pilots mentioned they preferred the yellow colour, used for the  $\beta$  display over the white colour used for lateral acceleration.

#### PILOT COMMENTS ON $V_c$ INDICATOR

After each run, pilots could freely comment on the displays. The most often heard comment was that it took time to learn how to control the  $V_c$ . A specific concern mentioned twice was that the  $V_c$  margin available could tempt the pilot to fly slower than 80 knots, what would lead to flight below  $V_c$  when increasing engine power. One pilot never used the display and did not see a need for it. On the other hand, when pilots had performed several runs, they became more familiar, and most of them were positive about the increase in situation awareness regarding the available aircraft roll performance.

## 7.8. DISCUSSION

### $V_c$ DISPLAY

When  $V_c$  exceedances were encountered, correct actions were taken in 36 of the 43 exceedances in the traffic pattern experiment, and in 16 out of the 19 exceedances in the go-around experiment. Based on these facts, the hypothesis that pilot awareness of available roll control would be enhanced by the  $V_c$  display, cannot be rejected. However, the present  $V_c$  display does not help pilots to make optimum use of available rudder.

This is also a direct consequence of presenting a minimum speed for lateral control. If the  $V_c$  would not have been shown, pilots would have increased power and increased rudder more, either accepting or being unaware of the fact that the aircraft had hardly any roll control left. In lateral control-limited situations, zero  $\beta$  is not always ideal. The zero  $\beta$  situation is of course minimizing the drag and when full power can be given the combination of full power and zero  $\beta$  will give the best climb performance. But in case roll control is limited and more power is needed, it is advantageous to use proverse yaw to increase roll performance and be able to use more power. The challenge is to make this choice visible to the pilot. A possible solution would be to present the  $V_c$  for maximum rudder to the pilot as well. This way the pilot can see that more roll control is indeed available if he adds rudder. However, further tests must be conducted to prove that this concept will work.

### GO-AROUND

Two specific problems were encountered related to the go-around. First, the sub-optimal energy management made the go-around profile much more challenging for most pilots than intended. It necessitated the constant adjustment of power to maintain or regain lateral control. This is typically a situation where normal pilot tendencies (i.e., to get away from the ground as soon as possible) are counterproductive. It could be advantageous to inform the pilot of the maximum sustained climb angle possible to prevent energy loss.

The second problem was the abrupt power application with delayed rudder. This situation occurred only once, but immediately led to a dangerously large bank angle, very close to the ground. There is no simple cure for this problem. As is explained in Chapter 3, the  $V_c$  presented is based on current power and current  $\beta$ , unless the current  $\beta$  cannot be maintained with maximum rudder. In the latter case, the  $V_c$  is based on maximum rudder and  $\beta$  is adapted to the  $\beta$  possible with full rudder at the predicted  $V_c$ . So, while our method predicts a velocity, it does not anticipate any power application but will react to it. However, the rapid  $V_c$  increase will coincide with the rapid bank angle change, which can be seen in Figs. 7.7c and 7.7a. An automatic rudder control that minimizes  $\beta$  could be a way to prevent these types of accidents. However, because we focus on manual control and not on automated control this solution is out of scope in this thesis.

#### SIDE-SLIP DISPLAY

It is clear that the hypothesis, that pilot control of side slip would improve with the new side-slip display, could neither be confirmed nor rejected. First, pilots were more focused on the outside world than on the slip indicator. Second, in the chosen scenarios zero  $\beta$  or zero side acceleration is not always the best option. In a follow-on experiment a scenario should be chosen that indeed requires zero  $\beta$  and would force pilots to focus more on the slip indicator.

### 7.9. RECOMMENDATIONS

In follow-up experiments, two  $V_c$  values should be displayed. The first is the current  $V_c$ ; the second one would present the  $V_c$  if the pilot were to use full rudder. The split of the two  $V_c$  values would give pilots an indication of the extra lateral manoeuvrability that can be gained by applying additional rudder. Furthermore, pilots should be more explicitly instructed that the strategy of achieving exactly zero  $\beta$  or zero side acceleration can be mitigated to gain roll control.

To aid in the go-around and the recovery from an airspeed below  $V_c$ , pilots should be prevented from climbing too steeply, causing a total energy decrease, which occurred in almost every go-around in this experiment. A possible option would be to present the maximum sustainable  $\theta$ , based on the current power setting to the pilot.

The scenarios where optimum slip is not always zero, and where pilots are looking more to the outside, are not suited to quantitatively evaluate if the central display improves pilot performance. A better scenario might be a single engine climb-out in instrument meteorological conditions (IMC), where power adjustments (e.g., level off) and heading changes are required. In such a scenario it is more likely to find performance differences. Finally, applying some damping to the side slip indicator must be investigated.

## REFERENCES

- [1] Anon., *Data and Statistics*, Tech. Rep. (NTSB, 2015)  
[www.nts.gov/data/index.html](http://www.nts.gov/data/index.html).
- [2] R. J. de Muynck and M. Van Hesse, *The A-Priori Simulator Software Package of the Piper PA34 Seneca III*, Tech. Rep. (TU Delft, 1990).
- [3] M. Laban, *On-line Aircraft Model Identification*, Ph.D. thesis, Technical University Delft (1994).
- [4] H. J. Koolstra, H. J. Damveld, and J. A. Mulder, *An Improved, Turbulence Proof, Reset Mechanism for Parameter Identification after System Change*, in *Proc. of the 2013 AIAA Guidance Navigation and Control Conference, Boston, USA, Aug. 19-22* (2013).
- [5] H. J. Koolstra, H. J. Damveld, and J. A. Mulder, *Application of SPRT Based Reset Methods for Damaged Aircraft Parameter Estimation*, in *Proc. of the AIAA Guidance, Navigation, and Control Conference, SciTech Forum 2015, Kissimmee, USA* (2015).
- [6] J. A. Mulder, J. C. van der Vaart, and M. Mulder, *Atmospheric Flight Dynamics* (Technical University Delft, Faculty LR, 2007).



# 8

## FINAL TESTS

*Press to Test at Max  $P_s$*

Motto USAF TPS Class 84-B

## 8.1. INTRODUCTION

In the previous chapters we have developed the models and methods to enable the estimation of the minimum lateral control speed ( $V_c$ ) and evaluated the accuracy of the  $V_c$  estimation in off-line scenarios. In Chapter 7 we did our initial tests with pilots in the loop, using TU Delft's SIMONA Research Simulator. The intent of these tests was to check whether pilots could use the new displayed information to their advantage, in situations where the lateral control was impaired. These tests revealed several shortcomings that have led to a number of modifications. First a 'climb bar' was added on the Primary Flight Display (PFD) to help the pilots in setting an attitude  $\theta$  that gives the climb angle ( $\gamma$ ) required to maintain airspeed. Second, instead of one  $V_c$  speed, two  $V_c$  speeds are now made available to the pilot,  $V_{c1}$  is the standard also displayed in the previous tests and  $V_{c2}$  shows the lateral control speed with full rudder. This additional  $V_{c2}$  shows the pilot whether additional rudder can enhance the lateral control and should prevent pilots from not making enough use of the rudder in cases where that would be advantageous, something that occurred regularly during the initial tests. Furthermore, a filter was applied to the displayed side slip signal to ensure a more usable display. Finally, an error in the aerodynamic model causing a wrong side force was corrected. All these new features will be discussed in more detail, later in this chapter.

### 8.1.1. OBJECTIVES

The experiment had three objectives: Firstly, to test if the experimental side slip display would improve pilot performance. Secondly, to investigate if the modified  $V_c$  display together with the new 'climb bar', which will be explained later, would enhance the handling of engine failures. Thirdly, to investigate whether pilots could use the  $V_c$  display to their advantage when they encountered a non-engine related lateral control problem.

### 8.1.2. OVERVIEW

In August 2015 the final tests were done with 19 participating pilots with a civil and/or military aviation background, covering a broad experience level from just graduated pilots to pilots with more than 10,000 flying hours. All pilots were acquainted with twin engine propeller aircraft. The following five experiments were used.

The first experiment was developed to have a dedicated evaluation of the new slip indicator as discussed in Chapter 7. In this experiment the pilot had to perform a climb from 200 to 1,000 feet with one-engine-inoperative (OEI) at the standard single engine climb speed of 90 KIAS. This experiment was repeated four times, each time with a different side slip indication and the performance was measured on how slip and heading were maintained.

The second experiment was the standard OEI go-around that was also used in Chapter 7. This experiment was also repeated four times, twice at low altitude, with visual reference to the runway, and twice at medium altitude, without visual reference to a runway. Furthermore, two runs were made with the new  $V_c$  display and two runs were done with the traditional display while the conventional side slip indicator was used. Safety and efficiency measures, which will be discussed in more detail later this chapter, were

used to evaluate the go-around.

The third experiment was an unexpected engine failure after take off (EFATO). This experiment was performed with and without the new  $V_c$  display and again safety and efficiency were measured.

The fourth experiment was initially intended as a demonstration of the use of the  $V_c$  indication in a situation with limited lateral control, in a similar manner as in Chapter 7. However, after the initial two evaluations it was noticed that most pilots were not acquainted with 'controllability checks'. It was therefore judged advantageous to let the remaining 17 participants first handle the limited lateral control situation without any additional guidance or information. Thereafter, the experiment was repeated with the additional  $V_c$  information and with guidance on how to perform a proper controllability check.

The fifth experiment was added halfway the test and 9 pilots participated. Initial evaluations of Experiment 2 revealed that the OEI go-around was too difficult a manoeuvre for most pilots. Therefore an additional experiment with the OEI go-around was added at the end of the regular test to investigate if the pilot performance in this experiment could be improved by additional training.

## 8.2. EXPERIMENTS

We will now discuss the five different experiments introduced above. All experiments used the same hardware, models, interface and group of participants. Therefore these items are discussed first in this section, and then each experiment will be treated separately.

### 8.2.1. SIMULATOR AND MODELS

#### APPARATUS: SIMONA RESEARCH SIMULATOR

The experiments were performed in the six-degree-of-freedom simulation, SIMONA Research Simulator (SRS). A description was already presented in Section 7.3.1 and no changes to the simulator hardware were made in this experiment.

#### VEHICLE MODEL

The non-linear Piper Seneca III (PA-34) aerodynamic model used in the real-time simulation was identical to the model used for all off-line simulations and is described in Chapter 5 and in Reference [1]. The side force error in the aerodynamic model, which affected the initial test, was corrected and validated.

#### $V_c$ CALCULATION

The major difference between the  $V_c$  calculation from the previous experiment described in Chapter 7 and this experiment is that two  $V_c$  values were calculated, which we shall label  $V_{c1}$  and  $V_{c2}$ .  $V_{c1}$  is the velocity that will give the required roll performance with maximum aileron while rudder is given to maintain the present  $\beta$ .  $V_{c2}$  is the velocity that will give the required roll performance with maximum aileron and maximum rudder.

$V_{c2}$  is smaller than  $V_{c1}$  as long as maximum rudder is not yet used. The spread between  $V_{c1}$  and  $V_{c2}$  is a good indication that maximum rudder was not used, which was a noted problem in the first experiment. The minimum lateral control speeds  $V_c$  were calculated in real time, based on pilot inputs, the aircraft state and the linear aircraft stability and performance parameters that were constantly updated by the parameter identification routine. The algorithms for the calculation of  $V_{c1}$  and  $V_{c2}$  are derived in Chapter 5.

#### SLIP INDICATION DAMPING

The only change in the slip calculation as compared to the initial experiment was that a lag filter was added to both the  $\beta$  and the  $\dot{y}$  indication, using a forgetting algorithm with  $\lambda = 0.95$  while the simulation used an update rate of 100 Hz.

#### CLIMB BAR

In the initial tests many pilots found it hard to set a correct pitch attitude when faced with an engine failure. Several times the attitude was set too steep causing a deceleration that reduced the lateral control. Our hypothesis was that when the pilot is presented with a climb bar that shows the  $\theta$  that would give a constant speed ( $\dot{V}_{tas} = 0$ ), he can set  $\theta$  below this bar to accelerate and on the bar to maintain speed. This climb angle was found by calculating the change in specific energy ( $E_s$ ) and transforming this to a climb angle using the present  $V_{tas}$ .

$$\gamma_{(\Delta V_{tas}=0)} = \arcsin\left(\frac{\sqrt{E_s}}{V_{tas}}\right) \quad (8.1)$$

Adding the present angle of attack gives the required pitch angle that was then displayed to the pilot.

### 8.2.2. PILOT INTERFACE

#### $V_c$ DISPLAY

The presentation of the  $V_c$  on the Primary Flight Display was changed; instead of presenting the  $V_c$  as an extension on the ‘Stall speed barber pole’, a separate box was presented to the right-hand side of the speed scale as shown in Fig. 8.1. The top of the box represents  $V_{c1}$  and the bottom of the box represents  $V_{c2}$ . When maximum rudder is used by the pilot, the scale reduces to a single line because then  $V_{c1} = V_{c2}$ . This is also an extra indication for the pilot that maximum rudder is used. It was also important for the pilots to understand that the application of rudder does not change the  $V_{c2}$  but ‘pushes’ the  $V_{c1}$  down to the  $V_{c2}$  and also that  $V_{c2}$  can only be changed by adjusting the thrust asymmetry. This fact was explained and demonstrated in the familiarization run.

#### CLIMB BAR

As shown in Fig. 8.1 the climb bar was presented as a short red bar. If the climb bar is aligned with the aircraft symbol, the present speed ( $V_{tas}$ ) is maintained.

#### DIFFERENCES WITH THE STANDARD PA-34

One configuration difference was added to the ones already described in Chapter 7. The heading display on the PFD, which is standard displayed below the attitude indicator was

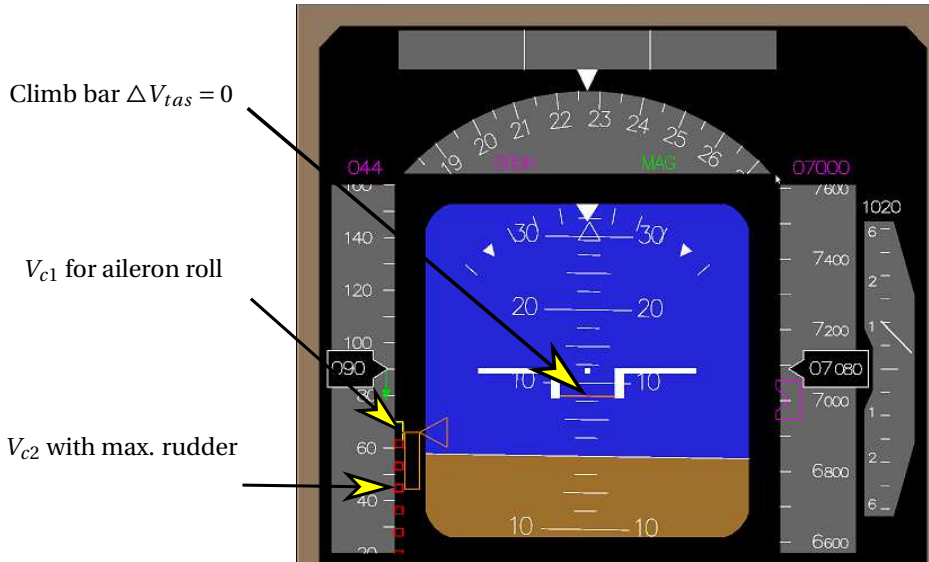


Figure 8.1: The PFD used in the experiments, augmented with the new  $V_c$  indications for aileron roll ( $V_{c1}$ ) and roll with maximum rudder ( $V_{c2}$ ). The climb bar in the centre is added to show the climb angle required to maintain the present speed.

moved on top because the cockpit lay-out made it impossible to see the heading scale when substantial aileron deflection was needed, as was the case in experiment one, the OEI climb.

### 8.2.3. SUBJECTS

Nineteen pilots participated in the experiments. Eighteen pilots had current flight experience on twin- or multi-engine aircraft and one was a retired airline pilot. The flight hours and other special qualifications are given in Table 8.1. All pilots were familiar with OEI approaches and go-arounds. Seven pilots had also participated in the initial tests. These pilots were divided over the different groups to minimize the effect of this previous experience.

#### INSTRUCTION TO SUBJECTS

For ease of reading, the instructions to the subjects are described separately for each experiment.

#### FAMILIARIZATION AND TRAINING

At the start of the experiment all subjects received a briefing on the new side slip display, the working of the  $V_c$  indication and the new climb bar. The five different experiments were explained and the required performance for each task was given. The required performance will be discussed in more detail in the discussion of the separate experiments. The briefing was followed by a familiarization run, where pilots were given some time to get adjusted to the feel of the aircraft by performing flight manoeuvres at altitude.

Table 8.1: Subject pilot background and experience.

Number	Flight. Hrs.	Special Qualifications
8	200-280	Just Graduated Civilian Pilots
1	1,550	Qualified Cessna Citation; Flight Instructor
1	3,600	Qualified Cessna Citation; Ex Military Pilot
1	3,100	Qualified twin prop and Cessna Citation
1	6,500	Qualified twin prop; Flight Instructor
1	14,000	Retired 747 pilot
2	5,000	Qualified twin prop
1	3,000	Military Pilot; Qualified C-130H; Experimental Test Pilot
1	1,300	Military Pilot; Qualified KDC-10;
1	1,300	Qualified B737
1	11,000	Qualified Airbus Pilot

Thereafter, they were instructed to select asymmetric power to generate side slip and subsequently the different slip indications were presented. The next step was to show the  $V_c$  indications and to let the pilots experience how the  $V_c$  indications changed with various power and rudder applications. They were then instructed to fly exactly the presented  $V_{cl}$  and to perform a maximum aileron roll to show that the presented  $V_c$  indeed gave the selected roll performance. Finally, the climb bar was demonstrated and it was shown that its position changed with the power setting and that setting the pitch attitude at the bar gave a constant speed.

#### WORKLOAD SCALE USED

For the first three experiments the subjective workload was measured with the Bedford Workload scale [2] as presented in Fig. 8.2. This scale has some resemblance in set-up with the Cooper Harper rating [3], however, the Bedford scale does not focus on the controllability of the aircraft as the Cooper-Harper scale does, but just on the workload to perform the task. In order to scale the workload, not the pilot effort but the spare capacity of the pilot is measured. It is the author's experience that this is easier for pilots than to estimate the workload itself. Because the controllability of the aircraft was not at stake, but we aimed to assess whether the new display indications alleviated workload, the Bedford scale was judged to be more appropriate than the Cooper Harper scale [3].

### 8.2.4. DATA PRESENTATION AND ANALYSIS

#### SCORING

When we use dependent measures to test hypotheses, we have the choice of testing each measure separately or to combine different measures in a single score. The latter approach has the advantage of simplicity. There are at least two ways to combine dependent measures: the first is the well known way of adding up the different measures, with the possibility of using weighting factors for each measure, and the second is to multiply the different measures used. The advantage of the multiplication method over the addition has been argued quite effectively by 'de Seversky' as early as 1942 [4]. One of the

## Bedford scale

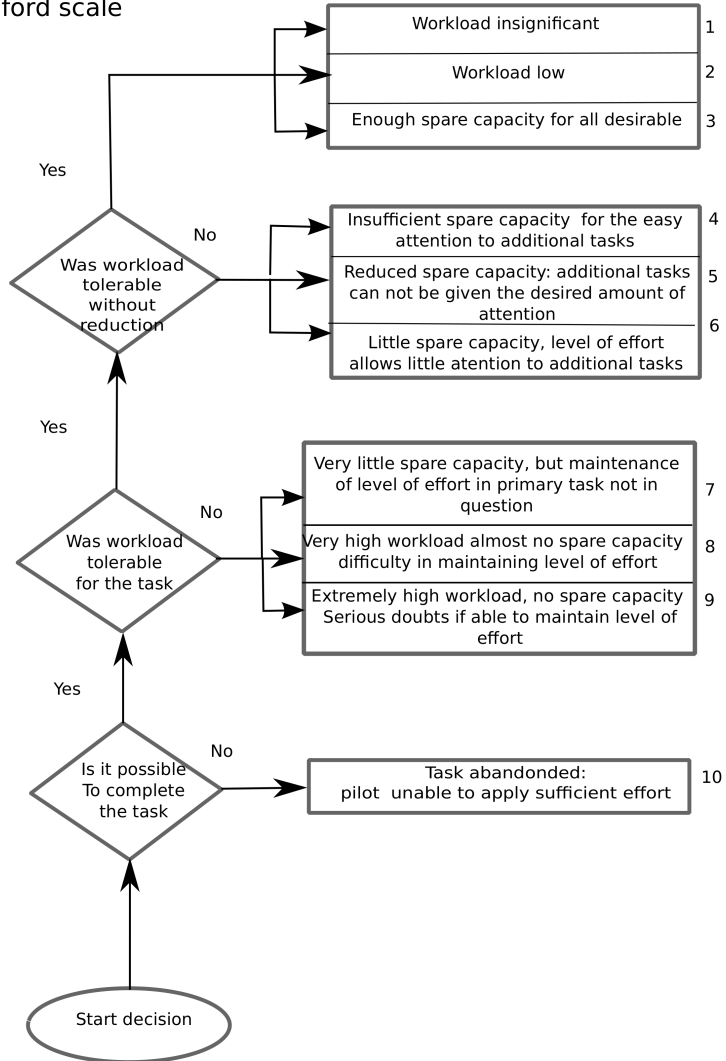


Figure 8.2: The Bedford workload scale from [2].

pleasant characteristics of the multiplication method is that the need for weighting factors vanishes and another favourable characteristic is that scaling does not matter. This is a direct consequence of the fact that both scaling and weighting factors can be combined into a single factor that affects all data in the same way, and consequently, can be omitted. The only restriction that we have to set is, not to use this method when one of the measures can be zero for a prolonged period.

#### BOX PLOTS AND SIGNIFICANCE LIMITS

The probability density distribution of the collected data is not known, furthermore, the number of participants is limited. Therefore the data are presented using box plots, which do not assume any known probability density distribution. However, to establish the significance limits for the change of the median, a Gaussian distribution of the median is assumed, as discussed in [5]. In their paper the authors state that the standard deviation of the median is given by  $s = 1.25R/1.35\sqrt{N}$  where  $R$  is the interquartile range and  $N$  is the number of samples. To establish the 95% confidence interval of the median, a factor  $C$  has to be found such that the 95% confidence limits of the median are:  $M \pm Cs$ . This factor  $C$  can vary from 1.96, when the standard deviation of two groups differs greatly to as low as 1.386 when the standard deviation of the two groups is similar. The common practice is to set  $C = 1.7$ , this is also used by Matlab <sup>1</sup>, which was used to generate our plots. However, this limit may be too restrictive in case of similar standard deviations of the different groups and too lenient when the standard deviations differ greatly. Using these box plots, a significant change ( $p \leq 0.05$ ) of the median is present when the notches don't overlap.

#### OTHER TOOLS

Because of the limitations of the box plots some other tools were used for data analysis. If only two groups had to be compared the single interval method [6] was also used to test for significance. In some experiments the change of the median or mean was not significant but the change in variation was. To establish the confidence limits for the variance the F-test [6] was used.

## 8.3. EXPERIMENT 1; ONE ENGINE OUT CLIMB

### 8.3.1. DESIGN AND PROCEDURES

The first experiment was intended to evaluate the different side slip displays. The scenario chosen was a standard OEI climb. The pilot started from take-off position and had to level off the aircraft with all engines working at 200 feet with an airspeed of 90 KIAS. This initial part was used to give the pilot some extra time to get acquainted with the aircraft before the measured part of the experiment started. The measured part started at the moment the pilot reduced one throttle to idle and advanced the other one to full power. The pilot had to climb to 1,000 feet maintaining speed and heading. At 1,000 feet the pilot had to level off the aircraft while maintaining heading and airspeed in the

<sup>1</sup>The Matlab document on box plots does not reveal exactly what constant is used but through inspection it proves to be 1.7, which equates to  $1.57R\sqrt{N}$ .

one-engine out configuration. When the aircraft was level at 1,000 feet, on heading and on speed, the run was terminated.

### OBJECTIVE

The objective of this experiment was to investigate whether the different side slip displays affected the workload or the precision with which the pilot could handle a situation where maintaining zero side slip required constant rudder inputs.

### INDEPENDENT VARIABLE

The independent variable was the change of type of display as explained in Chapter 7, the four possibilities being:

1.  $\dot{y}$  displayed at the top; white displaced square (Baseline);
2.  $\beta$  displayed at the top; yellow displaced square;
3.  $\dot{y}$  displayed at the centre; white variable size triangle;
4.  $\beta$  displayed at the centre; yellow variable size triangle.

The new displays are described in detail in Chapter 7, a short summary is repeated here. The first display type is the baseline, this type of display is common in aircraft with a modern PFD. The second display is optional in some aircraft<sup>2</sup> and both the third and fourth display are completely new.

### ORDER OF RUNS

Each pilot performed the experiment four times with all the possible side slip displays. To mitigate the learning effect, the order of the displays was semi-random using a 'Latin Square'. This guaranteed that each of the four display options appeared the same number of times as first, second, third or fourth. The basic Latin square requires four groups. With 19 subjects we could use 16 in the Latin Squares, and used the first 16<sup>3</sup>.

### PILOT PREFERENCES AND REQUIRED PILOT CONTROL

The OEI climb is a standard procedure familiar to all pilots. In an optimal OEI climb, drag should be minimized, which requires the pilot to maintain zero  $\beta$ . However, most aircraft are not equipped with a  $\beta$  indicator. The solution most commonly used, and also presented in PA-34 Flight Instructions, is to fly with the ball one half ball width off centre<sup>4</sup>. This setting is of course not valid for every combination of speed and power setting and therefore less precise. In our experiment, the actual  $\beta$  was displayed in half of the runs, this enables a more precise  $\beta$  control. However, when zero  $\beta$  is maintained, the

<sup>2</sup>According to a participating Airbus pilot, side slip angle ( $\beta$ ) can be displayed in Airbus aircraft. However, because Airbus aircraft are not equipped with *beta* vanes, it is not clear how this  $\beta$  is derived.

<sup>3</sup>If the additional requirement was set that also each order had to be used, we would have needed 4! or (24) subjects.

<sup>4</sup>Which means, displaced to the side of the working engine.

pilot has to fly with a roll angle that is also speed-dependent. This roll angle is required to compensate the side force of the rudder. It was therefore anticipated that flying with zero  $\beta$  would require more effort than flying with zero  $\dot{y}$ , which can be done with zero roll angle. Flying with the ball centred and zero roll angle is preferred by some pilots, as was discovered in the initial test. Therefore this technique was used in the runs where  $\dot{y}$  was displayed. Another PA-34 feature that affected the workload was the adverse yaw, not only speed and power changes, but also every aileron input requires a rudder input. The difficult parts for the pilot were the initiation of the engine failure, which caused a large side slip excursion, and to a lesser degree the level off while the part in between, where the aircraft was positioned in a steady climb, was relatively easy.

#### PILOT INSTRUCTIONS

Pilots were instructed to fly a constant heading of  $180^\circ$  and to maintain 90 KIAS. While it is a common practice to have the ball displaced 'half a ball width' in an OEI situation [7] some pilots favour to centre the ball, as became clear in the earlier experiments described in Chapter 7. The rationale behind the 'half ball width displaced' procedure is that it creates a condition that comes close to zero  $\beta$ . In our experiment the pilots were presented a  $\beta$  display option, and therefore we could instruct the pilots to 'centre the ball' at all times.

#### DEPENDENT MEASURES

The following dependent measures were used:

1. Speed and heading errors. The absolute speed and heading errors were multiplied to get a measure for the error and the average value of this measure is the score of the run.
2. The variation of the slip, where  $\beta$  or  $\dot{y}$  was collected based on the parameter displayed.
3. The workload given by the pilot after each run based on the Bedford scale.
4. The average climb rate over the steady part of the run. It was found that from 500 feet to the start of the level-off all pilots were in a stable climb, therefore these boundaries were used to define the steady part.

#### EXPERIMENT HYPOTHESIS

The first hypothesis was that the displays using the variable size triangle (3 and 4) would give a lower workload and a higher accuracy. The second hypothesis was that using the  $\beta$  displays (2 and 4) would give a higher workload and probably a lower accuracy than the  $\dot{y}$  display.

### 8.3.2. RESULTS EXPERIMENT 1

#### GENERAL

A typical profile is depicted in Fig. 8.3. In the shown profile, the initial 40 seconds, where the pilot is trimming the aircraft after the power change, show large excursions in speed and heading. Thereafter, the steady climb shows less speed and heading errors until

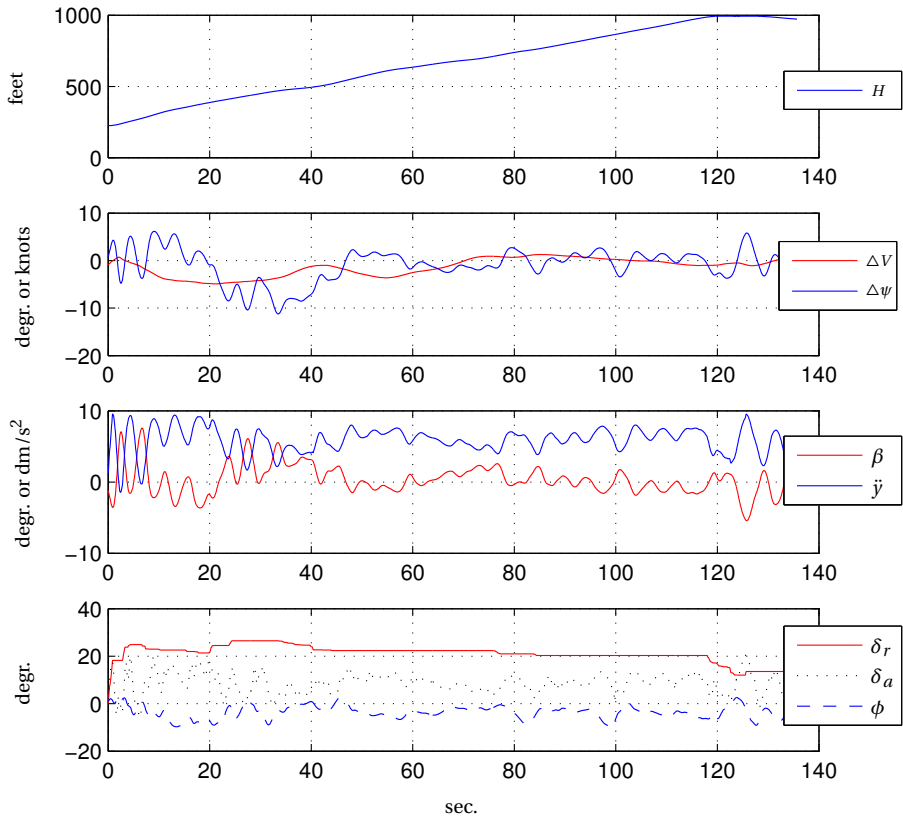


Figure 8.3: One-engine-inoperative (OEI) climb profile (run 614) where the pilot is using the triangle shape  $\beta$  display.

the 120 second point is reached. Here the pilots starts the level-off, which again shows an increase in heading and speed errors. Because of the different behaviour during the climb three different segments were defined for evaluation.

- The initial part from 200 to 500 feet altitude;
- The steady climb part from 500 feet to start level off;
- The level-off part, which started when the pilot reduced power and lasted until steady at heading and speed.

There was also a considerable difference in errors within the test group. Initial heading excursions of more than 20° were not uncommon. These errors became less during the different runs, which confirmed a strong learning effect, even in this familiar scenario. The probable cause could be that the PA-34, without rudder trim and without an aileron rudder interconnect to counter the effect of adverse yaw, is a difficult aircraft to fly with precision, even for experienced pilots.

#### SCORING

The basic question then was whether the new displays would enhance the pilot's accuracy in a OEI climb. As score for this performance the absolute value of product of speed and heading error was used. The scores are presented in Fig. 8.4. Fig. 8.4b shows the results over the complete trajectory while Figs. 8.4b, 8.4c and 8.4d respectively, show the results of the initial part, the steady part and the level-off. The following conclusions can be drawn from these figures:

- The median of the scores does not change much and the notches all overlap.
- The spread of the pilot scores is much reduced when we change from a display at the top to the presentation in the centre. This is true for both the  $\beta$  and  $\dot{y}$  display.
- The errors in the initial part of the climb are very large, and contribute most to the overall score; in this part of the run the differences between the four types of display are most prominent.

The implication of these results is that while the centre display does not significantly change the median of the performance score, it does change the spread. In other words, a considerable number of pilots had less extreme errors, particularly in the first part of the climb when the centre display was used.

Two other effects related to the score were evaluated. These effects are presented in Fig. 8.5. First, the strong learning effect was noted between the first and subsequent runs. To investigate if this had a masking effect on the score, a comparison between the original scores was made and a new set that was based on runs two to four. These results are shown in Fig. 8.5a and 8.5c. As can be seen there is little difference between these results.

We also looked at the sample size. We had 19 participants, but to have a perfect Latin square, where every display option appears the same number of times in each run, we

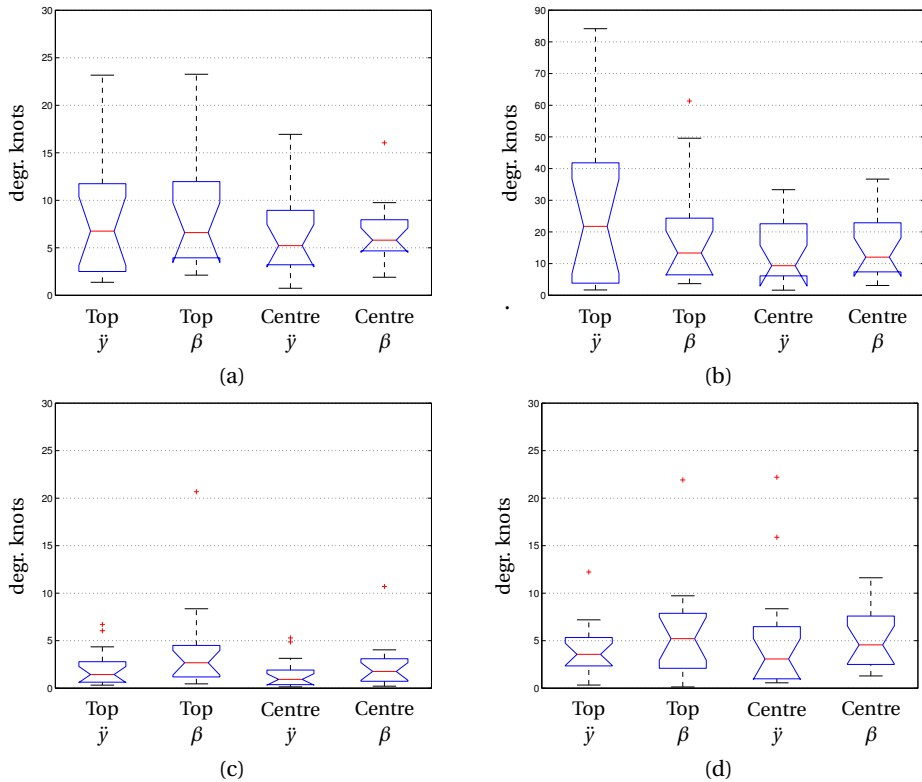


Figure 8.4: Scores for the different slip displays in the OEI climb; Scores are calculated by multiplying the absolute speed error in knots with the absolute heading error in degrees and taking the time average over the climb trajectory. (a) Represents the score over the complete trajectory, (b) represents the score for the initial part of the climb, (c) is the score over the steady part of the climb and (d) is the level off part. The large errors in the initial part necessitate a different scale for (b).

could only use 16. In Fig. 8.5b and 8.5d the result of using all 19 pilots instead of using the first 16 is displayed. Again, this does not change the initial conclusion that the major effect is in the spread of the data between the top and centre display and not in the change of the median.

### SLIP VARIANCE

A second point of interest was the variance in slip angle, which is after all the primary measure that is controlled by the pilot based on the new side slip display. In Fig. 8.6 the results of the slip variance are presented. Because the units of  $\dot{y}$  and  $\beta$  are different, these figures can only be used to compare the top and centre display and not the  $\dot{y}$  and  $\beta$  display. This led to the following observations:

- No significant change in median value was noticed between the top and centre displays when comparing  $\dot{y}$  (1 with 3) and  $\beta$  (2 with 4).

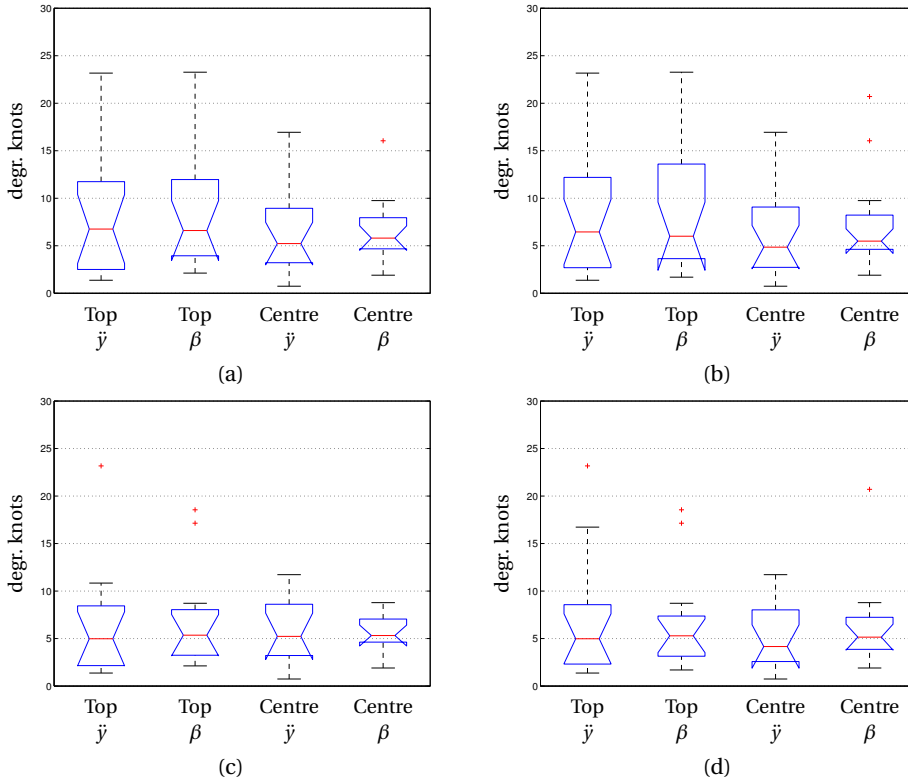


Figure 8.5: The total scores over the complete trajectory are compared for different numbers of pilots and for the effect of the omission of the first run. (a) All runs 16 pilots, (b) All runs 19 pilots, (c) Runs 2, 3 and 4 using 16 pilots and (d) Total score 19 pilots over runs 2, 3 and 4.

- The largest slip variance occurred in the initial climb. The variance difference between the steady part and the level-off was small.
- There was a significant difference in the spread of the data between the top and centre display for lateral acceleration, but this effect was not present for the  $\beta$  display.

We may conclude from the above facts that moving the slip indication to the centre of the display was not successful in lowering the variance of the  $\beta$ . This would be an indication that  $\beta$  control was more difficult for the pilots, as was already expected. This can be confirmed by the workload ratings, which we will discuss next.

#### WORKLOAD, CLIMB RATE AND PILOT PREFERENCE

The workload ratings, shown in Fig. 8.7a, revealed no significant change in the median of the workload. A noteworthy point is the large change in spread between the different displays. There was less variation in the workload rating—indicating more agreement between the pilots—about the  $\ddot{y}$  at the centre and the  $\beta$  display at the top than about

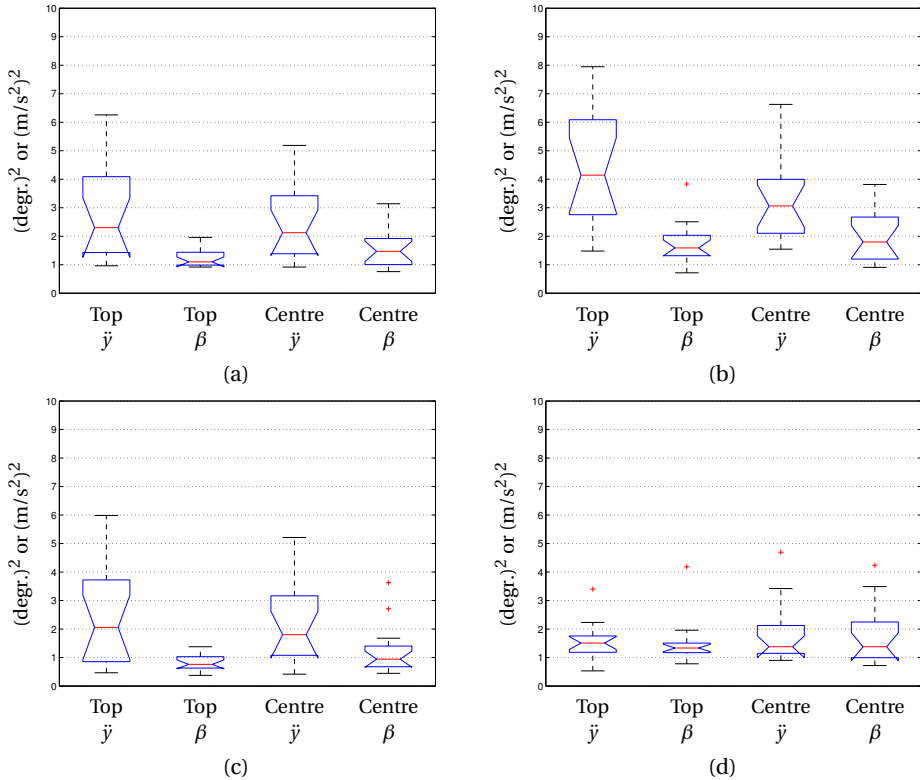


Figure 8.6: Slip variance for the different slip displays in the OEI climb; Variance in slip is for  $\beta$  in  $degrees^2$  and for  $\dot{y}$  in  $(0.1m/s^2)^2$  depending on the kind of display. (a) Represents the score over the complete trajectory, (b) represents the score for the initial part of the climb, (c) is the score over the steady part of the climb and (d) is the level off part.

the workload rating of the other two display combinations. Fig. 8.7b shows the achieved climb rate. The climb rate with  $\beta = 0$  is significantly higher than with  $\dot{y} = 0$ , as was to be expected for aerodynamic reasons, but it confirms that the lower drag is also achieved in practice. This fact was also noticed by all participants and would be a good reason to prefer the  $\beta$  display.

#### CHANGE IN VARIANCE

Until now we have seen that there were no significant changes in the medians of the score or slip variance but we did notice that there were large changes in spread of the scoring as can be seen in Fig. 8.8. This led to the question whether the change in variance of the score was significant. To evaluate this we used Fisher's F-test. The results are presented in Table 8.2. In this table we calculated the differences in variance between each display, and instead of presenting the F-value we transformed the F-value to the p factor to ease interpretation.

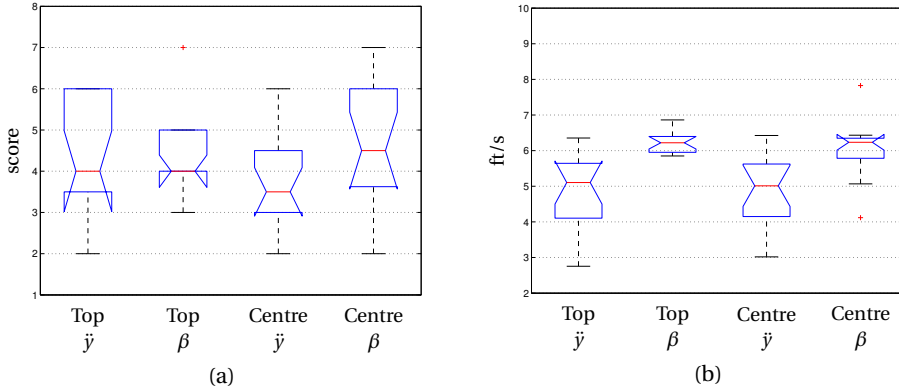


Figure 8.7: Workload and climb rate using different displays in the OEI climb. (a) represents the workload using the Bedford scale and (b) represent the average climb rate in *ft/s*

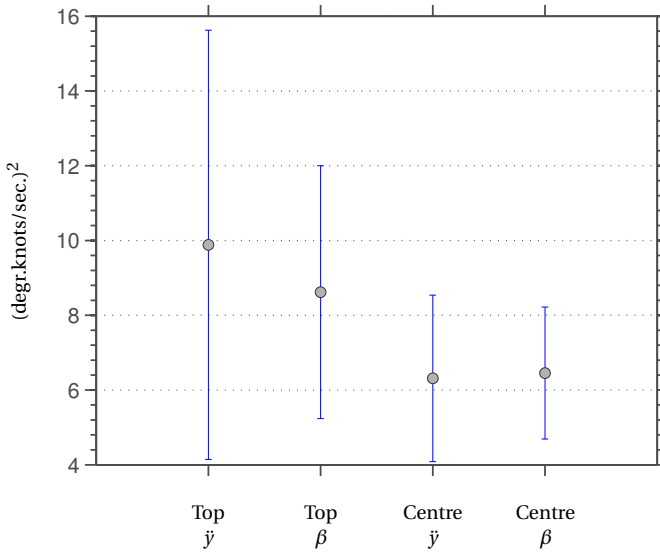


Figure 8.8: variance of the score.

From this calculation it is clear that over the complete run, the variance change of the score is significant at the  $p \leq 0.05$  level, for the comparison of  $\beta$  centre with  $\dot{y}$  at the top. Furthermore, while changing the  $\dot{y}$  display from top to centre gives a significance of only  $p = 0.076$  for the complete run, the change is significant over the first part, where the excursions are the highest.

Table 8.2: Significance score of the variance change between the different displays for (A) the complete run and (B) the score for the initial part of the climb to 500 feet.

		Top $\ddot{y}$	Top $\beta$	Centre $\ddot{y}$	Centre $\beta$
A	Top $\ddot{y}$	1	0.3165	0.0764	0.0287
	Top $\beta$	-	1	0.4276	0.2192
	Centre $\ddot{y}$	-	-	1	0.6581
	Centre $\beta$	-	-	-	1
B	Top $\ddot{y}$	1	0.2787	0.0400	0.0409
	Top $\beta$	-	1	0.3142	0.3189
	Centre $\ddot{y}$	-	-	1	0.9921
	Centre $\beta$	-	-	-	1

### CONCLUSION SIDE SLIP TEST

The mixed results presented above give rise to the following conclusion. Because the median of the score and the slip did not change significantly we may conclude that the new display did not significantly change the general performance of the participants. However, because the score variance decreased significantly when using the centre display, we may conclude that some pilots had less extreme errors. Less extreme errors is in itself a favourable result and we may conclude that this display could be beneficial, particularly when large excursions are present as in the initial part of the climb. At the end of the second experiment, which is discussed next, an additional test was performed to investigate the pilot's display preference.

## 8.4. EXPERIMENT 2; GO-AROUND

### 8.4.1. EXPERIMENT DESIGN AND PROCEDURES

The second experiment was the OEI go-around. This experiment was also carried out in the initial evaluation described in Chapter 7. The basic set up was the same. The pilots experienced an engine failure at exactly 80 knots IAS with the aircraft configured for landing with gear down and flaps set at 25°. After experiencing the engine failure, the pilots had to perform the OEI go-around. The differences with the initial evaluation were that the run was not only made at low altitude with reference to the runway but also at 3,000 ft without reference to the runway. The rationale behind the run at altitude was that in this situation, with less outside reference, pilots would receive more helpful information from the new displays when compared to the run at low altitude where their focus of attention was more outside as was described in Chapter 7. The second difference was that the side slip display was not changed. For all runs the standard  $\ddot{y}$  display at the top of the attitude indicator was used. Consequently, the only two new features tested in this experiment were the  $V_c$  indicator and the climb bar.

### INDEPENDENT VARIABLES

Two independent variables were used: Firstly, the new indications of  $V_c$  and climb bar were turned on and off. We will refer in the following to the first condition as the 'new' display and the latter as the 'old' display. Secondly, runs were performed both at low

altitude and at 3,000 feet.

#### ORDER OF RUNS

The order of runs was pseudo-random using the Latin square method to vary the independent variables.

#### PILOT INSTRUCTIONS

Pilots were told that the engine failure would be given at exactly 80 knots and that they had to perform a standard go-around. The only surprise for them was which engine would fail. Pilots were instructed that full rudder was required at this low airspeed and that the gear should be raised as quickly as possible in order to get a positive climb rate. Furthermore, the flaps should not be raised until 85 knots was reached and the aircraft had to be manoeuvred as quickly as possible into a safe climb with the standard OEI climb-speed of 90 KIAS.

#### OPTIMUM PILOT CONTROL

Optimum pilot control was already presented in Chapter 7. In summary, the main challenge for the pilot is to prevent airspeed loss and to quickly apply full rudder. Maintaining airspeed, combined with full rudder enables the use of more power on the working engine without losing lateral control. At 85 knots full power can be given. The earlier the gear is raised, the quicker the acceleration will be. The main challenge for pilots is that this scenario, which shows rather violent aircraft motions, requires fast synchronised inputs with all controls.

#### EXPERIMENT HYPOTHESIS

The experiment hypothesis was that the display of  $V_c$  and climb bar would lead to a safer and more efficient go-around.

#### DEPENDENT MEASURES

The dependent measures can be divided into two categories, firstly the measures that define the safety of the go-around and secondly those that determine the efficiency of the go-around. All dependent measures are presented in Table 8.3. In a properly executed go-around, the aircraft energy, which is decreasing slowly in the approach to land, should start to increase quickly. As a measure we used specific energy ( $E_s$ ), which is defined by the total energy divided by the mass and has  $(m/s)^2$  as unit.

### 8.4.2. RESULTS EXPERIMENT 2, GO-AROUND

#### GENERAL

All 19 pilots had to make four go-arounds with the two independent variables pseudo randomly changed using the Latin square method. This experiment was quite challenging for all pilots and a significant number of runs (17 out of 76) resulted in a crash. There were two pilots who had crashes in both the first and second run. Because the crash itself is already a demotivating factor for the pilots, the double crash was a reason to restart the test sequence with those two pilots after giving additional guidance. However, because these pilots had a different starting point in the Latin square, their results in this experiment were not used. Fortunately, the number of participants was large enough that their

Table 8.3: Dependent measures in the OEI go-around experiment.

Safety measures	comments
$V_c$ exceedance (knots)	Indicates the loss of sufficient lateral control
Time rudder response (s)	Time to $\delta_r > 25^\circ$
Maximum bank angle (degr.)	The actual lateral performance
Speed drop (knots)	80 minus minimum airspeed after failure
Efficiency measures	
Minimum $E_s$	Maximum loss in $E_s$ since after engine failure
Time minimum $E_s$	Should be as small as possible
Recovery time	Time to gear and flaps up and KIAS>85
Altitude loss	Loss of altitude in feet

sequence could be replaced by that from two other pilots. The complete Latin square required 16 pilots. From the first 16 pilots, two were removed because of the restart and their runs were repeated by pilot 18 and 19, and pilot 17 had to be omitted to apply the Latin square properly.

Because the crashes themselves also contain vital information, they should not be omitted from the results. However, the recovery time, which would be infinity, could not be used and was therefore changed to 'NaN', which automatically removed it from the calculation of mean, median and variance.

#### SAFE GO-AROUND

The safety related measures are depicted in Fig. 8.9. The 95% confidence intervals for each parameter are presented by the 'notches'.

In Fig. 8.9a we see that the median of the  $V_c$  exceedance is slightly lower for the new display compared to the old, however this difference is not significant because the 95% confidence limits overlap. More significant is the difference between the high and the low profile. It is clear that in the high profile the  $V_c$  exceedance is less. This might be partially caused by the fact that pilots have less problems lowering the nose to maintain airspeed at high altitude.

Fig. 8.9b shows the loss in airspeed after engine failure. Pilots lost less airspeed in the run at high altitude, and there is little difference related to the use of the new display. The fact that pilots in the run at low altitude were less inclined to lower the nose in order to maintain airspeed is of course a natural tendency. However, this tendency is dangerous because it impairs the lateral performance, which is most needed in the scenario close to the ground.

Fig. 8.9c shows the maximum bank angles reached. There are some excessive bank angles, clear indications of the crashes that occurred. There are no significant differences between the traditional and new display or between the high and low scenario.

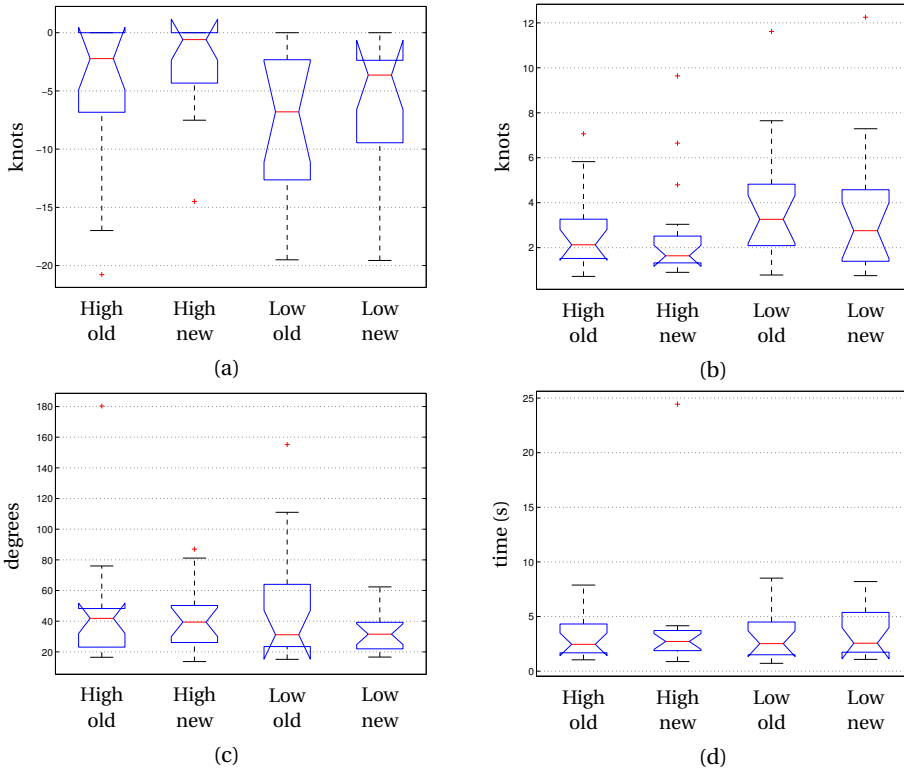


Figure 8.9: Safety related parameters in OEI go-around. (a) The  $V_c$  exceedance, (b) the maximum velocity decrease after the engine failure (c) the maximum bank angle and (d) the time required to get maximum rudder deflection.

Finally, the rudder response time is presented in Fig. 8.9d. It is clear that there is no significant difference between the use of the old or new display nor between the high and low scenario. It is however interesting to see that the spread in time is large, it is feasible to have full rudder within two seconds of the engine failure but as can be seen by the interquartile range, 25% of all participants in the low scenario used more than five seconds, which considerably impacts the fast recovery.

EFFICIENCY IN GO-AROUND

Fig. 8.10 presents the efficiency results of the go-around. In Fig. 8.10a the specific energy loss after the engine failure is presented and Fig. 8.10b shows the time where the minimum energy occurred. Ideally both values are low, a small drop in energy that is quickly transformed into an increase in energy. The two figures show that there is no significant difference in efficiency between the old and new display or between the high and low scenario. However, what is noteworthy is the large spread in data caused by the differences between pilots and the differences between the runs.

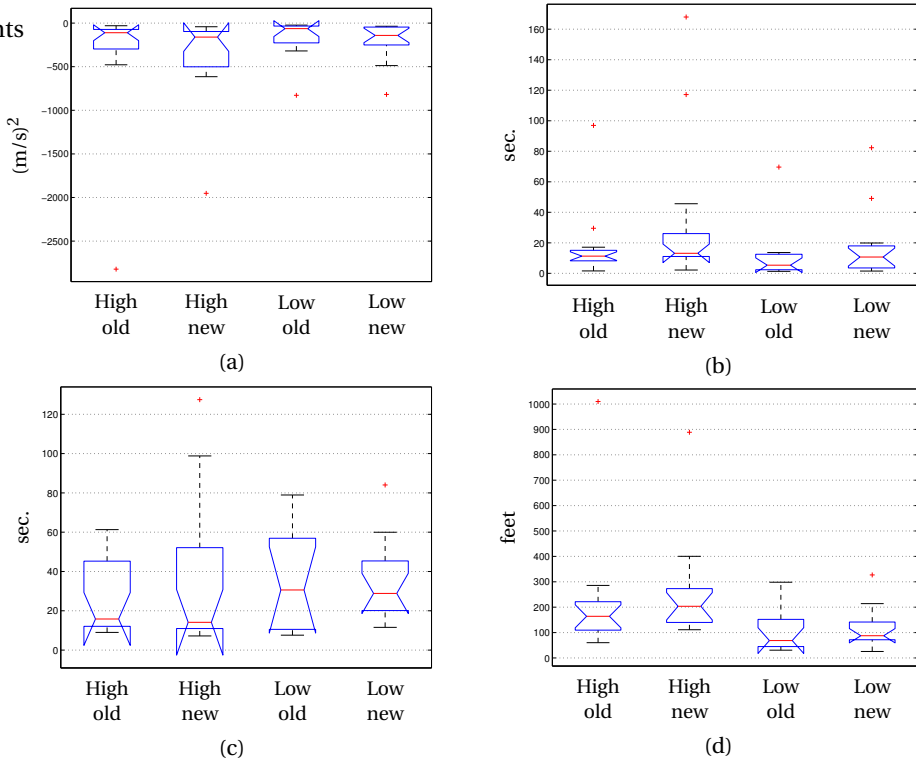


Figure 8.10: Efficiency related parameters in OEI go-around. (a) Minimum specific energy since engine failure, (b) Time minimum energy is reached after the engine failure (c) the recovery time and (d) the maximum altitude loss after the engine failure.

Fig. 8.10c shows the time from engine failure until the aircraft configuration is cleaned up and the aircraft is in a climb with an airspeed higher than 85 KIAS. From these data the crashes are removed. We note again that there is no significant difference between displays nor between scenarios and again we can observe the large spread in data.

Investigating the loss of altitude in Fig. 8.10d we see that there is no significant difference between the old and new display but we can see that the high scenarios in several instances had very large excursions in altitude loss, which would have caused a crash in the low environment.

#### WORKLOAD, COMMENTS, AND CRASHES

Fig. 8.11 shows the pilot workload ratings. The median of the new display is one scale level lower than the standard display, indicating that pilots were experiencing some help from the new display. However, this difference is not significant at the  $p \leq 0.05$  level. Another observation is that the absolute workload level is very high, indicating that this experiment was apparently extremely difficult for the pilots.

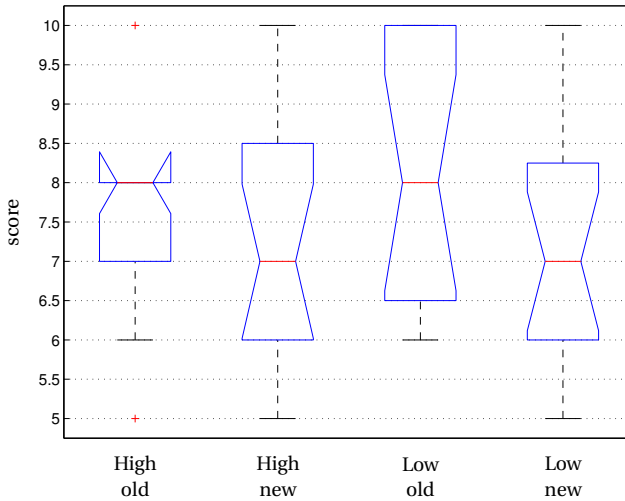


Figure 8.11: Workload scores for the OEI go-around

After each run, pilots were not only asked to rate the workload but also to give free comments on the display. It was interesting to note that out of 19 participating pilots 14 reported that they liked the climb bar and used it, or that they missed it when they had performed a run without the climb bar. However, it should be noted that they generally did not use the bar in the initial part of the run to maintain airspeed directly after the engine failure, but rather in the later part when the gear was raised and power set. Therefore the climb bar did prevent the over-rotations that were present in the initial test described in Chapter 7, but did less to prevent the initial speed loss. Further comments indicated that there was an initial tendency to use the bar as a flight director bar, which is of course possible, but only after the correct velocity is achieved.

There were only two out of the 19 pilots who were positive about the  $V_c$  display. Most pilots found it hard to use, only when the speed was above the  $V_c$  they noted it as a nice indication that they were on the safe side.

In the 64 runs used for the evaluation, 8 crashes occurred. From these 8 crashes there were only two at high altitude. In the high altitude scenario a crash was defined as a situation wherein the pilot was not able to control the aircraft any longer and the simulation was stopped. There was, in that situation, no collision with the ground. Of course there were several instances where excessive altitude loss was encountered but given the additional altitude the pilots were able to recover the aircraft.

The crashes at low level were all situations in which the collision with the ground was imminent. The simulation was normally stopped just before the ground impact because showing the impact itself did not serve any practical purpose. From the six crashes at low altitude only one crash was in a run where the new display was used, all others were

with the traditional display. One or less out of six has a binomial chance of 11.9% given that both results have the same likelihood. Consequently, the reduction in crashes is not significant at the  $p \leq 0.05$  level.

### CONCLUSION GO-AROUND

From the available data the following conclusions can be made:

- Recovering from a roll limited situation is extremely difficult for pilots;
- There are large differences in the performance of individual pilots;
- The increase in safety and efficiency between the runs with and without the new displays were not significant ( $p \leq 0.05$ ).

Halfway through the test it already became apparent that there was little difference in pilot performance with and without the new displays. A possible reason could be that this scenario required a far more extensive training than was given during the familiarization run. We may have underestimated the fact that pilots do not have any formal training in the recovery from a roll limited situation because it is not a part of standard pilot training. Pilots do of course train OEI go-arounds, but these are performed at a much higher airspeed where the roll limited situation is not encountered. Some pilots were so surprised by the controllability that they questioned the validity of the model. On these occasions pilots were given an additional demo after the formal test in which they could perform the same go-around with the standard airspeed of 90 KIAS instead of 80 KIAS, to their surprise the aircraft reacted exactly as expected.

To evaluate whether pilot performance could be improved by training, a new additional experiment was designed. In order not to interfere with the normal test sequence, this new test was added at the end of the regular test. However, because its flight profile is similar it will be discussed next.

## 8.5. TRAINING THE GO-AROUND

### 8.5.1. EXPERIMENT DESIGN AND PROCEDURES

The experiment design was similar to the previous test with the following changes:

- Only the new display was used with  $V_c$  indication and climb bar;
- The side slip display used was  $\beta$  in the centre position;
- The same run was repeated four times.

### INDEPENDENT VARIABLES

There were no independent variables for this test.

### PILOT INSTRUCTIONS

Pilots were instructed to use a step-wise approach where they deliberately had to use the  $V_c$  information and the climb bar. The steps were:

1. When noting the engine failure, lower nose to the climb bar in order to maintain airspeed;
2. Apply full rudder;
3. Advance throttle as far as  $V_c$  indication allows;
4. Raise the gear;
5. Maintain  $\theta$  below the climb bar to increase airspeed, throttle can be advanced based on the  $V_c$  indication;
6. If full throttle is given and  $V_c$  is below the present airspeed, set  $\beta$  to zero to achieve minimum drag;
7. Raise the flaps at 85 KIAS.

#### ORDER OF RUNS

For the evaluation, the first run shown is the run that the pilot had performed in the previous test using the new displays at low altitude. The next four runs show the changes that were achieved in the training experiment.

#### DEPENDENT MEASURES

The dependent measures were the same as in the previous test.

#### EXPERIMENT HYPOTHESIS

The hypothesis was that pilot performance in this experiment would increase over the runs.

### 8.5.2. RESULTS EXPERIMENT 5, GO-AROUND TRAINING

#### SAFETY

In Fig. 8.12 the results of the training sessions on the safety related parameters are shown.

Comparing the different parameters we can see that in Fig. 8.12a the learning effect is visible in the decrease of  $V_c$  exceedance and the spread in  $V_c$  data. A similar observation can be made about the decrease in maximum bank angle as shown in Fig. 8.12c. The learning effect is less visible in the time required to achieve maximum rudder, shown in Fig. 8.12d, and in the velocity decrease shown in Fig. 8.12b. While the trend is clearly visible, the variation in data is too large and the number of participants too low to make a statement with 95% confidence about the improvement in safety due to training.

#### ENERGY CONTROL

In Fig. 8.13 the results of the training sessions on the efficiency-related parameters are presented. The learning effect is visible in the recovery time, as shown in Fig. 8.13c. The recovery time is defined as the time from engine failure until the aircraft is configured gear and flaps up and the airspeed is above 85 knots. To a lesser degree, it is also visible in the decrease in spread of the altitude loss data as shown in Fig. 8.13d. It should be noted that initially some altitude loss is needed to maintain airspeed while the power

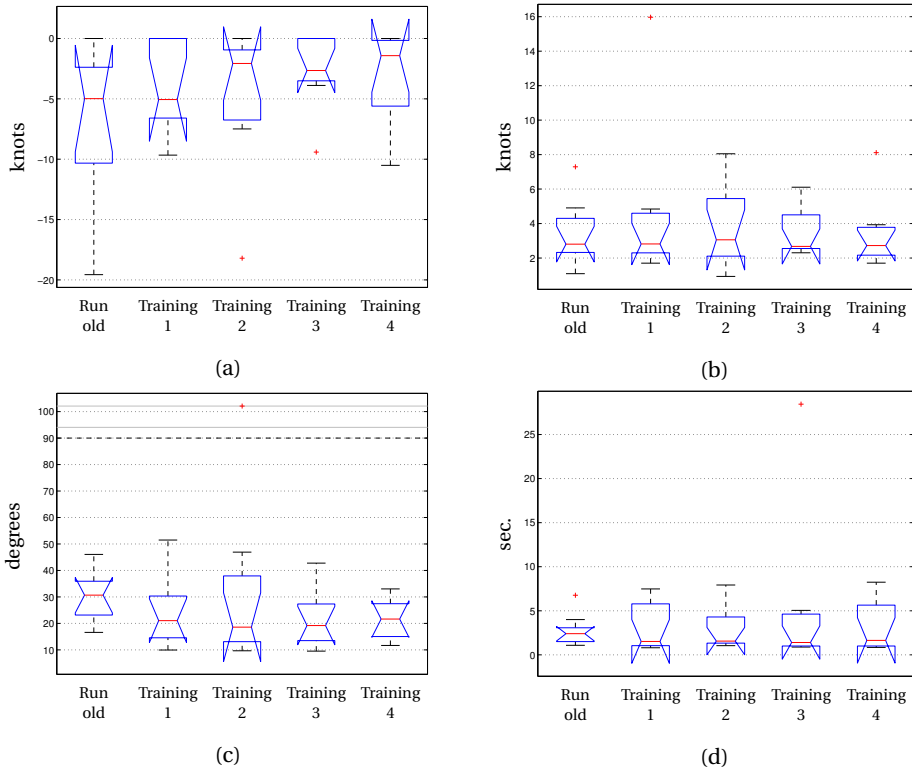


Figure 8.12: Safety related parameters in OEI go-around during training session. (a) The  $V_c$  exceedance, (b) the maximum velocity decrease after the engine failure (c) the maximum bank angle and (d) the time required to get maximum rudder deflection.

is not yet advanced and the gear is still down. From this data one can conclude that a 100 feet altitude loss is generally required to perform the go-around. A smaller altitude loss is not always advantageous because it will cause speed loss and delay recovery. If we look at the loss in specific energy, Fig. 8.13a, and the time of minimum energy shown in Fig. 8.13b we see the trend that the specific energy loss converges to  $200(m/s)^2$  and occurs after 12 seconds. Similar to the safety results, the trend in the data is clear but does not yet give a change in median that is significant.

### LEARNING CURVES

To view actual learning curves per pilot we made plots of how the  $V_c$  exceedances, the maximum bank angle, the reaction time of the rudder and the total time needed for recovery changed per run per pilot. These results are shown in Fig. 8.14.

Fig. 8.14d shows that the curves per pilot differ considerably. The next question is what adequate performance we might expect in this experiment, because if we can define an adequate performance we can also judge if the pilot reached an adequate performance. An adequate performance should at least have no excessive  $\Delta V_c$ . We have

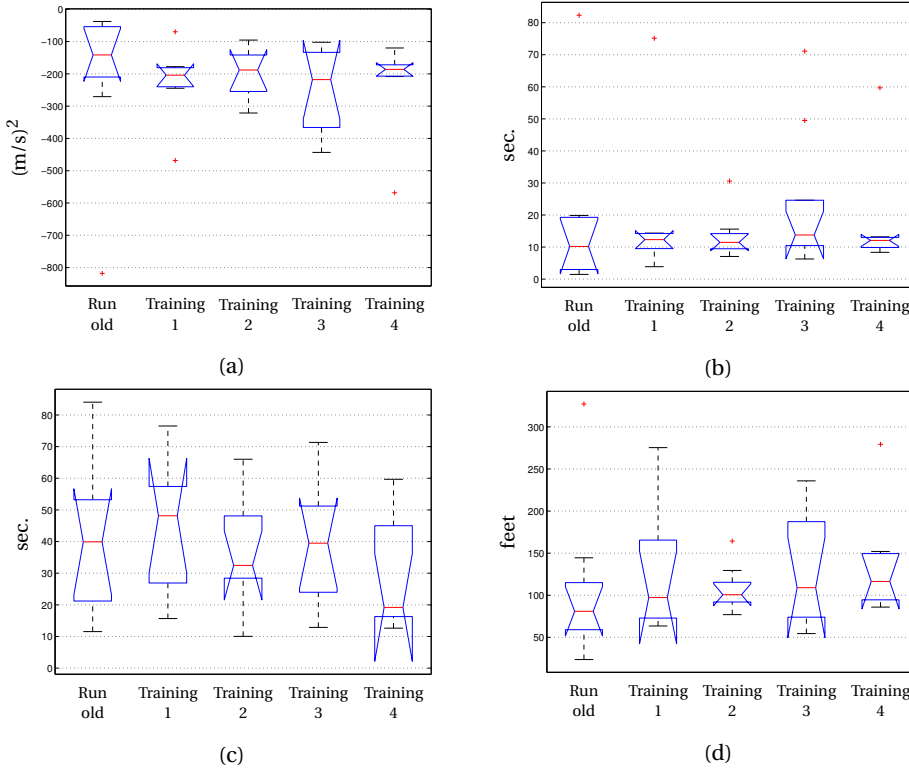


Figure 8.13: Efficiency related parameters in OEI go-around training. (a) Minimum specific energy since engine failure, (b) Time minimum energy is reached after the engine failure (c) the recovery time, which is defined as the time from engine failure until the aircraft has a speed above 85 knots with gear and flaps up; (d) the maximum altitude loss after the engine failure.

to realize that these are always possible with throttle movements and delays in rudder applications but the excursions are preferably smaller than 5 knots. Furthermore, excessive bank angles of more than 30 degrees must not occur. In addition, we want a short recovery time. The trends in Fig. 8.14c indicate that a recovery shorter than 20 seconds is possible. Quite a few pilots met these requirements or came close, while other pilots, particularly numbers 1,2 and 4 clearly needed more time to train to an adequate performance level. However, because time in the simulator was limited, the number of training runs was also limited and as shown by the result in Fig. 8.14, training to proficiency could not be achieved for every pilot.

#### CONCLUSION GO-AROUND TRAINING

The available data indicate that training does improve pilot performance in the go-around. It was also clear from the comments that pilots were using the climb bar and the  $V_c$  indication according to the instructions given. However, we also have to realize that a (very) large part of the pilot attention is devoted to maintaining the aircraft level and countering the yaw leaving little time to accurately position the climb angle, correctly position

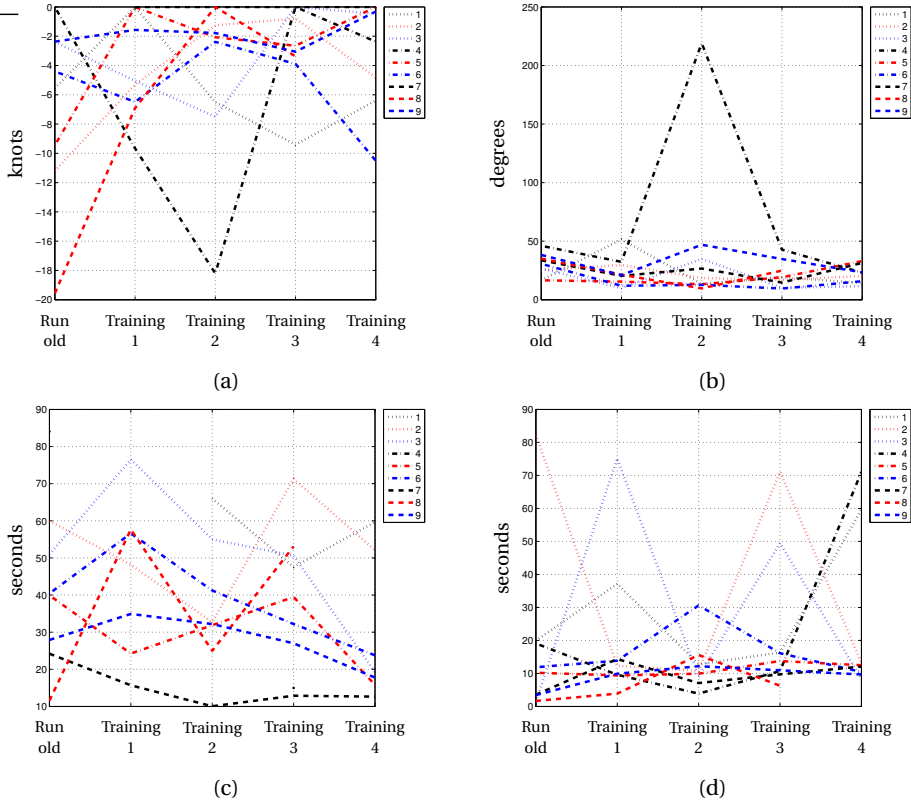


Figure 8.14: Subjects learning curves in OEI go-around training. (a) maximum  $\Delta V_c$ , (b) Maximum bank angle excursion in degrees (c) the recovery time and (d) time minimum energy is reached after the engine failure.

the throttles and raising the gear. Still, six out of the nine pilots showed a good progression while three clearly required more time than could be given in this experiment.

ADDITIONAL PILOT’S PREFERENCE TEST

At the end of the second experiment, pilots were allowed to choose their favourite side slip display for the remaining experiments. Their choice was an additional indication for pilot’s preference. The results are presented in Table 8.4. The Table shows that 13 pilots out of 19 preferred the centre display, an outcome with a binomial probability of 8.3% if there was no real preference. There was a similar division between  $\dot{y}$  and  $\beta$ , 13 out of 19 pilots preferred  $\dot{y}$  over  $\beta$ , again the probability is 8.3% that this is a random outcome when there is no real preference.

Table 8.4: Type of side slip display and the number of pilots that selected this display for test number 3 and 4.

Type of display	Times selected
Standard display $\dot{y}$ on top	5
$\beta$ on top	1
$\dot{y}$ centre	8
$\beta$ centre	5

## 8.6. EXPERIMENT 3; EFATO

### 8.6.1. EXPERIMENT DESIGN AND PROCEDURE

This experiment was a classic situation for all pilots: the engine failure after take-off (EFATO). This experiment was conducted in a similar way as performed in simulator training. In particular, this failure was not previously announced but came as a surprise. Because we can only surprise the subjects once, we had to make this test a between subjects test. For half of the pilots the test was done with the new display with climb bar and  $V_c$  indication while the other half had no  $V_c$  and climb bar displayed. The aim of this test was to see whether the new display would enhance the correct execution of the EFATO. The engine failure was given at 85 KIAS when the gear was already selected up and the experiment was stopped when a safe climb was established. The prime results were from the first run, where the EFATO came as a surprise. The run was however repeated, and every participant made four runs and had the opportunity to perform the EFATO with and without the new features. The side slip display for this test was a free choice for the pilot as mentioned before.

#### INDEPENDENT VARIABLES

The only independent variable was the on/off setting for the  $V_c$  and climb bar display.

#### PILOT INSTRUCTIONS

The instructions for the pilot were minimal, to enhance the surprise effect. The instruction was simple: perform the take off and climb to 1,000 feet, if something happens act as you would normally do.

#### DEPENDENT MEASURES

The following dependent measures were used:

- The time needed to recover the aircraft, which was defined by reaching a velocity of 88 KIAS;
- The time it took to give full rudder;
- The maximum loss in airspeed since the engine failure;
- The maximum loss in altitude since the engine failure;
- The pilots assessment of his workload.

### EXPERIMENT HYPOTHESIS

It was expected that the new display would facilitate the pitch control of the pilot by the presentation of the climb bar. This would then prevent or reduce the loss of airspeed and expedite recovery to a safe single-engine climb out. There was no special effect expected based on the  $V_c$  indication. The  $V_c$  indication in an engine failure would only become important as a large velocity loss was encountered. The hypothesis was therefore that velocity loss could be reduced and recovery expedited.

## 8.6.2. RESULTS EFATO

### GENERAL

All pilots experienced this experiment as easy, at least a lot easier than the previous experiment in which many of them crashed. One of the contributing reasons why this experiment was easier is undoubtedly that no extra actions were needed to raise the gear and flaps and that the throttles could be held in the same position<sup>5</sup>. The consequence was that all attention could be devoted to the primary flying task: reduce side slip, maintain heading and reset the pitch attitude if required.

In Fig. 8.15 the results of the first run are presented. The differences between the runs with and without the new display are small. Fig. 8.15a shows that the median of the recovery time is longer with the new display. This result, even being below the significance level, was unexpected and could be caused by the fact that pilots were strongly inclined to use the climb bar as a flight director bar. Consequently, setting the pitch to the climb bar will keep the airspeed at its present value and delays the acceleration to the required climb speed. On the other hand, keeping the nose at the bar will prevent the airspeed loss in the initial phase of the EFATO. This was indeed happening as can be seen in Fig. 8.15c, where the airspeed loss was slightly less in the situations when the new display was used. Looking at the rudder reaction time in Fig. 8.15a it is clear that in this experiment the rudder reaction was quite fast. It was also investigated whether the type of side slip display had any influence on the rudder reaction time and this proved not to be the case. This is quite logical because the outside view and the motion cues are so dominant that the side slip display was hardly needed in this situation and the pilot could control the side slip completely on outside references. Finally, 17 out of 19 runs did not have any altitude loss as shown in Fig. 8.15d, and for the two runs that did, the loss was at a maximum of 7 feet. This makes sense, since pilots are quite familiar with this type of scenario.

In Fig. 8.16 the combined results are depicted for all four runs. It is interesting to compare these results with those in Fig. 8.15. There are no significant differences regarding the rudder reaction time and altitude loss. It is however interesting to see that the recovery time with the new display becomes smaller, a good indication that pilots started to know how to use the climb bar. On the other hand, the airspeed loss without the climb bar is also decreasing, which can be attributed to the learning effect. But even with this learning effect it is evident that the spread in airspeed loss with the standard display is larger than with the new display.

<sup>5</sup>There was no need to feather or reduce the failed engine because auto feather was included in the model.

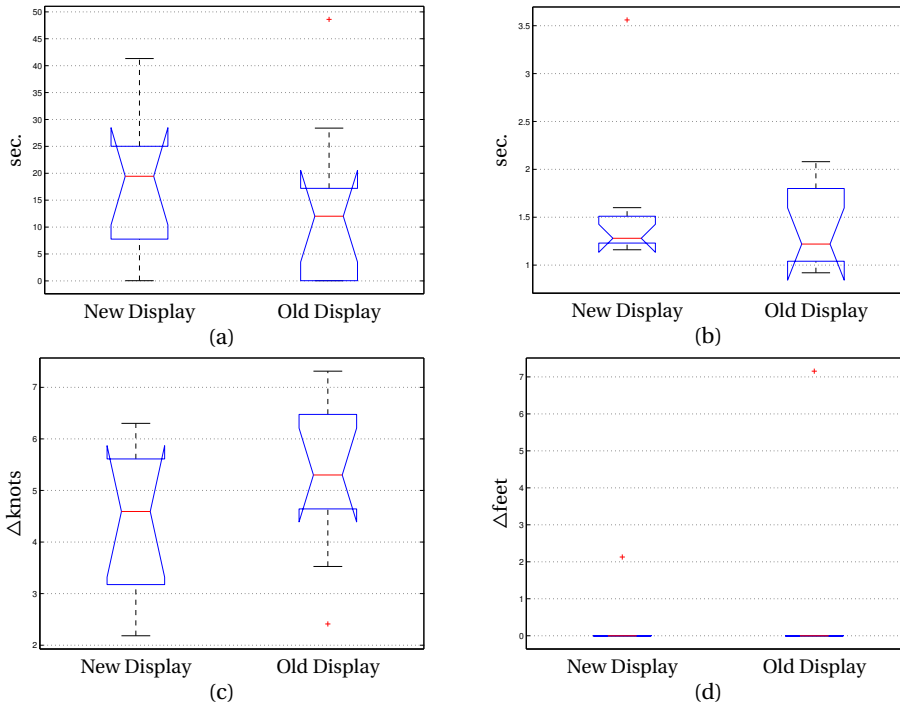


Figure 8.15: Engine Failure after take off (EFATO), results of different display types in the first run. (a) the needed recovery time to velocity >88 KIAS, (b) the time required to achieve full rudder, (c) the maximum airspeed loss in knots and (d) the altitude loss if present; most pilots did not experience any altitude loss consequently, the box plot is compressed to a line.

### WORKLOAD AND COMMENTS

In Fig. 8.17 the workload scores are presented. The difference between the two displays appears to be small. In the free comments that were collected after each run, 14 out of 19 pilots mentioned that they liked the climb bar and considered it helpful information.

### DISCUSSION AND CONCLUSION EFATO

The data show that there are differences between the results with and without the new displays, but they never reach significance, as shown in Fig. 8.15, 8.16 and 8.17 where the 95% confidence notches in the box plot all overlap. While the box plots focus on the change in median and interquartile range, an investigation of the change in variance was also conducted using the Fisher test. This evaluation showed that all variance changes were not significant. On the other hand, pilots appreciated the climb bar and used it, which could be reason enough to install it in the aircraft anyway.

It is conceivable that the effect of the climb bar would have been more pronounced if the engine failure was given at a lower airspeed. However, at 80 knots with gear down there is no climb potential for this particular aircraft, and the best option for the pilot in that situation is to put the aircraft back on the runway.

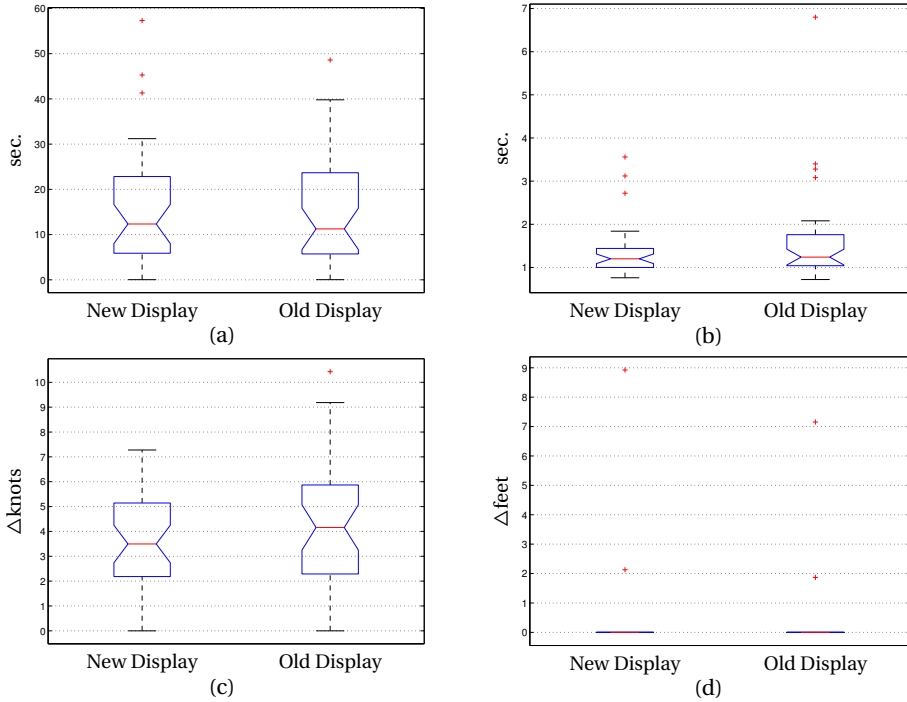


Figure 8.16: Engine Failure after take off (EFATO), results of different display types over all runs. (a) the needed recovery time to velocity >88 KIAS, (b) the time required to achieve full rudder, (c) the maximum airspeed loss in knots and (d) the altitude loss if present.

A point of discussion is whether pilots are better off with the standard flight director command bars or with this simple climb bar. When the aircraft is already equipped with a flight director, a climb bar might be superfluous, the flight director can easily be programmed to maintain airspeed or regain airspeed after an engine failure. However, for aircraft without a flight director the climb bar is a technically easy to install display addition, that can aid the pilot in regaining airspeed and maintaining it without the added complexity of navigational guidance.

## 8.7. EXPERIMENT 4; DAMAGED AIRCRAFT

### 8.7.1. EXPERIMENT DESIGN AND PROCEDURE

The last experiment was initially intended as a demonstration of how the  $V_c$  indicator could be used in case of a failure, in a similar manner as was done in the initial test described in Chapter 7. The failure chosen was a lateral mass asymmetry of 200 kg, positioned 4 meter right of centre, and a reduction in the aileron efficiency of 50%. This configuration gives a similar effect as the loss of a small part of the wing and the loss of one aileron. The aim was to let the pilots first experience the failure, and thereafter

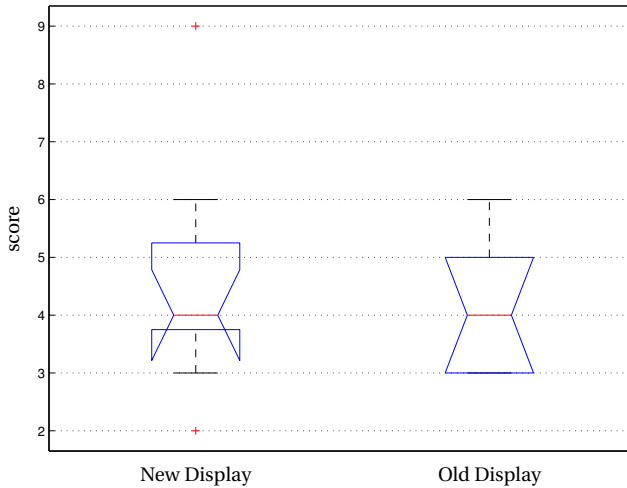


Figure 8.17: Workload scores for the EFATO for the first run.

instruct them to apply control inputs, in order for the PID program to determine the change in control and stability derivatives. Finally, the test would then be completed by landing the aircraft safely with a speed that was above the newly calculated  $V_c$ . In this initial set-up of the experiment only subjective comments from the pilots would be collected about the use of the  $V_c$  indicator in case of a failure that influenced the lateral-directional control.

However, after two participants had received this demonstration, it became clear that this experiment was an excellent opportunity to investigate how pilots would cope with an emergency that they had never before encountered. This required just a small extension of the experiment. In this revised set-up the pilots were first given the emergency without the  $V_c$  indicator and with the failure detection software turned off. When this first run was completed they repeated the run with  $V_c$  information available and detection software turned on. In this last set-up they were given additional instructions on how to perform the control inputs and to select a safe speed for approach and landing. Subsequently, the approach and landing were carried out.

#### INDEPENDENT VARIABLE

There was one independent variable in this experiment:  $V_c$  indication and error detection software was selected off in the first run and on in the second run.

#### IDEAL PILOT PERFORMANCE

The handling of control problems was already discussed in Chapter 2. An excellent check list for control problems is given in the US Navy NATOPS [8] but is also available in many check lists from military aircraft. If we use, and annotate (in *italic*) this procedure for this particular control problem the following steps should be taken:

- After detection of the problem the aircraft should be brought to a safe altitude over a preferably uninhabited or sparsely populated area;
- The pilot should decrease airspeed in slow steps (10 knots) until the speed is reached where the gear can be lowered. At every step the controllability must be checked. *The NATOPS does not dictate an engine check at every step, however, if this is done, pilots can note what the effect of asymmetric power is on the controllability and this is particularly useful in emergencies where the lateral-directional control is affected.*
- *When the gear is selected down the steps must be made with 5 knot intervals and flaps can be lowered when no visual damage is present.*
- *After the lowest speed is reached with adequate control, the pilot should increase the airspeed with 10 knots and use that velocity for the remainder of the flight as minimum speed. Here the NATOPS procedure must of course be vague because there is no means in flight to easily quantify adequate control. With the  $V_c$  indication a quantitative measure is available but this measure is of course also dependent on the amount of proverse rudder and asymmetric power that is applied.*

#### PILOT INSTRUCTIONS AND FLIGHT PROFILE

The run started on runway 18R of Amsterdam Airport. Pilots were instructed to perform a normal take off, followed by a climb to 1,000 feet. At 1,000 feet a left hand turn was made to downwind and the airspeed was increased to 120 KIAS. When straight and level on downwind the failure was introduced into the system. The pilots were given some time to investigate the problem. The simulation was then paused to enable pilots to give their assessment of the situation and their plan for landing. Three specific questions had to be answered :

- What do you think is the problem with the aircraft?
- Which speed are you going to use on final?
- Where in the profile to land are you going to configure the aircraft for landing?

After this, the simulation was restarted and pilots were given the opportunity to execute the landing in the way they had just had explained. After landing the same experiment was repeated, but now with the  $V_c$  and fault detection system on, but without giving the pilots any information on the type of emergency. The failure was introduced again on downwind and now the fault detection software would notice the change in aircraft stability and control derivatives and alert the pilot with the message 'Manoeuvre'. At that moment pilots were instructed to give sinusoidal inputs in the all controls, and they were shown that the  $V_c$  indication was converging. Thereafter the landing was made with a speed based on the  $V_c$  indication.

## 8

#### DEPENDENT MEASURES

The following dependent measures were collected from the first run:

- Where in the profile the gear and flaps were selected;

- The actual speed on final;
- The amount of rudder on final;
- If asymmetric thrust was used.

On the second run, pilots were instructed to follow the controllability check and to use the  $V_c$  indicator to establish a safe approach speed. This gave them less freedom of action, so the only data that could be collected were their qualitative comments to relate this procedure to their initial approach to solve the problem.

#### HYPOTHESIS

In the first run there was no hypothesis to be tested, the aim was to collect data on how pilots would react to an unknown type of control problem without any additional guidance on the controllability of the aircraft. The second run was also not suited for hypothesis testing because there is also a bias because of the learning effect by the repeated scenario.

#### 8.7.2. RESULTS ASYMMETRY

The results are based on 17 pilots, because the first two pilots only had the scenario with the  $V_c$  displayed. In Table 8.5 the assumed cause is given in column 2. If gear and flaps were selected on final, the altitudes are given in column 3 and 4 respectively, 'dwnd' means the selection was done on down wind and 'C Ch' means the pilot decided to select gear and flaps at altitude in a control check. The rudder deflection during the final approach is given in column 6 and the last column indicates if asymmetric power was used. From this data the following observations can be made.

#### ASSUMED CAUSE

Not a single pilot could completely determine the actual cause, this was also intended. Not surprisingly, almost all pilots assumed some problem with a control surface, either rudder, aileron or flaps. However, those types of failure normally require a fixed control input, which does not change with airspeed. One of the participants remarked after experiencing the emergency: 'Not to worry because there was still adequate control'. A clear indication that no additional loss of control was expected at lower airspeeds.

#### CONTROLLABILITY CHECK

Only three pilots decided to do the controllability check. Two of them were active military pilots and the third was a civilian pilot with a military flying background. So, we see that those pilots just did as they were trained to do; one of the three had done the same controllability checks in an actual flight situation just less than a month ago.

#### CONFIGURATION CHANGE

Out of the 14 pilots that did not use the controllability check, only three decided to configure at downwind, another three decided to configure at long final and the rest decided to configure late. Of course all pilots did exactly as they were trained to do, or decided on this course of action due to lack of training in these type of emergencies.

Table 8.5: Pilot assessment and actions during combined asymmetry and partial aileron failure. Pilots with a military training background are marked with an (m) behind their number. For the configuration changes the acronym 'dwnd' means downwind and 'C Ch' means that the configuration change was done as part of the controllability check.

P	Assumed Cause	Gear Selection feet	Flap Selection feet	Final Speed KIAS	Rudder at final degr.	Asym Pwr
1	Aileron damage	800	550	90	10	yes
2	Roll/yaw problem	400	400	100	10	no
3	Heavy aileron	600	500	100	10	no
4	Jammed aileron	300	dwnd	95	5	no
5	Aileron or flaps	700	up	110	0	no
6	Jammed control	1050	300	90	4	no
7	Asymmetric drag	1000	1000	92	5	no
8	Some disturbance	dwnd	700	80	30	no
9	Limited aileron	500	dwnd	90	8	no
10	Aileron problem	1000	not	110	15	no
11	Control cables	dwnd	dwnd	83	10	no
12	Asymmetric Flap	dwnd	up	105	5	no
13(m)	Aileron problem	C Ch	C Ch	90	10	no
14	Aileron heavy	1000	up	110	6	no
15	Heavy aileron+ $\beta$	900	up	90	9	no
16(m)	Aileron problem	C Ch	C Ch	78	-5	yes
17(m)	Adverse yaw	C Ch	C Ch	90	20	no

### USE OF RUDDER

Pilots had the option to use rudder in order to counter the roll tendency. About 5° of positive rudder was needed to counter the adverse yaw caused by the aileron deflection (The exact amount depended on the actual speed). Nine pilots used more than 5° which is a good way to improve roll performance, and landing with a side slip is not uncommon. One pilot even used almost maximum rudder, this allowed for a safe low approach speed, but also an excessive side slip during landing. However, a safe landing was performed.

### USE OF ASYMMETRIC POWER

Only two pilots used asymmetric power. The first pilot used a little bit of thrust differential as a way to trim the aircraft. The second pilot, using the controllability check, was deliberately searching for a more balanced configuration, and discovered that with a large power differential full aileron control was regained and that even negative rudder was required to counter the asymmetric thrust. This pilot was very professionally applying the findings of the controllability check, while not necessarily aware that he was using the fact that the asymmetric thrust also generated asymmetric lift that countered the moment caused by the asymmetric mass distribution. This illustrates the fact that a pilot does not have to know what the cause of the problem is to find a suitable configuration to land the aircraft.

### RESULTS WITH $V_C$ INDICATION ON

The second run was a repeat of the first run but now with error detection and  $V_C$  display enabled. This part was primarily used as a demonstration that using the  $V_C$  indication a safe approach speed could be selected. All pilots were instructed to do the complete slow down and configuration at downwind, simulating that they were at a safe altitude over uninhabited terrain. Upon the error detection in the roll channel, pilots were instructed to perform the control inputs and were shown that the  $V_C$  slowly converged. After some time a second error detect was generated. This second detect was triggered by the yaw channel. The error in this channel is much smaller, therefore the detection software, as described in Appendix C, needs more time. Upon the second detect, the pilots were again instructed to perform control inputs. Finally, the approach was made at an airspeed close to the  $V_C$ , but not lower than the normal approach speed of 80 KIAS. The result of this effort is displayed in Table 8.6. During this approach pilots were also alerted by the supervisor on the effect of g-load on the  $V_C$  and the use of rudder. On this second approach seven pilots used asymmetric thrust and 6 pilots were now using more rudder deflection.

In this second run there was of course no surprise effect what would happen to the aircraft. However, all pilots were still unaware of the exact cause. Also, except for the three pilots that performed controllability check, they were unaware about the safety margins. For these pilots the second run was their first option to set a safety margin for their approach, so it is interesting to note how these margins changed.

Table 8.6: Improvement in safety per pilot when using the new display in final approach from 300 to 50 feet; Columns two and three shows the speed margin  $V_{tas} - V_c$ , a negative value indicates lack of sufficient roll capability. Columns 4 and 5 give the maximum aileron in the final approach phase, and columns 6 and 7 show the fraction of time the  $V_{tas}$  was below the  $V_c$ .

pilot	$V_{tas} - V_c$	$V_{tas} - V_c$	Max $\delta_a$	Max $\delta_a$	$V_{tas} < V_c$	$V_{tas} < V_c$
	old	new	old	new	old	new
1	<b>-10.0</b>	<b>-3.8</b>	38.2	46.4	0.8	0.6
2	22.7	0.2	41.8	43.0	0.3	0.7
3	17.5	0.0	27.1	0.0	0.0	0.0
4	23.5	26.5	27.3	34.2	0.0	0.1
5	43.1	<b>-15.6</b>	30.1	45.5	0.0	0.8
6	<b>-10.2</b>	27.9	52.8	42.5	0.6	0.0
7	<b>-7.7</b>	18.2	39.8	44.7	0.7	0.1
8	<b>24.8</b>	40.3	19.2	27.9	0.0	0.0
9	<b>-24.6</b>	9.6	34.5	24.9	1.0	0.0
10	44.8	24.5	10.2	41.2	0.0	0.1
11	<b>-28.2</b>	28.1	55.0	45.2	1.0	0.0
12	<b>-13.2</b>	12.4	33.1	11.9	1.0	0.0
13(m)	<b>-19.1</b>	15.9	35.1	31.8	1.0	0.0
14	<b>-29.2</b>	<b>-1.2</b>	18.0	32.9	1.0	0.5
15	<b>-9.8</b>	3.8	27.4	25.5	1.0	0.3
16(m)	18.0	19.0	24.6	35.7	0.0	0.0
17(m)	18.0	4.4	19.7	26.9	0.0	0.2
Mean	3.6	12.4	31.4	33.0	0.5	0.2

### SAFETY OF THE APPROACH

There were two indications of how dangerous the approach was. The first was the amount of  $V_c$  exceedance, and the second indication was the maximum aileron used. In Table 8.6 both are presented. The maximum available aileron deflection is  $60^\circ$ , however aileron effectiveness decreases rapidly above  $45^\circ$  as can be seen in Fig. 5.15 in Chapter 5. Table 8.6 shows that in two runs aileron deflection exceeded  $50^\circ$ , which is a clear indication that roll control was at the limit and wind shear or gust could easily have led to an excessive bank angle close to the ground with a risk of ground impact.

In Table 8.6 we can see that most pilots considerably increased the safety margin during the second run. Especially the mean time the  $V_{tas} < V_c$  changed in the second run. Some lines need further clarification. Pilot number three could, for personal reasons, not complete the last run with the  $V_c$  indication, therefore these data points are missing. Pilot 5 was the only pilot who had a considerable  $V_c$  exceedance in the second run and not in the first run. Further analysis showed that the first run was made at a very high speed ( $>110$  KIAS), which was of course above the  $V_c$ , but also quite high for landing. On the second approach he was invited to try a lower speed, however, he failed to use adequate rudder, which might also be attributed to inadequate instruction by the supervisor.

## 8.8. DISCUSSION

In this discussion let us first consider some conclusions and recommendations that were made by the Dutch Flight Safety Board [9] after the accident with El AL Flight 1862, on October 4, 1992. Finding number 9 reads:

‘Current standard industry training requirements and procedures do not cover complex emergencies like that encountered by El AL 1862.’

And recommendation 4.6 reads:

‘Evaluate and where necessary improve the training and knowledge of flight crews concerning factors affecting aircraft control when flying in asymmetrical conditions such as with one or more engines inoperative including: advantages and disadvantages of direction of turn limitation of bank; use of thrust in order to maintain controllability.’

And finally recommendation 4.10 states:

‘Expand the training of pilots and ATC personnel to include the awareness that in the handling of emergency situations not only the safety of aeroplane /passengers but also the risk to third parties especially residential areas should be considered.’

From these quotes it is clear that the handling of complex emergencies is in the interest of civil aviation. The military practice of using the controllability check is a good starting point for handling these emergencies, because it is not based on coping with or solving the emergency at hand, but it establishes the remaining manoeuvrability, re-

regardless of the type of emergency. It is, however, worrying to see that 24 years after the aforementioned accident this procedure is not known to most civilian pilots. This is of course not their fault, they fly as they are trained to, but is due to the fact that the regulating authorities have not implemented the accident recommendations into the training requirements.

Our prime objective was to see whether pilot control improves using the new display features in situations where the lateral control is impaired. To this end the different display options, including a new side slip indicator, a minimum lateral control speed indicator and a 'climb bar' were tested separately as well as combined in five different experiments using 19 pilots. In these experiments pilot performance with and without the new display features were compared to evaluate if the new display options would enhance safety and enable an efficient recovery from lateral control limited situations.

For the main findings we can differentiate between two types of scenarios: The familiar scenarios such as the one-engine-inoperative (OEI) climb out and the engine failure after take off, and the unfamiliar scenarios such as the OEI go-around at low speed and the asymmetry combined with an aileron failure. The OEI go-around is in itself not an unfamiliar scenario but it was done at such a low speed that it became a recovery from a roll limited situation, which was unfamiliar to all participating pilots.

The familiar failures were all handled quite well, and the new features had limited effect on the performance level in these scenarios. The only statistically significant improvement that could be measured was the decrease in the variance of the combined heading and side slip error when using the new slip indicator in the OEI climb out scenario. Furthermore, pilots appreciated having a climb bar in the engine failure after take off scenario, but it did not show significant improvements in either the safety, or the efficiency measures.

Handling of the unfamiliar scenarios was quite different. In the OEI go-around at low airspeed dangerous situations and even crashes did occur, and no statistically significant improvement was seen when pilots could use the climb bar and  $V_C$  indicator over the runs where these new features were not shown. It seemed that this scenario was too complex to be mastered in the available familiarisation time. Pilots were generally so absorbed in basic aircraft control that no or hardly any time was spent in looking at the new display items. Therefore an additional experiment was added, flown by nine participants, in which the OEI go-around was extensively trained using the new display features. These training sessions showed that 6 out of 9 pilots showed a decent training curve and were able to improve their performance, while using the  $V_C$  display and climb bar, while three pilots seems to need more training time than could be made available in this experiment.

This says absolutely nothing about the proficiency or ability of the pilots but proves that the handling of unknown and complex scenarios requires training. In this respect this scenario is not different from stalls, spins or unusual attitudes which are often part

of basic training<sup>6</sup>. An additional observation is that the number of pilot actions required in the one-engine go-around at low airspeed is higher than in the recovery from unusual attitudes, spins and stalls.

The final experiment evaluated the use of the new display features using a scenario with a damaged aircraft that had reduced lateral control due to asymmetric weight and a partial loss of aileron. Initially this experiment was done without the new display features to evaluate the 'natural' reaction of the pilot. This initial run revealed a difference between military and civilian trained pilots. Military trained pilots all performed the controllability check, safely at altitude, where they also configured the aircraft for landing, and were therefore able to derive a safe approach condition. Civilian trained pilots did not perform a controllability check and showed quite a variance in chosen approach speeds and altitudes where they configured the aircraft for landing.

This experiment was repeated with the new  $V_c$  indication available and where all pilots were instructed to perform a controllability check. In this experiment the  $V_c$  indicator proved to be a valuable tool to find a safe airspeed in case of an unknown failure. All qualitative comments of the pilots that for the first time performed the controllability check were positive, such as: 'Nice that you can see the  $V_c$ '.

Finally, this discussion would not be complete without the following observation: All participating pilots enjoyed taking part in this experiment, the tasks were challenging and asked a lot from their piloting skills. Everyone worked hard to perform to the best of their ability. Sometimes they got frustrated because the aircraft crashed in spite of their efforts. The most frequent comment after the completion of the test was: 'I learned a lot from this experiment and I would like to participate again'. For the author, this confirms his belief that pilots will not stand in the way when this type of training is added to the syllabus. The next step might be to convince the rest of the flying community to allocate training time and funds to incorporate these scenarios in pilot training. This thesis might be a step in that direction and might also inspire other researchers to tackle other control situations where pilot performance can be improved.

## 8.9. CONCLUSIONS

Based on the second series of pilot-in-the-loop experiments the following conclusions are reached:

1. The new side-slip display, which uses the variable size triangle, does not significantly improve pilot performance but does lower the variance. This indicates that the amount of excessive errors decreases.
2. The  $V_c$  indication and climb bar can help the pilot in recovering from 'roll limited situations' when this is combined with sufficient training.

<sup>6</sup>In the military training of unusual attitude, stalls and spins are done in basic training while in civilian training they are not always included or part of advanced training.

3. When the controllability check is done in case of a damaged aircraft with reduced lateral-directional control, this experiment shows that pilots can use this  $V_c$  indication to select a safe speed for approach and landing.

### 8.10. RECOMMENDATIONS

In practical tests one is always limited in time and not all conditions that are of interest can be evaluated. For future tests with the new display the following research items are recommended:

1. What is the effect of the new side slip indicator compared to operating the old side slip indicator, but now comparing pilots that use 'half a ball width displacement' in side slip with using the  $\beta$  display.
2. Research the effect of the 'Controllability Check' with and without  $V_c$  indication, using a set of different damage situations to counter the learning effect, and quantify the effect of the  $V_c$  on the safety of the recovery.
3. What is the transfer of training from the dedicated training of the controllability check to the actual behaviour of the pilot when confronted with an unexpected and unknown failure situation.

## REFERENCES

- [1] R. J. de Muynck and M. Van Hesse, *The A-Priori Simulator Software Package of the Piper PA34 Seneca III*, Tech. Rep. (TU Delft, 1990).
- [2] A. H. Roscoe and G. A. Ellis, *A Subjective Rating Scale for Assessing Pilot Workload in Flight: A Decade of Practical Use*, Tech. Rep. TR 90019 (Royal Aerospace Establishment, 1990).
- [3] G. E. Cooper and R. P. Harper, *The Use of Pilot Rating in the Evaluation of Aircraft Handling Qualities*, Tech. Rep. Report 567 (AGARD, 1969).
- [4] A. P. de Seversky, *Victory Through Air Power* (Garden City Publishing Co, 1942).
- [5] R. McGill, J. W. Tukey, and L. W. A., *Variation of Box Plots*, *The American Statistician* **32**, 12 (1978).
- [6] anon, *Online Statistics Education: An Interactive Multimedia Course of Study*, Tech. Rep. (Rice University, 2015)  
<http://onlinestatbook.com/2/index.html>.
- [7] anon, *Flying Light Twins Safely*, Tech. Rep. (FAA, 2008)  
<https://www.faa.gov/.../FAA%20P-8740-66%2>.
- [8] Anon., *US Navy Air Operations Publication (NATOPS)* (USNavy, 1995)  
<http://navyflightmanuals.tpub.com/P-1242/P-12420132.htm>.
- [9] anon, *FAA Lessons Learned*, Tech. Rep. (FAA, 1992)  
[http://lessonslearned.faa.gov/11\\_main.cfm?TabID=1&LLID=38&LLTypeID=2](http://lessonslearned.faa.gov/11_main.cfm?TabID=1&LLID=38&LLTypeID=2).



# 9

## **DISCUSSION, CONCLUSION AND RECOMMENDATIONS**



## 9.1. DISCUSSION

### 9.1.1. INTRODUCTION

The prevention and recovery from the loss of lateral-directional control has historically received much less attention than the recovery and prevention of longitudinal control, or stall prevention. However, the loss of lateral-directional control, especially for twin propeller aircraft, is a frequent accident cause. The focus on longitudinal control is also reflected in the instrumentation available to the pilot. For longitudinal control and stall prevention the pilot can, for instance, use the Angle of Attack (AoA) indicator. The AoA will give the pilot a measure how close he is in relation to the stall AoA, and this indication is valid for any g-level. For lateral-directional control the pilot is presently only given a fixed limit, the minimum control speed air or  $V_{mca}$ . In this thesis we researched if we could present the pilot with a better indication to prevent the loss, or assist the recovery from the loss, of lateral-directional control that will work in all flight situations, even when the aircraft is damaged.

#### CHOSEN MEASURES

The first step is to define lateral-directional control and find a measure for adequate lateral-directional control that is usable for pilots. In aircraft dynamics lateral control, or the roll control about the body X-axis, and directional control, the yaw around the top axis, are normally combined because these motions are coupled. We will however choose separate measures for lateral and directional control. In our research we exclude lateral-directional limits that are not related to control, because the combination of different flight envelopes in a single limit might become too restrictive as explained in Chapter 2.

In a normal flight situation, the required directional control can be defined as the ability to maintain zero side slip ( $\beta = 0$ ), even in a situation with maximum asymmetric thrust. For lateral control, roll limits can be used as defined in the Military Specification 8785C [1]. Our analysis showed that for a damaged aircraft the  $\beta = 0$  limit can be relaxed, aircraft can fly with a considerable  $\beta$  before departing directionally. The roll control authority for both a damaged and an undamaged aircraft can be based on Mil. Spec. 8785C using the minimum requirements set for the highest workload level. Our analysis showed that this lateral limit will normally be reached before the directional limit. Consequently, we can limit ourselves to providing the pilot with this lateral control limit. This lateral control limit can be linked to a minimum velocity, which makes the limit easily interpretable for the pilot. This minimum velocity can be based on different flight situations, for example using maximum asymmetric thrust and using maximum rudder control, or using just enough rudder to maintain  $\beta = 0$ . Because we wanted to present the pilot with feedback on his control actions, we chose to present the pilot with the minimum lateral control speed, which we named  $V_c$ , for the actual thrust setting and actual side slip angle  $\beta$ .

The next step was to predict the  $V_c$  accurately. The normal situation will be that the aircraft flies at a safe speed well above the  $V_c$  and therefore we need to know how aircraft characteristics change with airspeed. Especially effects of the propeller thrust and

induced flow are critical, because their influence increases with a decrease in airspeed. Furthermore, we needed a model that is usable for damaged aircraft, where the c.g., mass and inertia tensor may be unknown. Based on this model we derived an algorithm and applied corrections to enable an accurate  $V_c$  prediction.

### 9.1.2. $V_c$ PREDICTION- THEORY

#### VELOCITY DEPENDENCIES PROPELLER AIRCRAFT

For the prediction of the  $V_c$  it is essential to know how roll performance is influenced by velocity. Without any engine influence, the available roll moment would change with  $V^2$ . If we do take the thrust effect into account, the situation is different for jet and propeller aircraft. For jet-powered aircraft this relation is simple: thrust is almost constant over the speed range and the effect of induced airflow over the wing is small. For propeller aircraft the situation is different. Generally [2] one assumes that engine power is constant and because power is thrust times velocity, the propeller thrust is approximated by  $\frac{Power}{V}$ . Our analysis, based on the PA-34 model and the propeller model in Appendix B showed that this relationship overestimates the engine thrust at low speed but is reasonably accurate at higher speeds.

Another important effect of the propeller is the cross flow over the fuselage giving an additional moment around the top axis. This effect is usually [2] accounted for by multiplying the thrust moment by a factor  $k$  whose value depends on the turning direction of the propeller, its position on the wing and the placement of the wing relative to the fuselage [3]. Comparing the original wind tunnel results with tests performed with the RNLAF C-130 [4] showed that the effect was less linear with the normalized thrust than expected based on [3] which resulted in an overestimation of the cross flow effect at lower speed.

The last propeller effect investigated was the roll moment caused by the lift increase due to the induced airflow over the wing behind the working propeller. Normally this effect is accounted for by a constant  $C_{l_{TL,TR}}$ , where the subscript  $TL$  means left engine input and  $TR$  right engine input. Because this constant is multiplied by the normalized engine thrust, it assumes a linear relation with this normalized thrust. Investigating this effect more closely, using a propeller model to calculate the induced airflow, we found that the roll moment increases at low speed and should be modelled by  $\frac{Power}{V^2}$ <sup>1</sup> instead of  $\frac{Power}{V}$  as used for the propeller thrust. The consequence is that, if the standard normalization is used and the model parameters are based on tests at a higher airspeed, the predicted roll effect at low airspeed will be under-estimated.

The conclusion is that we should be careful with the use of the standard normalization of engine power to calculate the propeller effect. In the further evaluation, different normalizations were investigated for their suitability in predicting the correct  $V_c$  for the Piper Seneca aircraft. Also, for this effect an aircraft type-specific solution is required. The next question to be answered is whether the turn direction affects the roll perfor-

<sup>1</sup>But will not increase any further when  $C_L$  has reached its maximum value.

mance.

#### RELATION $V_c$ WITH ROLL ANGLE

In the pilot community, the question whether you can turn in the direction of the 'dead' engine is a heavily debated issue. It is obvious that the roll performance in the direction of the failed engine is much larger than into the opposite direction, therefore there is a serious risk of over-banking. However, the effect of the roll angle on the roll performance is quite low as our analysis showed. It is limited to the ' $C_{l_r}$ ' effect, the fact that the wing at the outside of the turn has a slightly larger velocity than the inboard wing. For the PA-34, compensating for this effect required no more than 2° additional aileron deflection. Therefore we conclude that, as long as the roll is made carefully, no restriction in the roll directions is needed.

#### MODEL DEVELOPMENT AND $V_c$ ALGORITHM

For the determination of the available roll control of a damaged aircraft we need a model where c.g., mass and inertia tensor are unknown. In Chapter 4 we developed this model based on the equations for a shifted reference point [5]. Based on the parameters of this model, the  $V_c$  algorithm and the needed corrections for the  $V_c$  calculations were developed. From the model parameters the airspeed for the minimum required roll performance could be calculated directly if thrust was constant and no lateral asymmetry existed. However, to account for thrust and slipstream effects of propeller driven aircraft and for lateral asymmetry, an iterative algorithm is required. Furthermore, corrections are needed to account for present roll rate and roll acceleration, as well as for the possibility that at the  $V_c$  speed,  $\beta = 0$  is no longer maintained because the rudder has reached maximum deflection. When this last situation arises, an additional correction is needed for the ensuing induced adverse yaw that will affect the roll performance. All these corrections were implemented in the  $V_c$  algorithm.

#### $V_{mca}$ VERSUS $V_c$

The above developed  $V_c$  is not a replacement for  $V_{mca}$ . Each limit has its own use.  $V_{mca}$  is a certification requirement while  $V_c$  reflects the resulting manoeuvrability considering the pilot inputs. However, our analysis did also reveal that the  $V_{mca}$  requirement can be defined more precisely.  $V_{mca}$  is based on a static equilibrium point, a steady heading side slip, with the most critical engine failed and the others at maximum power, using maximum rudder<sup>2</sup> and a bank angle not more than 5° away from the failed engine. Because the aircraft manufacturer has some freedom in choosing the bank angle, this limit does not equate to a fixed  $\beta$ . However, as we have seen in the example of the PA-34, this  $V_{mca}$  limit is very close to the velocity where  $\beta = 0$  can just be maintained. Therefore we may conclude that the  $\beta = 0$  limit, for the situation where the most critical engine<sup>3</sup> has failed, is a more precise requirement. Furthermore, the basic  $V_{mca}$  requirement in FAR23.149 does not define any lateral control, however, in FAR25.149 additional lateral control requirements are presented. But these conditions do not set a specific minimum

<sup>2</sup>The limit is either a full deflection or a maximum force of 150 lbs (Civil) or 180 lbs (Military).

<sup>3</sup>The most critical engine depends on the propeller turn direction, this is further explained in Appendix A

roll performance at  $V_{mca}$ . It would be more precise to define  $V_{mca}$  as the minimum velocity, where an aircraft with the most critical engine failed and the others at full power, can maintain  $\beta = 0$  and still has the required minimum roll performance.

### 9.1.1.3. OFF-LINE SIMULATIONS WITH THE PA-34

Up to this point we developed a theoretical framework that is not aircraft type specific. In the following step we evaluated and optimized our  $V_c$  calculation for the  $V_c$  prediction of the Piper Seneca. In Chapters 5 and 6 we used off-line simulations with a non-linear model described in [6]. This addressed two problems: Firstly the model size; due to the unknown mass, c.g. position and inertia tensor, the model has many variables. A possible anticipated risk was that parameter identification would converge slowly. Therefore we investigated if we could optimize the model size. Secondly, there are several choices possible for the optimum configuration of the  $V_c$  prediction algorithm, which needed to be addressed before the start of pilot-in-the-loop testing.

#### OPTIMUM MODEL SIZE FOR ROLL PERFORMANCE PREDICTION

There are several methods available to optimize the model size to get a good fit with the model data and the experimental data. For our objective: ‘the prediction of  $V_c$ ’ the aim is not to fit the model data with the experimental results but to make a good prediction that is outside the envelope where the data is collected. The two dimensions where the prediction is outside the ‘data collecting envelope’ are airspeed and control inputs. The typical scenario for which we develop the  $V_c$  prediction is a failure that occurs at cruise speed, while we want to calculate the minimum speed at which the pilot can make a safe approach<sup>4</sup>. During the cruise phase the pilot will avoid excessive control inputs, to minimize additional loads on the damaged aircraft. However, we must calculate the roll performance for maximum control inputs.

In Chapter 5 we investigated the traditional model size criteria such as ‘Akaike Information Criterion’ (AIC), ‘Bayesian Information Criterion’ (BIC), the partial F (Fisher) test, the coefficient of determination ( $R^2$ ) and the Predicted Squared Error (PSE). We showed that the above criteria use a (very small) relative improvement in the error variance. While this might be statistically significant, it lacks practical application. It is possible that a relatively small improvement in the error variance has an insignificant contribution to the actual  $V_c$  accuracy, while it is also possible that no significant improvement in the error variance can be achieved but that the  $V_c$  still has not reached the desired accuracy. Next we applied these methods for the optimization of the model size in the second step of the ‘two step method’ [7], which is a least squares approximation of the linearised model. Evaluation revealed that all standard methods selected too many model parameters, which degraded the accuracy of the prediction. Using an alternate method, that was based on the improvement of the final prediction, the number of the selected model parameters was much lower. This alternate method can however only be used in simula-

<sup>4</sup>The case that the failure occurs at approach speed is the easier problem which typically does not require prediction over a large velocity range.

tions where the outcome is known. The conclusion of this evaluation was that the model size should be based on simulations and that the real time model adaptation, based on standard model size selection criteria should be avoided.

Investigating the causes of over-fitting revealed that the accuracy of the linearised higher order parameters was the cause of the increase in prediction error. The only way to achieve a good accuracy for these parameters is to make large control inputs at lower speeds, however this is no longer a prediction of the  $V_c$  but a confirmation.

#### CONFIGURATION CHOICES AND $V_c$ PREDICTION ACCURACY

Based on the  $V_c$  algorithm, a  $V_c$  Prediction System (VPS) was designed in Chapter 6 to be used for pilot-in-the-loop testing. The VPS uses a Parameter Identification (PID) module, an error detection module, the  $V_c$  prediction module and the display. Several configuration choices had to be made: the type of PID, model size, normalization and initial values used.

For the PID the two-step method was used [7], however, in a simulation the first step, the determination of the state, can be omitted because the state is perfectly known. This leaves the second step, the approximation of the model parameters using recursive least squares (RLS). Four different RLS methods were compared, two normal RLS methods that required a reset after the detection of the failure, and two PID methods that used a forgetting algorithm (FA), which nullified the need for a reset.

The effect of model size was evaluated for three different model sizes, first the smallest model with 10 independent variables, second a model with thirteen independent variables which included as additional independent variables:  $\left(\left(\frac{pb}{2V}\right)^2 + \left(\frac{rb}{2V}\right)^2\right)$ ,  $\left(\frac{pb}{2V} \frac{qc}{2V}\right)$  and  $\left(\frac{pb}{2V}\right)^2$ . These parameters were selected because the alternate selection method of Chapter 5 chose these parameters most frequently. Third, the largest model was incorporated to confirm the earlier findings on model size with  $V_c$  accuracy calculations.

In developing the  $V_c$  algorithm, we had already found that the additional lift effect of the induced airflow, which causes the roll, is dependent on  $\frac{1}{V^2}$  instead of  $\frac{1}{V}$ . This was the reason to evaluate if an improved normalization could be used. The model parameters, derived at different airspeeds showed that three model parameters changed considerably with airspeed. These parameters were: the yaw due to roll ( $n_p$ ), the roll due to yaw ( $l_r$ ) and the roll due to engine power ( $l_{TL}$  and  $l_{TR}$ ). Based on the discovered parameter change over the speed trajectory, a new normalization was made that minimized the airspeed dependency. The new and old normalization were both used in the evaluation.

Finally, two sets of initial model parameter values were used based on 85 KTAS, the approach airspeed, and based on 120 KTAS, which is the standard cruise speed. Initial parameter values are required for two reasons. Firstly, they enable the VPS to start the  $V_c$  prediction right away, without having to determine the model parameters first. Secondly, normal pilot control is not sufficient for the determination of all required model parameters, e.g., the pilot will normally not use asymmetric power and consequently the

effect of roll due to power asymmetry is not assessed.

The total number of configuration options was 48 and these were all included in the evaluation. A good  $V_c$  prediction is accurate and on time. To evaluate if these requirements could be met, off-line simulations were performed with different failure scenarios using a non-linear model of the PA-34 [6]. To make these tests operationally relevant, smooth as well as turbulent flying conditions were simulated, with either one or two sets of control inputs to enable parameter identification.

The evaluation of the  $V_c$  prediction capability was done separately for engine failures and all other failures. This was necessary for two reasons, firstly the normal profile with power changes is not suited to measure the convergence of the  $V_c$ , every time power is adjusted the  $V_c$  changes. Secondly, the engine performance is in the model and does not require a reset nor changes in the model parameters. Three different model sizes, four PID methods and two different normalizations were compared as to their capability to predict  $V_c$ .

For the non-engine failures, the 22 variable model was the least accurate and showed the slowest convergence while the 13 and 10 variable model did not differ much in performance. The two RLS methods that used a reset (Standard RLS and modified Kalman MKM) performed better than the two RLS methods that used a forgetting algorithm. The effect of the improved normalisation was small. The best combinations were the RLS method with 13 variables and the standard normalization and the MKM method with 10 variables and the modified normalization.

The evaluation of the engine failures showed that for an engine failure the large models also predict well. This is logical, the engine performance is in the model, and when the model parameters are not adjusted it stays accurate. However, there was a large difference between the two forgetting algorithms. The standard FA diverged because of the constant adaptation of the model parameters while the forgetting algorithm with damping (FAD) worked quite well.

The overall performance of the  $V_c$  prediction was, however, below the desired accuracy. The desired accuracy was a mean absolute error in  $V_c$  of less than one knot ( $0.5m/s$ ), which is typically the reading accuracy of the speed indicator. In our evaluation the lowest mean absolute  $V_c$  error was  $1.9m/s$ . A further evaluation showed that this inaccuracy was due to a problem in accurately predicting the adverse yaw effect. It turned out that the important parameters to calculate the adverse yaw effect,  $n_p$  and  $n_r$  would diverge after a failure and very slowly converge back to the correct value. For a correct determination of the values of  $n_p$  and  $n_r$  large inputs and manoeuvres are required, which are typically avoided during failures. Two improvements were made: the first, an adjusted reset based on theoretical maximum values of a parameter, reduced the divergence of  $n_p$ . A second improvement was to predict the roll for a shorter time period,  $0.75s$  instead of  $1.5s$ . With these two improvements the mean absolute error could be reduced to  $1.0m/s$ .

Finally, it was found that turbulence was favourable for the RLS method that used a reset but unfavourable for RLS using a FA. For additional control inputs, the situation was reversed, FA methods did benefit with a faster convergence while for the RLS method there was only a reduction in the  $V_c$  error variance.

With the previous model evaluation the following choice was made for the pilot-in-the-loop evaluation. We chose the small model with 10 independent variables and used the Modified Kalman Filter for parameter identification. For the normalization we chose the standard option and the pre-set values based on 85 knots. Two pilot-in-the-loop test series were done. First the initial tests in October 2014, after which modifications were made in the display, and the final tests in August 2015.

#### 9.1.4. RESULT PILOT-IN-THE-LOOP SIMULATIONS

##### INITIAL TESTS

In October 2014 Pilot-in-the-loop experiments were conducted in the SIMONA research simulator at TU Delft. These tests are described in Chapter 7. In the simulator the model of the PA-34 was used, which was modified to enable control failures. In the tests 10 pilots participated who were all familiar with twin propeller aircraft. These initial tests were exploratory in nature and were intended to investigate if pilots could work with the new  $V_c$  indication to prevent and recover from situations with reduced lateral control. Additionally a new side slip indicator was installed in the centre of the Primary Flight Display, which was designed to be better noticeable, especially at larger side slip angles. The first two scenarios were One Engine Inoperative (OEI) scenarios, the first in a standard traffic pattern and the second was an OEI go-around. In both scenarios, the initial velocity was 10 knots below the standard OEI approach velocity, but above  $V_{mca}$ , to invoke situations with limited lateral control. The third scenario was a (partial) rudder hard-over that was used to evaluate if the pilot could work with an advisory system that calculated a new safe lateral control velocity. During these scenarios many  $V_c$  exceedances did occur and from these events and the pilot comments the following conclusions were drawn.

##### TRAFFIC PATTERN

From the traffic pattern scenario, 40 runs could be used for analysis. In 20 of these runs  $V_c$  exceedances occurred, the total number of separate exceedances was 43. In 22 of these 43 exceedances the speed was less than 78 KIAS, more than two knots under the recommended approach speed, however, this would only give a  $V_c$  exceedance if it was combined with full power. In 27 cases the adverse  $\beta$  was more than  $2^\circ$  at the start of the  $V_c$  exceedance and in 13 cases even more than  $4^\circ$ . This adverse  $\beta$  was never caused by reaching the rudder limit, because rudder deflection at the start of the  $V_c$  was in all cases less than the maximum value. This adverse  $\beta$  cause for  $V_c$  exceedance was not expected and indicated that correct rudder control in the traffic pattern was difficult for some pilots. This was also in line with pilots' comments that they often did not notice the new side slip display because they were more focused on the outside view. Eight out the ten pilots were also unaware of the possibility to use proverse yaw in order to increase lateral

control. The two pilots that did use proverse yaw were not doing this in relation to the  $V_c$  indicator but to minimize aileron deflection. From this scenario the most important result was that pilots need additional information on the available rudder to improve recovery from situations with reduced lateral control.

#### OEI GO-AROUND

Twenty three runs were analysed in the go-around scenario. In 8 out of 23 runs no  $V_c$  exceedance occurred at all, indicating that the pilot was using cautious throttle, using the  $V_c$  display and enough rudder. In the remaining 14 runs a total of 20  $V_c$  exceedances occurred. The reasons for the exceedances were: using insufficient rudder, too abrupt power application and inadequate energy management. The too abrupt power application was a one time event for which the  $V_c$  warning does not help, because it is based on present power settings. However, it also illustrates how an impulsive reaction can cause a dangerous situation even when flying well above  $V_{mca}$  and  $V_c$ . The findings on the proper use of rudder were similar to the traffic pattern scenario. Only in three  $V_c$  exceedances full rudder was applied at the start of the exceedance and in only three more instances full rudder was achieved at some point during the time of  $V_c$  exceedance. In other words, in 14 instances rudder was not used as a means to improve the lateral control and to lower the  $V_c$ . The major problem during the go-around was not the control of power to prevent  $V_c$  excursions or the control of side-slip. Rather, pilots overestimated the aircraft single engine climb performance. They increased the pitch angle too much when the gear was raised, which led to a fast speed bleed off and often to a reduction well below the initial 80 knots, and also below the present  $V_c$  value.

#### RUDDER HARD-OVER

This scenario was intended to see if the  $V_c$  calculation would enhance the safe recovery of a damaged aircraft. When the failure occurred, all pilots were unaware of the cause, except for one pilot. The required identification manoeuvres for the model parameter estimation had as side benefit that it helped the pilots in their analysis and to find a practical solution: to use differential thrust to counter the yaw. All pilots did find a safe approach speed with the help of the  $V_c$  indication and were able to make a safe approach with the damaged aircraft.

#### CHANGES MADE

Based on this initial test it was decided to add the  $V_c$  speed for maximum rudder. This way the pilots could be given an additional indication that additional rudder was available. Secondly, the climb angle to maintain constant speed was added to the display, to prevent pilots from selecting climb angles that would lead to a loss of airspeed.

#### 9.1.5. FINAL TESTS

Here the prime objective was to see if pilot control significantly improved using the new display features in situations where the lateral control is impaired. To this end four different scenarios were used. The first scenario was used to evaluate if the new side slip indication would enhance pilot performance. The chosen scenario was an OEI climb on a steady heading. The second scenario was the OEI go-around, similar to the previous

tests, but with the additional condition that 50% of the tests were performed at altitude without reference to a runway. The third scenario was the engine failure after take off (EFATO) and the fourth scenario was the handling of an unknown failure that limited lateral control. The chosen failure was a lateral asymmetry. Nineteen pilots participated in these tests, experience levels varied from recently graduated pilots to very experienced pilots with more than 10,000 flying hours. These test are described in Chapter 8. We will now discuss the results of each scenario separately.

#### SIDE SLIP TEST

Pilot performance was scored based on the combination of heading and velocity errors. Comparing the pilots' results for the different display options showed no significant improvement in the scoring ( $p \leq 0.05$ ). However, with the new display there were fewer extreme errors, and a significant decrease in variance. Taken combined with the pilots' preference for the centre display, we may conclude that this display could be beneficial, particularly when large side-slip excursions are present as in the initial part of the climb. Furthermore, pilots preferred the lateral acceleration display over the  $\beta$  display. A point for further research is to investigate how pilots would perform if they use the technique of 'half a ball width displacement', which is intended to fly close to zero  $\beta$  without a dedicated  $\beta$  indicator.

#### OEI GO-AROUND

The OEI go-arounds were performed with and without the new  $V_c$  display and climb bar in scenarios close to the runway and at altitude. It was noticed during these tests that this scenario was extremely difficult for the pilots. In training a go-around is normally initiated at the single engine climb speed (90 KIAS for the PA-34), but in this scenario the airspeed was the normal approach speed of 80 KIAS. This go-around from a lower airspeed was unfamiliar to all pilots. Furthermore there were large differences in the performance of individual pilots. Pilots commented that they liked the climb bar but it was only used when a climb was already established and not in the initial phase of the scenario to prevent airspeed loss. The  $V_c$  display was only positively commented upon by two out of 19 pilots during this scenario, most found it hard to use it to their advantage. In the safety and efficiency scores no increase between the runs with and without the new displays was achieved at the  $p \leq 0.05$  significance level.

Halfway during the test it already became apparent that the standard familiarisation run was probably inadequate in this scenario. For the remaining participating pilots an additional experiment was added at the end of the test to evaluate if pilot performance in the OEI go-around could be improved by more extensive training with the new display. This experiment, with 9 participants, showed that pilot performance did improve. It was also clear from the comments that pilots were using the climb bar and the  $V_c$  indication according to the instructions given. However, a (very) large part of the pilot attention is devoted to maintaining the aircraft level and countering the yaw, leaving little time to accurately position the climb angle, correctly position the throttles and raise the gear. Still, six out of nine pilots showed a good progression while three clearly required more time than could be given in this experiment. The overall conclusion of this scenario

was that the new display can help the pilot in the recovery from a lateral control limited situation, but only after extensive training.

### EFATO

Pilot performance in this (known) scenario was quite good with and without the new display. The data show that there are differences between the results with and without the new displays, but they never reach the required  $p \leq 0.05$  significance levels. On the other hand, pilots appreciated the climb bar and used it, which could be reason enough to further investigate incorporation into the aircraft.

### LATERAL ASYMMETRY

A sudden unknown damage to the aircraft was evaluated in two runs per pilot. In the first run the pilot was asked to 'act as he would do in real life' without any additional  $V_c$  display. In the second run the  $V_c$  was displayed and pilots were instructed to act in accordance with the 'controllability check' as described in [8]. There was a significant difference between three pilots with a military flying background<sup>5</sup> and the others. The first group carried out the standard controllability check on the first run and configured at altitude, allowing for a safe approach without configuration changes. The second group showed a large variety in procedures, generally configuring the aircraft was done late and approach speeds varied widely from excessively fast to dangerously slow. In the second run, when everybody followed the 'controllability check' and the  $V_c$  display was active, a considerably increased safety margin was achieved, which proves the validity of using the controllability check combined with a  $V_c$  display.

## 9.2. CONCLUSIONS

In summary the main conclusions are:

- There exists a hierarchy in flight envelopes, based on the urgency of pilot actions. Mixing flight envelopes with a different hierarchy should be avoided to prevent having overly restrictive limits.
- Impaired lateral-directional control normally leads to a roll departure and not to a yaw departure.
- The certification requirement for  $V_{mca}$  can be better defined on the capability to maintain zero side slip in the most limiting asymmetric power condition while being able to achieve the desired minimum roll performance.
- Prediction of roll performance for damaged aircraft requires reduced-size models.
- Recovering from a roll limited condition can be enhanced by presenting an adaptive minimum velocity, but will only work after extensive training.
- Pilots often have problems in establishing the right attitude in an OEI go-around. Displaying a 'climb bar' can ease this problem.

<sup>5</sup>Two were active military pilots and one was an ex-military pilot.

- Civil trained pilots should be trained in the controllability check, similar as is customary in military training.

### 9.3. RECOMMENDATIONS

The following recommendations are given:

1. Instead of basing  $V_{mca}$  on a steady heading side slip with a maximum bank angle using maximum asymmetric thrust, it is more logical to base it on the maximum of the two following speeds: (i) the speed required to maintain zero  $\beta$  with maximum asymmetric thrust and (ii) the speed required to give a minimum lateral control with maximum asymmetric thrust.
2. Pilots of twin engine aircraft should be trained in the recovery from lateral control limited situations.
3. Civilian pilot training programs should incorporate the 'controllability check' in their training syllabus.
4. Further research is needed to quantify the effect of the 'controllability check' with and without  $V_c$  indicator on the handling of unknown failure situations, and also the transfer of 'controllability check' training on the handling of a pilot of unexpected failure situations.
5. Further research can establish the effect of the new and old side slip indicators, e.g., comparing 'the half ball width' displaced procedure with using  $\beta$  indication.

## REFERENCES

- [1] Anon, *Military Standard, Flying Qualities of Piloted Airplanes; MIL-STD-1797*, Tech. Rep. (DoD, 1987).
- [2] J. A. Mulder, J. C. van der Vaart, and M. Mulder, *Atmospheric Flight Dynamics* (Technical University Delft, Faculty LR, 2007).
- [3] J. Manné, *N.L.L. Rapport A 1508 B; Windtunnel Investigation on the Influence of the Aircraft Configuration on the Yawing and Rolling Moment of a Twin Engined, Propeller-Driven Aircraft with one Engine Inoperative*, Tech. Rep. (NLR, 1963).
- [4] M. J. T. Schroijen, L. L. M. Veldhuis, and R. Slingerland, *Propeller Empennage Interaction Effects on Vertical Tail Design of Multiengine Aircraft*, *Journal of Aircraft* **47**, 1133 (2010).
- [5] P. H. Zipfel, *Modeling and Simulation of Aerospace Vehicle Dynamics* (AIAA, 2007).
- [6] R. J. de Muynck and M. Van Hesse, *The A-Priori Simulator Software Package of the Piper PA34 Seneca III*, Tech. Rep. (TU Delft, 1990).
- [7] M. Laban, *On-line Aircraft Model Identification*, Ph.D. thesis, Technical University Delft (1994).
- [8] Anon., *US Navy Air Operations Publication (NATOPS)* (USNavy, 1995)  
<http://navyflightmanuals.tpub.com/P-1242/P-12420132.htm>.

# A

## PROPELLER-INDUCED FLOW EFFECTS ON CONTROL

### PROPELLER AIRCRAFT PERFORMANCE

An often used approximation of the thrust of a propeller-driven aircraft [1, p. 458] is  $T = \frac{P}{V_{true}}$ , where  $T$  is engine thrust and  $P$  is engine power. This approximation is relatively accurate at higher velocities but can not be correct at lower airspeeds because then thrust would go to infinity at  $V_{true} = 0$ . Because we are especially interested in the controllability at low speed, a closer look is required.

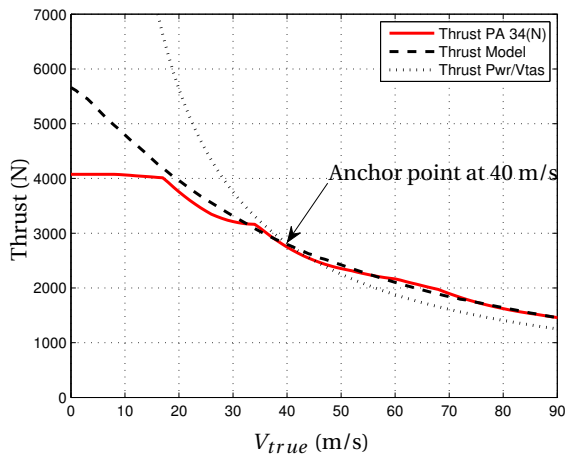


Figure A.1: Thrust of a PA-34; Comparing three models: the non-linear model based on [2], the blade model (Appendix B) and the  $\frac{P}{V_{true}}$  approximation from [1, p. 458].

In Fig. A.1 a comparison is made between three thrust models. The first is the thrust

as calculated by the non-linear PA-34 model that we used in our simulations.[2] This model uses look-up tables and first calculates the available engine power. Based on engine power and propeller characteristics, it calculates the thrust. Noteworthy is that thrust increases with decreasing airspeed but remains almost constant below  $18m/s$ . This is due to the fact that in the propeller graphs, the thrust coefficient will not increase further when the advance ratio ( $\frac{V}{(rpm/60)\pi D}$ ) drops below a certain value. The second model is based on a program made by the author that uses the blade strip method. This model is presented in Appendix B. Based on the propeller size and its lift and drag coefficient, an iterative method is used that adjusts the propeller pitch and induced flow until an equilibrium is reached where all power is absorbed and the induced air flow is stable. The data of this program fit the PA-34 model quite well at airspeeds above  $20m/s$ . For this simulation  $C_L$  and  $C_D$  were based on the NACA 5406 profile, while the propeller blade area was tuned to match the PA-34 data at  $40m/s$ . The third model shows the result if we assume that  $T = \frac{P}{V_{true}}$ . For the last model we used the thrust level at  $40m/s$  as anchor point. Fortunately the models are reasonably close at speeds above the stall speed. However, we have to realize that the standard used  $\frac{1}{V}$  relationship is only valid around the 'anchor point'. For the experimentally derived  $V_{mca}$  this relationship is unimportant, but if we want to calculate  $V_{mca}$  and  $V_c$  based on engine thrust, this relationship with airspeed is important.

#### THRUST AND INDUCED FLOW

A second point of interest is the induced airflow, or slipstream, of propeller-driven aircraft. From the thrust we can estimate the induced airflow based on Newton's momentum equation Thrust =  $\dot{m}\Delta V$ , where  $\dot{m}$  is the mass flow through the propeller, that can be estimated by:

$$\dot{m} \approx (V + 0.5V_{ind}) \rho 0.25\pi D^2 \quad (\text{A.1})$$

Eq. A.1 is based on the assumption that half of the airflow acceleration occurs before the propeller, and is therefore contributing to mass flow, while the other half of the acceleration happens behind the propeller [3, p.15]. In Fig. A.2 the induced flow presented is derived using the propeller blade element method. From the induced flow over the wing the additional lift can be estimated to be:

$$\Delta L = 0.5\rho\bar{c}D(V_{ind}^2 + 2V_{ind}V)C_L, \quad (\text{A.2})$$

where  $D = 1.93m$  is the diameter of the PA-34 propeller,  $\bar{c} = 1.61$  is the mean aerodynamic chord of the PA-34 and  $V_{ind}$  is the induced airflow. The lift is also affected by the swirl generated by the propeller. The upward moving blade will increase the AoA, while the downward moving blade will decrease AoA and lift. If we assume that the aircraft is in the linear part of the  $C_L$  curve, we can expect that these effects will cancel each other. Consequently, the additional lift generated will remain the same but the moment around the body axis depends on the turn direction of the propeller. The consequence is that the Outward Up (OU) turning blade will generate a larger roll moment than the Inward Up (IU) moving blade because the OU turning blade has the highest AoA at the largest distance from the aircraft centre line. For level flight,  $C_L$  can also be written as

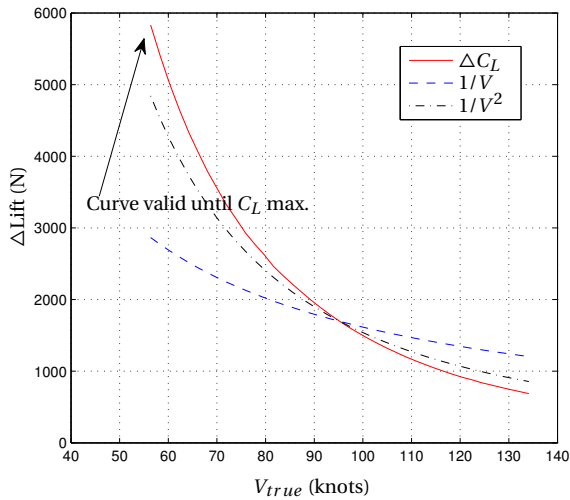


Figure A.2: Additional lift caused by propeller slipstream for the PA-34 using maximum power. Graph only valid until maximum  $C_L$  is reached. The  $1/V$  and  $1/V^2$  curves are 'anchored' to the  $\Delta L$  at 97.2 knots.

a function of  $V^{-2}$  because  $C_L = \frac{mg}{0.5\rho V^2 S}$ , and we can change Eq. A.2 in a form that only depends on  $V_{ind}$  and  $V$ .

The slipstream-induced additional lift is calculated for the PA-34 with a mass of 1900 kg and is presented in Fig. A.2. The results are of course only valid until the maximum  $C_L$  is reached. As illustrated in Fig. A.2, the effect can be approximated by a  $\frac{c}{V^2}$  curve. This means that the velocity effect of the asymmetric thrust on the roll moment,  $\frac{c}{V^2}$ , is much stronger than the effect on the yaw moment, which is  $\frac{c}{V}$ . The consequence is that, using the standard normalisation of propeller thrust ( $\frac{P}{V^3}$ ) to predict the roll moment at lower speeds, we may under-estimate the roll effect. A solution can be to use a different normalisation for the engine thrust if it is applied for the roll coefficients rather than for yaw parameters. This option is further explored in Chapter 6.

#### CROSS FLOW AT THE VERTICAL TAILPLANE

Research by Mannée [4], [5] revealed that the yaw moment of a propeller aircraft was much larger than could be expected based on engine thrust. Wind-tunnel tests using a model with and without a vertical tail revealed that installing the vertical tail could more than double the yaw moment. This additional yaw moment was dependent on the engine position and turn direction of the propeller. A low wing with a low placed propeller had less additional moment than a high wing with a high placed propeller. This effect can be explained by the fact that the cross flow is at its maximum in the horizontal plane of the slipstream and when this plane is situated higher, it affects a larger part of the vertical tail. A good description of the flow at the vertical tail is given in [6]. When the engine is placed more outboard, the additional yaw moment becomes smaller. This effect is explained in [7] and [6] by the fact that the flow originates from the difference in wing

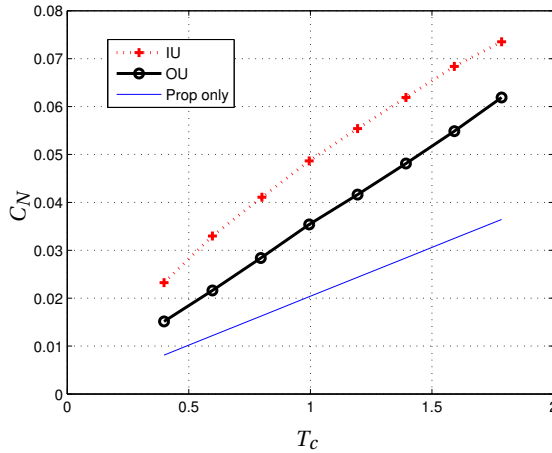


Figure A.3: Mannée [5]: Effect  $T_c$  on  $C_N$  for Inboard Up (IU) and Outboard UP (OU) turning propellers compared to the effect without vertical tail for a high wing configuration

loading, consequently, when the engines are placed further apart, the pressure gradient is less and the cross flow will be smaller.

#### CROSSFLOW AND PROPELLER TURN DIRECTION

A surprising effect was that turn direction of the propeller had a major influence on the cross flow. The IU turning propeller created a much larger moment than the OU turning propeller. The results of Mannée for the high wing configuration is shown in Fig. A.3. Instead of using the actual thrust, the non-dimensional thrust coefficient  $T_c$  is used, which is defined as  $\frac{T}{qS}$ .

The interaction of the propeller swirl with the cross flow on the vertical tail has been extensively studied, however, results of e.g., [6] show that there is still a considerable difference between the calculated moment, based on potential flow and Reynolds Average Navier Stokes (RANS) simulations, and wind-tunnel experiments. For our analysis, we are interested in the effect of this cross flow on the aircraft controllability. Here it is less important what source is used, than to know its dependency on airspeed or  $T_c$ . Fig. A.3 shows the effect of the IU and OU propeller. This figure supports the procedure [1] to account for cross flow by multiplying the calculated propeller moment, based on engine thrust and arm, with a constant that is different for the IU and OU propeller. However, the effect on the IU propeller is less linear at the higher  $T_c$  values.

This non-linear effect in wind tunnel tests also manifests itself in flight tests. In [7] the results are presented from a test flight performed in 2002 with a C-130H of the Royal Netherlands Air Force. In [7] the results are compared with predictions based on potential flow theory. In Fig. A.5 we have plotted the cross flow effect against airspeed that was derived from flight tests with the RNLAF Hercules. The Hercules has right turning

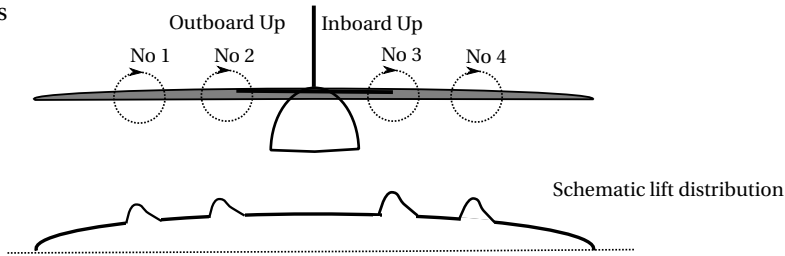


Figure A.4: Rear view of the C-130 with propeller numbers, propeller turn direction and schematic lift distribution over the wing due to propeller slipstream effect.

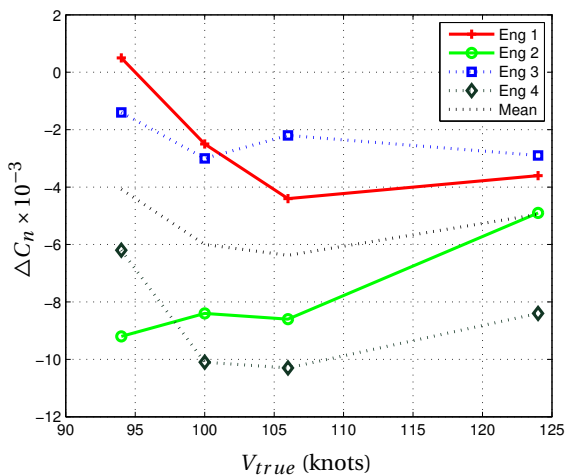


Figure A.5: The cross flow effect as function of the failed engine and  $V_{true}$ . Data based on a test flight with a RNLAf C-130H in 2002. The Hercules has right turning propellers, consequently the left engines (1 and 2) are OU and the right engines (3 and 4) are IU.

propellers, consequently the left propellers (1 and 2) turn OU and the right propellers (3 and 4) IU ( See Fig. A.4).

#### EFFECT OF FEATHERING ON CROSS FLOW

Fig. A.5 shows the effect of the feathering of one engine on the calculated cross flow moment. This cross flow moment was calculated by subtracting the thrust moment from the total aircraft yaw moment, while the total yaw moment was derived from the rudder deflection required to maintain zero side slip. This zero side slip angle was derived during a gliding flight with all engines at idle. Surprisingly, almost all moments were negative. Surprisingly, based on the results of Mannée (Fig. A.3) one would have expected a failure (and feathering) of number 3 engine, giving less lift and consequently more pressure above the wing at the position of engine 3, would enable a cross flow with a positive  $\beta$ , giving an increasing  $C_n$ . However, apparently the cross flow effect of the outside engines

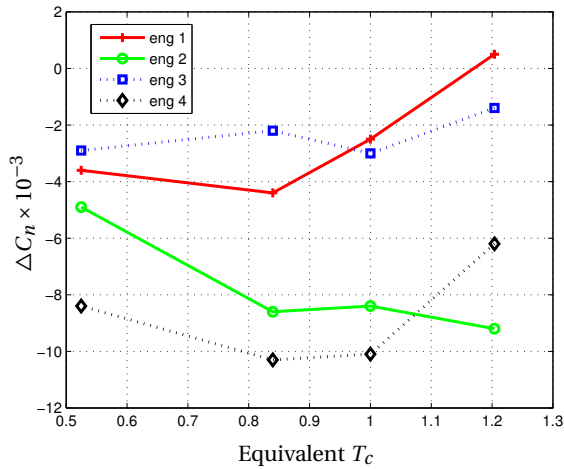


Figure A.6: The cross flow effect caused by failing one engine as function of equivalent  $T_c$ . The  $\Delta C_n$  is calculated by subtracting the engine moment from yaw moment based on  $\delta_r$ . Data are based on a test flight with a RNFAC C130H in 2002

and the turning direction of the number two propeller more than compensated for this<sup>1</sup>. This feature was also confirmed by the calculated change in moments from [7] using potential flow calculations. Assuming that we can superimpose the data from the different failures, the average value is indicative for the cross flow moment of the C-130H with all engines running. This negative cross flow moment is caused by the difference in moment generated by the IU and OU propellers as predicted by [5]. A problem is that the dependency on airspeed seems to be different for each engine. To be able to compare these data with the results from Mannée, the cross flow moments were also plotted against equivalent  $T_c$ . If we assume that power is constant and thrust can be approximated by  $\frac{P}{V_{true}}$  then  $T_c = \frac{c}{V^3}$  where  $c$  is a constant. In Fig. A.6 the results are plotted against  $T_c$ .

Fig. A.6 differs considerably from the wind tunnel results. Based on the results of [5] one would expect the cross flow effect to be linear with  $T_c$  for the outward up propeller and almost linear for the IU propeller, but decreasing at the higher  $T_c$  levels. Some of the probable causes are inaccuracies in the measured  $\beta$  and the derivation of  $T_c$ . In the flight experiment with the C-130H the  $\beta$  was determined by a tuft of cloth fixed to the left windshield and marking the zero position on the windshield with the engines at idle. Given the fact that the C-130H is not equipped with a  $\beta$  indicator this was the optimum solution, but the authors rightly argue that the accuracy is not high, probably  $1^\circ$  at most, which is equivalent to  $2.2 \times 10^{-3}$  change in  $C_n$  or in the same order as the cross flow effect.

Another contributing factor could be the calculation of the  $T_c$ . We previously dis-

<sup>1</sup>But the  $\Delta C_n$  caused by feathering number 3 was the least negative  $\Delta C_n$ .

cussed the effect of the propeller blade on the angle of attack of the wing behind it, but the AoA of the wing also influences the propeller blade AoA. From [8] we know that with an increase in aircraft AoA, the up-wash increases and this up-wash will increase the AoA of the down going blade, while decreasing the AoA of the up going blade. This will not only change the moment arm of the thrust, decreasing the arm for the OU propeller and increasing it for IU, but will also cause a small decrease in  $T_c$ . The problem is that the  $T_c$  value is calculated from engine power charts and propeller efficiency charts. The propeller efficiency charts use pressure ratio ( $C_p = Pwr \times \rho N^3 D^5$ ) and advance ratio  $J$ , but do not correct for AoA. The consequence is that the calculated cross flow could be incorrect because the wrong thrust moment is subtracted at the low speed points where the AoA and  $T_c$  value reach their maximum.

This last effect is also confirmed by tests performed by the USAF Test Pilot School in 1985, in which the author participated [9]. These tests evaluated the possibility of using non-dimensional methods to derive  $V_{mca}$  for propeller aircraft. The tests showed that there were non-linear effects in the relation between required rudder deflection and the change in the engine moment coefficient  $C_{n_e}$  that could also be caused by AoA.

#### CONCLUSION ON THE CROSS FLOW EFFECT

The wind tunnel tests by Mannée showed that a linear relation between  $C_N$  and  $T_c$  exists for the OU propeller, but that for the IU propeller the relation is less linear with a decreasing slope at higher  $T_c$  values. Flight tests show that more non-linearities exist that could be due to AoA changes. Because the wind tunnel tests from [5] and [7] are performed at fixed AoA, it is not surprising that these differences do show up. For the correct theoretical derivation of the  $V_{mca}$  the exact relation between  $C_N$  and  $T_c$  must be known for each AoA as well as the exact relation between  $V_{true}$  and  $T_c$ .

These results are also important for the real-time derivation of the minimum lateral control velocity in this thesis. For these derivations we can conclude that if the yaw moments at low speed (and high  $T_c$ ) are extrapolated from measurements at a higher speed (and low  $T_c$ ) the yaw effect could be exaggerated. This situation might occur if we perform aircraft parameter identification at high speed to predict the controllability at a lower speed. Fortunately this means that the controllability would be underestimated. We err on the side of safety.

#### REFERENCES

- [1] J. A. Mulder, J. C. van der Vaart, and M. Mulder, *Atmospheric Flight Dynamics* (Technical University Delft, Faculty LR, 2007).
- [2] R. J. de Muynck and M. Van Hesse, *The A-Priori Simulator Software Package of the Piper PA34 Seneca III*, Tech. Rep. (TU Delft, 1990).
- [3] G. J. D. Zondervan, *A Review of Propeller Modelling Techniques Based on Euler Methods* (Delft University Press, 1998).
- [4] J. Manné, *N.L.L. Rapport A 1508 A; Windtunnel Onderzoek naar de Invloed van de*

- Vliegtuigconfiguratie op Gier- en Rolmoment ten Gevolge van het Uitvallen van een Motor Bij een Tweemotorig Schroefvliegtuig*, Tech. Rep. (NLR, 1962).
- [5] J. Manné, *N.L.L. Rapport A 1508 B; Windtunnel Investigation on the Influence of the Aircraft Configuration on the Yawing and Rolling Moment of a Twin Engined, Propeller-Driven Aircraft with one Engine Inoperative*, Tech. Rep. (NLR, 1963).
- [6] M. J. T. Schroyen, L. L. M. Veldhuis, and R. Slingerland, *Propeller Empennage Interaction Effects on Vertical Tail Design of Multiengine Aircraft*, *Journal of Aircraft* **47**, 1133 (2010).
- [7] M. J. T. Schroyen and R. Slingerland, *Propeller Slipstream Effects on Directional Aircraft Control with One Engine Inoperative*, in *Collection of Technical Papers - 45th AIAA Aerospace Sciences Meeting, Reno, USA, January 8–11*, Vol. 18 (2007) pp. 12592–12604.
- [8] L. L. M. Veldhuis, *Propeller Wing Aerodynamic Interference*, Ph.D. thesis, Technical University Delft (2005).
- [9] L. P. Trottier, H. J. Koolstra, G. K. Bruce, T. H. Thacker, J. P. P., and H. H. Reda, *Limited Static Air Minimum Control Speed Testing using the Thrust-Moment-Coefficient Method*, Tech. Rep. (USAF TPS, Edwards AFB, CA, 1985).

# B

## PROPELLER SIMULATION

### INTRODUCTION

In the derivation of the  $V_c$  algorithm for propeller aircraft (Chapter 3) it is important to know how the thrust and the induced airflow change with airspeed. Quite often a simple relationship as  $T = \frac{P}{V}$  is used where  $T$  is the thrust,  $P$  is the engine power and  $V$  is the true airspeed. To get a better understanding of the airflow and thrust generated by a propeller as function of the aircraft airspeed, this program was made. The general idea is that the propeller performance can be estimated by calculating the lift and drag, based on the NACA profile, of a representative blade segment. The program is iterative as can be seen in Fig. B.1. In the inner loop the induced inflow velocity is calculated, after the inflow velocity has stabilized the pitch is adjusted that power required equals the power available.

### INPUT VARIABLES

The following input parameters are required:

1. Shaft Horse Power SHP  $\Rightarrow P_a = SHP \times 750 Nm/s$ ;
2. Rpm  $\Rightarrow \omega = Rpm \times 2\pi/60$ ;
3. Radius spinner ( $r_1$ ) in meter;
4. Radius propeller ( $r_2$ ) in meters;
5. Aspect ratio of the propeller blade (AR);
6. Number of blades (n);
7. Air density ( $\rho$ )  $kg/m^3$ ;
8. NACA profile look up tables for  $C_L$  and  $C_D$  as function of  $\alpha$ .
9. The  $V_{tas}$  range for the calculation.

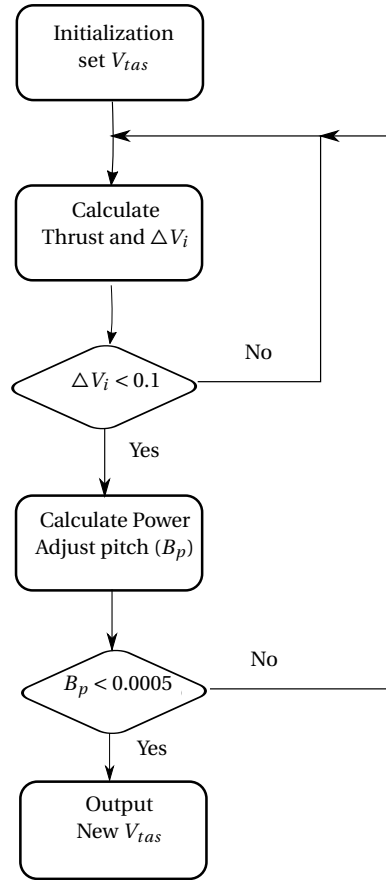


Figure B.1: The flow diagram of the propeller performance program.

### INITIALIZATION

For the effective radius  $R_e$  75% of the propeller is often used. In this program we use the quality that the relative airspeed over the blade increases with the radius and hence its thrust with the radius squared. The effective radius is then:

$$R_e = \sqrt{\left(\int_{r_1}^{r_2} r^2 dr\right) / (r_2 - r_1)} \quad (\text{B.1})$$

Which equates to:

$$R_e = \sqrt{(1/3)(r_2^3 - r_1^3) / (r_2 - r_1)}; \quad (\text{B.2})$$

The affected area in the air stream  $S = \pi(r_2^2)$ .

The total blade area  $S_b = ((r_2 - r_1)^2 / AR)n$ .

The radial velocity at the effective radius;  $V_r = \omega R_e$ .

The initial estimates for the first  $V_{tas}$  are made before starting the iterative calculation. These estimates are:

1. Initial maximum lift estimate:  $L = 0.5\rho S_b 1.37V_r^2$ ;
2. Estimated initial inflow based on  $L = \dot{m}\Delta V$ , where the mass flow for  $V_{tas} = 0$  is  $\dot{m} = dVS/\rho$ , which gives  $dV = \sqrt{(2L)/(S\rho)}$ ;
3. Estimated initial propeller blade pitch angle  $B_p$  is based on an AoA of  $17^\circ$  giving:  $B_p = \arctan(0.5\frac{dV}{V_r}) + 17\pi/180$ .
4. Improved inflow velocity:  $V_e = \sqrt{V_r^2 + dV^2}$ .
5. Estimated initial lift is:  $L = 0.5\rho S_b 1.37V_e^2$ ;
6. Estimated initial drag is based on the maximum  $C_D$  value:  $D = 0.5\rho S_b 0.0365V_e^2$ ;
7. Estimated angle ( $\theta$ ) of the relative wind with the propeller blade plane is:  $\theta = B_p - 12\pi/180$ ;
8. Estimated propeller thrust is then:  $T_p = L\cos\theta - D\sin\theta$ .
9. Estimated propeller drag at  $R_e$  is:  $D_p = D\cos\theta + L\sin\theta$ .
10. Estimated required power ( $P_r$ ) is:  $P_r = \omega R_e D_p$ .

If the power available is larger than this power required at maximum angle of attack and for maximum drag, the program is halted in order to adjust either engine power or the propeller dimensions.

#### CALCULATING THE INFLOW

In the inflow calculation the pitch is fixed and  $V_i$  is adjusted until  $\Delta V_i < 0.1\text{ m/s}$ . The lift and drag coefficients are from NACA look up tables based on AoA. The calculation is based on the concept that 50% of the induced airflow speed is realized in front of the propeller and 50% behind the propeller. Therefore only 50% of  $V_i$  is used to calculate the mass flow which is  $((V_{tas} + V_i/2)\rho S)$ . The loop is exited when the change in  $V_i$  is smaller than 0.1 m/s. The calculation steps are:

1. Calculate relative air velocity:  $V_x = V_{tas} + V_i/2$ ;  $V_e = \sqrt{V_x^2 + V_r^2}$ ;
2. Calculate angles:  $\theta = \arctan V_x/V_r$ ;  $\alpha = B_p - \theta$ ;
3. Retrieve  $C_L$  and  $C_D$  by interpolation from NACA tables;
4. If  $\alpha$  is greater than the maximum of the tables, which might occur as a result of the iteration, the  $C_L$  and  $C_D$  are extrapolated to prevent instability. To prevent negative lift at high AoA  $C_L$  above the stall angle will never be less than  $C_L = 2 \sin \alpha$ .
5. Calculate lift and drag:  $q = 0.5\rho V_e^2$ ;  $L = qC_L S b$ ;  $D = qC_D S b$ ;
6. Convert to thrust:  $T_p = L \cos \theta - D * \sin \theta$ ;
7. Recalculate  $V_i$  based on thrust and mass flow:  $V_i = -V_x + \sqrt{V_x^2 + 2T_p/(S\rho)}$ ;
8. For stability the new  $V_i$  is averaged with the previous  $V_i$ ;

#### ADJUSTING PITCH

The pitch adjustments are made to make the required power equal to power available. The required power is:

$$P_r = \omega R_e (L \sin \theta - D \cos \theta) \quad (\text{B.3})$$

The initial iterative adjustment ( $\Delta B_p$ ) is given by:

$$\Delta B_p = ((P_a - P_r) / P_r) \alpha \quad (\text{B.4})$$

For the following iterations the effect of the change of  $B_p$  on the change in  $P_r$  is used:

$$B_p = 0.4 * (P_a - P_r) * (B_{p_{prev}} / (P_r - P_{r_{prev}})) \quad (\text{B.5})$$

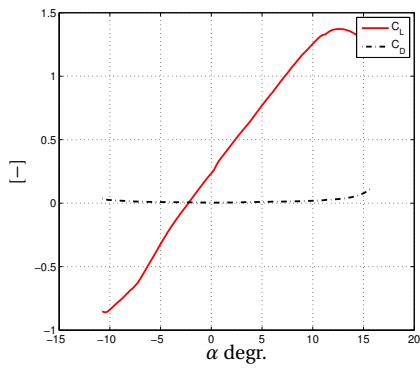
where the suffix 'prev' indicates the value from the previous step.

#### RESULTS

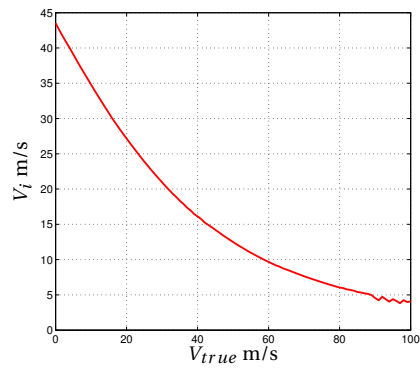
Next the results are presented for a propeller and engine that are close to the PA-34 specifications. The program settings are presented in Table B.1 and the simulation results are presented in Fig. B.2.

Table B.1: Specifications

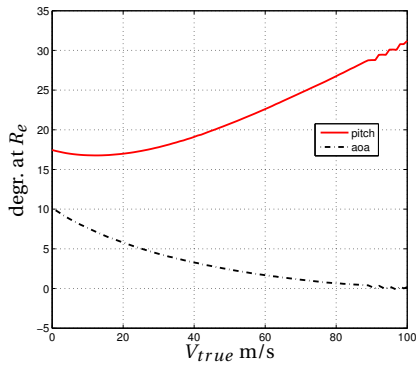
Shaft Horse power	211
rpm	2600
Radius spinner	0.20m
Radius propellor	0.965m
Number of blades	2
Aspect Ratio blade	4.1
Blade profile	NACA 5406



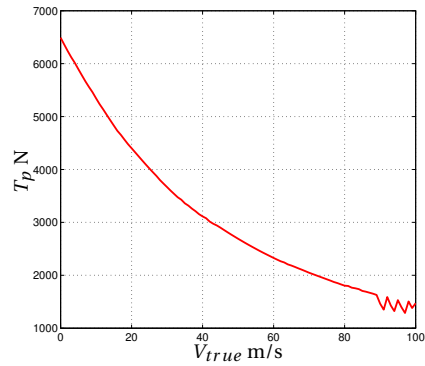
(a)



(b)



(c)



(d)

Figure B.2: Result simulation with propeller blade element program for the data of Table B.1; (a)  $C_D$  and  $C_L$  for NACA 5406; (b) Induced velocity in slipstream; (c) AoA and pitch change at  $R_e$ , (d) Thrust.



# C

## ERROR DETECTION IN REALISTIC SCENARIOS WITH LATERAL CONTROL PROBLEMS

### C.1. PROBLEM OUTLINE

When aircraft model parameters suddenly change, e.g., due to equipment failure or damage to the aircraft, parameter identification is essential to the determination of the flight envelope. Parameter identification methods that use a sliding window or a Forgetting Algorithm (FA) automatically adjust to a change in the parameter(s), but are consequently less stable [1]. Other methods, such as Recursive Least Squares (RLS) and the Modified Kalman Method (MKM) do not discard old data and are therefore more stable, but will adjust slowly when parameters change. However, when these latter methods use a covariance matrix reset (MKM), or a  $P$  matrix reset (RLS), on the detection of a failure, the gain is temporarily increased and the innovations become larger, while the initial value of the parameters is not affected. Through this reset, the stability of these methods can be combined with a quick adaptation to the changed model parameter(s).

The standard failure detection methods [2] use the innovation, the difference between the predicted and measured state as input for the detection method. Innovation Based Methods (IBM) [2] can use the mean value, its auto-correlation, or its variance. In earlier research [3] these detection methods have shown problems with turbulence, noise and lack of excitation in cruise flight. Lack of excitation will give very low innovation values. Consequently a sudden large input results in a considerable increase of the innovation. This might be mistaken for the detection of failure although the innovation is actually small in relation to the input. Turbulence and noise have a different effect. They will increase the average error level and can either hide parameter changes or give multiple false alarms. The effect of turbulence and noise can be reduced by increasing the sample size, however, this will also decrease the visibility of a failure that manifests

itself only during a short control input.

The purpose of our research was to select, modify or develop a reset mechanism for parameter identification to achieve the following characteristics:

- Fast detection of failure;
- No false alarms;
- Ability to work in turbulence;
- Capability to identify both slow and abrupt failures;
- Identifies the parameters that have changed.

## C.2. SPRT FOR ERROR DETECTION

### THE CONCEPT

Searching for a fault detection method we found the Sequential Probability Ratio Test (SPRT) described in [4]. The SPRT was designed to measure a sudden change in an observed parameter and can be used directly on the observed innovation. However, our intent was to detect a change in the model parameters. Because the model parameters are not directly observed we needed an additional step to convert the innovation to control parameter errors. We developed two methods for transforming innovation to control parameter errors. These two methods are the direct division (DD) method and the projection (P) method. The combinations SPRT-DD and SPRT-(P) can theoretically determine the error in each model parameter. This enables a precise reset of the covariance matrix. A block diagram of the method is depicted in Fig. C.1. In this appendix we have chosen to use the MKM as the parameter identification method. The differences between RLS and revised MKM are small and already explained in Chapter 6.

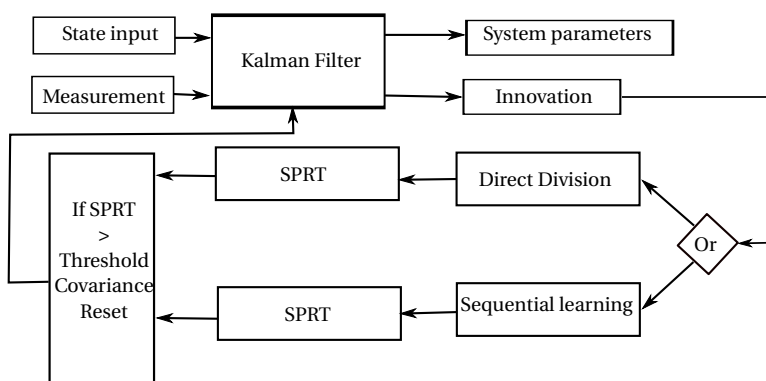


Figure C.1: Block diagram of the concept.

## OVERVIEW

In this appendix the following steps are taken. First, a short overview of the SPRT method will be given, explaining its most important characteristics. Next the direct division and projection method will be derived. Thereafter the improvements and settings developed in [5] and [6] will be discussed. Finally the performance of the two SPRT based methods will be compared with the results of innovation based methods; for this evaluation we will use the same Piper Seneca runs as used in Chapter 6.

### C.2.1. THEORY

There have been many studies during the last century on change detection algorithms. In [4] many change detection algorithms are presented from which we have chosen to use the Sequential Probability Ratio Test (SPRT) developed by Page in 1954. The basic concept is briefly repeated here and we use the same notation as the authors of [4]. The main point is to explain the unique features of this routine for change detection. For a full description we refer to [4].

SPRT is based on the log likelihood ratio. If the measured parameter  $y$  has a probability distribution  $p\theta_0$  before the change and  $p\theta_1$  after the change, the log likelihood ratio of measurement  $i$  is defined as:

$$s(y_i) = \ln \frac{p\theta_1(y_i)}{p\theta_0(y_i)} \quad (\text{C.1})$$

In the case of the following Gaussian distribution:  $\theta_0$  with mean  $\mu_0$ ,  $\theta_1$  with mean  $\mu_1$  and a common standard deviation  $\sigma$  the log likelihood ratio of sample  $y_i$  is:

$$s(y_i) = \frac{\mu_1 - \mu_0}{\sigma} \left( y_i - \frac{\mu_0 + \mu_1}{2} \right) \quad (\text{C.2})$$

This example illustrates that  $s(y_i)$  is negative when  $y_i$  is closer to  $\mu_0$  than to  $\mu_1$ . Therefore the cumulative log likelihood  $S_j^k = \sum_{i=j}^k s_i$ , will be a continuously decreasing function under distribution  $p\theta_0$ . Consequently a change may be detected by the change in sign of the mean value of the log likelihood ratio, and the exceeding of the cumulative sum (cusum) of a pre-set value can be used to detect the time of change.

For the same Gaussian distribution as used for Eq. C.2 the combined likelihood ratio for samples  $j$  to  $k$  is the product of the likelihood ratio of the samples and equates to:

$$\Lambda_k^j = e \left[ b \bar{S}_j^k - \frac{b^2}{2} (k-j+1) \right], \quad (\text{C.3})$$

where:

$$\bar{S}_j^k = \frac{1}{\sigma} \sum_{i=j}^k (y_i - \mu_0), \quad (\text{C.4})$$

and the Signal to Noise Ratio (SNR),  $b$  is defined as:

$$b = \frac{\mu_1 - \mu_0}{\sigma} \quad (\text{C.5})$$

In the case of a damaged aircraft neither the magnitude nor the direction of the parameter change is known. To account for that uncertainty, by [7] the idea was introduced to weigh all possible  $\theta_1$  values. There are several possibilities, e.g., a uniform or a Gaussian distribution, however a simple and useful realization is the distribution of the mean values,  $F(\theta) = F(\mu)$ , over two points,  $(\mu_0 - \nu)$  and  $(\mu_0 + \nu)$ . In this case, the weighted likelihood ratio for a Gaussian distribution becomes:

$$\tilde{\Lambda}_j^k = \int_{-\infty}^{\infty} e^{\left[ b\tilde{s}_j^k - \frac{b^2}{2}(k-j+1) \right]} dF(\nu) \quad (\text{C.6})$$

Because the probability density function has only two points, the integration becomes the summation of these points or:

$$\tilde{\Lambda}_j^k = e^{\left[ -b\tilde{s}_j^k - \frac{b^2}{2}(k-j+1) \right]} \cdot \frac{1}{2} + e^{\left[ b\tilde{s}_j^k - \frac{b^2}{2}(k-j+1) \right]} \cdot \frac{1}{2} \quad (\text{C.7})$$

This can be changed to:

$$\tilde{\Lambda}_j^k = \cosh\left(b\tilde{s}_j^k\right) e^{-\frac{b^2}{2}(k-j+1)}, \quad (\text{C.8})$$

and after taking the logarithm we arrive at the decision function to be used:

$$g_k = \ln \cosh\left(b\tilde{s}_j^k\right) - \frac{b^2}{2}(k-j+1) \quad (\text{C.9})$$

An important parameter of the cumulative sum is the sample size. If the sample size is small, only large deviations will be detected. If the sample size is large, small changes can be detected but detection may take much longer. Several options are available for the sample size: weighted average over time with a forgetting function, the sliding window approach or the SPRT. The reason to choose the SPRT is that it uses an adaptive sample size. It exploits the fact that under the  $\theta_0$  distribution the log likelihood ratio is always decreasing. The routine restarts every time when  $g_k < 0$ . If the log likelihood ratio is positive,  $g_k$  will continue to increase until a pre-set threshold (the alarm level) is exceeded. This makes the decision function into a SPRT capable of detecting large, small and slowly developing parameter changes. The sequential steps are:

$$N_k = N_{k-1} + 1 \quad (\text{C.10})$$

$$\tilde{S}_k = \tilde{S}_{k-1} + \frac{y_k - \mu_0}{\sigma} \quad (\text{C.11})$$

$$g_k = -\frac{1}{2}N_k b^2 + \ln(\cosh(b\tilde{S}_k)) \quad (\text{C.12})$$

The alarm time is defined as the first time  $g_k$  exceeds the pre-set threshold  $h$ .<sup>1</sup>

<sup>1</sup>The calculation of  $\ln(\cosh(\tilde{S}_k))$  by computer can easily exceed the floating point accuracy, leading to incorrectly establishing the value to infinity. Therefore it is prudent to use  $|S_k| + \ln(0.5)$  for values of  $S_k$  larger than 10.0 instead of  $\ln(\cosh(\tilde{S}_k))$ . The error will be less than  $2.2 \exp -8\%$

$$t_a = \min\{k : g_k \geq h\}, \quad (\text{C.13})$$

and if  $g_k < 0$ ,  $N_k$  and  $S_k$  are both reset to zero.

### C.2.2. ERROR DETECTION IN CONTROL AND STABILITY PARAMETERS

The SPRT method is capable of detecting changes in the observed parameters. However, the model parameters are not directly observed. The essence of our addition to the SPRT method is to find ways to transform the observed error between prediction and measurement to parameter errors, in such a way that the SPRT method can be used to detect changes in the system parameters. The transformation to parameter updates is precisely what Kalman filtering does, however, when the values in the covariance matrix are low, this update is small and the adaptation slow. The essence of our method is to transform the full innovation to parameter errors and let the SPRT detect if the change in the parameter(s) is significant.

The system used for the parameter identification with the modified KF[8] is:

$$\dot{Z} = M\Theta + v, \quad (\text{C.14})$$

where  $\dot{Z}$  is the vector of measured state derivatives,  $M$  is the block diagonal matrix with in each block the extended state as a row vector. The extended state augments the state with the control inputs,  $v$  is the noise vector and  $\Theta$  is the column vector containing the system parameters. When one or more of the control parameters in  $\Theta$  change the system can be reformulated as:

$$\dot{Z} = M\Theta + M\Delta\Theta + v \quad (\text{C.15})$$

Assuming that the Kalman gain is low, and therefore  $\Theta$  is only slightly adjusted, the summation over  $N$  samples gives:

$$\sum_{i=1}^N P_r + \sum E = \sum M\Theta + \sum M\Delta\Theta + \sum v, \quad (\text{C.16})$$

where  $P_r$  is the predicted  $\dot{Z}$ , which is equal to  $\sum M\Theta$ ;  $E$  is the innovation, the difference between measured and predicted  $\dot{Z}$ . Under the assumption of zero mean noise  $\sum v$  will approach zero. This gives the equality:

$$\sum E \approx \sum M\Delta\Theta \quad (\text{C.17})$$

This value of  $\Delta\Theta_i$  is the input for the SPRT. Before the change occurs its mean ( $\mu_0$ ) is 0 and it changes to an unknown value  $\mu_1$ . It is assumed that the failure (e.g. a single aileron failure) is affecting only the value of the parameter (e.g.,  $l_{\delta a}$ ) and not its variance  $P(i, i)$ . This does not imply that variance can not be influenced by turbulence or other factors, but that it is not influenced by the failure. Solving Eq. C.17 for  $\Delta\Theta$  if the time of change would be known is simple, it can be done with a standard least square approximation. However, the issue at hand is to use this to estimate the time of change.

### DIRECT DIVISION METHOD

The first approach we developed is named Direct Division, this method divides the error by  $M$ :

$$y_{i,j} = \frac{E_j}{M_{i,j}} \quad (\text{C.18})$$

To prevent the SPRT value to become  $\infty$ , a minimum value had to be set for the input  $M(i, j)$ . Some of the extended state parameters are quite small, necessitating a low minimum value. However, a very low minimum value increases the noise. On the other hand, during a large part of the flight trajectory, some of these extended state parameters are small and a too rigid threshold can eliminate most of the data. A solution to this problem was found in [6] by changing the original equation C.18 to:

$$y_{i,j} = E_j \frac{M_{i,j}}{M_{i,j}^2 + \eta} \quad (\text{C.19})$$

In these equations  $y_{i,j}$  is the input value for the SPRT calculation,  $E_j$  is the error of row  $j$ ,  $M_{i,j}$  is the extended state parameter  $j$  of row  $i$  and  $\eta$  is the cut-off value of the independent parameter. By using this equation  $M_{i,j}$  values much smaller than  $\eta$  will cause  $y_{i,j}$  to approach 0 and not lead to noisy inputs, while for much larger  $M_{i,j}$  values the effect is almost similar to equation C.18.

### C

### PROJECTION METHOD

A second approach is to use the projection of the innovation on the input [5]. If  $\hat{x}$  is the measured extended state vector and  $e$  is the innovation vector then the projection of the error on the extended state vector is:

$$\text{Projected error on the input} = \frac{\hat{x}}{\hat{x}^T \hat{x}} e \quad (\text{C.20})$$

The expectation of the change in model parameter is:

$$E(\Delta\theta) = \frac{1}{N} \sum \frac{\hat{x}}{\hat{x}^T \hat{x}} e \quad (\text{C.21})$$

Two things are noticeable: Firstly this correction is identical to the Kalman gain (Eq. 6.9) for a single row where  $M$  is replaced by  $\hat{x}$ ,  $R = 0$  and  $P = I$ . Secondly, the method to perform parameter identification based on this projection, but multiplied with a fixed constant  $\alpha$ , ( $0 < \alpha < 1$ ) is called the Sequential Learning Method in [8]. Sequential Learning is an older method for parameter identification in non-linear models. Therefore we will use this name 'Sequential Learning' (SL) for the combination of the projection method with single variable SPRT. In our SL method we use  $\alpha = 1$  to project the full error. Similarly as DD, this transformed error can be incorporated into the same SPRT algorithm.

In [6] it was discovered that this method did not work when the input parameters differ in order of magnitude. To overcome the problem with extremely large or small parameters, a normalization had to be used that did not change the basic characteristics of the SL method. The important characteristic, which must be maintained in normalization, is that  $\hat{x}^T SL(i) = e(i)$ . Therefore the normalization has the following form:

$$SL(i) = \frac{N\hat{x}}{\hat{x}^T N \hat{x}} e(i), \quad (\text{C.22})$$

where  $N$  is the normalization matrix. The normalization equation has similarity to the Kalman gain equation, but there the normalization is done with the covariance matrix and the measurement covariance  $R$  is added. However, the Kalman gain is a correction based on the uncertainty of the parameter, while our normalization is a correction for the magnitude of the extended state variables. Therefore the normalization should give all extended state variables the same order of magnitude. The normalization matrix  $N$  is a diagonal matrix, the value of the diagonal elements was based on the mean value of each independent variable in typical runs.

### C.2.3. SETTINGS, IMPROVEMENTS AND RESULTS

#### SNR SETTINGS

The first setting to discuss is the Signal-to-Noise Ratio (SNR). The expectation was that a too low SNR value might cause false alarms and a too high value might make the system insensitive to small errors. Evaluation in [5] and [6] showed that the SNR setting for the SL and DD method were not critical. The results for  $SNR = 0.1$  to  $SNR = 6$  show similar behaviour, detection occurs at the same time and the difference between the affected and not-affected parameters is also similar. However, the absolute SPRT value is directly related to the SNR setting. This effect proved to be linear between  $0.3 < SNR < 13$ . The consequence is that the detection threshold for the SPRT must be chosen in conjunction with the SNR setting.

#### THRESHOLD SETTINGS

The threshold level was based on the maximum SPRT levels for each parameter in the 8 runs without failure and in 8 runs with left or right engine failures. This maximum SPRT level was multiplied by 1.5 to achieve the threshold level. The runs included flight in turbulent as well as in smooth flying conditions. The engine failure runs should not lead to high SPRT values because the engine performance is incorporated in the model, but engine failures do generate sudden attitude changes and are therefore a good test for the robustness of the detection methods.

Because the influence of turbulence on threshold levels is large, it is important to choose relevant, but not extreme, turbulence conditions. However, exploring the effect of turbulence in the PA-34 aircraft showed that the main influence for the threshold level was the engine failure and not the turbulence. Part of the explanation might be that the engine failures caused already large excursions. It is important that threshold levels are determined based on experiments that encompass all relevant conditions.

Because every parameter has its own unique SPRT value, based on the residue of its row, the inputs of its related independent parameter and its variance, it is logical to use separate threshold values for each parameter and not a single threshold per row, which will lead to a delayed detection as shown in [6].

### RESETS

Initially the intent was to detect the changed parameter and to reset only the covariance for the affected parameter. The evaluations in [6] show that a single parameter covariance reset is not feasible in the case of a failure that gives a constant error (like an asymmetry or a rudder hard-over), but seems possible for control failures and all other changes that give a fluctuating error. One way to cope with this problem is to revert back to row resets, another option investigated was the use of individual resets per parameter based on the individual thresholds of those parameters. Unfortunately this did not work either. Even in the case of a simple 50% aileron failure, the correct parameter was initially reset, but if further resets were not suppressed during the new stabilization period, the reset was followed by incorrect resets in other parameters, influencing the errors of the remaining parameters and eventually leading to a continuous reset process as illustrated in Fig. C.2 rather than to a stable calculation of the lateral control envelope.

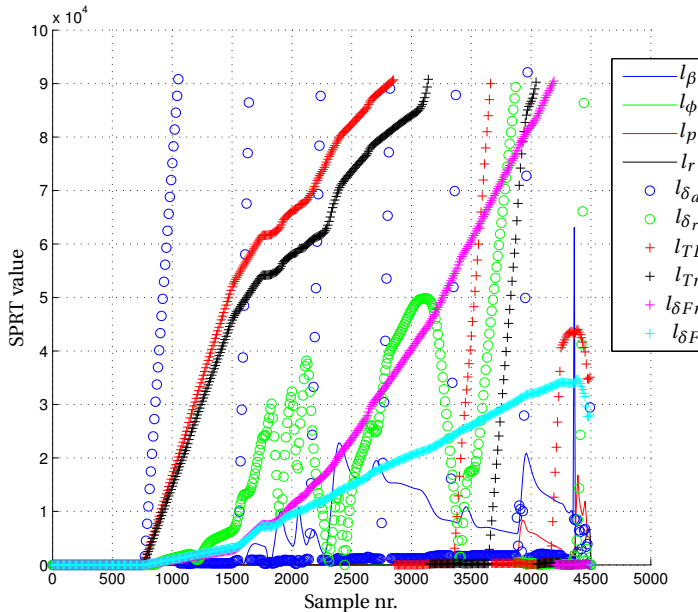


Figure C.2: Effect of individual parameter resets for SPRT SL, run is lateral asymmetry of the Citation aircraft in smooth flying conditions [6].

### IMPROVEMENTS

With the above described settings, evaluation runs were made with PA-34 model in [6]. It turned out that, with the exception of rudder failures, all failures could be detected. Investigation revealed that threshold value for  $n_{dr}$  is quite large due to engine failures. This high threshold levels for  $n_{dr}$  is to be expected because continuous rudder inputs are required to minimize the side slip during an engine failure. Because we could not lower

the threshold as this would introduce false alarms, a different solution had to be found. The solution found and tested was to incorporate a second threshold, not based on the SPRT level, but on its rate of increase. The threshold level for this rate test was again based on flights with and without engine failures in smooth and turbulent conditions. The rate algorithm uses a damping, based on a sample rate of  $25\text{Hz}$ , it is:

$$SPRT_{rate}(i) = 0.95SPRT_{rate}(i - 1) + 0.05(SPRT(i) - SPRT(i - 1)) \quad (\text{C.23})$$

This extra threshold check proved to be very effective. Not only did it made the rudder failures more detectable, but the detection time for all failures decreased.

### C.2.4. RESULTS

#### INNOVATION BASED METHODS

Finally we like to compare the new methods with the traditional methods based on the residue. When we evaluate the residue to detect failures we can use the mean[3], the variance or the auto correlation[2]. In order to reduce the noise, e.g. due to turbulence, all IBM based methods need to be averaged over a sample size. But the effect of sample size will be different for each type of failure. For control failures the residue is only large during control applications and using a large sample size will decrease detectability of the control error. Asymmetries give a constant residue and increasing the sample size will increase the visibility of the asymmetry error. We evaluated four different samples sizes  $N = 25, 50, 100$  and  $200$ . For these evaluation we used the same PA-34 failures as used in Chapter 6 and determined the number of correct detections. The results are presented in Table C.1.

Table C.1: Effect of sample size on correct detections for innovation based methods. Total number of runs is 32.

N	Mean	Auto Cor.	Variance
25	0	2	2
50	0	2	2
100	12	2	2
200	7	2	2

This evaluation showed that both the variance and the auto correlation based method detected only two failures out of the 32, and these detections were also very late, more than two minutes after the failure. The best IBM method was the mean. A closer investigation revealed that from the twelve detects using a sample size of 100, eight detections were within 10 seconds after the failure and four were more than two minutes after the failure. From the 7 detects using a sample size of 200, only two were within ten seconds after the failure and the remainder was more than 90 seconds after the failure. This makes the sample size of 100 the best choice.

The large number of missed detections is due to the high error level in runs with tur-

bulence and in runs with engine failures. This effect is graphically shown in Fig. C.3. Fig. C.3a shows the three IBM errors for a 50% aileron failure in smooth flying conditions. In this situation the aileron failure is clearly visible. However, the threshold levels has to be based on the error levels encountered in turbulence condition without failures (Fig. C.3b), as well as engine failures in smooth flying conditions (Fig. C.3c) and engine failures in turbulent flying conditions (Fig. C.3d).

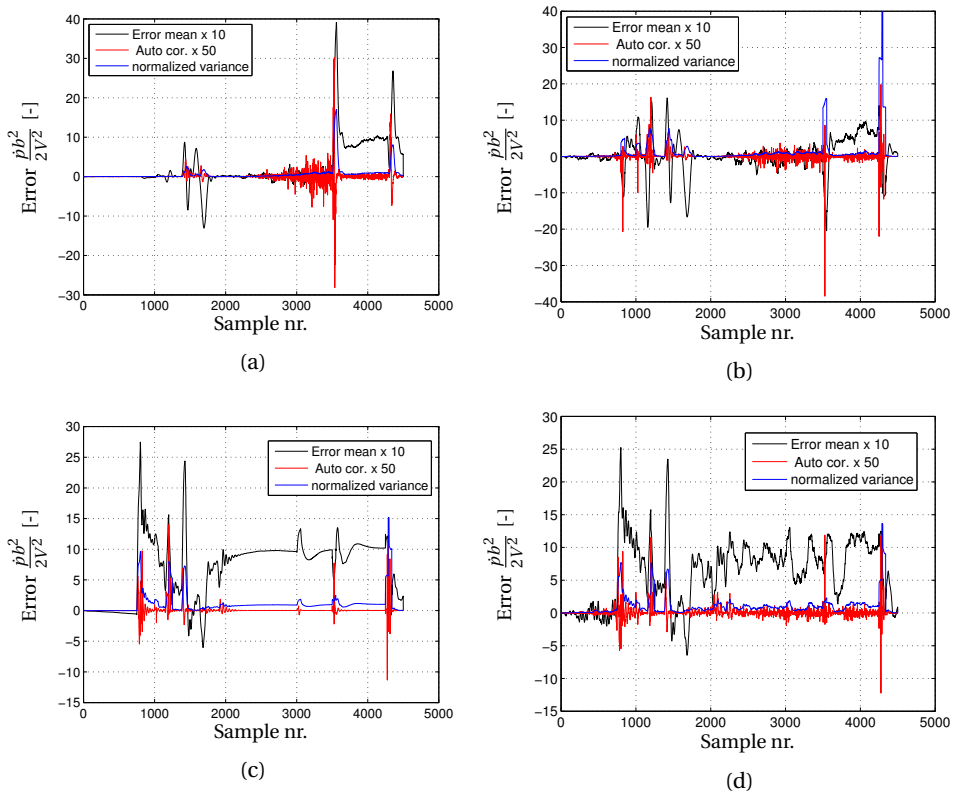


Figure C.3: Mean, Auto correlation and variance error in roll channel for different runs: (a) 50% aileron failure in smooth flying conditions, (b) non failure profile in turbulent flying conditions, (c) engine failure in smooth flying conditions and (d) engine failure in turbulent flying conditions.

### SPRT BASED METHODS

The results of the SPRT based methods are summarized in Table C.2. The most important finding is that both the SL and DD method did not miss any detection at all. There is a slight difference between the two methods but the results of both methods are acceptable.

The results in Table C.1 show that the rudder failure detection takes the longest. This is due to the fact that rudder applications are small and limited. The detection is therefore delayed till the first large rudder input. The difference in detection time between SL

Table C.2: Detection time in seconds after the occurrence of the failure for the different types of failures. Total number of runs is 32.

Failure	SPRT DD	SPRT SL
50% aileron failure	10.9	5.4
Rudder failure	29.5	29.9
Lateral Asymmetry	1.2	0.5
Rudder Hardover	1.3	1.3

and DD for an aileron failure is due to the fact that the DD detection in turbulent flying condition is slower.

### C.2.5. CONCLUSION

Firstly, our research showed that SL and DD were both capable of detecting all failures. A second finding was that single parameter resets instead of row resets did not work, even in simulations where the correct parameter was identified. Therefore it was necessary to use the row reset. Thirdly, adding an additional test for the rate of change of the SPRT value prevented missed detection of rudder failures in the PA-34 simulations and aided in the faster detection for both the DD and SL methods. The SPRT-SL method was incorporated in the real time simulation described in Chapters 7 and 8 because it gave the fastest error detection. Finally, both SPRT methods proved to be significantly better than the traditional residue based methods.

## REFERENCES

- [1] C. Kamali, A. A. Pashilkar, and J. R. Raol, *Evaluation of Recursive Least Squares Algorithm for Parameter Estimation in Aircraft Real Time Application*, Aerospace Science and Technology **1**, 165 (2011).
- [2] C. Hajiyev, *Fault Diagnosis and Reconfiguration in Flight Control Systems* (Kluwer Academic Publishers, 2003).
- [3] H. J. Koolstra, H. J. Damveld, and J. A. Mulder, *Envelope Determination of Damaged Aircraft*, in *Proc. of the AIAA Guidance, Navigation, and Control Conference 2012, Minneapolis, USA, Aug. 13-16* (AIAA, 2012).
- [4] M. Basseville and I. V. Nikiforov, *Detection of Abrupt Changes: Theory and Application* (Prentice-Hall, Inc, 2004).
- [5] H. J. Koolstra, H. J. Damveld, and J. A. Mulder, *An Improved, Turbulence Proof, Reset Mechanism for Parameter Identification after System Change*, in *Proc. of the 2013 AIAA Guidance Navigation and Control Conference, Boston, USA, Aug. 19-22* (2013).
- [6] H. J. Koolstra, C. C. de Visser, and J. A. Mulder, *Effective Model Size for the Prediction of the Lateral Control Envelope of Damaged Aircraft*, in *Proc. of the AIAA Guidance, Navigation, and Control Conference, the AIAA SciTech Forum 2015, Kissimmee, USA* (2015).
- [7] M. Pollack and D. Siegmund, *Approximations to the Expected Sample Size of Certain Sequential Tests*, Annals Statistics **3**, 1267 (1975).
- [8] D. Graupe, *Identification of Systems* (Robert E. Krieger Publishing Company, 1976).

# SUMMARY

In commercial and general aviation, Loss of Control in Flight (LOC-I) has been the major cause of fatalities over the past years. Over the last decades several efforts have been made to mitigate this problem such as improved flight control systems, pilot stall training and unusual attitude recognition and recovery. This thesis researches whether the pilot response to an impending loss of lateral-directional control can be improved. This thesis focuses on twin engine propeller aircraft. These aircraft are the most limited in lateral-directional control, especially during loss of an engine. It was tested whether, similar to the way an Angle of Attack (AoA) indicator can warn for impending stall, a warning can be given for an impending loss of lateral-directional control.

Investigating research done in the field of safe-flight envelopes, it became clear that many researchers combine different envelopes. Furthermore, the categorisation of the envelopes is not uniform. In Chapter 2 we show that it is advantageous to make the following envelope categorization: Structural, Performance, Control, Stability and Situational Awareness envelope. The introduction of a ‘Situational Awareness’ envelope is useful to address the limits, such as roll angle limits, that are not based on aerodynamic limits but that can serve as boundary for normal flight conditions. Our investigation shows that exceeding envelope limits does not always lead to an imminent dangerous situation, however, for both the control and the structural envelope it does. This is the reason we restrict ourselves to the control envelope in order to prevent that the combination with other envelopes will make it overly restrictive.

In Chapter 3 we develop a theoretical framework for the lateral-directional control warning system. The following conclusions are derived. Firstly, the loss of lateral control normally precedes the loss of directional control. Consequently, an aircraft that loses lateral-directional control will normally enter an unstoppable roll. Secondly, it is feasible to use airspeed as a boundary measure for sufficient lateral control. Sufficient control is, conform the Military Specifications, defined as a roll angle change in a fixed time interval and has different values for each aircraft type. This minimum control speed ( $V_c$ ) differs from the well known ‘Minimum Control Speed Air’ or  $V_{mca}$ . While  $V_{mca}$  is a fixed value,  $V_c$  depends on the aircraft state and pilot inputs. The third conclusion is that the  $V_{mca}$  definition can be improved, by changing the ‘Steady Heading’ requirement into a zero slip angle ( $\beta$ ) requirement and add a minimum roll control requirement.

Investigations into the roll control after an engine failure lead to some additional findings. The standard assumption that thrust is power divided by airspeed, is reasonably accurate when compared to the non-linear model of the Piper Seneca (PA-34). However, this assumption can’t of course be correct at very low airspeeds. The thrust dependent cross-flow that is responsible for a decrease in the directional control, increases

less with thrust at low airspeeds. On the other hand, the roll moment, due to the additional lift generated by the slipstream behind the working engines, increases much more strongly at low airspeeds, namely, power divided by the airspeed squared. This non-linearity was a reason to try different normalizations for thrust, in order to see if this would improve the  $V_c$  estimation.

Another area investigated was to what extent the controllability with one-engine-inoperative (OEI) is influenced by a turn. It is evident that the roll control into the dead engine is much larger than rolling into the opposite side, which constitutes a potential risk of over-banking. However, the turn itself has only a very limited effect on the available roll control. Through off-line simulations, using a non-linear model of the PA-34, it is shown that for this aircraft the additional aileron deflection to counteract this effect is just two degrees.

In order to be able to calculate the  $V_c$  for damaged aircraft as well, a model is derived in Chapter 4 that is based on an unknown mass, unknown inertia tensor and an unknown centre of gravity position. The parameters of this model are estimated on-line and are then used for the prediction of the  $V_c$  and the required corrections.

One possible disadvantage of the above mentioned model is that the number of needed parameters is much larger than if mass, inertia tensor and centre of gravity position would have been known. In Chapter 5 we describe the off-line tests in which we evaluate how model size influences the prediction of maximum rate roll at low airspeed. The finding is that small model sizes, where several parameters are omitted, predict the roll more accurately. Additionally, it is shown that the standard (statistical) methods for model size optimization add too many parameters. It seems therefore more practical to base model size on experimental evidence. Investigations into the causes of the failure of the statistical methods reveal that the prime causes are the parameters that depend on higher order variables. Those variables are not estimated accurately enough in standard flight conditions and generate excessive errors in manoeuvres with maximum control deflection.

In Chapter 6 we investigate different configuration settings for the  $V_c$  Prediction System (VPS), using off-line simulations with a non-linear PA-34 model. This simulation involves flights with different types of failures, including engine failures, control failures, rudder hard-over and lateral asymmetry. The flight profiles involve flights in turbulent as well as smooth air conditions. In these simulations, the VPS continuously predicts the  $V_c$  and, because at the end of the run a maximum rate roll was performed at low airspeed, the predicted  $V_c$  can be compared with the actual measured  $V_c$ .

Four configuration options are tested: Parameter Identification Methods (PID), model size, normalization and initial parameter settings. For PID the well-known two-step method is used. Within the two-step method there are possible choices for the 'second step'. One can use a PID with a forgetting algorithm, that constantly adapts and does not need a separate error detection algorithm, or a PID method that needs a reset af-

ter a failure is detected. In our evaluation the PID methods using a reset have a more stable  $V_c$  prediction, especially in turbulent air conditions. In this evaluation the initial model size findings are confirmed, smaller models also predict the  $V_c$  more accurately. The improved normalizations are intended to reduce the speed dependency of the  $V_c$  prediction. However, the tests show that the effect on  $V_c$  accuracy is small. A similar conclusion can be made for the initial conditions, this effect on accuracy is also small.

The off-line tests also reveal that the  $V_c$  mean absolute error is  $1.9\text{m/s}$ , deviating considerably from the desired accuracy of  $0.5\text{m/s}$ , which is equivalent to the displayed accuracy of most airspeed indicators. Further investigation reveals that the drag difference between the up-going and down-going aileron—the adverse yaw effect—excites the Dutch roll. To correct effectively for the Dutch roll effect in the  $V_c$  calculation, the accurate value of a number of stability derivatives is crucial. However, two important parameters,  $n_p$  and  $n_r$ , change strongly after the covariance matrix reset that is initiated by the detection of the failure and these parameters only slowly converge back to their initial, and correct, values. With two adaptations this effect can be minimized. Firstly, the reset value of the covariance matrix can be decreased, which affects a smaller change of  $n_p$  and  $n_r$ , while at the same time the PID remains adequate to adapt the parameters after a failure detection. The second adaptation is the decrease of the time interval for the predicted roll angle change from 1.5 second to 0.75 second. This decreases the mean absolute error to  $1\text{m/s}$ .

Finally the practical feasibility of the  $V_c$  indication was investigated experimentally using the TU Delft's Simona Research Simulator. Two test series were accomplished, the first one in October 2014 and described in Chapter 7. In the first trials ten pilots participated; these trials were exploratory in nature and concentrated on the most common emergency, the engine failure. One test scenario was devoted to a damaged aircraft that experienced a rudder hard-over. These tests reveal that pilots are not always aware of the fact they are using less than maximum rudder in situations where maximum rudder is required. Another problem is that many pilots find it hard to establish the correct climb angle with one engine inoperative. Another feature tested in these trials was a new slip indicator. This slip indicator can display either side slip angle ( $\beta$ ) or side acceleration. The slip can be displayed in the standard position in the top of the attitude indicator, but also in the centre of the attitude indicator as a variable size triangle, which has the advantage that the visibility increases with the square of the slip error.

Based on these initial tests the following modifications are made. Firstly, a double  $V_c$  is presented, the first  $V_c$  gives the minimum speed for the required roll performance using aileron only and maintaining the present side slip. The second  $V_c$  gives the minimum speed for the same roll performance using both maximum aileron and rudder. The difference between the two speeds is an indication for the pilot that additional rudder is still available to aid in lateral control. Secondly, a climb bar is added to the attitude indicator, indicating the attitude that will give a constant speed. This enables the pilot to see directly if the climb attitude will give an acceleration or deceleration. Finally, a filter is added to stabilize the slip indication.

In August 2015 the second series of tests were conducted with 19 pilots participating. These tests are described in Chapter 8. Again, the majority of tests were devoted to the handling of engine failures with pilots alternately using the standard and the new display. Four different scenarios were flown.

The first scenario was intended to measure whether the slip indicator would give a more precise aircraft control in a climb with one engine inoperative. The results show that the average score did not change significantly using the new display. However, the error variance does decrease significantly. The practical implication of this finding is that the new display does help some pilots to prevent large slip errors. Pilots preferred the side acceleration display over the display of  $\beta$ , although the latter does give a significantly better climb performance. The majority of the subjects (13 out of 19) had a preference for the centre triangle display.

The second scenario was a one-engine-inoperative go-around, starting with a critically low airspeed (80 knots). This scenario was by far the most difficult and ended several times with a (near) crash. The tests show no significant improvement in pilot performance when  $V_c$  and climb bar are displayed. Halfway through the test it already became apparent that this test reveals more how difficult this scenario is for the pilots, who hardly noticed the new display, although they had been given ample familiarisation time with the new display. Therefore a new scenario was added halfway through the experiment that was added at the end of the regular test series. In this scenario the subjects were given dedicated training in this scenario, using the new display, and we measured the performance improvements of the subject. The results show that 6 out the 9 participating subjects showed a good learning curve while three needed more time to master this scenario. The conclusion of this test is that the recovery of a roll-limited situation using this new display can only improve after being given adequate training. Additionally, the tests reveal how dangerous the recovery from a roll limited situation is for pilots that have had no training in this scenario. Unfortunately this is true for almost all pilots.

The third scenario was a known scenario for all subjects, a sudden engine failure directly after take-off. All subjects performed well in this scenario and there is no significant improvement when using the new display. However, pilots did appreciate the climb bar.

Finally, the fourth scenario was devoted to investigating the handling of a damaged aircraft. The damage condition was a partial loss of aileron combined with a lateral c.g. shift. This scenario was used to investigate how pilots would handle this scenario without any extra information, and how they performed when instructed to follow the 'Controllability Check' procedure combined with the  $V_c$  display. Results show that all subjects that had received military flight training (3) executed the 'Controllability Check' and out of those with civilian flight training nobody did. These latter subjects showed large variations in approach speeds, from dangerously fast to dangerously slow, while configuration changes were often made late. Neither military trained nor civilian trained pilots

were able to correctly explain the cause of the strange aircraft behaviour. This was also the intention as the damage had to be of an unknown type.

In the second run of the fourth scenario the  $V_c$  was displayed. Here all pilots were instructed to follow the 'Controllability Check' procedure. With this combination of  $V_c$  presentation and 'Controllability Check' all subjects found a safe approach speed. Furthermore some subjects discovered by themselves that they could use asymmetric thrust to increase lateral control.

The first overall conclusion of this thesis is that the limits for 'One Engine Out' operation can be improved. Rather than using the present  $V_{mca}$  definition, it is better to base  $V_{mca}$  on the zero side slip angle requirement with maximum asymmetric thrust and on the Mil. Spec. requirements for lateral control. Secondly, lateral control limits are normally exceeded before directional control limits, which allows us to focus on the former limits for an in-flight warning systems. Thirdly, the decrease in lateral control with air-speed is quite rapid, because of the non-linear effects of engine moment and induced roll moment due to the propeller slipstream. Fourthly, experiments show that the visual presentation of the  $V_c$ , climb bar and the new slip indicator can all help recover from flight situations where the roll performance is limited, but their use must be combined with adequate training. Finally, the handling of damaged aircraft can be improved by incorporating the 'Controllability Check' in civilian pilot training.

Further research is needed to quantify the effects of the 'Controllability Check' with and without the  $V_c$  indicator developed in this thesis, on the handling of unknown failure situations. Also the transfer of 'Controllability Check' training on the pilots' handling of unexpected failure situations needs to be further evaluated.



# SAMENVATTING

Het verlies van controle over de besturing van het vliegtuig is de laatste jaren de belangrijkste oorzaak van fatale vliegongevallen, en dit geldt zowel voor de commerciële als ook voor de kleine (privé) luchtvaart. In de laatste decennia zijn diverse inspanningen gedaan deze problemen te reduceren, onder andere door de vliegers te trainen in overtrek en ongebruikelijke neusstanden als ook door het ontwikkelen van betere automatische besturingssystemen. Deze studie onderzoekt of de respons van een piloot bij een dreigend verlies aan laterale directionele bestuurbaarheid kan worden verbeterd. Deze studie concentreert zich op tweemotorige propellervliegtuigen, omdat deze vliegtuigen, met name bij motorverlies, de grootste beperkingen ervaren in laterale directionele bestuurbaarheid. Het doel was te onderzoeken of op een soortgelijke wijze als een invalshoekmeter waarschuwt voor een dreigende overtrek, er een waarschuwing kan worden gemaakt voor een verlies aan laterale directionele controle.

In de bestudering van het onderzoek dat is gedaan naar veilige vluchtdomeinen werd het duidelijk dat veel onderzoekers een combinatie van vluchtdomeinen gebruiken. Tevens bleek dat de indeling in de diverse vluchtdomeinen niet uniform is. In Hoofdstuk 2 laten we zien dat de volgende indeling nuttig is: Structureel, Prestatie, Controle, Stabiliteit en een Situationeel Bewustzijns vluchtdomein. De introductie van het 'Situationeel Bewustzijns' vluchtdomein is nuttig om limieten, zoals onder andere rolhoeklimieten, die niet gebaseerd zijn op aerodynamische limieten, maar op het normale vluchtdomein, een plaats kunnen krijgen. Ons onderzoek laat zien dat overschrijding van een vluchtdomein niet altijd leidt tot een direct gevaarlijke situatie, echter, bij zowel het structurele als het controle domein is dit wel het geval. Dit is de reden om het controledomein niet te combineren met andere domeinen om te voorkomen dat de limieten te beperkend worden.

In Hoofdstuk 3 wordt het theoretisch fundament gelegd om te komen tot een lateraal directioneel waarschuwingssysteem. Deze analyse leidt tot de volgende conclusies. Ten eerste blijkt dat het verlies van laterale controle normaliter eerder komt dan het verlies van directionele controle. Een vliegtuig met verlies van laterale-directionele bestuurbaarheid zal dus standaard in een niet te stoppen rol komen. Ten tweede blijkt dat het mogelijk is de gewenste minimum controle in rol te koppelen aan een vliegsnelheid. Voor de gewenste rolcontrole is gekozen voor een verandering van rolhoek in een bepaalde tijdsinterval, die in overeenstemming met de Military Specifications, voor elk type vliegtuigtype kan worden vastgesteld. Deze minimum snelheid voor toereikende laterale controle ( $V_c$ ) is in tegenstelling tot de bekende 'Minimum Control Speed Air' ( $V_{mca}$ ) geen vaste snelheid, maar is afhankelijk van de toestand van het vliegtuig en de besturing door de vlieger. Een derde bevinding is dat de huidige  $V_{mca}$  beter gedefinieerd kan worden door deze niet te baseren op de capaciteit om met kleine rolhoek nog

rechtuit te kunnen vliegen, maar op de eis om de sliphoek ( $\beta$ ) op nul te kunnen houden, met als aanvullende eis dat tevens voldoende rolcontrole aanwezig is.

Onderzoek naar de rolcontrole bij motorverlies leidt tot een aantal aanvullende bevindingen. Zo blijkt de (standaard) aanname dat de stuwkracht gelijk is aan het vermogen gedeeld door de snelheid, redelijk te kloppen bij simulaties met een niet-lineair model van de Piper Seneca (PA-34), hoewel deze aanname bij zeer lage snelheden natuurlijk niet correct kan zijn. De met de stuwkracht samenhangende laterale stroming over de romp, die de directionele controle van propellervliegtuigen verder vermindert, blijkt echter bij lagere snelheden iets minder sterk toe te nemen dan de stuwkracht. Anderzijds blijkt het door de slipstream veroorzaakte rolmoment veel sterker toe te nemen bij lagere snelheid, namelijk met het vermogen gedeeld door het kwadraat van de vliegsnelheid. Dit rolmoment wordt veroorzaakt doordat de slipstream van de werkende motor extra lift genereert. In de latere  $V_c$  proeven werden daarom naast de standaard normalisatie, ook andere verhoudingen getest om te bezien of hierdoor de schatting van de  $V_c$  kon worden verbeterd.

Verder werd onderzocht in hoeverre, met één motor uit, de bocht de bestuurbaarheid beïnvloedt. Het is duidelijk dat het inrollen van de bocht in de richting van de niet werkende motor, altijd veel sneller kan dan naar de andere kant, waardoor er een risico bestaat van te ver doorrollen, echter, de bocht zelf heeft slechts een zeer klein effect op de beschikbare bestuurbaarheid in rol. In simulaties met een niet-lineair model van de PA-34 bleek dat de extra benodigde rolroeruitslag slechts twee graden is.

Omdat het doel is ook de  $V_c$  te kunnen berekenen voor beschadigde vliegtuigen, is een model ontwikkeld voor vliegtuig parameteridentificatie dat uitgaat van een onbekende traagheidstensor, massa en zwaartepuntligging. De parameters van dit model worden gedurende de vlucht geschat en gebruikt in het algoritme voor de  $V_c$  berekening waarbij de benodigde correcties worden toegepast.

Eén van de mogelijke nadelen van het gebruikte model is dat het aantal parameters groot is ten opzichte van een model met bekende massa, traagheidstensor en zwaartepuntligging. In Hoofdstuk 5 wordt daarom het effect van de modelgrootte onderzocht en bezien in hoeverre de voorspelling van de maximale rol beïnvloed wordt door de modelgrootte. Dit onderzoek leidt tot de conclusie dat een klein model, waarin verschillende parameters zijn weggelaten, leidt tot een nauwkeuriger voorspelling. Tevens blijkt dat standaard (statistische) methoden voor het optimaliseren van de modelgrootte leiden tot een te groot model. Het is daarom beter de modelgrootte te optimaliseren aan de hand van praktijktesten. Onderzoek naar het tekortschieten van de statistische methoden onthulde dat de belangrijkste oorzaak ligt bij de parameters die afhankelijk zijn van hogere orde variabelen. Deze parameters worden in standaard vluchtcondities te onnauwkeurig bepaald en genereren excessieve fouten voor manoeuvres met maximale roeruitslagen.

In Hoofdstuk 6 worden verschillende configuratie mogelijkheden voor het  $V_c$  Voor-

spellingssysteem (VVS) behandeld. Deze mogelijkheden zijn getest in 'offline' simulaties met een niet-lineair model van de Piper Seneca. Met dit model werden vluchten gesimuleerd waarbij diverse soorten storingen optraden: motorstoring, verlies van stuurvlakken, vastgelopen uitgeslagen richtingsroer en laterale asymmetrie. Deze testen werden uitgevoerd in normale en in turbulente vliegcondities. Tijdens deze vluchten voorspelde het VVS de  $V_c$  en aangezien aan het eind van elke test een maximale rol werd gemaakt bij lage snelheid kon de voorspelde  $V_c$  worden vergeleken met de gemeten  $V_c$ .

Vier configuratie-opties werden getest. Ten eerste was er een keus in gebruikte Parameter Identificatie (PID) methode, ten tweede werden ook in deze test verschillende modelgroottes meegenomen, ten derde werden verschillende normalisaties geprobeerd en ten vierde was er een keus in initiële parameterwaarden. Voor de PID werd de bekende 'Twee Stap Methode' gebruikt. Binnen deze methode zijn er echter nog keuzes mogelijk voor de tweede stap. Er kan worden gekozen voor een PID gebaseerd op een vergeet-algoritme dat zich constant aanpast en dus geen aparte foutdetectie nodig heeft, of een PID die gereset moet worden bij detectie van een storing. In onze vergelijking blijken de methoden gebaseerd op een reset veel stabiel, met name in turbulentie. Bij het analyseren van het effect van modelgrootte worden de eerdere conclusies bevestigd in een nauwkeuriger  $V_c$  berekening met de kleine modellen. De verbeterde normalisaties zijn bedoeld om de  $V_c$  berekening minder snelheidsafhankelijk te maken. In de testen blijkt echter dat de verbetering in  $V_c$  nauwkeurigheid klein is, en datzelfde is ook het geval met de initiële condities die een gering effect hebben op de voorspellingsnauwkeurigheid.

Het bleek echter dat de gewenste nauwkeurigheid in  $V_c$  voorspelling bij lange na niet werd gehaald. De gemiddelde absolute fout was  $1,9\text{ m/s}$  terwijl het doel was  $0,5\text{ m/s}$  (gelijk aan afleesnauwkeurigheid van de snelheidsmeter). Onderzoek leerde dat het 'haak effect', veroorzaakt door het verschil in weerstand van het naar boven en naar beneden uitgeslagen rolroer, de 'Zwierbeweging' opwekt. Om het effect van deze zwierbeweging goed te compenseren in de  $V_c$  berekening zijn een aantal stabiliteitsparameters cruciaal. Het bleek dat twee van deze parameters,  $n_p$  en  $n_r$  na het ontstaan van een storing sterk veranderen en maar langzaam terugconvergeren naar hun initiële (en correcte) waarden. Met twee aanpassingen kon dit probleem worden verkleind. Ten eerste bleek het mogelijke de reset (van de covariantie matrix) zodanig te dimensioneren dat bij een reset  $n_p$  en  $n_r$  minder gingen veranderen terwijl de reset toch adequaat blijft voor het aanpassen van de parameters na detectie van een storing. Een tweede aanpassing was het verkorten van de tijdsinterval van de rolhoek verandering van 1,5 tot 0,75 seconde. Na deze aanpassing was de gemiddelde fout teruggebracht tot  $1\text{ m/s}$ .

Tenslotte werd de praktische bruikbaarheid van  $V_c$  presentatie onderzocht in de Simona Research Simulator van de TU Delft. Er vonden twee testseries plaats, de eerste in oktober 2014, waaraan 10 piloten deelnamen. De eerste testen staan beschreven in Hoofdstuk 7. Deze testen hadden een verkennend karakter en concentreerden zich voornamelijk op de meest voorkomende noodsituatie, de motorstoring terwijl één testscenario een beschadigd toestel ('Rudder Hardover') betrof. Uit deze testen kwam naar voren dat piloten zich niet altijd bewust waren van het feit dat zij minder dan maximaal

richtingsroer gebruikten, terwijl dat toch gewenst was. Een ander probleem was dat veel piloten het moeilijk vonden om de juiste klimhoek te vinden bij een doorstart met één uitgevallen motor. In deze testen werd tevens een nieuwe slip indicator getest waarbij, of de dwarsversnelling kon worden getoond, of de sliphoek. Tevens kon de slipindicatie op de standaard wijze bovenin de attitude indicator worden getoond maar ook als driehoek met variabele grootte, centraal in de attitude indicator, waarbij de zichtbaarheid kwadratisch toeneemt met de sliphoek of de dwarsversnelling.

Gebaseerd op deze initiële testen werden er een aantal wijzigingen aangebracht. Ten eerste werd een dubbele  $V_c$  gepresenteerd, de eerste  $V_c$  geeft de minimum snelheid voor de vereiste rolprestatie met uitsluitend gebruikmaking van de rolroeren en het handhaven van de initiële slip. De tweede  $V_c$  geeft de minimum snelheid voor de vereiste rolprestatie gebruikmakend van zowel vol rolroer- als richtingsroeruitslag. Het verschil tussen deze snelheden is dus een indicatie voor de piloten dat er nog meer richtingsroeruitslag beschikbaar is. Ten tweede is een balk toegevoegd aan de attitude indicator die de klimhoek aangeeft waarbij de snelheid constant blijft. De piloot kan dan direct zien of de neusstand leidt tot versnelling of vertraging. Tenslotte is ook een filter toegevoegd om de slip en  $\beta$  indicatie beter te stabiliseren.

In augustus 2015 werden de laatste testen uitgevoerd, waaraan 19 vliegers deelnamen. Deze testen staan beschreven in Hoofdstuk 8. Wederom zijn de meeste testen gebaseerd op het onderzoeken van de prestaties van de piloten bij motorstoring, waarbij afwisselend met en zonder de nieuwe indicaties werd gevlogen. In totaal werden vier scenarios gebruikt.

Het eerste scenario was bedoeld om te meten of de nieuwe slip indicator tot een nauwkeuriger vliegtuigbesturing zou leiden in een klim met een niet-werkende motor. Het bleek dat de gemiddelde score niet significant veranderde als gebruik werd gemaakt van de display met de variabele driehoek. Wel bleek dat de variantie significant afnam. De implicatie hiervan is dat deze nieuwe display voor sommige vliegers helpt om grote sliphoeken te vermijden. Vergelijken we de  $\beta$  indicatie met die van de dwarsversnelling dan blijkt dat proefpersonen er de voorkeur aan gaven te sturen met nul dwars acceleratie in plaats van  $\beta = 0$  terwijl de laatste vliegsituatie toch een significant hogere klimsnelheid geeft. Het merendeel van de proefpersonen, 13 van de 19, hadden een voorkeur voor de display met de variabele driehoek.

Het tweede testscenario was een doorstart met één motor uit, vanuit de situatie waar de snelheid kritisch laag was (80 knopen). Dit bleek verreweg het moeilijkste scenario waarin ook meerdere malen de simulatie eindigde in een (bijna) ongeval. Uit de testen komt geen significant verschil in prestatie door het presenteren van de  $V_c$  en de klimbalk aan de piloten. Halverwege de testen werd al duidelijk dat deze test eerder aantoont dat dit scenario te moeilijk is voor de proefpersonen en dat zij er nauwelijks aan toe kwamen om de gepresenteerde nieuwe indicaties waar te nemen ondanks dat zij daarmee in de familiarisatie fase geruime tijd hadden mogen oefenen. Daarom werd halverwege de testen een nieuw scenario toegevoegd na afloop van de reguliere testen. Hierbij werd

gekeken of de prestaties door oefening met de nieuwe displays verbeterden. Het blijkt dat 6 van de 9 proefpersonen die bij dit experiment betrokken waren een goede leercurve vertoonden, terwijl drie proefpersonen nog meer tijd nodig hadden. De conclusie is dan ook dat de nieuwe presentatie pas de rolgelimeerde vliegsituatie zal verbeteren als de piloot daarvoor getraind wordt. Tevens maakt deze test het potentiële gevaar van deze situatie duidelijk voor de piloot die hierin niet is getraind. Dat is momenteel het geval voor nagenoeg alle piloten.

Het derde scenario was een voor alle proefpersonen bekend probleem, een plotselinge motorstoring direct na de start. Het bleek dat alle proefpersonen in dit scenario goed presteerden en dat er geen significant verschil was als gevolg van de getoonde extra informatie. Wel werd de klimbalk positief gewaardeerd door de proefpersonen.

Tenslotte was het vierde scenario ontworpen rond een onbekende schade aan het vliegtuig, in dit geval een laterale asymmetrie gecombineerd met het verlies van de helft van de rolroeren. In dit experiment werd vergeleken hoe de diverse proefpersonen een dergelijk probleem standaard oplossen, en hoe dit scenario verloopt indien consequent de 'Bestuurbaarheidscontrole' wordt uitgevoerd en de  $V_c$  informatie getoond wordt. Het bleek dat proefpersonen met een militaire vliegopleiding (3) allen de standaard 'Bestuurbaarheidscontrole' uitvoerden en van de piloten met een civiele opleiding niemand. Deze laatste groep proefpersonen liet een zeer gevarieerd beeld zien: grote variaties in naderingssnelheid van gevaarlijk snel tot gevaarlijk traag, terwijl configuratie wijzingen vaak pas laat werden gemaakt. Geen van de proefpersonen, onafhankelijk van de soort vliegopleiding, was in staat de oorzaak van het vreemde vlieggedrag juist te verklaren. Dat laatste was ook bedoeld, omdat de vraag was hoe een vlieger omgaat met onbekende schade aan het vliegtuig.

Elke proefpersoon kreeg dit scenario twee keer. Bij de tweede keer werd de  $V_c$  getoond en werden de proefpersonen tevens, zover nodig, geïnstrueerd in de 'Bestuurbaarheidscontrole'. De combinatie van  $V_c$  indicatie met 'Bestuurbaarheidscontrole' had tot gevolg dat de proefpersonen een veilige naderingssnelheid vonden en sommigen zelfs ontdekten dat zij asymmetrische stuwkracht konden gebruiken ter vergroting van de laterale bestuurbaarheid.

De eerste conclusie van deze thesis is dat de limieten voor bestuurbaarheid met één motor uit, beter kunnen worden gedefinieerd. In plaats van de huidige  $V_{mca}$  definitie te gebruiken kan  $V_{mca}$  beter worden gebaseerd op de eisen dat nul sliphoek mogelijk moet zijn met maximale asymmetrische stuwkracht en op de laterale besturingseisen van de 'Military Specifications'. Ten tweede, de rol-besturingslimieten worden doorgaans eerder bereikt dan de gier-limieten, daarom kan worden geconcentreerd op deze limieten. Ten derde, de afname van de bestuurbaarheid in rol met snelheid is abrupt vanwege het niet lineaire effect van het motormoment en het rolmoment dat wordt veroorzaakt de door slipstroom van de propeller. Ten vierde, uit de experimenten in de vluchtsimulator blijkt dat de presentatie van de  $V_c$ , klimbalk en nieuwe slip-aanwijzer een bijdrage kan leveren in het herstellen van vliegsituaties waarbij het rolvermogen is gelimiteerd,

maar uitsluitend indien dit gepaard gaat met voldoende training. Tenslotte blijkt dat de besturing van een beschadigd vliegtuig kan worden verbeterd door de 'Bestuurbaarheidscontrole' procedure in te brengen in de civiele vliegopleiding.

Verder onderzoek is gewenst om het effect van de 'Bestuurbaarheidscontrole' procedure te onderzoeken bij onbekende schade aan het vliegtuig zowel met als zonder dat er gebruik kan worden gemaakt van de  $V_c$  indicatie. Verder onderzoek naar het effect van de 'Bestuurbaarheidscontrole' training op het omgaan met dit soort situaties in de praktijk is gewenst.

# CURRICULUM VITÆ

## Herman Johan KOOLSTRA

17-03-1952      Born in Rijk, The Netherlands.

### EDUCATION

1964-1970      HBS-B  
Chr. Lyceum, Hilversum  
The Netherlands

1970-1971      Kweekschool v.d. Zeevaart  
Amsterdam, The Netherlands

1975              Koninklijk Instituut v.d. Marine  
Den Helder, The Netherlands

1976-1977      Military Pilot Training  
Moose Yaw, Canada

1982-1983      Koninklijke Militaire Academie  
Breda, The Netherlands

1984-1985      USAF Test Pilot School  
Edwards Air Force Base, USA

## PROFESSIONAL CAREER

1971-1974	Maritime Officer, Shell Tankers B.V.
1975-1976	Officer, Netherlands Navy. Task: Hydro-graphic survey
1977-1984	Military Pilot, Royal Netherlands Air Force.
1985-1990	Experimental Test Pilot NF5.
1990-1996	Experimental Test Pilot F-16.
1996-1997	Test Director Multinational Operational Test and Evaluation Mid Life Update F-16.
1998-2001	Head Fighter Operational Requirements RNLAf.
2001-2004	Head Flight Test Branch RNLAf
2005-2007	Assistant Professor Military Operations, KMA Breda
2007-2011	Flight Inspector Military Aviation Authority (part time)

# LIST OF PUBLICATIONS

9. **H.J. Koolstra , H.J. Damveld, and J.A. Mulder**, *Application of SPRT Based Reset Methods for Damaged Aircraft Parameter Estimation* , 2015 AIAA Modeling and Simulation Technologies Conference.
8. **H.J. Koolstra , C.C. de Visser, J.A. Mulder**, *Effective Model size for the prediction of the lateral control envelope of damaged aircraft*, 2015 AIAA Modeling and Simulation Technologies Conference.
7. **H.J. Koolstra , H.J. Damveld, and J.A. Mulder**, *An Improved, Turbulence Proof, Reset Mechanism for Parameter Identification after System Change*, 2013 AIAA Guidance Navigation and Control Conference
6. **H.J. Koolstra , H.J. Damveld, and J.A. Mulder**, *Envelope Determination of Damaged Aircraft*, 2012 AIAA Guidance Navigation and Control Conference
5. **H.J. Koolstra and H. Jansen**, *Background Information on Military Aviation Requirements-Flight Simulation Training Devices (MAR-FSTD)* , MAA- Den Haag (2010).
4. **H.J. Koolstra and H. Jansen**, *Military Aviation Requirements- Flight Simulation Training Devices (MAR-FSTD)* , MAA- Den Haag (2010).
3. **H.J. Koolstra et al.**, *Introduction to Military Air Operations*, KMA-Breda (2007).
2. **H.J. Koolstra and H. Gemmink**, *De beperkingen van het 'See and Avoid' systeem*, KLu- Den Haag (2004).
1. **H.J. Koolstra, P.M.N. Hollestelle and J.M. Klijn**, *A data acquisition system for the RNLAf MLU F-16; Requirements and proposal*, NLR TP 96588 1996.



$t=0.0s$



$t=1.0s$



$t=2.0s$



$t=3.0s$



$t=4.2s$